RAPPORT DE THESE

IRSN
INSTITUT
DE RADIOPROTECTION
ET DE SÛRETÉ NUCLÉAIRE

Faire avancer la sûreté nucléaire

INFLUENCE OF OSMOTIC PROCESSES ON THE EXCESS-HYDRAULIC HEAD MEASURED IN THE TOARCIAN/DOMERIAN ARGILLACEOUS FORMATION OF TOURNEMIRE

ISRN/IRSN-2011/149

UPMC
PARISUNIVERSITAS

AMPHOS 21

IRSN
INSTITUT
DE RADIOPROTECTION
ET DE SÛRETÉ NUCLÉAIRE

DIRECTION DE L'ENVIRONNEMENT ET DE L'INTERVENTION
Service d'analyse des risques liés à la géosphère

Université Pierre et Marie Curie - Paris 6
École Doctorale Géosciences et Ressources Naturelles

THÈSE de DOCTORAT

pour obtenir le titre de

Docteur en Sciences

de l'Université Pierre et Marie Curie - Paris 6
Spécialité : Hydrologie et Hydrogéologie quantitative

Présentée et soutenue par

Joachim TRÉMOSA

Influence of osmotic processes on the excess-hydraulic head measured in the Toarcian/Domerian argillaceous formation of Tournemire

---

soutenue le 30 novembre 2010
devant le jury composé de

Président :	M Pierre M. ADLER	Université Pierre et Marie Curie
Rapporteurs :	M Philippe COSENZA	Université de Poitiers
	M Philippe GOUZE	Université de Montpellier 2
co-Directeur :	M Julio GONÇALVÈS	Université Paul Cézanne
co-Directrice :	Mme Sophie VIOLETTE	Université Pierre et Marie Curie
Examinateurs :	M Daniel COELHO	ANDRA
	M Eric C. GAUCHER	BRGM
Encadrants :	M David ARCOS	AMPHOS XXI Consulting S.L.
	M Jean-Michel MATRAY	IRSN
Invité :	M Frédéric SKOCZYLAS	Ecole Centrale de Lille

Par une belle matinée de mai,
une svelte amazone, montée sur
une superbe jument alezane,
parcourait les allées fleuries du
Bois de Boulogne.

Albert Camus — La Peste

Acknowledgements, remerciements, agradecimientos...

First of all, in this nice but difficult task of the acknowledgements, I would like to thank the French Institute for Radiological Safety and Nuclear Protection (IRSN) and Amphos XXI Consulting S.L. for funding my PhD thesis. In a long-term occupation such as a thesis, feeding the student is quite important. I also really appreciated the excellent material conditions in which I performed my thesis. Sur ce point, je tiens en particulier à remercier Didier Gay, Denise Stammose et Corinne Bauer à l'IRSN y quiero agradecer a Jordi Bruno y Lara Duro en Amphos 21.

Mes remerciements s'adressent ensuite à Pierre Adler pour avoir accepter de présider mon jury de thèse. Je remercie aussi Philippe Cosenza at Philippe Gouze pour leur lecture attentive de mon manuscrit et leurs remarques pertinentes, tant dans le rapport de thèse que lors de la soutenance. Pour compléter les remerciements aux membres de mon jury de thèse, je tiens à remercier Daniel Coelho et Eric Gaucher pour l'examen de mon manuscrit et pour leurs remarques constructives.

Mille merci à mon directeur, ma directrice et mes encadrants de thèse. Julio est un type formidable! Il a pleins d'idées lumineuses, il est toujours disponible, il est patient et toujours prêt à ré-expliquer sa dernière idée lumineuse et il est toujours de bonne humeur. Je le remercie aussi pour m'avoir fait confiance et me laisser me dépatouiller à partir de ses grandes idées. Je n'ai pas travaillé régulièrement avec Sophie mais je le regrette car ses conseils sont toujours excellents. Quant à Jean-Michel, je tiens à le remercier bien évidemment pour ses conseils en tutage de grillons mais aussi pour m'avoir passé les clés du tunnel de Tournemire et m'avoir laissé m'y amuser pendant 3 ans. La confiance qu'il m'a accordé est aussi importante à mes yeux. Quiero también agradecer a David por sus consejos y por haber encontrado tiempo para seguir mi trabajo.

J'ai aussi eu, au cours de ma thèse, la chance de travailler avec d'autres équipes de recherche que je souhaite remercier. Je pense en particulier à l'équipe du Laboratoire de Mécanique de Lille (LML) de l'Ecole Centrale de Lille. Merci à Frédéric Skoczylas de m'avoir aidé à la conception des expériences d'osmose chimique et d'avoir trouvé de la place pour héberger mes manips. Merci aussi à Thierry Dubois pour le suivi de ces expériences. Pour leurs discussions sur mon travail traitant de la géochimie des eaux porales de Tournemire et pour leur aide dans l'application de leur modèle au cas de Tournemire, je souhaite remercier Eric Gaucher (pour la deuxième fois ici) et Christophe Tournassat du BRGM.

À l'IRSN, sur le projet Tournemire, je tiens en particulier à remercier Justo Cabrera, Pierre Dick, Jean-Do Barnichon, Sébastien Savoye, Karim Ben Sli-

mane, Patrice Desveaux et Claude Combes. Toujours à l'IRSN, mais côté labo à Fontenay-aux-Roses, je remercie Sylvain Bassot et son équipe: Olivier, Nadia, Julia et Aurélie.
Pour l'émulation scientifique pendant ces 3 ans, des routes californiennes à la croix de Crépougnac en passant par la dune de Taghit et Couverpuits, c'était avec Fethi.
Pour avoir partagé café et repas, merci aux collègues du 76/2. Parmi ceux que je n'ai pas déjà cité: Charles, Lise, Gilles, François, Majda, Gonça, Pierre, Vincent, Laurent, Claire-Marie, Stéphane, Philippe, Aurélia, Angélique, Pauline, Nathalie, Isabelle, Elisabeth, Christophe, Vannapha, Caroline, Alexandre et pardon à ceux que j'oublie. Gracias también a todos los colegas de Amphos 21.
Merci aux copains et copines, aux collocs y compañeros y compañeras de piso. C'est bien d'oublier les argiles de temps à autres.
Enfin, grosses bises à toute la famille et chapeau bas à Céline pour me supporter et partager ma soupe quotidienne.
Et surtout, merci à toi lecteur!

Abstract

In the framework of the studies dealing on ability to store radioactive wastes in argillaceous formations, signification of interstitial pressures is an important point to understand water and solutes transport. In very low permeability argillaceous formations, like those studied in the Callovo-Oxfordian of the Paris basin by ANDRA, pore pressure is frequently higher than the theoretical hydrostatic pressure or than the pressure in the surrounding aquifers. Such an overpressure is also measured in the Toarcian/Domerian argillaceous formation ($k = 10^{-21}$ m^2), studied by the IRSN in the underground research laboratory of Tournemire (Aveyron, France). The hydraulic head profile has been specified in this manuscript and found to present a 30 ± 10 m excess-head. This excess-head can be due to compaction disequilibrium of the argillaceous formation, diagenetic evolution of the rock, tectonic compression, changes in hydrodynamic boundary conditions or osmotic processes. Amongst these potential causes, chemical osmosis and thermo-osmosis, a fluid flow under a chemical concentration and a temperature gradient, respectively, are expected to develop owing to the small pore size and the electrostatic interactions related to the charged surface of clay minerals.

The goal of the work presented here was to study and quantify the contribution of each cause to the measured excess-head. Chemo-osmotic and thermo-osmotic permeabilities were obtained by experiments and using theoretical models. Theoretical models are based on the reproduction of the interactions occurring between the charged surface of clay minerals and pore solution and their upscaling at the representative elementary volume macroscopic scale. Chemical osmosis phenomenon is related to anionic exclusion and the determination of the chemo-osmotic efficiency requires the resolution of an electrical interactions model. A triple-layer-model which considers diffuse layers overlapping was improved during this thesis to be able to take into account the effect of multi-ionic solutions, i.e. nearest than the natural waters composition, and, thus, to constrain better the chemo-osmotic efficiency ε. Thermo-osmosis process is poorly characterized so that no satisfactory macroscopic expression to calculate the thermo-osmotic permeabil-

ity k_T was available nor thermo-osmotic experiments performed on natural shales, so far. This process is interpreted as being related to changes properties of water sorbed at clay minerals surface compared with bulk water. A thermo-osmotic permeability predictive model is proposed here, based on the modifications of the hydrogen bounds associated with water molecules located at the vicinity of the solid surface. Input parameters of this model only consist in petrophysical parameters and medium conditions (porewater concentration and temperature). Chemical osmosis and thermo-osmosis experiments were performed on Tournemire argillite samples and in a test interval equipped borehole at the Tournemire URL. These experiments have consisted in inducing a concentration or temperature gradient across a sample for the laboratory experiments and between the borehole test interval and the formation for the in situ experiments. Osmotic flows were identified by the interpretation of the pressure evolution in the test interval using a hydro-thermo-chemo-mechanical model based on the mass balance equations and the coupled-flow equations. Inversion of the measured pressure signals allowed identifying a chemo-osmotic efficiency ε ranging between 0.014 and 0.31 and a thermo-osmotic permeability k_T ranging between 6×10^{-12} and 2×10^{-10} m^2 K^{-1} s^{-1} for the Tournemire clay-rock.

In parallel to the characterization of the osmotic processes in the argillaceous formation of Tournemire, porewater composition and temperature profiles were established. Temperature profile was obtained by direct measurement in different boreholes. Porewater composition profile was calculated by a geochemical model developed to reproduce the thermodynamic equilibrium reactions with mineral phases and cation exchange between the clay-rock and the pore solution. Added to the requirement of the temperature and concentration profiles across the Tournemire argillaceous formation as force gradients to reproduce the osmotic flows through the formation, the porewater composition is also needed as it is an essential input parameter to predict the chemo-osmotic efficiency coefficient.

At last, the characterization of the osmotic processes and the different force gradient profiles allowed estimating the contribution of the osmotic and hydraulic processes to the measured excess-hydraulic head profile measured in the argillaceous formation of Tournemire. Considerations on the hydro-mechanical behaviour of the argillaceous formation allowed rule out the other possible causes of excess-head and lead to the conclusion that only the hydraulic processes, related to the intrinsic permeability variation across the formation, and osmotic processes can explain the pressure field in the Toarcian/Domerian formation. The results particularly highlight the importance of the spatial variations of the hydraulic and osmotic permeability coefficients in the generation of an excess-hydraulic head.

Résumé

Dans le cadre des études portant sur la faisabilité d'un stockage de déchets radioactifs dans des formations argileuses, la signification des pressions interstitielles est une question importante pour comprendre les transports d'eau et de solutés. Dans les formations argileuses de très faible perméabilité, comme celle étudiée par l'ANDRA dans le Callovo-Oxfordien du bassin de Paris, la pression interstitielle est fréquemment supérieure à la pression hydrostatique théorique ou à la pression dans les aquifères encaissants. Une telle surpression est aussi enregistrée au sein de la formation argileuse du Toarcien/Domérien ($k = 10^{-21}$ m^2), étudiée par l'IRSN au laboratoire souterrain de recherche de Tournemire (Aveyron). Le profil de charge hydraulique, qui présente un excès de charge de 30 +/- 10 m, est précisé dans ce manuscrit. Cette surpression peut-être due à des déséquilibres de compaction de la formation argileuse, à l'histoire diagénétique de la roche, à des compressions tectoniques, à des changements de conditions hydrodynamiques aux limites de la formation ou à des phénomènes d'osmose. Parmi ces causes potentielles, l'osmose chimique et l'osmose thermique, respectivement, un flux d'eau sous un gradient de concentration et sous un gradient de température, sont susceptibles de se développer dans les milieux argileux par le fait de la faible taille des pores et des interactions électrostatiques liées aux charges de surface des minéraux argileux.

Le travail effectué a consisté à étudier et quantifier l'importance de chacun des processus responsables des surpressions à Tournemire. Les paramètres de couplage associés aux deux processus osmotiques, l'osmose chimique et la thermo-osmose, ont été acquis expérimentalement et à l'aide de modèles théoriques. Les modèles théoriques se fondent sur la reproduction des interactions qui ont lieu entre la surface chargée des minéraux argileux et la solution porale et leur mise l'échelle macroscopique du volume élémentaire représentatif. Le phénomène d'osmose chimique est lié à l'exclusion anionique et nécessite la résolution d'un modèle électrique d'interactions. Un modèle triple couche considérant le recouvrement des couches diffuses a été amélioré durant cette thèse pour prendre en compte l'effet des solutions multi-ioniques,

i.e. plus proche de la composition des eaux naturelles, et de mieux contraindre l'efficacité chemo-osmotique ε. La thermo-osmose est moins bien caractérisée de telle sorte qu'il n'existait pas d'expression macroscopique satisfaisante pour calculer la perméabilité thermo-osmotique k_T, ni d'expériences de thermo-osmose sur matériaux naturels. Ce processus est interprété comme étant causé par un changement des propriétés de l'eau liée à la surface des minéraux argileux par rapport à celles de l'eau libre. Nous proposons ici un modèle prédictif de la perméabilité thermo-osmotique basé sur la modification des liaisons hydrogène autour des molécules d'eau proche de la surface du solide et ayant pour seules données d'entrée des paramètres pétrophysiques et les conditions du milieu (concentration de l'eau porale de température). Les expériences d'osmose chimique et thermique ont été réalisées sur échantillons d'argilite de Tournemire et dans un forage équipé d'une chambre de test à la Station Expérimentale de Tournemire. Ces expériences ont consisté à induire un gradient de concentration ou de température à travers un échantillon pour les expériences en laboratoire et entre la chambre de mesure d'un forage et la formation pour les expériences sur site. Les flux osmotiques associés sont évalués grâce à l'interprétation de l'évolution des pressions dans les intervalles de mesure avec un modèle hydro-thermo-chemo-mécanique fondé sur les lois de conservation de la masse combinées avec les équations de flux couplés. L'inversion des signaux de pression mesurés permettent d'obtenir l'efficacité d'osmose chimique (ε entre 0.014 et 0.31) ainsi que la perméabilité thermo-osmotique (k_T entre 6×10^{-12} et 2×10^{-10} $\mathrm{m^2\ K^{-1}\ s^{-1}}$) de l'argilite de Tournemire.

En parallèle à la caractérisation des processus osmotiques dans la formation argileuse de Tournemire, les profils de composition de l'eau porale et de température ont été établis. Le profil de température a été obtenu par mesure directe dans plusieurs forages. Le profil de composition de l'eau porale a nécessité le développement d'un modèle géochimique visant à reproduire les réactions d'équilibre thermodynamique avec les phases minérales et par échanges cationiques entre la roche argileuse et la solution porale. Ajouté au fait que le profil de concentration chimique est la force motrice de l'osmose chimique dans la formation, la composition de l'eau porale est une donnée nécessaire pour calculer le coefficient d'efficacité chemo-osmotique.

Enfin, la caractérisation des processus osmotiques et des différents profils de force motrice nous a permis d'estimer la contribution des phénomènes osmotiques et hydrauliques au profil d'excès de charge hydraulique observé dans la formation de Tournemire. Des considérations sur le comportement hydromécanique de la formation argileuse ont permis d'écarter les autres causes possibles d'excès de charge et ont conduit à la conclusion que seuls les processus hydraulique, lié à la variation de la permabilité intrinsèque au

sein de la formation, et osmotiques expliquent le champ de pression dans la formation. Nos résultats pointent particulièrement l'importance de la variation au sein de la formation des coefficients de perméabilité hydraulique et osmotique dans la génération d'un excès de charge.

Contents

List of Figures

List of Tables

Part I

Introduction

The safety of deep geological nuclear wastes repositories needs the identification and the quantification of all the phenomena expected to contribute to mass transport in the geological medium. Indeed, this later can be considered as a barrier as in the French concept of a repository. The occurrence of overpressures in the low permeability argillaceous formations of sedimentary basins is frequently noted, i.e. fluid pressures higher than the theoretical hydrostatic pressure or than the linear pressure evolution of the surrounding aquifers.
The study of these overpressures can provide large informations on the hydrodynamic phenomena occurring in the shale layer [115]. Amongst the causes of overpressures, it can be distinguished those linked to a pore volume reduction, occurring mainly in the early basin evolution, those linked to an increase of the water volume and those linked to fluid flow processes (changes of hydraulic boundary conditions, osmotic flows or density driven flow). The determination of the processes inducing an overpressure is an important task for constraining the convective contribution to mass transport.

This doctoral thesis was launched by the French Institute for Radiological protection and Nuclear Safety (IRSN), in collaboration with the Université Pierre et Marie Curie - Paris 6 and AMPHOS XXI, within the framework of the evaluation of the ANDRA industrial project of geological repository in the Callovo-Oxfordian argillaceous formation in the East of the Paris basin. In the "Dossier Argile 2005" [4], a milestone established by ANDRA and presenting the repository host abilities of the Callovo-Oxfordian argillite, the 50 to 60 m excess-head observed in the formation was entirely attributed to chemical osmosis. It was in contradiction with Gonçalvès *et al.* [60] work and the IRSN safety notice [73], which argued that chemical osmosis is not as well efficient as hypothesized by ANDRA and that further processes could also be responsible of the observed overpressure.
Due to the scarcity of the knowledge on chemical osmosis behaviour in natural shales and in particular for the Callovo-Oxfordian argillite, further studies were needed to state on the interpretation of the pressure field in the Callovo-Oxfordian formation.
Osmotic efficiency for the Callovo-Oxfordian formation was established by Rousseau-Gueutin [135] and a contribution by chemical osmosis of 10 to 20 m on the 50 to 60 m of excess-head was calculated. Other processes are consequently required to explain the excess-head in the Callovo-Oxfordian formation. For this purpose, two additional processes were proposed such as thermo-osmosis and the role of pergelisol in the changes of hydraulic boundary conditions [74].

The purpose of the present thesis is to demonstrate the ability to interpret the measured excess-head, with a special emphasis to osmotic processes, in an argillaceous formation with properties clos enough to those of the Callovo-Oxfordian. The Toarcian/Domerian Tournemire formation, studied by the IRSN for research purposes was considered for this purpose.

A full characterization of the excess-head and hydrodynamic phenomena is presented in this study. It includes field data compilation, characterization of the hydrogeochemical system of Tournemire, in situ and off site laboratory osmotic flow experiments, theoretical developments for the characterization of the osmotic processes and modelling at the formation scale for assessing the influence of the different flow processes on the pressure field.
This manuscript is organized in four parts to deal with the origin of the excess-head in the Tournemire argillaceous formation.

The first part consists in the state of the art and presents some elements about abnormal pressures in sedimentary basins, the concepts of hydrogeology in argillaceous formations with a special emphasis to the osmotic processes and the geological and hydrogeological settings of the Tournemire Toarcian/Domerian argillaceous formation.

In the second part, entitled contribution to the hydrogeochemical characterization of the argillaceous formation of Tournemire, the profiles of hydraulic head, temperature and porewater chemical composition were established. Hydraulic head and temperature profiles are obtained through a collection and selection of data obtained in equipped boreholes. The porewater composition profile is needed for osmotic coefficients prediction and osmotic flow interpretation but can not be directly obtained by sampling due to the very low rock permeability and water content. It thus required the use of a clay-rock - solution geochemical interactions model able to calculate the porewater composition from relevant properties of the rock and the solution.

The third part aims at characterizing the chemical osmosis and thermo-osmosis coefficients in the Tournemire argillaceous formation. For both osmotic processes, the coefficients are established through theoretical models, accounting for the electrical interactions between the charged surface of clay minerals and the water and solutes in the pore space, and by experiments. The experiments have permitted assessing the clay-rock ability for driving an osmotic flow and determining a range of osmotic coefficients for given conditions, i.e salinity, temperature and porosity. Experiments results can

be compared to the predictions. Whereas the theoretical models provide coefficients as a function of the medium conditions and, consequently, a profile of the osmotic coefficients can be obtained across the formation as a function of the medium properties.
The predictive model for chemo-osmotic efficiency consists in the improvement of a triple-layer-model considering the interaction of the diffuse layers [59, 89] to consider multi-ionic solutions, i.e. in conditions nearest than the natural conditions found in clay-rocks. Two predictive models for thermo-osmosis in argillaceous media, so far poorly predicted, were established from a theory at molecular and pore scale [39]. These models correspond to the first general estimate of the thermo-osmotic permeability. They allow leading a discussion on the influence of this osmotic process on fluid flow in argillaceous formations.
The experimental determination of chemo- and thermo-osmotic coefficients were performed on samples in off site laboratory and in equipped boreholes, respectively.

The fourth and last part of this disertation concerns the interpretation of the pressure fields in argillaceous formations and includes the interpretation of the pressure profile in the Toarcian/Domerian argillaceous formation of Tournemire. The first chapter of this part consists in a discussion on the natural attenuation of chemo-osmotically induced abnormal pressures considering the effect of the natural waters composition on the osmotic efficiency. It is a contribution to the discussion on the ability of shales to generate overpressures by chemical osmosis, initiated by the Neuzil [116] observation that an osmotic flow can develop at the formation scale.
The last chapter deals with the interpretation of the hydraulic head profile measured in the Tournemire formation. In the calculations of the resulting hydraulic head, the impact of the osmotic processes was mainly considered. However, the influence of alternative processes were also discussed and introduced in the calculations. The calculated hydraulic head profiles were next compared to the excess-head previously determined, allowing to conclude on the origin of the excess-head in the Tournemire argillaceous formation and to discuss the influence of the osmotic processes on the fluid flow across the formation.

Part II

State of the art

Chapter 1

State of the art

1.1 Abnormal pressures in sedimentary basins

1.1.1 Abnormal pressures: overview and definition

Abnormal fluid pressures, especially overpressures, are frequently found in sedimentary basins and can reach some tens of MPa [33, 72, 88]. Indeed, around 180 worldwide located sedimentary basins were listed to present overpressures [70]. These overpressures can be observed in different kind of rocks (mainly carbonates, detrital rocks and evaporites) but most often in argillaceous layers or in relation with these layers [146]. The overpressures were historically studied in petroleum geology in areas affected by high fluid pressures prior their drilling. An unrecognized overpressure region suddenly found during drilling can lead to a kick effect in the borehole and to potentially dangerous and very costly blowouts and important economic losses [11, 106]. Overpressures are also studied in basin modelling to constrain the hydrocarbons expulsion from the source rock [33], shales typically.
In the context of radioactive waste storage in argillaceous formations, abnormal pressures were also found. These overpressures are moderate, lower than 1 MPa, most likely because the studied argillaceous formations are shallower than the ones studied for petroleum issues and are located in inactive sedimentary basins. The interest of studying overpressures in argillaceous formations mainly rests on the fact that the analysis of the causes of overpressures and the physical constrain of their magnitude allows understanding the mechanisms of fluid flow in clay-rocks [69].

A fluid (water, oil or gas) pressure is defined as abnormal if it differs from the theoretical hydrostatic pressure, calculated from the ground surface to the formation of interest considering a continuous groundwater column which writes:

$$P_h = \rho_f \, g \, z \tag{1.1}$$

where P_h is the hydrostatic pressure (Pa), ρ_f is the fluid density (kg m^{-3}), g is the acceleration due to gravity (m s^{-2}) and z is the depth (m). A fluid pressure lower than the hydrostatic pressure is then described as a subpressure and a fluid pressure higher than the hydrostatic one as an overpressure.
The example of the pressure evolution with depth (Fig. 1.1) in the Gulf Coast region of United States, i.e. a young and active basin with high sedimentation rate, provides an illustration of the occurrence of overpressures compared to the hydrostatic pressure and the lithostatic pressure. It is worth noting that the formation with normal fluid pressure and the geopressured zone can only coexist because of an impermeable caprock at the top of the overpressured region.

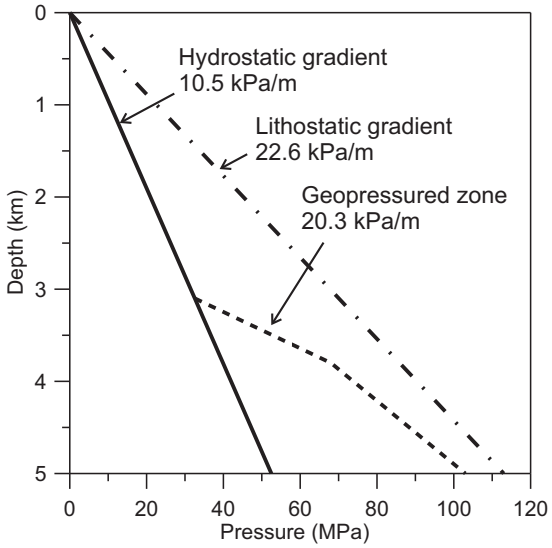

Figure 1.1: Average subsurface pressures evolution in the Gulf Coast region showing a geopressured zone (after [33, 72])

The definition previously presented corresponds to that used in petroleum geology, however this simple definition presents limitations as it includes situations where an overpressure can be explained by the topography, e.g.

in the case of an artesian aquifer [69]. Another definition, more appropriate to fluid flow perturbations and hydrodynamic phenomena [115], is proposed by Horseman *et al.* [69]. The overpressures term is restricted to the overpressures that can not been explained by the assumptions of a standard hydrogeological model. These standard assumptions [69] corresponds to a groundwater flow associated with negative hydraulic gradients arising from elevation differences between the recharge, at the surface, and the discharge area. It requires that the single phase flow can be described by the Darcy's law. It is also assumed that boundary conditions are constant with time and that a steady-state flow occurs at isothermal conditions. The last assumption is that the physical properties of the system, including the geometry, are time-independent and that solid and fluid volumes are conserved.
It appears that some standard conditions are particularly questionable in a low permeability shale and that such formations are especially subjected to present abnormal pressures. It mainly concerns the steady-state conditions requiring that boundary conditions are constant during enough time so that flow equilibrates in the shale, the validity of the Darcy's law to describe fluid flow or the constant physical properties since a hydromechanical behaviour is expected when mechanical stresses (e.g., loading, tectonic compression) act on the rock.

Most of the abnormal pressures consist in a hydrodynamic phenomenon which tends to recover equilibrium conditions after a perturbation in the hydraulic conditions of the system [115]. The abnormal pressure consequently tends to vanish with time, as a function of the hydraulic diffusivity of the low permeability rock or of the cap-rock. Abnormal pressure at equilibrium conditions can also be found and linked to fluid density or temperature contrasts or to dependence of flow parameters on system properties.

1.1.2 Causes of abnormal pressures

Three mechanisms causing abnormal fluid pressures can be identified [33], resulting from of changes in: i) rock pore volume; ii) the volume of interstitial fluids; and iii) fluid pressure and movement of fluids.
In the following paragraphs, the most common causes of generation of overpressures are presented.

Compaction disequilibrium

During basin burial, the sediments are subjected to a compaction because of the lithostatic pressure, i.e. the overlying sediments weight. This compaction tends to reduce the porosity (e.g., see Athy's relationship [8]) and, as a consequence, to expel the pore fluids. However, with a rapid compaction, e.g. with a high sedimentation rate and a low rock permeability, fluids keep trapped in the porosity and fluid pressure increases [24, 33, 69, 95].
Compaction disequilibrium is one of the most frequent cause of overpressures which can exceed tens of MPa. The example of abnormal pressures by compaction disequilibrium often cited is the case of the Gulf Coast region in United States [42] (Fig. 1.1).

Tectonic compression

A lateral tectonic compression can lead to the development of overpressures in shales by a pore volume reduction consecutively to compressive forces. This phenomenon also induces a squeezing of shale porewater which tends to induce overpressures in the core of anticlinal folds in the sealed underlying layers [33].
Tectonically induced overpressures are frequently found in orogenic belts. As an example, abnormally high formation pressures were encountered in the foothills of the Himalaya Mountains, associated with folding, on the Potwar Plateau [3] or in the Khaur Fields [78], in western Pakistan.

Visco-plastic behaviour of clays

The visco-plastic behaviour of argillaceous rocks consists in a time-dependent deformation at constant load. It can lead to a reduction of porosity and to the persistence of overpressures during large geological time scales [139]. In limestones and sandstones, this process results from pressure dissolution mechanism and can be quantified using stylolitic textures. In clay-rocks, macroscopic creep is the consequence of an aggregate deformation by sliding and rotation of grains [45].

Aquathermal effect

Overpressures induced by an aquathermal effect are linked to the 300 times higher thermal expansion of water during temperature changes compared with the rock thermal expansion [69, 92, 93, 94]. When sediment is heated, i.e. during burial or due to a geothermal gradient change, the porewater vol-

ume increases and, in a low permeability formation or because of a caprock, this water can not migrate, leading to the development of an overpressure.

Diagenetic effects

Mineralogical changes and dissolution - precipitation processes during diagenesis can be envisaged as a cause of overpressures [33, 146]. Illitization, i.e. the transformation of smectite clay to illite, occurs during burial at a temperature between 80 and 120 ℃ and releases an amount of water equal to one half of its volume [128]. In a low permeability formation, this water release can lead to overpressure generation.
The dissolution precipitation processes occurring during diagenesis can lead to a reduction of the pore volume, i.e. a clogging, and, consequently, to an increase of the fluid pressure.
These diagenetic effects on abnormal pressure are most likely a secondary cause [146], associated to the causes acting during burial, mainly compaction disequilibrium.

Organic matter maturation

During burial, with temperature and pressure increase, organic matter maturates to generate hydrocarbons by cracking. This reaction causes modifications in the formation pressures of the source rock by a coupled increase of porosity and of the fluids volume [33, 69]. An upward migration of hydrocarbon gases from lower to upper horizons can also result in overpressuring of upper horizons.
As an example, various basins in the Rocky Mountains region present overpressures identified to be generated by hydrocarbon generation in an organic-rich source rock, caused at present day and in the last few million years [142].

Density contrasts

The pore fluid heterogeneity in a sedimentary basin can lead to the development of abnormal pressure, without fluid movement [115]. The density contrasts can result from salinity differences or, to a greater degree, from differences in secondary fluid phases (oil and natural gases) contents between different rock regions.
Overpressures linked to density contrasts are reported for sand unit upwarded along a salt dome and containing water, oil and gas in the Louisiana Gulf Coast [42]. The phases repartition in the formation depends on their densities and leads to an overpressure generation in the upper part of the formation.

Osmotic processes

Among osmotic processes, chemical osmosis is the osmotic process most studied for its relation with formation pressures [97, 110, 116, 136]. Chemical osmosis, a fluid flow driven by a chemical potential gradient can be considered as a plausible cause of abnormal fluid pressures in clay-rich and highly compacted formations in presence of a chemical concentration gradient. This process was able to explain moderate overpressures or part of overpressures in Cretaceous sediments intercalations of sands and illitic clays in Dunbarton basin of South California [46, 97] and in the Callovo-Oxfordian clay-rock of the Paris basin [136].
The osmotic flow describing fluid flow under a temperature gradient, i.e. thermo-osmosis, can also be envisaged as a cause of abnormal pressures, as suggested by Rousseau-Gueutin [135].
The effect of chemical osmosis and thermo-osmosis on the fluid pressure can be linked to changes in the concentration or temperature gradient and in the osmotic flow coefficient. Details on the occurrence of these processes are addressed in the following section.

1.2 Hydrogeology of argillaceous formations

Hydrogeology of argillaceous formations is a recent section of the hydrogeological science, classically dedicated to the understanding and characterization of water, solutes and heat flows in aquifers. Shales are defined as aquicludes, which correspond to layers presenting a very low permeability and enable to give rise to any appreciable leakage, at least on small time scale [38].
Generally, the fluid flow in a sedimentary basin is parallel to the bedding plane in aquifers (horizontal) and normal to the bedding in low permeability formations (vertical flow). This vertical flow across the low permeability layer is called drainance and allows, associated with diffusion, chemical exchange between two aquifers separated by the low permeability formation. With the exception of the works of Bredehoeft and Neuzil [26, 25, 111, 112, 113, 114], the interest for the understanding of the hydrodynamic behaviour of argillaceous formations was mainly motivated by the studies on the confinement ability of clay-rocks for radioactive wastes storage.

The aim of the studies on confinement ability of clay-rocks is to assess that a contaminant stored in a clay-rock will not migrate out of this host-rock

during a determined time duration, so that the concentration of contaminant is at acceptable values out of host-rock. It thus requires the evaluation of mass transport through the clay-rock, considering diffusion and convection processes.
In the convection process, dissolved solutes are carried through the porous medium by the fluid displacement. The other way to transport solutes in a porous medium is diffusion. The expression combining the mass balance equation describing convection and the second Fick's law writes [38]:

$$div(D_e \nabla C - qC) = \omega \frac{\partial C}{\partial t} \tag{1.2}$$

where C is the solute concentration (mol L^{-1}), q the specific discharge (m s^{-1}) calculated using the Darcy's law, D_e is the effective diffusion coefficient (m^2 s^{-1}) and ω_c is the kinematic porosity.

In shales, because of the low permeability, diffusion is considered as the dominant mass transport process [32, 123] and convection is often neglected. However, a re-evaluation of the Darcy's law in clay-rocks is rarely considered, which can lead to an underestimation of the fluid movement. Indeed, the contribution of osmotic processes on the fluid flow has to be considered for a reliable description of the water movement in such rocks as demonstrated by theoretical developments on osmotic flows and experimental evidences [22, 27, 32, 50, 51, 58, 68, 79, 103, 110, 116, 136, 137]. These osmotic processes consist in fluid flows induced by driving forces different than the hydraulic one and therefore must be added to the Darcy's flow.
Let's now have a description of the hydrodynamic behaviour of argillaceous rocks, first, using a classical hydrogeological approach and, then, introducing coupled flows.

1.2.1 Hydraulic behaviour of clay-rocks

In a classic way, the fluid flow in porous media is described by the Darcy's law:

$$q = -\frac{k}{\eta}(\nabla P + \rho_f g \nabla z) \tag{1.3}$$

where q the specific discharge (m s^{-1}), k is the intrinsic permeability (m^2), η is the fluid dynamic viscosity (Pa s), P is the fluid pressure (Pa), ρ_f is the fluid density (kg m^{-3}), g is the acceleration due to gravity (m s^{-2}) and ∇z is (0,0,1) vector if the vertical axis z is directed upward.

The intrinsic permeability is the critical parameter to describe fluid flow in a porous medium. Natural shales found in sedimentary basins are highly compacted and present low permeability, making difficult their determination. Measurements methods of the intrinsic permeability were established to detect the low filtration velocities of such media. For in-situ measurements, the inversion of the pressure evolution after a pulse-test or a slug-test in a hydraulically isolated measurement chamber is the more reliable method for obtaining the hydraulic parameters. Analytical and numerical methods [26, 56, 111] are used to analyze the transient-state evolution to the formation steady-state. It is worth noting that the pore-pressure steady-state must be reached before performing the pulse-test for a correct analysis of the pressure recovery as a function of the imposed pressure gradient.
Intrinsic permeability as a function of porosity is reported in Fig. 1.2 for different compacted natural clay-rocks. A log-linear correlation between porosity and intrinsic permeability is often observed [69, 99, 114] and a mathematical relationship can be established. The Kozeny-Carman relation allows calculating the intrinsic permeability as a function of petrophysical parameters of the porous medium, i.e. the tortuosity and the specific surface area. Its expression for clay-rocks, using plane parallel pore geometry assumption writes [85, 122]:

$$k = \frac{b^2}{3F} \tag{1.4}$$

where b is the half pore-size (m) and F is the dimensionless formation factor, given by the Archie's law $F = \omega^{-m}$ [7] where ω id the total porosity and m is the cementation factor. The cementation factor value varies between 1.3 and 5.4 as a function of the rock [69]. For shales, its value is expected to be around 2 for deeply buried compacted sediments according to Ullman and Aller [149] and between 2.5 and 3.5 for smectite rich materials according to Revil *et al.* [129]. Here a cementation factor of 2.3 is obtained by fitting the permeability data as a function of porosity as represented in Fig. 1.2. This value is confirmed by the fit of the diffusion coefficient as a function of the porosity (Fig. 1.4).

Pressure evolution through time is calculated using the continuity equation, which describes a mass balance at the Representative Elementary Volume (REV):

$$\nabla(\rho_f\, q) + \frac{\partial(\rho_f \omega)}{\partial t} = 0 \tag{1.5}$$

In sedimentary basins argillaceous formations, the fluid is generally confined and the variations of fluid pressure induce a deformation of the solid skeleton as well as fluid density changes. A hydromechanical coupling and state

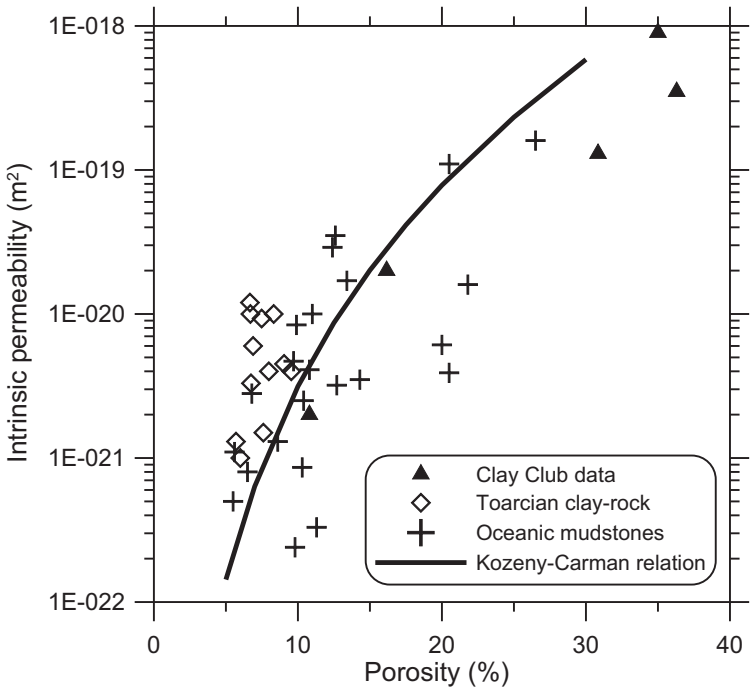

Figure 1.2: Data of intrinsic permeability and porosity for different shales: Toarcian Tournemire clay-rock [20]; oceanic mudstones collected at depths between 2 and 5 km in wells from North Sea, Gulf of Mexico and Caspian Sea [154]; clay-rocks from Clay Club Catalogue [19] including Paris basin Callovo-Oxfordian argillite, Mont Terri Opalinus clay, Zurcher weinland clay, Boom clay, Ypresian clay, Wakkanai formation and Spanish reference clay. Permeability evolution calculated with the Kozeny-Carman relation ($m = 2.3$) is also represented.

.

equations for fluid and solid are introduced to express the second term of Eq.(1.5) as pressure.
This development is generally made in the framework of the poroelasticity theory by e.g. de Marsily [38], leading to the equation:

$$\nabla(\rho_f\, q) = -\frac{S_s}{g}\frac{\partial P}{\partial t} \tag{1.6}$$

where S_s is the specific storage coefficient (m^{-1}), which considers the porous medium deformation and the compressibility of the fluid and solid grains. It writes:

$$S_s = \rho_f\, g\, \omega \left(\beta_l - \beta_s + \frac{\alpha}{\omega}\right) \tag{1.7}$$

where, β_l, β_s and α are the compressibilities (Pa^{-1}) of the fluid, the solid grains and the porous medium, respectively.
The specific storage coefficient can be calculated as a function of porosity, considering the expression of the porous medium compressibility in its full expression and the fact that the Biot coefficient, equal to 1 in standard case, becomes lower than 1 for clay-rocks and varies with porosity [36]. These considerations modify Eq.(1.7) and lead to [58]:

$$S_s = \rho_f\, g\, \omega \left(\beta_l - \beta_s + \frac{\gamma_B}{\omega}\right) \frac{3(1-2\nu)}{E_Y} \tag{1.8}$$

where, γ_B is the dimensionless Biot coefficient, related to the porosity by the expression $\gamma_B = 1 - (1-\omega)^{3.8}$ [55, 86], ν is the dimensionless Poisson coefficient and E_Y is the Young modulus (Pa) which can be expressed as a function of the porosity by the relation $E_Y = E_Y^0(1-\omega)^n$ [108]. E_Y^0 and n were determined [55] equal to 10 GPa and 8, respectively, from available measurements of Young modulus for compacted clay-rocks [14, 54, 108].

Other sources of pressure variation through time can be introduced in the right hand side of the continuity, or pressure-diffusion, equation (1.5). These sources may concern variations of the total stress in the porous medium, variations of temperature or other term source like an input or a withdrawal of fluid.

1.2.2 Coupled-flows in clay-rocks

Many experiments evidence that the Darcy's flow is not enough to describe fluid movement in clay-rich media and that fluid flow can also be induced by gradients other than the hydraulic one [76, 69, 103]. In soil science

and petroleum engineering these experiments mainly consisted in chemical osmosis experiments performed at laboratory, on purified or remoulded material (e.g., [27, 80, 81, 83, 82, 91, 103, 155]). The demonstration of the occurrence of chemical osmotic flow at the formation scale in clay-rocks is recent [116] and proved the need of reevaluating the Darcy's law to describe fluid flow in such rocks.

The origin of the coupled-flows lies on the electrochemical interactions occurring at the pore scale between the charged surface of clay minerals and the water and electrolytes. Because of isomorphic substitutions of cations by other having a lower valence, in tetrahedral and octahedral layers, clay minerals present a surface charge, negative at natural pH, which induces a non-uniform distribution of cations, anions and water molecules. The solutes distribution in the pore space results from the combination of the attraction by the charged surface and their diffusion towards the pore center, where solute concentration is lower [103]. The ion distribution, as well as the electrical potential, can be described using double layer or triple layer electrical models [103, 151]. These models allow considering a compact layer at the surface vicinity presenting high solute concentration strongly adsorbed to the surface and, farest from the surface, a diffuse layer presenting a progressive decrease of the solute concentration.
Owing to these non-homogeneities in ion distribution, restrictions on ion movement caused by electrostatic attraction and repulsion and, because of the temperature dependence of these interactions, flows driven by potential gradients non-usually associated to these flows may be observed.

The Onsager's matrix (Table 1.1) summarizes the flows which can develop under the different potential gradients. The fluxes related to their natural gradient, the diagonal flows are reported in, as well as the flows occurring under the other potential gradients, i.e. the non-conjugated flows.

Two approaches can be considered for the characterization of the coupling coefficients relating a flux to a driving force: the phenomenological approach and the mechanistic one.

The phenomenological approach is based on the principles of the irreversible thermodynamics, based on the notion of entropy, [76] and assumes a linear relation between the flows J_i and the gradients X_i, as follows [69]:

$$J_i = -\sum_{j=1}^{n} L_{ij}\, X_j \qquad\qquad n = 1, 2, 3 \ldots n \tag{1.9}$$

Flux	Gradients			
	Hydraulic head	Electrical	Chemical concentration	Temperature
Fluid	Darcy	Electro-osmosis	Chemical osmosis	Thermo-osmosis
Current	Electrofiltration	Ohm	Membrane potential	Thermo-electricity
Ion	Ultrafiltration	Electrophoresis	Fick	Soret effect
Heat	Thermal filtration	Peltier effect	Dufour effect	Fourier

Table 1.1: Onsager's matrix with coupled-flows terminology [38, 103, 120, 121]

where the subscripts i and j correspond to the various kinds of flows and gradients, respectively and L_{ij} are the phenomenological coefficients. The Onsager reciprocal relations [120, 121] assume that the coefficients are related so that $L_{ij} = L_{ji}$.
This approach leads to the following matrix which describes both flows to the driving forces by their relating coupling coefficients [22, 131]:

$$\begin{pmatrix} q \\ J_e \\ J_i \\ H \end{pmatrix} = \begin{pmatrix} L_{11} & L_{12} & L_{13} & L_{14} \\ L_{21} & L_{22} & L_{23} & L_{24} \\ L_{31} & L_{32} & L_{33} & L_{34} \\ L_{41} & L_{42} & L_{43} & L_{44} \end{pmatrix} \cdot \begin{pmatrix} \nabla P \\ \nabla \varphi \\ \nabla \mu_s \\ \nabla T/T_0 \end{pmatrix} \tag{1.10}$$

where q, J_e, J_i and H are the fluxes of fluid, current, ions and heat, respectively, and ∇P, $\nabla \varphi$, $\nabla \mu_s$ and $\nabla T/T_0$ are, respectively, the gradients of pressure, electrical potential, solute chemical potential and temperature. Note that the chemical potential gradient if often expressed as an osmotic pressure gradient $\nabla \Pi$.
The coefficients of the coupled flow matrix can then be obtained during experiments, i.e. measuring the flow associated to a force gradient.

The mechanistic approach lies on the resolution of the flow equations at the pore scale [22, 76], i.e. Navier-Stockes's equation for fluid flow and Nernst-Planck's equation for the solutes movement, including the different forcing acting in the porous medium. These microscopic equations are then homogenized for obtaining the coupling coefficients at the adequate macroscopic scale for hydrogeological application, i.e. at the Representative Elementary Volume (REV).

The mechanistic method provides analytical expressions for the coupling coefficients and use average petrophysical, electrochemical or magnetic properties of the porous medium. Such a method was developed by, e.g. Coelho *et al.* [34], Gupta *et al.* [63, 64] Moyne and Murad [107] or Revil *et al.* [130, 131].

A special attention is paid, in the manuscript, to the osmotic processes, i.e. the fluid flows induced by chemical concentration, temperature and electrical gradients, in natural compacted clay-rocks. When chemical osmosis, thermo-osmosis and electro-osmosis are considered together with the Darcy's flow, the fluid flow equation (Eq.1.3) is extended and writes:

$$q = -\frac{k}{\eta}(\nabla P + \rho_f g \nabla z) + \varepsilon \frac{k}{\eta} \nabla \Pi - k_T \nabla T + \beta \nabla \varphi \tag{1.11}$$

where ε is the chemo-osmotic efficieny (dimensionless), k_T is the thermo-osmotic permeability ($m^2\ s^{-1}\ K^{-1}$) and β is electro-osmotic conductivity ($m^2\ s^{-1}\ V^{-1}$). The osmotic flows are detailed hereafter.

Chemical osmosis

Chemical osmosis is the fluid flow across a material exhibiting a membrane behaviour, induced by a difference of chemical potential. A membrane is a material which restring ionic species transport but not the movement of neutral species like water. A ideal membrane impedes totally the ionic transport, while in a non-ideal membrane (e.g. clays or biological membranes) only a partial restriction of the ionic transport is observed. Negative surface charges of clay minerals induce a partial exclusion of anions in the clay porosity, i.e. anionic exclusion. It consequently results in a partial restriction of ionic transport between two reservoirs separated by such a material. Indeed, for electroneutrality requirements in the two reservoirs, cations and anions must be transported together and restrictions in the non-ideal membrane have an influence on both ions.
Differences in concentration between two reservoirs also induce a difference in osmotic pressure [81] which leads to a fluid movement across the membrane and is interpreted as an osmotic flow. The osmotic pressure of a fluid writes:

$$\Pi = -\frac{RT}{\Omega_{water}} ln\, a_w \tag{1.12}$$

where Π is the osmotic pressure (Pa), R is the gas constant (8.32×10^{-3} m^3 Pa K^{-1} mol^{-1}), T is the temperature (K), Ω_{water} is the molar volume of water

(L mol^{-1}) and a_w is the water activity in solution. The osmotic pressure can also be approximated by the Van't Hoff relationship, which hold for solutions with concentrations lower than 1 mol L^{-1} [46]:

$$\Pi = \nu RTC_f \tag{1.13}$$

where ν is the number of dissociated ions in solutions and C_f is the solute concentration (mol L^{-1}).
The ability of a membrane to generate a fluid flow under a concentration gradient is described by the chemo-osmotic efficiency, or reflection coefficient. Most generally, the chemo-osmotic efficiency varies between 0 and 1 and its value equals 0 when the material does not present a membrane behaviour. Osmotic efficiency value is 1 for an ideal membrane, which totally impedes the solute transport. It is worth noting that the chemo-osmotic efficiency is strongly dependent on concentration and pore-size. The higher osmotic efficiency values are observed in very compacted materials filled by fresh water.

Experiments for chemical osmosis characterization in argillaceous materials were performed at the sample scale and the formation scale. Materials studied during laboratory experiments are remoulded or synthetic clays and bentonites [12, 47, 81, 82, 83, 91, 96, 119] or non-remoulded natural clay-rocks [32, 68, 136, 155]. These experiments were generally performed on centimeter-size samples. Most chemical osmosis experiments were carried on sampled, but some experiments were made in-situ, in equipped boreholes [51, 116, 118, 137].
A very large range of osmotic efficiency was measured during these experiments on argillaceous materials, from 0.002 [12] to 0.98 [81]. A dependence of the osmotic efficiency on the experimental conditions (clay, compaction state, concentration and composition of the test solution) is noted. A good agreement between the osmotic efficiency and the product of the half pore-size and the squared root of the concentration is observed through the Bresler [27]'s curve (Fig. 1.3). This curve corresponds to a fit of various osmotic efficiency measurements on bentonites, kaolinite, illite and loam. The Bresler's curve is often used for osmotic efficiency prediction in argillaceous rocks. A synthesis of the osmotic efficiencies measured on natural clay-rocks is available in Fig. 4.2. These available measurements were made on Oligocene Boom clay [51], Cretaceous Pierre shale [1, 50, 116], Cretaceous Bearpaw formation [32], Jurassic Opalinus clay [68], Paris basin Callovo-Oxfordian (COx) formation [136, 137] and different non localized shales [1].
Studies of chemical osmosis on natural clays were dedicated to the interpretation of abnormal hydraulic pressures in shale layers of sedimentary basins

or to the safety assessment of shales as natural barriers of radioactive waste repositories.

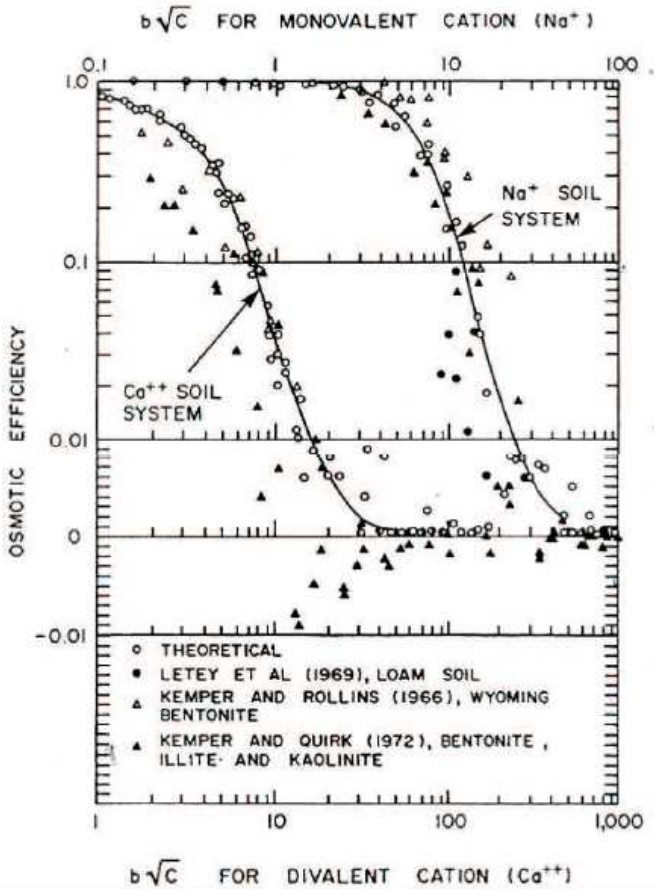

Figure 1.3: Bresler [27]'s curve relating the osmotic efficiency coefficient of argillaceous materials to the half pore-size ($\AA$) and the solution concentration. Experimental data come from [82, 83, 91].

.

Thermo-osmosis

Thermo-osmosis is a fluid flow driven by a temperature gradient. Several warnings were addressed [31, 141] on the possible effect of thermo-osmosis on modifying the overall fluid fluid in argillaceous rocks and, in particular, in exothermic nuclear wastes repository conditions. However, this osmotic process is poorly characterized as very few experiments on argillaceous materials are available in the literature [43, 65, 133, 144, 145, 156] and no one, so far,

on natural and undisturbed clay-rock. A reliable model for characterizing the thermo-osmotic permeability of an argillaceous material also misses. The few experiments on argillaceous materials give a thermo-osmotic ranging between 10^{-14} and 10^{-10} m^2 K^{-1} s^{-1}.

Electro-osmosis

Electro-osmosis describes the flow of fluid due to an electrical potential gradient [34, 64, 132]. When an electrical field is applied to an electrolyte, the cations migrate to the cathode and the anions to the anode. During their movements, water molecules are dragged by the ions because of a viscous process [61]. Cations are the dominant charged species in the porosity of a clay material and a flux of water is observed towards the cathode.
Electro-osmosis has practical applications in clay de-watering for civil engineering purposes or for soils remediation. However, in natural systems, the macroscopic current density J_e is considered null [22, 131]. This hypothesis allows writing the electrical potential gradient as a function of the other gradients and coupling coefficients:

$$J_e = L_{21}\nabla P + L_{22}\nabla\varphi + L_{23}\nabla\mu_s + L_{24}\nabla T/T_0 = 0 \tag{1.14}$$

$$\nabla\varphi = -\frac{L_{21}}{L_{22}}\nabla P - \frac{L_{23}}{L_{22}}\nabla\mu_s - \frac{L_{24}}{L_{22}}\nabla T/T_0 \tag{1.15}$$

The introduction of this electrical potential gradient expression in the other flow expressions (Eq.1.10) leads to an implicit integration of electro-osmosis in the flow coefficients related to the pressure, chemical potential and temperature gradients [22, 131].

1.2.3 Fick's diffusion in clay-rocks

Diffusion is recognized as the main process controlling mass transport in clay-rocks and its expression is given in Eq.(1.2). It consists in the diffusion of chemical species in the water filled space of a porous medium along the network of pore channels. The irregularity of this network with endless pores and solute unaccessible pores makes this diffusion slower than that occurring in the absence of the rock framework. The porosity, the constrictivity and the tortuosity of the porous medium relate the effective diffusion coefficient of a solute in a porous medium to its diffusion in free water. This relationship can be written [69, 141]:

$$D_e = \omega\frac{\chi}{\tau^2}D_0, \tag{1.16}$$

or

$$D_e = \frac{D_0}{F}, \tag{1.17}$$

where, χ and τ are the dimensionless constrictivity and tortuosity of the porous medium, respectively, D_0 is the molecular diffusion coefficient of the considered solute in water ($m^2\ s^{-1}$) and F is the formation factor.
The effective diffusion coefficient value for different argillaceous formations is represented in Fig. 1.4 as a function of the porosity. An approximative value of the effective diffusion coefficient can be provided by calculating D_e using Eq.(1.17) and the cementation factor m of 2.3 obtained by fitting the intrinsic permeability values in Fig. 1.2.

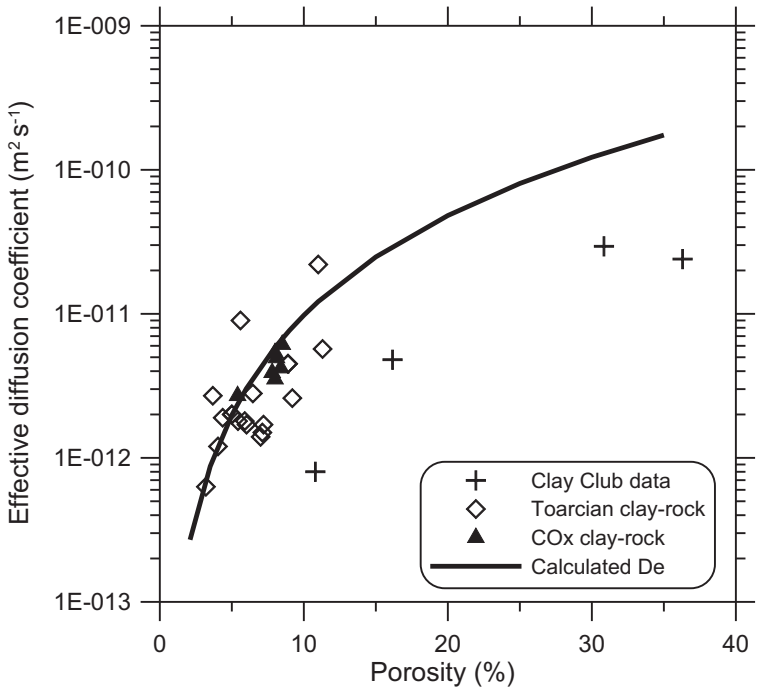

Figure 1.4: Data of effective diffusion coefficient and porosity for different shales: Toarcian Tournemire clay-rock [15]; Paris basin Callovo-Oxfordian argillite [40]; clay-rocks from Clay Club Catalogue [19] including Mont Terri Opalinus clay, Zurcher weinland clay, Boom clay and Spanish reference clay. D_e evolution calculated with the Eq.(1.17) is also represented, using $m = 2.3$.

.

1.3 Geological and hydrogeological settings of the Toarcian/Domerian argillaceous formation at Tournemire

1.3.1 Geological context

The Toarcian/Domerian argillaceous formation is studied in the IRSN underground research laboratory (URL) at Tournemire (Aveyron, France). The URL facility (Fig. 1.5) consists in a century-old tunnel giving a direct access to a clay-rock of upper Toarcian age. More recent galleries were excavated from the tunnel and hundreds of boreholes drilled from the tunnel and the galleries.

At Tournemire [30], the highly-compacted Toarcian/Domerian argillaceous formation is 250 m thick and is sub-horizontal with a bedding around 4 °[30]. 4 sublevels can be distinguished in (Fig. 1.5).
The Domerian is 40 m thick and composed of shales and marls with lateral facies variations.
The lower Toarcian is 25 m thick and composed of organic matter (around 10 %) rich marls. This level is also called "schistes cartons" and considered as the source rock for hydrocarbons expelled in the past.
The intermediate Toarcian is composed of 20 m thick shales and marls with little carbonates intercalations and carbonated nodules.
The upper Toarcian represents the thickest level of the argillaceous formation and is composed by shales with some carbonated nodules. In its upper part, intercalation of carbonates-rich layers are also observed.

The Mesozoic formations sandwiched between the argillaceous formation and the red permian sandstones are, from the older to the younger: the 200 m thick Hettangian formation, composed of dolomitic limestones and dolostones; the Sinemurian, made with limestones and dolostones and is 70 m thick; and the 45 m thick Carixian limestones which presents an enrichment in clays in its upper part.
There are about 250 m of limestones and dolostones between the top of the Toarcian and the plateau groundlevel. The transition between the Toarcian and the Aalenian is progressive: the lower part is composed by clay-rich nodulous limestones and the limestones being more massive at the top of the Aalenian. Aalenian layer is 60 m thick at Tournemire. Next, the 140 m thick Bajocian formation is observed and composed of massive limestones and dolostones. The Bathonian is a massive and thick formation, composed

of limestones at its basis and dolostones in its upper part. This formation is eroded and forms the groundsurface of the Causse plateau.
The argillaceous is therefore sandwiched between two karstified limestones formations: the Carixian and the Aalenian. The 250 m of sediments above the argillaceous formation ensure the formation to be still compacted (vertical stress of about 4 MPa at the tunnel level in the upper Toarcian [30]).

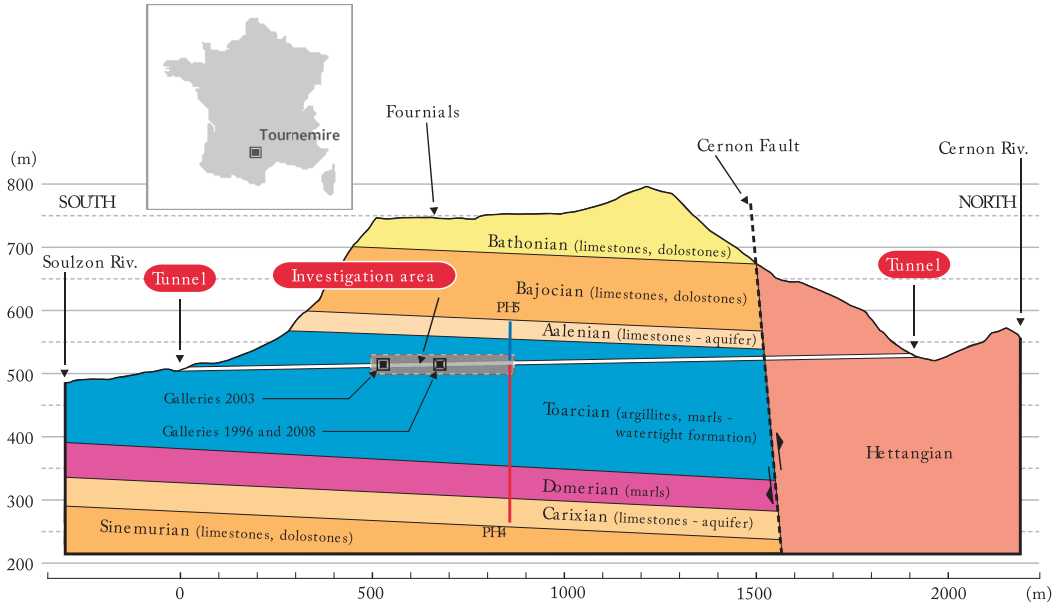

Figure 1.5: Geological cross section at the Tournemire URL [30].

.

The Tournemire stratigraphic series forms part of the Permo-Mesozoic Grands Causses basin and is related to the Tethys, a paleo-ocean axed on the East-West direction which widest extension occurs during Mesozoic. Stratigraphic record indicates an evolution from a continental depositional environment during the Permian towards a marine environment during the Jurassic [30].
The geological map (Fig. 1.6) shows the extension of the North-South Grands Causses basin and its delimitation by the hercynian crystalline and metamorphic regions.
Basin filling starts with transgressive epicontinental episodes during the Triassic and Sinemurian epochs. Sediments corresponds to a shallow sea and lagunar depositional environments [134]. During Carixian the sea became deeper and an argillaceous sedimentation is recorded during Domerian and Toarcian. A calcareous sedimentation is then observed from the Aalenian

to the Portlandian [134], at the end of the Jurassic with the regression of the Tethys sea. Basin evolution during the Jurassic is related to a tectonic in extension [30]. The Grands Causses basin evolved next under continental conditions from the lower Cretaceous [29, 30, 140]. An erosion of 1300 ± 400 m during the lower Cretaceous was deduced by thermal history reconstruction [127] and explain well the overconsolidation of the clayey formation. A first karstification episode of the calcareous formations is assumed to have occurred at this age [140].
A North-South compression is observed since the upper Cretaceous with the first stages of the pyrenean orogenesis. The major pyrenean compression took place during the Eocene with a N30°E compression. During this tectonic event, hercynian and syn-sedimentary mesozoic structures are reactivated in inverse movements and North-South thrust faults [30]. At the Tournemire URL, it concerns the regional Cernon fault, crossed in the northern part of the tunnel, and different families of calcified fractures in the clay-rock formations. This event led to the massif exhumation and karstification of limestones and dolostones.
The pyrenean compression was followed by a regional extension tectonic during the Oligo-Miocene resulting in the elevation of the Massif Central and the Cévennes regions compared to the Grands Causses, without faults activation in the Causses.
The most important karstification episode occurred during the Neogene and the valley incision occurred mainly during early and middle Miocene [2, 140].

1.3.2 Hydrogeological context

The aquiclude formations of the Toarcian and Domerian are surrounded by two karstic aquifers (Fig. 1.5).
The lower aquifer includes the Hettangian and Carixian formations. It is a regional aquifer which recharge occurs 2 km at the South of Tournemire. Because of the North-East slight bedding of the series, water movement is directed from the South-West to the North-East. This aquifer presents an artesian behaviour at the Tournemire URL location under the argillaceous series [30].
The upper aquifer is a local one, which is recharged by the local precipitations on the Causse plateau. The Aalenian, Bathonian and Bajocian formations compose this aquifer.
Note that the upper aquifer is connected to the lower aquifer by the transmissive Cernon regional fault [30], as well as the role of tectonic discontinuities in the water movement in these karstic aquifers.

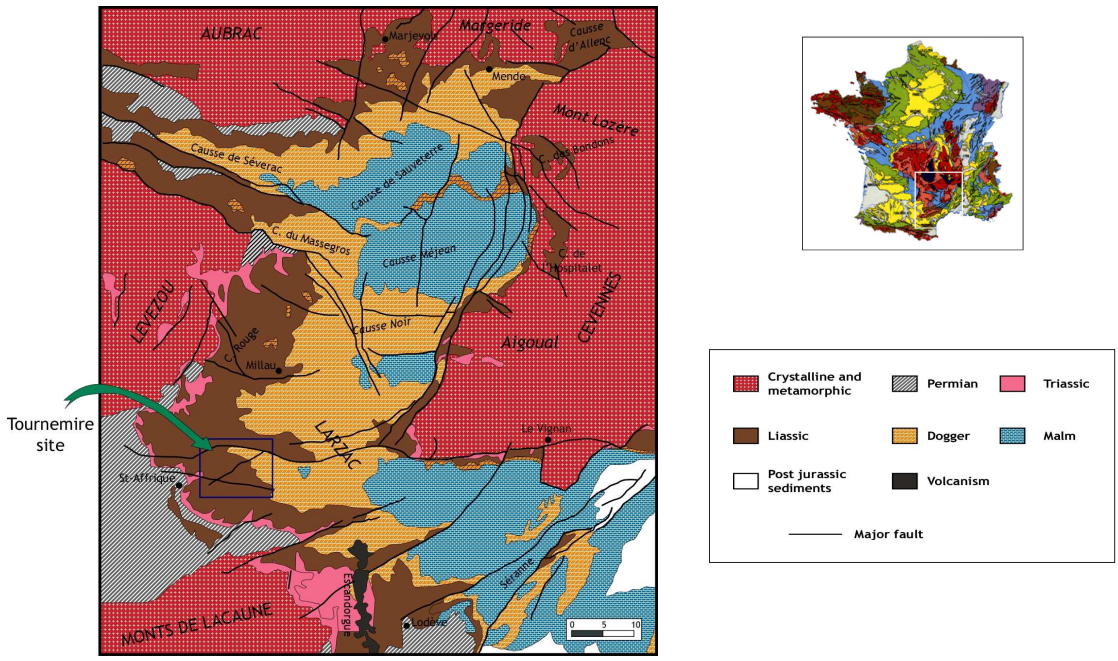

Figure 1.6: Geological map of the Grands Causses basin.

.

The Domerian and Toarcian compacted argillaceous formations exhibit very low hydraulic conductivities, diffusion coefficients and water contents. The Tournemire shale presents an intrinsic permeability ranging in between 10^{-22} and 10^{-20} m^2. Indeed, the measured range spreads on 6 orders of magnitude [20, 21, 123], between 10^{-22} and 10^{-16} m^2, but these variations are mainly related on the difficulties in performing fluid flow measurements in such impervious materials. Measured permeability being very sensitive to the sample damages during drilling and to the experimental method and conditions, e.g. duration of the test, transient or steady-state initial pressure conditions, confined or unconfined sample, preservation of the sample. Values considered as representative of the unperturbed rock were obtained on samples from CD and ID180 boreholes [20, 21], maintained under mechanical confinement. Intrinsic permeabilities ranging between 1 $\times$ 10^{-21} and 9.3 $\times$ 10^{-21} m^2 were measured during pulse-tests, by inversion of the pressure recovering in a measurement chamber after inducing a pressure increase or decrease [26, 56, 111]. An in situ measurement in unperturbed conditions [17] with an adequate borehole device using a long-term permanent probe indicated an intrinsic permeability ranging between 6 $\times$ 10^{-22} and 2 $\times$ 10^{-21} m^2.

The effective diffusion coefficients of the Tournemire clay-rock were measured for natural (deuterium, helium, chloride, bromide) and artificial (tritium, iodide) tracers [15, 105, 124, 138, 153]. Water effective diffusion coefficient ranges in between 4×10^{-12} and $1.3\ 10^{-11}$ $m^2\ s^{-1}$ [138, 105, 15]. For anions diffusion (chloride or bromide), the effective diffusion coefficient ranges in between 6×10^{-13} and 9×10^{-12} $m^2\ s^{-1}$ [15]. For iodide the effective diffusion coefficient ranges between 2 and 7×10^{-12} $m^2\ s^{-1}$ [153]. It is worth noting that an anisotropy related to the rock orientation is observed on the diffusion coefficient value, the water diffusion coefficient being three times higher when determined parallel to the bedding compared with a measurement normal to the bedding [21, 105].

The porosity describes the open, fluid-filled voids in a rock. In a compacted clay-rock, where non-negligible proportions of volume of water and solutes content are adsorbed at the solid surface, some part of the total void space is not available to solute or water transfer [69, 125].
For flow and transport considerations, the total physical porosity, the kinematic porosity and the anions accessible porosity are of special interest. The total porosity corresponds to the ratio of the pore volume to the total volume and, for Tournemire, ranges in between 6 and 12 % for the upper and intermediate Toarcian and the Domerian layers and in between 3 and 5 % for the lower Toarcian.
The anions accessible porosity corresponds to the volume available for the anions transport, i.e. the pore volume out of the solid surface induced electrical field influence and a part of the diffuse layer [126]. This porosity is lower than the total porosity and, for chloride and bromide, ranges in between 3 and 9 % [15].
The kinematic porosity corresponds to the pore space volume available for fluid displacement, excluding the water adsorbed at the solid surface [38]. Kinematic porosity value is between the total porosity and the anions accessible porosity values.

The profiles of natural tracers (chloride, water isotopes, helium) were established across the Tournemire argillaceous formation [15, 124, 138]. They provide useful information on the transport processes at the formation scale. The profiles (Fig. 1.7) indicate a dilution of the solutes in the argillaceous porewater and the porewater itself by the fresher water from the surrounding aquifers.
Using the assumption of a transport occurring entirely by diffusion and considering sea water as the initial porewater, the water isotopes profile (Fig. 1.7.b) is obtained after 15 My [138] and the chloride profile (Fig.

1.7.a) after 80 My of diffusion [15]. Such a difference can be explained by a possible equilibration of the water isotopes with another fluid than sea water during the geological history and by a second episode of water diffusion from this intermediate state.

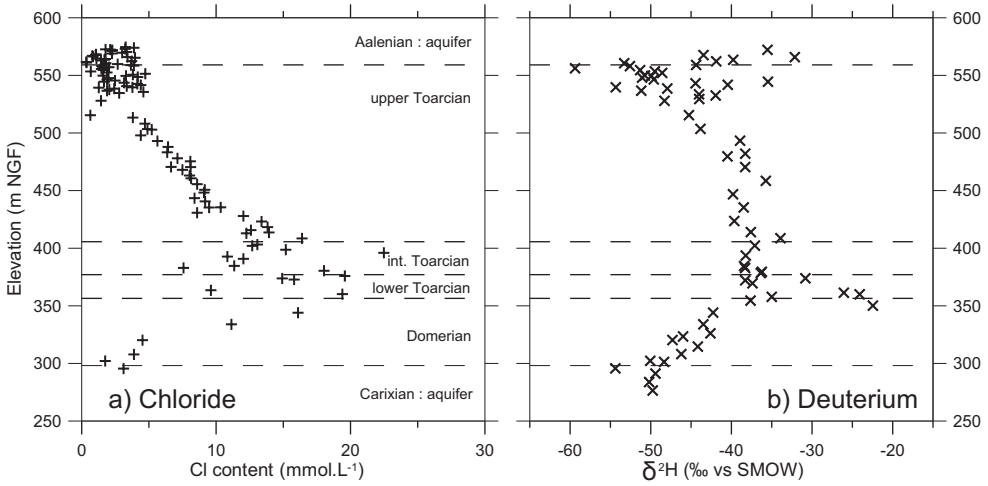

Figure 1.7: Profiles of natural tracers across the Tournemire argillaceous formation: a) Chloride [15, 124]; b) Deuterium [15, 138].

.

The Tournemire formation is affected by a tectonic subvertical fractures network organized in relay (Fig. 1.8). These fractures are sealed and water can only be found in the geodic cavities in the echelon faults zone. The equivalent hydraulic conductivity in these fractures can reach 10^{-10} m s^{-1}, i.e. 4 orders of magnitude higher than the rock matrix conductivity, and the water sampled in these geodic cavities present an apparent ^{14}C age of about 20000 $\pm$ 5000 yr [13]. However, the natural tracers profiles (Fig. 1.7) present a regular evolution and do not seem to indicate an actual effect of fractures on the transport at the formation scale [15, 123, 138]. A possible moderate effect of fractures on ionic transport in the lower and intermediate Toarcian is suspected by the dispersion of tracers content in these levels (Fig. 1.7). The effect on the transfers in the argillaceous formation is not precisely constrained but appears limited, most likely due to the non-connection of the different fractures. Indeed, Neuzil [114] stated that most argillaceous formations present scale independent permeability, unless if affected by connected discontinuities.

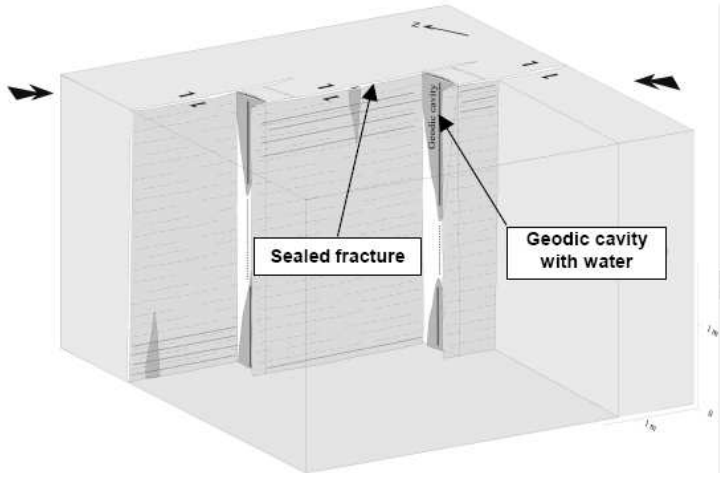

Figure 1.8: Schematic view of the sub-vertical fracture network organized in relay [13].

.

Part III

Contribution to the hydrogeochemical characterization of the argillaceous formation at Tournemire

Chapter 2

Hydraulic head and temperature profiles

2.1 Introduction

The aim of this chapter is to establish the profiles of hydraulic head and temperature across the Tournemire clayrock. The hydraulic head (or pressure) profile previously established [20, 21] needed an actualization since the conditions for non-perturbed pressure measurements in Tournemire clayrock were better constrained [17] and since the long term hydromechanical influence of the tunnel was better understood [98]. The pressure profile actualization was also motivated by the fact that the only one long-term and non-affected by experimental artefact pressure measurement out of the tunnel influence (in ID180 borehole) presented a hydraulic head value higher than the corresponding hydrostatic head for the same elevation. The profile establishment is then emphasized to the investigation of the occurrence of an overpressure in the Tournemire shale. It required the drilling of two boreholes crossing the whole argillaceous formation (PH4 and PH5 boreholes) and their equipment by a completion allowing pressure and temperature measurements and a data selection of pressure measurements representative of the formation conditions. The data selection is a crucial task because pressure measurements representative of the formation are difficult to obtain. Indeed, pressure measurements are easily perturbed and the pressure equilibrium achievement can last years because of the low rock hydraulic conductivity.
The temperature profile is established in the second part of the chapter. Its main interest here is that temperature is the force gradient of thermo-osmosis coupled-flow and this profile will be useful for determining the thermo-osmotic contribution on flow and pressure regimes in the Tournemire clay

formation. It is worth noting that it is the first temperature profile established at Tournemire so far.

2.2 Hydraulic head profile

The previous hydraulic head profile across the Tournemire argillaceous formation [20, 21, 123] did not indicate the presence of abnormal pressures in the formation. However some of these pressure measurements were affected by the effect of the Tournemire URL access tunnel [21, 98]. Indeed, the 125 years old tunnel has induced a depression explained by a coupled effect of a hydromechanical effect and a suction subsequent to its natural ventilation. Both phenomena are assumed to have considerably lower the pore pressure. The extension of this pore pressure perturbation (named the excavation hydraulically disturbed zone) was observed on about 40 meters around the tunnel [98]. Other pore pressure measurements were most likely not representative of the in situ conditions as measurements were made at transient state [17, 20, 21]. Because of the very low hydraulic conductivity of the formation, the steady state is only reached after a very long time after the perturbation induced by the drilling. Only one measurement was assumed in equilibrium, in borehole ID180 where the pressure acquisition lasted 7 months and the pressure reached an equilibrium value [18, 20, 21]. The aim of this section is to establish a profile of the hydraulic head across the Tournemire clayrock, out of the tunnel influence and representative of the in situ pore pressure. For this aim, a review of pressure measurements on various equipped borehole was performed. At last the possibility of an overpressure in the Toarcian/Domerian clayrock is investigated by combining these measurements on a profile.

2.2.1 Review of the pore pressure measurements

ID180 borehole

The ID180 borehole was drilled, in 1994, vertically and downward from the tunnel of the Tournemire URL (at the metric point 675.7 from the South entrance of the tunnel). It is 160.52 m deep and crosses part of the upper Toarcian, the whole intermediate Toarcian and reaches the lower Toarcian [18]. It was drilled for investigations on fluid transfer and mass transport in the formation. In situ measurements for fluid transfer characterization was made in two steps by the ANTEA company by using a multi-packer device classically used in oil exploration. In a first step, six shut-in chambers were isolated and the hydraulic conductivity was obtained at different levels in

the formation by interpretation of the pulse-tests. However, the pressures monitored before and after these tests were not stabilized and not representative of the formation pressure because of the low hydraulic conductivity of the rock and the short duration time of the stabilization phase (from 1 to 2 days) [18].
In the second step of the experiments on the ID180 borehole, a 78 m height chamber was isolated at the bottom of the borehole and a long term monitoring of pressure measurement was performed from the 07/09/1996 to the 26/03/1997. The pressure evolution (Fig. 2.1) indicated a rapid equilibrium reached two months after the completion installation. After the packer deflating in November 1996 during some hours for works in the URL, it was re-inflated and the pressure stabilized in the interval at the same pressure (hydraulic head of 533.4 m NGF) even more rapidly, in one month. Despite lasting one or two months, this pressure stabilization was considered as rapid for the Tournemire clay-rock (see for comparison the pressure evolution in PH4 borehole on Fig. 2.2 which last years). This result suggests a water inflow by a natural fracture with a much higher transmissivity than the rock matrix, like the zone of calcite-filled microfractures observed at 383 +/- 1m NGF in the intermediate Toarcian or more likely in the fault zone identified at 370 +/-1 m NGF in the lower Toarcian [18]. Consequently the elevation range corresponding to this measured head can be limited by geological evidences to a part of the interval (369.5 to 412.8 m NGF, versus 356.4 to 438.5 m NGF for the whole measurement chamber).

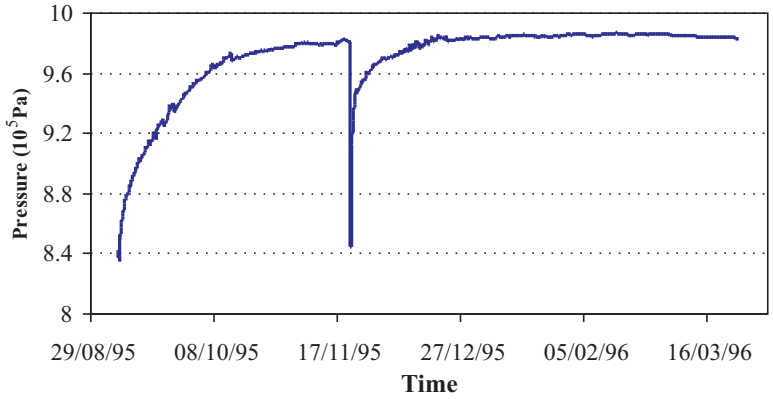

Figure 2.1: Absolute pressure evolution in ID180 borehole [21, 18].

PH4 and PH5 boreholes

The aims of the PH4 and PH5 boreholes were the characterization of the transport and flow processes in the Tournemire formation at the formation scale. It mainly included the obtention of profiles of the natural tracers and their transport parameters including the accessible porosity and effective diffusion coefficient, the hydraulic head out of the tunnel influence, the petrophysical parameters and the mineralogy. Both boreholes were vertically air-drilled from the tunnel at metric point 840. PH4 borehole was drilled downward to a depth of 250 m, during the Autumn of 2006. It crosses part of the upper Toarcian, the intermediate and lower Toarcian, the Domerian and reaches the Carixian aquifer. PH5 borehole was drilled in October 2008 upward on 50.1 m in the upper Toarcian and the Aalenian aquifer.
The PH4 borehole was equipped by the HydroInvest company with a Westbay completion individualizing 6 shut-in chambers for the pressure and temperature measurement [71]. These chambers are 0.6 m length, except the chamber in the Carixian aquifer (4.8 m length, with the pressure sensor located in the interval at 297.6 m NGF) and a 59.1 m length chamber in the upper Toarcian (sensor at 432.9 m NGF). The pressure evolution in the 6 PH4 chambers since the completion installation, in February of 2007, is shown in Fig. 2.2. The pressures evolve slightly to an equilibrium value which seems most likely reached for only 3 probes after 3 years of evolution: the two probes located in the Domerian plus that situated in aquifer layers. It is worth noting that the 3 chambers located in the upper Toarcian (sensors at 432.9, 434.4 and 478.9 m NGF) present low pressure values attributed to an air trapping during drilling. The Westbay completion does not present hydraulic lines allowing a resaturation of the perturbed chambers. One only can act on the measurement chambers by inflating or deflating of the completion packers and this operation was not enough for pressure correction. Thus, equilibrium pressure values at only three elevations were obtained from the PH4 borehole, in the lower Toarcian, in the Domerian and in the Carixian aquifer.
The PH5 borehole was equipped by the SolExperts company by a multi-packer system completion allowing the pressure measurement in a 0.35 m length chamber in the upper part of the upper Toarcian and in a 14.9 m length chamber in the Aalenian aquifer [101]. The pressure evolution since the completion installation in November 2008 is presented in Fig. 2.3. The chamber in the upper Toarcian is installed at only 16 m from the tunnel and the measured pressure is under the tunnel influence. The pressure measurement in the Aalenian gives the hydraulic head in the upper aquifer.

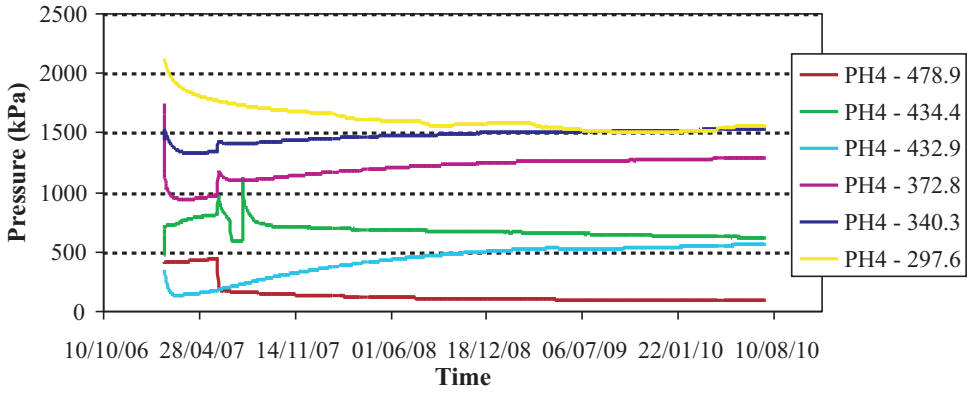

Figure 2.2: Absolute pressure evolution in PH4 borehole with the elevation of the intervals pressure sensor given in the legend.

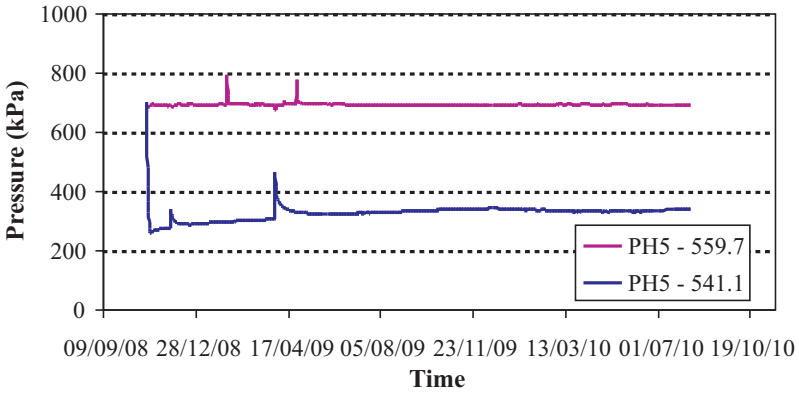

Figure 2.3: Absolute pressure evolution in PH5 borehole with the elevation of the intervals pressure sensor given in the legend.

ID270 borehole

The ID270 is a horizontal borehole drilled from the tunnel at the metric point 675.5. It was first drilled on 40 m in 1994 and extended to 110 m in 2007 for the monitoring of the hydromechanical response of the formation to a drift excavation (the 2008 West gallery). After its extension, ID270 was equipped with a multi-packer system completion by the SolExperts company which isolated 5 pressure measurement chambers located at 102.75, 105.05, 105.65, 106.25 and 109.80 m from the borehole head [41]. The aim was thus to monitor the pressure evolution in the formation before, during and after the excavation, in a non-perturbed zone far from the tunnel influence and in a borehole parallel to the gallery. The pressure evolution since the completion installation up to the beginning of the hydromechanical response to the gallery excavation is represented in Fig. 2.4. For reaching rapidly the pressure equilibrium in the measurement chambers, several water injections were successively performed. A pressure stabilization of about two weeks was likely achieved (indicated by a rectangle on Fig. 2.4) just before the pressure rise subsequent to the passage of the excavation front (see the excavation progress on the right axis of Fig. 2.4). The values of pressure stabilization were evidenced since they were first obtained in the pressure decrease following a water injection and the same pressures were reached again after the next water injection.
In spite of the hydromechanical response monitored in the measurement chambers few times after the observed pressure stabilization, these values can be considered as representative of the formation pressures. These measurements then give access to a pressure value at the tunnel elevation but out of its hydraulically disturbed zone.

2.2.2 Hydraulic head profile establishment

The pressure measurements selected in the previous section are now used to establish an hydraulic head profile across the Tournemire clayrock. The data selection allowed identifying measurements representative of the formation pressures, i.e. achieving a pressure equilibrium at long term, and out of the tunnel influence and of disturbances induced by its excavation and ventilation. These measurements come from a limited number of boreholes (ID180, ID270 and PH4) and are represented in Fig. 2.5 as elevation as a function of the hydraulic head. Because of the bedding of the Toarcian/Domerian formation (about 4), a correction of the measurement chambers elevation to a same hypothetic borehole was applied for obtaining

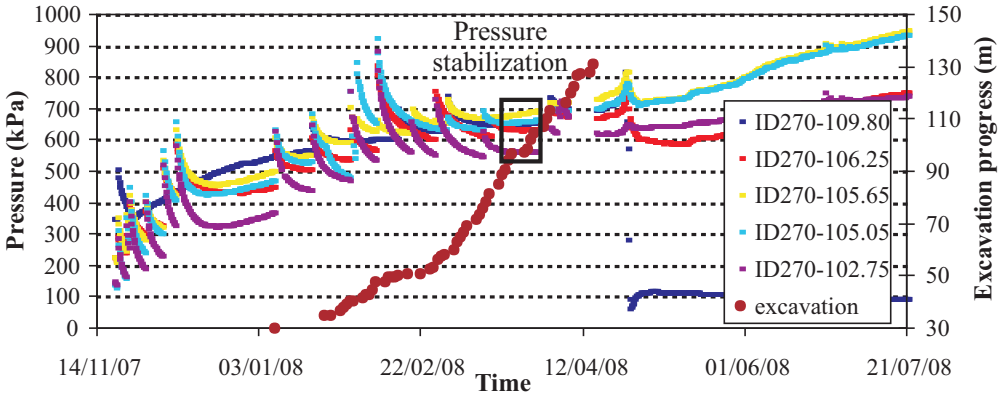

Figure 2.4: Absolute pressure evolution in ID270 borehole after the completion installation and before the hydromechanical response due to the 2008 West gallery excavation. The gallery excavation progress is also represented on the right axis and the distance of the intervals pressure sensor from the borehole head is given in the legend.

a profile at equivalent stratigraphic level. The comparison between the boreholes is made on the PH4-PH5 vertical axis, as a very complete rock characterization was made on these boreholes. The hydraulic head in the Aalenian, the upper aquifer, was monitored in PH5 and CA boreholes and the hydraulic head in the lower aquifer of the Carixian was measured in the PH4 and DC boreholes.

The resulting hydraulic head profile and data are reported in Fig. 2.5 and Table 2.1, respectively. The hydraulic head profile indicates an excess-head of about 30±10 meters with respect to the hydrostatic head profile. This slight excess-head seems to establish between 20 and 40 m, as a function of the uncertainty on the elevation of the water inflow in ID180 borehole.

It is worth noting that the measured excess-head in the Tournemire argillaceous formation (corresponding to 0.3 ± 0.1 MPa) is of the same order of magnitude as the 50 to 60 m MPa excess-head measured in the Callovo-Oxfordian clayrock of the Paris Basin. However, the hydraulic head in the argillaceous formation is lower than the hydraulic head of the surrounding aquifers. A detailed interpretation of the pressure profile monitored in the Tournemire formation will be assessed in Chapter 7.

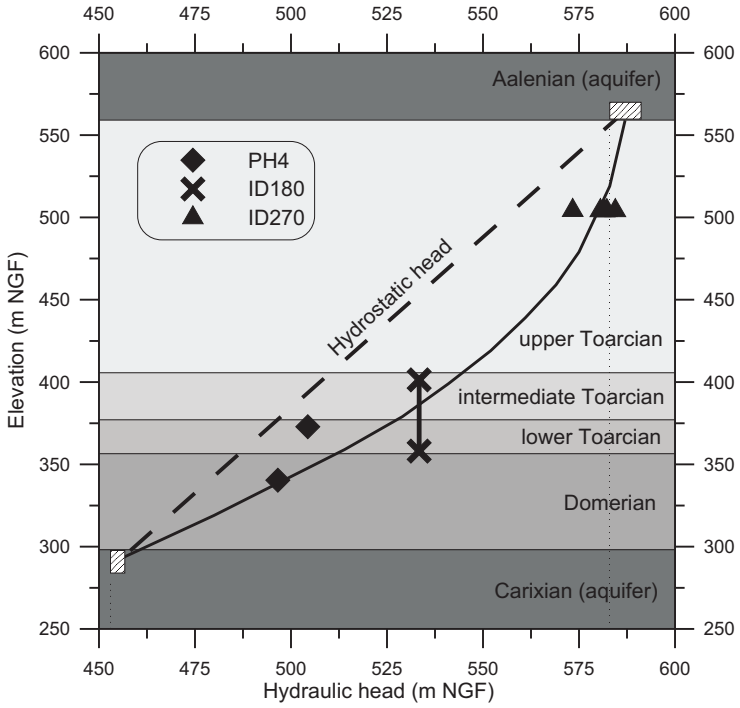

Figure 2.5: Hydraulic head profile across the Tournemire argillaceous formation. Data were selected so that the measurements are representative of in situ conditions and not affected by the tunnel influence.

Borehole	Chambers elevation	Elevation on PH4 z-axis	Hydraulic head
PH4	339.9 - 340.5	339.9 - 340.5	504.36
	372.5 - 373.1	372.5 - 373.1	496.57
ID180	412.82 - 369.5	401.3 - 358.0	533.37
ID270	515.5	504.0	581.65
	515.6	504.1	580.56
	515.7	504.2	584.46
	515.7	504.2	582.24
	515.8	504.3	573.36

Table 2.1: Hydraulic head and elevation of the selected measurement chambers for the hydraulic head profile establishment. Elevations and hydraulic heads are in m NGF.

2.3 Temperature profile

In this section, the temperature profile across the Toarcian and Domerian layers is established from measurements on different boreholes equipped with a temperature sensor in their borehole completion. Many equipped boreholes at Tournemire URL leave a temperature sensor but most of these boreholes are not deep enough so that the temperature show seasonal variations with temperature changes in the tunnel and the galleries. The extension of the temperature seasonal variations in the formation has not been studied but it seems these variations are noticed in measurement chambers up to 10 meters in the rock from the URL drifts. For the temperature profile establishment, measurements out of this influence are selected, so that the measurements present a constant value through time. After the completion installation in the borehole and its saturation with water, a thermal equilibrium between the formation and the measurement chamber is reached after only some hours.
The temperature profile is mainly based on measurements performed in the different intervals of PH4 and PH5 boreholes (see section 2.2.1) and it is completed and validated by measurements on PH1 and PH3 boreholes. The temperature evolution in the different intervals of PH4 and PH5 boreholes is presented in Fig. 2.6. We can see that the monitored temperature is constant for each sensor and that the temperature decreases for increasing elevations.
The PH1 and PH3 boreholes are vertical descendant boreholes drilled from the tunnel at metric points 745.45 and 725.70, respectively, from the South entrance of the tunnel. The PH1 borehole was equipped in October 2000 by the ANTEA company and a temperature sensor was installed in the shut-in chamber at 478.1 m NGF. The temperature was monitored during several month and a constant value of 15.1℃ was reported [5]. The PH3 borehole was also equipped by the ANTEA company, in January 2003. The temperature measurements in a shut-in chamber at 501.8 m NGF indicated a constant value of 13.2℃ [6].

These temperature data are reported as a function of their measurement elevations in Fig. 2.7 in order to establish a profile. The temperature presents a linear and continuous evolution across the formation. It varies in between 24.2℃ at the Carixian/Domerian boundary to 11.5℃ in the upper Toarcian, over the tunnel. It results in a relatively elevated temperature gradient of 5.2℃ per 100 m across the formation. This high geothermal gradient is most likely to be linked to the context of the Massif Central volcanic area, such as the volcanic intrusion of a dyke located in the close-by Roquefort village

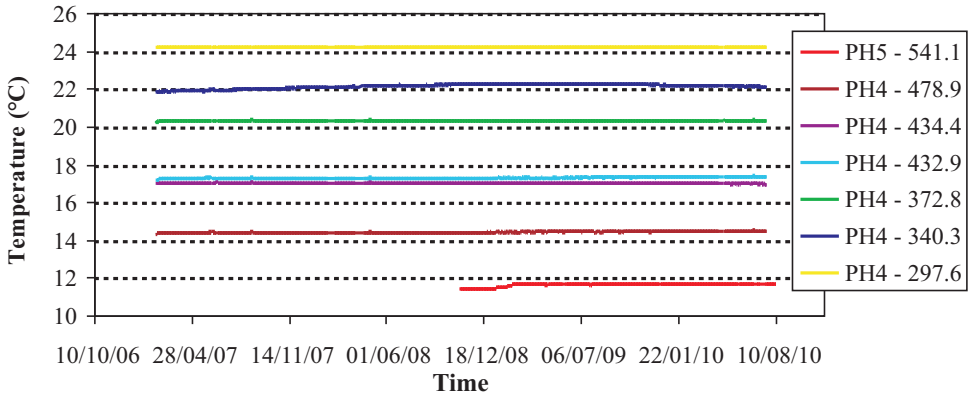

Figure 2.6: Temperature evolution in PH4 and PH5 boreholes with the elevation of the intervals pressure sensor given in the legend.

and dated 5 Ma [84]. High geothermal gradients are also reported in the edge of the Massif Central (4.1°C/100 m in Randels (Aveyron, at the North of Millau); 3.8°C/100 m in St Saturnin de Lenne (Aveyron, at the North of Séverac) [152]), in the Permian basin of Lodève (Hérault; 4.6°C/100 m [152]) and in the Cevennes (5.2°C/100 m in Durfort (Gard) [48]).

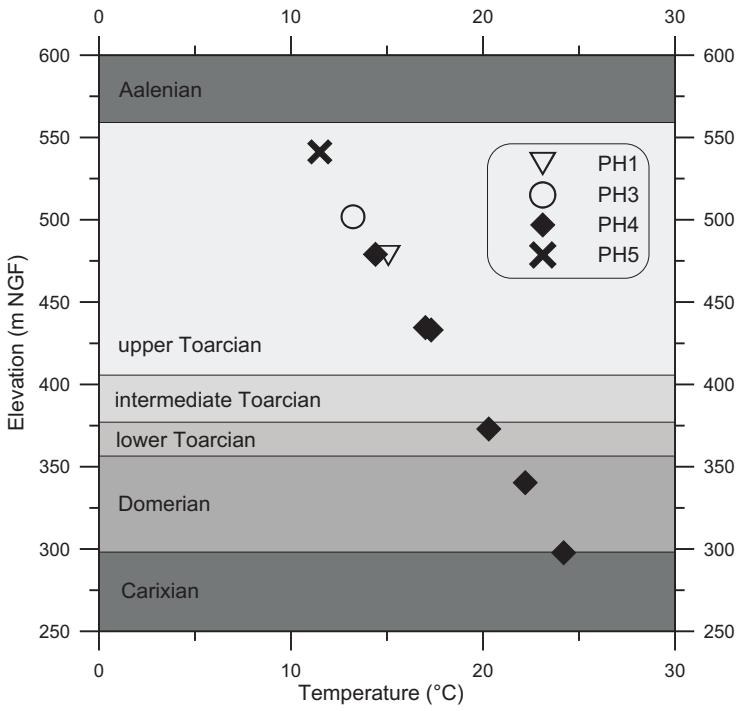

Figure 2.7: Temperature profile across the Tournemire argillaceous formation.

2.4 Conclusion

The hydraulic head profile allowed the identification of a 20 to 40 m excess head in the argillaceous formation, respectively to the hydrostatic head between the two surrounding aquifers. This is an important observation as this results tends to confirm that abnormal pressures are frequent in argillaceous formations in sedimentary basins. The higher difficulty being their detection, especially when the overpressure is moderated.
The interpretation of the origin of this measured excess-head at Tournemire will be carried in Chapter 7, after the characterization of the coupled-flow processes in the Tournemire clayrock.
A temperature profile across the formation was also obtained. It indicates a relatively high geothermal gradient of 5.2℃/100 m. The temperature profile will be useful for the assessment of the thermo-osmosis influence at Tournemire. This study will be conducted in Chapter 7.

Chapter 3

Chemical composition profile

The chemical composition profile across the Tournemire argillaceous formation is required for the interpretation of the characterization of the influence of the chemical osmosis in the formation.
It is need as the driving force of chemical osmosis in the shale. With a maximal salinity is the shale layer and minimum salinity in the surrounding aquifers, an overpressure can be observed, because of a converging osmotic flow towards the argillaceous formation.
Porewater composition is more especially required for the calculation of the theoretical chemical osmotic efficiency, as the model developed in section 4.2 is able to account for both monovalent and divalent counterions. This consideration allows calculating the osmotic efficiency for natural conditions, i.e. with complex composition solutions. The availability of the chemical composition profile across the Tournemire argillite is then needed to calculate the chemo-osmotic efficiency profile (see section 4.2.5).
The obtention of a reliable porewater composition presents also a more general interest for the different studies performed with Tournemire clay-rock which require a reference porewater composition.

Owing to the difficulties to sample porewater without inducing perturbations on the water composition linked to the very low permeability and water content, a undirect method for obtaining the porewater composition is required. This method consists in reproducing the adequate interaction reactions occurring between the solid and the solution and within the water itself, using geochemical modelling.
The geochemical system was then characterized by a set of characteristics of the Tournemire argillite (e.g., exchangeable cations, mineralogy and petrology, porosity) and its porewater (e.g., mobile anions, CO_2 partial pressure).

The interaction model was then established, considering mainly the different cation exchange properties of the clay minerals contributing the the cation exchange. The model results were compared with two other models: the BRGM model [53] which considers cation exchange only on one site; and a previous model only based on mineral equilibrium [13]. Models comparison and validation is made using water composition sampled in fractures [13], corrected here from its perturbations linked to the drilling.
The geochemical model was then applied across the argillaceous formation accounting for the changes in rock and water properties to obtain a water composition profile.

This Chapter is presented as a paper, submitted to Applied Geochemistry.

Geochemical characterization and modelling of the Toarcian/Domerian porewater at the Tournemire underground research laboratory.

J. Tremosa[a,b,c,*], D. Arcos[c], J.M. Matray[b], F. Bensenouci[b,d], E.C. Gaucher[e], C. Tournassat[e], J. Hadi[e,f]

[a] *UPMC Univ. Paris 06, UMR-7619 SISYPHE, 4 place Jussieu, F-75252 Paris, France*
[b] *IRSN, DEI/SARG/LR2S, BP 17, F-92262 Fontenay-aux-Roses, France*
[c] *Amphos XXI Consulting, S.L., Passeig de Garcia i Faria, 49-51, E-08019 Barcelona, Spain*
[d] *Univ. Paris Sud 11, UMR-8148 IDES, Bât. 504, F-91405 Orsay, France*
[e] *BRGM, EPI/MIS, 3 av. Claude-Guillemin, BP 36009, F-45060 Orléans, France*
[f] *Univ. Grenoble 1, LGIT-OSUG, F-38041 Grenoble, France*

Abstract

For the safety evaluation of hazardous waste repositories in clay-rocks, a thorough assessment of porewater chemistry and water-rock interactions is required. However, this objective is a challenging task due to the low hydraulic conductivity and water content of such rocks, which subsequently renders porewater sampling difficult (without inducing perturbations). For this reason, an indirect approach was developed here to determine porewater composition of clay-rocks, by a geochemical model of water-rock interaction using some properties of the rock and the contacting solution. The goal of this paper is to obtain the porewater composition of the Toarcian/Domerian argillaceous formation at Tournemire (South of France), for which a reliable model is still lacking. The following work presents a comprehensive characterization of the geochemical system of the Tournemire clay-rock, including mineralogy, petrology, mobile anions, cation exchange properties, accessible porosity and CO_2 partial pressure. Perturbation corrections from fracture water sampling were also computed. These water were found in sealed fractures (Beaucaire et al., 2008) and their radio-

*Corresponding author
Email address: j.tremosa@brgm.fr (J. Tremosa)

carbon apparent age is estimated at 20000 years. Their age together with their equilibrium situation allow considering these fracture waters as representative of the formation porewater. The model developed to calculate the Tournemire porewater composition is essentially based on cation exchange by a multi-site approach, but equilibrium with some mineral phases (calcite, quartz and pyrite) is also considered. Different exchange sites of different affinities towards cations are used, which proportions are given by the mineralogy. Exchange on illite is performed with Bradbury and Baeyens (2000) three-sites model, while one site is considered for smectite phases (Tournassat et al., 2009). Multi-site model results are compared with corrected fracture water data and two other models: a model only based on mineral equilibrium (Beaucaire et al., 2008) and a model using cation exchange on one global site (Gaucher et al., 2009). The best results were obtained with the models that take into account cation exchange and particularly with the multi-site model. The interest of considering a model with exchange sites of different affinities is especially obvious for a satisfactory representation of the K^+ content in solution. A dependence of K^+ content to the amount of high affinity sites was observed, leading to an improvement of its simulation when uncertainty on mineralogical data is considered. Once validated, the multi-site model was applied at different levels of the Tournemire argillaceous formation to obtain a profile of the porewater composition.
Keywords: porewater modelling, multi-site cation exchange, Tournemire argillite, Toarcian

---

1. Introduction

Understanding porewater chemistry and water-rock interactions in overconsolidated clay formations is an important task in studies dealing with safety evaluation of hazardous waste repositories in clay-rocks (Altmann, 2008). Chemical conditions in the porewater and buffer abilities of the rock will control the concentrations of contaminants within a repository, in case of engineered barrier failure. Furthermore, a reference porewater composition and its variation with

depth are required in a series of studies performed at the IRSN's underground test facility built in a Toarcian/Domerian argillite at Tournemire (South eastern France), dedicated to the safety assessment of nuclear repositories in clay-rocks. The Tournemire experimental station is solely used for scientific and technical research, namely studies involving confinement properties of clay-rocks, including the analysis of the transport and flow phenomena and the study of natural tracers, and on the interactions between the repository components and the natural medium. Thus, it is necessary to reach a good knowledge on porewater composition, its variations across the clay-rock formation and the water-rock interaction processes. A consequent research is ongoing on the characterization of porewater geochemistry in the different clay-rocks studied in the framework of radioactive waste storage (Beaucaire et al., 2008, 2000; Bradbury and Baeyens, 1998; Gaucher et al., 2006, 2009; Pearson et al., 2003) and in bentonite engineered barrier systems envisaged in geological repositories (ENRESA, 2008; Wersin, 2003). The main difficulty arises from the argillite low water content and permeability preventing any direct water sampling despite the development of experimental methods for such rocks (Gaucher et al., 2009; Pearson et al., 2003; Sacchi et al., 2000), i.e. leaching, squeezing or centrifugation, but unsuitable at Tournemire. However, a direct acquisition of the Tournemire clay-rock water was obtained in-situ from water-bearing fractures. The residence time of waters collected in these boreholes was estimated by radiocarbon dating in between 17000 and 30400 years (Beaucaire et al., 2008). Concerning the non-fractured medium and compared to other compacted clay rocks studied for repository purposes — Callovo-Oxfordian at Bure (Delay et al., 2006) and Aalenian at Mont Terri (Fernandez-Garcia et al., 2007) —, the Tournemire URL gives access to one of the most impervious clay-rock studied so far with extremely low permeabilities (10^{-14} – 10^{-15} m.s^{-1}) and porosities (9 – 10%) (Boisson et al., 2001). These properties exclude therefore any porewater production at the human scale in the non-fractured medium as diffusion is dominating advection. Thus, an indirect method for porewater composition determination is required. Properties of the rock and some properties of the porewater can be determined and, by

combination with a geochemical model of water-rock interactions, a good estimation of the porewater composition can be reached. The model consists in reproducing the processes occurring between the argillite and its porewater, mainly mineral dissolution/precipitation reactions and surface reactions such as cation exchange and protonation/deprotonation, until the system reaches equilibrium.

This paper aims to propose a specific-site model for the acquisition of the porewater composition in the Toarcian/Domerian clay-rock at Tournemire. Two water–rock interaction models were initially proposed by Beaucaire et al. (2008), nevertheless, these models still have to be improved in order to represent fracture water in a satisfactory way. Indeed, an organic matter biodegradation by sulphate-reducing bacteria activity affecting the evolution of water composition with time and linked to drilling perturbation was identified in the fracture waters but not taken into consideration in the initial model.

In the present work, we first present the data obtained for implementing the proposed geochemical system, including corrections applied to fracture-waters composition. Next, a model for porewater composition calculation, based on mobile anions, mineralogy and cation exchange modelling on various surface sites, is proposed and evaluated. This evaluation is highlighted by comparing the multi-site model with the reference fracture waters composition and with other models: the previous models proposed for the Tournemire argillite (Beaucaire et al., 2008) and the BRGM model proposed for the Callovian-Oxfordian porewater (Gaucher et al., 2009) and adapted here for Tournemire argillite . Finally, a water composition profile is obtained, applying the model presented in this paper.

2. Description of Tournemire clay-rock geochemical system

2.1. Geological settings

The formation of interest, the Tournemire clay-rock, is a subhorizontal Domerian and Toarcian argillaceous sequence, which forms part of the *Grands Causses*

basin. This basin is related to the Tethys opening and presents sediments from the Permian to the upper Jurassic. At Tournemire, Jurassic geological series consist in 300 m thick limestones and dolostones layers from Hettangian, Sinemurian and Carixian. They are overlaid by 250 m thick compacted shales and marl formation deposited in a deep marine environment during the Domerian and Toarcian and followed by limestones and dolostones from Aalenian, Bajocian and Bathonian which form the the present day Causses plateau (Fig. 1). Several faults affect the massif in consequence to the two main tectonic events: an extension during the Jurassic and a compression at the Neogene during the Pyrenean orogenesis, which also leads to massif exhumation (Boisson et al., 2001; Cabrera et al., 2001).

Domerian and Toarcian shales and marls are of very low hydraulic conductivity, ranging in between 10^{-14} and 10^{-15} m.s^{-1}, in Boisson et al. (2001) after laboratory pulse tests performed on 40 cm long test piece core samples and in Bertrand et al. (2002) after in situ pulse tests performed in 1 m height-long term monitoring probe. These aquitard formations are surrounded by two limestones aquifers: in the Carixian and in the Aalenian formations. Karstification of these formations started at the Neogene and river-valleys incision at the beginning of the Miocene (Ambert and Ambert, 1995).

Temperature profile at the Tournemire URL was obtained by long-term temperature measurements from various boreholes equipped with packers. The temperature profile obtained across the Domerian and Toarcian levels is linear and gives a geothermal gradient of 0.052 °C.m^{-1} (Tremosa, 2010). This high geothermal gradient is most likely linked to the vicinity of the *Massif Central* volcanic area.

The IRSN underground research laboratory at Tournemire consists in a century-old tunnel crossing the upper Toarcian formation, recent galleries excavated from the tunnel and different sets of boreholes. The data described below comes from samples collected in two vertical boreholes drilled from the tunnel downwards to the Carixian (PH4) and upwards to the Aalenian formations (PH5) (Fig. 1). The goal of these boreholes was to establish a set of parameters of

interest across the argillaceous sequence to and from the surrounding aquifers.

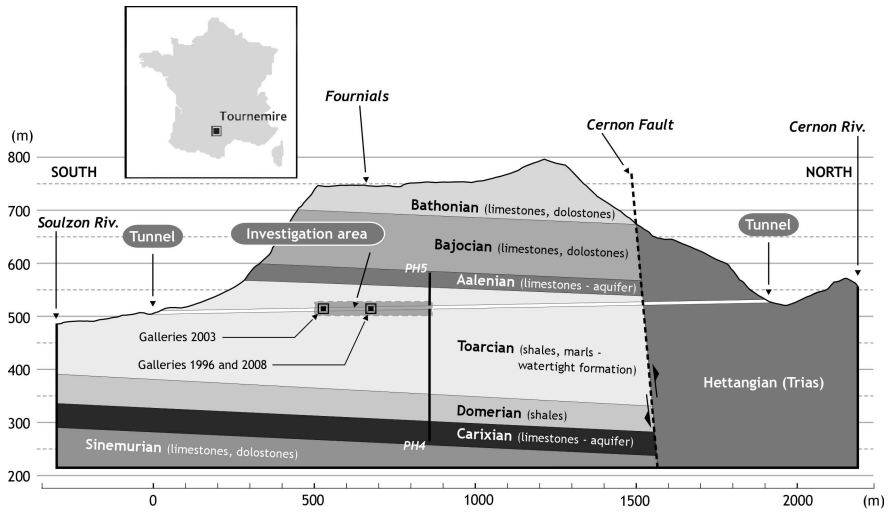

Figure 1: Geological cross-section of the Tournemire URL.

2.2. Mineralogical and petrological characterization

Clay-rock mineralogy and petrology are essential to buildup a sound conceptual model of the water–rock interaction processes. The identification of the different minerals present in the rock along with their cristalline state give information on the minerals in equilibrium within the formation. For this purpose, a mineralogy profile (Fig. 2) across the Tournemire argillaceous sequence was established from samples collected in PH4 and PH5 boreholes. The mineralogical analysis were performed by Etudes Recherches Matériaux ERM and consisted in X-ray diffraction analysis, major elements chemical analysis and measurements of the cation exchange capacity and the carbonates content. These analysis allow a semi-quantitative estimation of the mineral contents. The mineralogical analysis show that the formation presents a relatively homogeneous mineralogical composition, except for the lower Toarcian level. Tournemire clay-rock is rich in 2:1 minerals, illite and illite/smectite mixed-layers rich in illite (with 50 to 90% of illite) and some detrital micas. The 2:1 minerals content is about 50% of the whole rock in the upper Toarcian, 30% in the lower Toarcian and 60% in the

Domerian. Other clay minerals present are kaolinite (10%) and chlorite (5%). The clay-rock also contains non negligible amounts of quartz and carbonates (about 15% each), mainly calcite but also dolomite and siderite. Furthermore, and even if strontianite has not been directly observed in Tournemire clay-rock, 200 to 500 ppm of Sr were measured in calcite minerals at Tournemire (Mathieu et al., 2000). This measurement indicates a Sr-carbonate phase is most likely present at low amount in the rock. The carbonates content in lower Toarcian is higher (30%). Some other minerals with lower contents are also found: pyrite, feldspars, apatite and rutile. It is worth noting the absence of sulphate minerals in the Tournemire clay-rock. Consequently, sulphate concentration in porewaters is not controlled by sulphate minerals saturation. Petrological observations indicate the occurrence of authigenic calcite and illite in rock joints as well as pyrite and some glauconite crystals. These authigenic minerals do not show dissolution signal and clearly indicate the porewater is at thermodynamic equilibrium with these minerals. Equilibrium with unaltered pyrite allows the assessment of the redox conditions, as it occurs in similar formations (Gaucher et al., 2006; Pearson et al., 2003). Organic matter content in the argillite is about 1% in the upper Toarcian and Domerian and up to 10% in the lower Toarcian (Cabrera et al., 2001).

The clay sequence is surrounded by two carbonate formations: the Aalenian is a marly limestone and the Carixian is a sandy limestone.

2.3. Determination of exchangeable cations occupancy and cation exchange selectivity coefficients

Exchangeable cations give a very valuable information on the porewater cation population in clay-rocks for which there is no possibility to extract water without inducing experimental artefacts. The sorbed cations at the clay minerals surface can be considered as a "fingerprint" of the solution (Bradbury and Baeyens, 1998) and, once the population repartition of the sorbed cations (i.e. the fractional occupancy) and the surface to porewater exchange ability of the cations (i.e. the selectivity coefficients) are known, one can calculate the cations

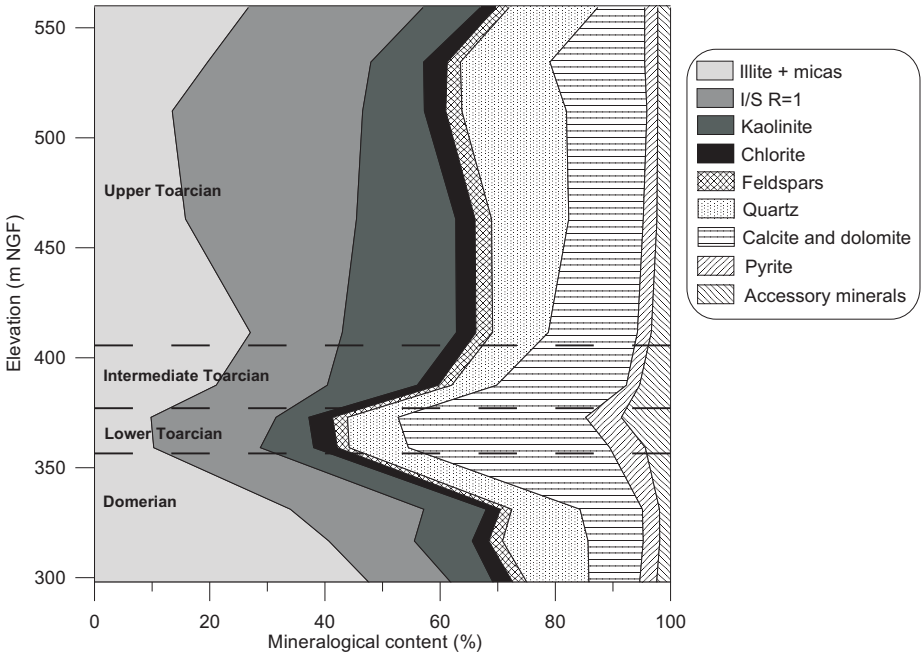

Figure 2: Mineralogical composition profile of the Tournemire clay-rock

concentrations in the porewater.

Cations occupancy was determined under anoxic conditions using the <100 μm fraction with CsCl extracting solutions, at different rock/solution ratio (0.25:1, 0.5:1 and 1:1). A short contact time (1h) between the rock and the extractant was selected for limiting perturbations due to dissolution of carbonates minerals. Rock crushing and sieving and extraction of exchangeable cations was performed under anoxic conditions (in a glove-box under a N_2 atmosphere, with a O_2 content <50 ppmv) for avoiding pyrite dissolution. After centrifugation — during 10 min at 10000 rotations per min — of the rock–extractant mud, the supernatant was analyzed by ionic chromatography in IRSN's facilities at Fontenay-aux-Roses. Possible dissolution and accuracy of exchangeable cation data were assessed by comparing extracts obtained at different rock/solution ratio (Dohrmann, 2006) and led to a data selection. A profile of exchangeable cations is thus obtained (Table 1) and indicates the exchanger composition is

dominated by Ca and the cation exchange capacity ranges between 0.08 and 0.12 $mmol_c.kg^{-1}$.

Cation exchange selectivity coefficients for the illite/smectite mixed layer fraction of the Tournemire clay-rock were also determined, at BRGM's facilities. The method proposed by Gaucher et al. (2009) was followed and applied to the <2 μm fraction of an upper Toarcian sample (elevation 431.0 m NGF). Sample was several times equilibrated with a synthetic water close to the assumed Tournemire porewater composition, then centrifugated. Cation exchange selectivity were calculated in the Gaines and Thomas (1953) convention from supernatant composition and cations extracted from clay slurry by Cobalthexamine (Tournassat et al., 2009). Results are shown in Table 2 for an exchange reaction corresponding to:

$$i\,NaX + Me^{i+} = MeX_i + i\,Na^{+}, \tag{1}$$

where Me is a cation species, i is its valence and $K^{Na/Me}$ is the selectivity coefficient. These exchange selectivity coefficients are higher than those commonly found for such clay-rocks (Gaucher et al., 2009; Pearson et al., 2003).

Elevation (m NGF)	CaX_2	MgX_2	NaX	KX	SrX_2	sum
509.0	3.82±0.05	1.85±0.04	1.68±0.07	1.19±0.05	0.10±0.01	8.64±0.22
461.5	3.46±0.04	1.81±0.03	1.83±0.03	1.14±0.06	0.12±0.02	8.36±0.18
399.3	5.04±0.07	2.48±0.07	2.98±0.12	1.66±0.07	0.17±0.003	12.33±0.33
370.4	3.97±0.12	1.89±0.06	1.82±0.09	1.44±0.09	0.20±0.02	9.32±0.38
329.1	4.60±0.19	2.02±0.06	0.88±0.06	1.31±0.04	0.10±0.02	8.91±0.37

Table 1: Cation occupancy (in $mmol_c.100\ g^{-1}$) profile across the Tournemire clayrock.

2.4. Determination of chloride and sulphate contents

Studies on Tournemire anion population, and especially on conservative species, were mainly performed for diffusion study purposes (Bensenouci, 2010;

log K	$K^{Na/K}$	$K^{Na/Ca}$	$K^{Na/Mg}$	$K^{Na/Sr}$
Measured from exchange experiment (<2 μm)	1.35	1.32	1.23	1.23
Illite/smectite model	1.18	0.67	0.72	0.60
In situ experimental determination	1.81	0.88	0.64	0.96

Table 2: One site cation exchange selectivity (log K) (i) measured on an upper Toarcian sample fraction, (ii) predicted by generic models (Tournassat et al., 2009, 2007) and (iii) determined from fracture waters composition and in situ cation occupancy (average value).

Patriarche et al., 2004; Savoye et al., 2006). These data are used here to characterize the ionic strength of solutions. Several methods for chloride and sulphate contents determination have been performed, developed and assessed (Sacchi et al., 2000; Savoye et al., 2006; Witterbroodt et al., 2007). It results that anion content is less affected by experiment artefacts and more representative of the pore water when obtained by diffusion methods than by lixiviation (Savoye et al., 2006; Witterbroodt et al., 2007).

Figure 3 synthesizes profiles of chloride and sulphate obtained by Patriarche et al. (2004) on different boreholes and Bensenouci (2010) on boreholes PH4 and PH5. Patriarche et al. (2004) obtained a chloride profile by immersion of argillite samples in distilled water and by following the chloride concentration in the water until equilibrium. Bensenouci (2010) applied the radial diffusion method developed by Van der Kamp et al. (1996) and adapted to compacted clay-rocks by Savoye et al. (2006). The radial diffusion method presents the advantage to directly determine the tracer-accessible porosity on the transient pattern of the tracer restitution curve and also the value of the effective diffusion coefficient in the steady-state phase of the pattern. The same cells were used to determine both stable isotope, chloride and sulphate contents in the same experiment (Savoye et al., 2006). This experiment consists in equilibrating a synthetic water, the composition of which tends to buffer carbonates dissolution, with an argillite core wherein a borehole is drilled lengthwise at one end and at the center of the core diameter. This borehole is filled with the synthetic water and equilibration occurs through this borehole surface. Water composition is fre-

quently analyzed until equilibrium. Moreover, sulphate content determination that samples were prepared and maintained under anoxic conditions to avoid any perturbation by pyrite oxidation: samples were conditioned in epoxy resin in less than one hour after the drilling and next prepared in anoxic glove-box (atmospheric O_2 concentration <50 ppmv) where diffusion cells were maintained under a N_2 atmosphere.

Chloride and sulphate content repartition across the formation (Fig3) shows a bell-shape curve with higher contents at the center of the formation and a progressive content decrease towards the Aalenian and Carixian aquifers, indicating a diffusion process from the argillite to the aquifers (Bensenouci, 2010). Cl^- and SO_4^{2-} contents from fracture waters (Beaucaire et al., 2008) (corrected in section 2.7) are also represented in Fig.3 and present a similar trend for both anion species.

2.5. Measurements of CO_2 partial pressure

CO_2 and alcanes partial pressures measurements were performed by BRGM on samples from the upper and lower Toarcian following the method developed by Gaucher et al. (2010, 2009). Just after sampling, during the PH4 borehole, samples were conditioned in hermetic cells under a He or an Ar atmosphere after several cycles of vacuum/rare gas flushing to remove the atmospheric gas. The cells were then sealed on to allow degassing of the core till stabilization of the gas composition. Mesaurements were performed by gas ionic chromatography enabling the determination of CO_2 and alcanes partial pressure. Isotopic measurements on gases were also performed following the protocol detailed in Girard et al. (2005). The absence of N_2 in the cell atmosphere after degassing indicated the lack of atmospheric contamination. N_2 is a better indicator of atmospheric contamination than O_2 as O_2 tends to react with the clay-rock and is not easily analyzable at trace content in an Ar environment. In cells affected by an atmospheric contamination, PCO_2 was observed to rise with PN_2 because of an oxidation of alcanes. Non contaminated CO_2 partial pressure measurements give a PCO_2 value of 3.6 mbar ($\log PCO_2$=-2.4) the upper Toarcian and a PCO_2

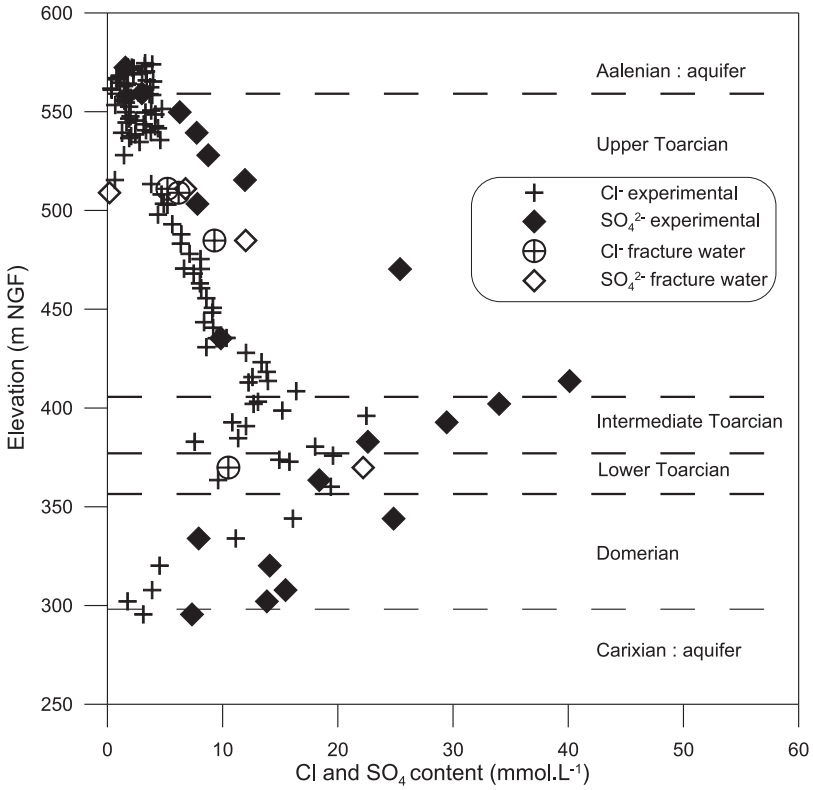

Figure 3: Chloride and sulphates contents profile in Tournemire formation (Beaucaire et al., 2008; Bensenouci, 2010; Patriarche et al., 2004)

value of 6.4 mbar (log PCO_2=-2.2) for the lower Toarcian. These values are in the range of PCO_2 measured in similar clay-rock formations, thus indicating that the PCO_2 is closely related to the mineralogical sequence (Gaucher et al., 2010; Girard et al., 2005). Alcanes partial pressures are particularly high, especially in the lower Toarcian with rich organic matter content (about 10%wt). The gas composition indicates a thermogenic origin of the alcanes, and not a biogenic one (Gaucher et al., 2010). Experiments also suggest that high alcanes contents could control the total reductive capacity of the clay-rock, as they are very sensitive to oxidant conditions. Isotopic measurements of $\delta^{13}C$ (-6.6 ‰) and $\delta^{18}O$ (34 ‰) on outgassed CO_2 indicate that CO_2 is in equilibrium with the carbonate minerals contained in the clayrock (Gaucher et al., 2010; Girard et al., 2005).

2.6. Petrophysical parameters of the Tournemire clay-rock

The porosity and the grain density are necessary to define the rock/water ratio and principally to convert the exchangeable cations content by rock mass into a porewater volume. These parameters may be considered as homogeneous at each level of the clay sequence, hence a mean value was chosen for each level (Tab. 3).

The total or physical porosity and the gravimetric water content were determined by measurements of water content and volume on samples from PH4 and PH5 boreholes, following the procedure described in Matray et al. (2007). These measurements were performed at the Tournemire test facility just after removing the core from the boreholes. The total porosity ranges between 8 and 9% in the formation, expect for the lower Toarcian level which presents a total porosity of 3.5%. The gravimetric water content is more homogeneous across the argillaceous formation and ranges between 2.6 and 3.8%.

Anion accessible porosity seems conceptually the best estimate of the pore space to be considered in a geochemical model (Pearson et al., 2003), as anions are excluded from a part of the porosity because of electrical repulsions in the vicinity of the negatively charged clay minerals surface. The anion accessible porosity

corresponds to the pore space not affected by anion exclusion and corresponds to the free water as described in electrical surface models and to some of the water in the diffuse layer (Appelo et al., 2010; Horseman et al., 1996). Anion accessible porosity was determined in radial diffusion experiments, as described in section 2.4. Anion accessible porosity ranges between 1 and 3%, depending on the clay-rock layer (Bensenouci, 2010).

Grain density was obtained by helium pycnometry measurements performed by Etudes Recherche Matériaux and by IRSN. Grain density appears very homogeneous across the argillaceous formation, except for the lower Toarcian which exhibits a lower density. This lower measured density in the lower Toarcian is likely due to its high content in sedimentary organic matter.

Formation level	Anion accessible porosity	Gravimetric water content	Total porosity	Grain density ($g.cm^{-3}$)
Upp. Toarcian	0.020	0.038	0.091	2.720
Int. Toarcian	0.025	0.034	0.088	2.724
Low. Toarcian	0.020	0.026	0.035	2.398
Domerian	0.013	0.030	0.080	2.738

Table 3: Average petrophysical parameters for the different levels of the Tournemire clay-rock.

2.7. Fracture water data

The Tournemire clay-rock is affected by a fracture network organized in relay systems (Beaucaire et al., 2008) and most of which are filled by calcite. However, a water inflow was observed in some geodic fractures crossed by air-drilled boreholes. A packer system was installed in these boreholes, in order to sample fracture water inflows. Four fracture waters — from boreholes M2, TN2 and TF5 in the upper Toarcian and TN3 in the lower Toarcian — were regularly sampled and identified to be representative of the formation porewater. Different reasons suggest these waters are representative of the formation porewater. The first reason is provided by the consequent contact time between the

fracture waters and the clay-rock. Indeed, these waters present residence times estimated in between 17000 and 30400 years by radiocarbon dating (Beaucaire et al., 2008). Furthermore, the composition of these fracture waters agrees with the expected equilibrium of the carbonate system for this rock. Fracture waters given in Table 1 from Beaucaire et al. (2008) with available pH and alkalinity measurements were used to calculate the saturation index of these waters relatively to calcite and dolomite and the CO_2 partial pressure (Fig.4). For these calculations sit.dat thermodynamic database was used and the dolomite phase used in these calculations corresponds to a medium order dolomite. The calculations indicate the fracture waters are close to calcite and dolomite equilibrium. In most cases the waters are slightly oversaturated with calcite and dolomite, suggesting the measured pH value is higher than in situ pH because of CO_2 outgassing during sampling. The calcite and dolomite saturation indices of these waters tend to increase with time span since drilling. Calculated CO_2 partial pressure (Fig. 4) are in the range of the measured PCO_2 for the Tournemire argillite (section 2.5). As a consequence, sampled waters are considered to be representative of the in situ porewater chemical composition provided that pH values are readjusted to calcite equilibrium.

As yet noted by Beaucaire et al. (2008), an organic matter biodegradation by Sulphate-Reducing-Bacteria (SRB) was identified between the different samplings. It is evidenced by a sulphate decrease and related bicarbonate increase in solution (eq.2, where organic matter is represented as CH_2O) and by isotope evidences (increase in δ^{34}S and δ^{18}O in the residual sulphate).

$$CH_2O + 0.5\, SO_4^{2-} \rightarrow HCO_3^- + 0.5\, HS^- + 0.5\, H^+ \qquad (2)$$

SRB were identified in the Tournemire fracture water (Daumas, 2005) and in the rock porosity (Urios et al., 2010). Due to the very low pore size of some nm of the intact rock, the bacteria were inactive before the drilling. Drilling is assumed (i) to reactivated bacteria by either inducing a mechanical unloading around the borehole which lead to microcracks opening in the rock and introducing nutrients (De Cannière et al., 2011; Stroes-Gascoyne et al., 2011); or (ii)

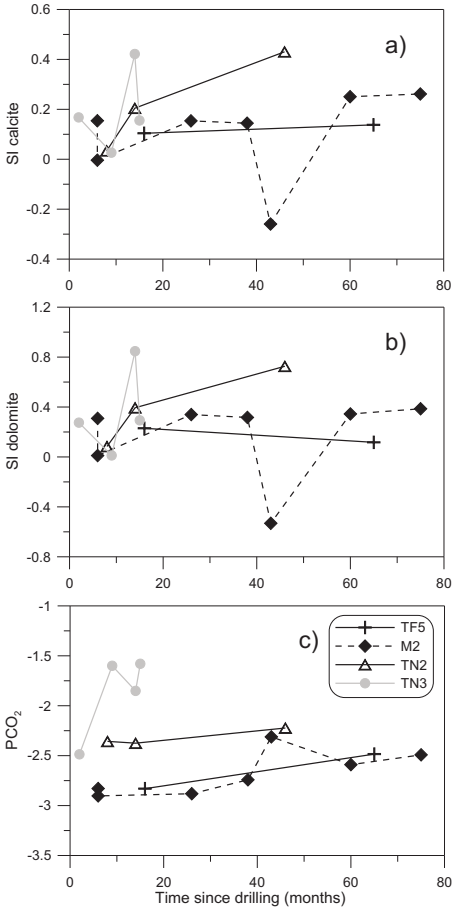

Figure 4: Calculated (a) calcite and (b) dolomite saturation indices and (c) PCO_2 for sampled fracture waters since drilling.

introduced active allochtonous bacteria responsible for the observed bacterial activity (Stroes-Gascoyne et al., 2011).

Our interest in organic matter biodegradation is limited to the initial reactants and final products evolution in the system, as expressed in eq.2. The effects of microbial physiology and population dynamics can be described by an overall kinetic law. The system evolution will also depend on system parameters, commonly reactants concentrations and temperature, however organic matter and sulphates contents are unlikely to induce reaction limitations. The biodegradation rate constant (k, in mol.L^{-1}.s^{-1}) can be obtained performing a mass balance through time on sulphate content:

$$k = \frac{d\,CH_2O}{dt} = \frac{2 \times d\,SO_4^{2-}}{dt} \tag{3}$$

Calculated organic matter biodegradation rate constants for the different fracture waters are -8×10^{-12} mol.L^{-1}.s^{-1} for M2 water, -1.2×10^{-10} for TN2 water and -2.2×10^{-10} for TN3 water and seemingly to decrease with the aqueous sulphate concentration.

These biodegradation rates are introduced in a simple batch model to reproduce the evolution of the water composition considering organic matter biodegradation via a 0-order kinetic law and equilibrium with calcite, dolomite and quartz. For the sake of simplicity, a closed system is elected in this model which, in particular, does not consider transport between the borehole and the surrounding rock porewater (Arcos et al., 2004; Tournassat et al., 2011). Indeed, the biodegradation rate constants previously established are overall rate constant describing sulphate evolution in the system.

These calculations were performed with PHREEQC v2.17 (Parhurst and Appelo, 1999) calculation code, using sit.dat thermodynamic database (Duro et al., 2007). Good fittings are obtained with this model for both sulphates, bicarbonates and pH evolutions in waters from boreholes TN3 and M2 (Fig.5). These results confirm the effect of organic matter degradation via SRB activity in the fracture waters. However, bicarbonates and pH evolutions in TN2 water are not reproduced and simulated bicarbonates contents are larger than those observed,

indicating a sink of carbonates possibly attributed to a CO_2(g) outgassing. TF5 water presents low sulphate content and no effect of SRB activity can be identified, but PCO_2(g) evolution shows a gradual outgassing with time.

Perturbation of the sampled fracture waters with time since coring indicate that only the firsts sampled fracture water compositions are likely to present a good estimate of the porewater of the Tournemire clay-rock formation, provided their pH is readjusted to calcite equilibrium (see above). The reference waters which will be used in the next sections for comparison with rock–water equilibrium models results are summarized in Table 4.

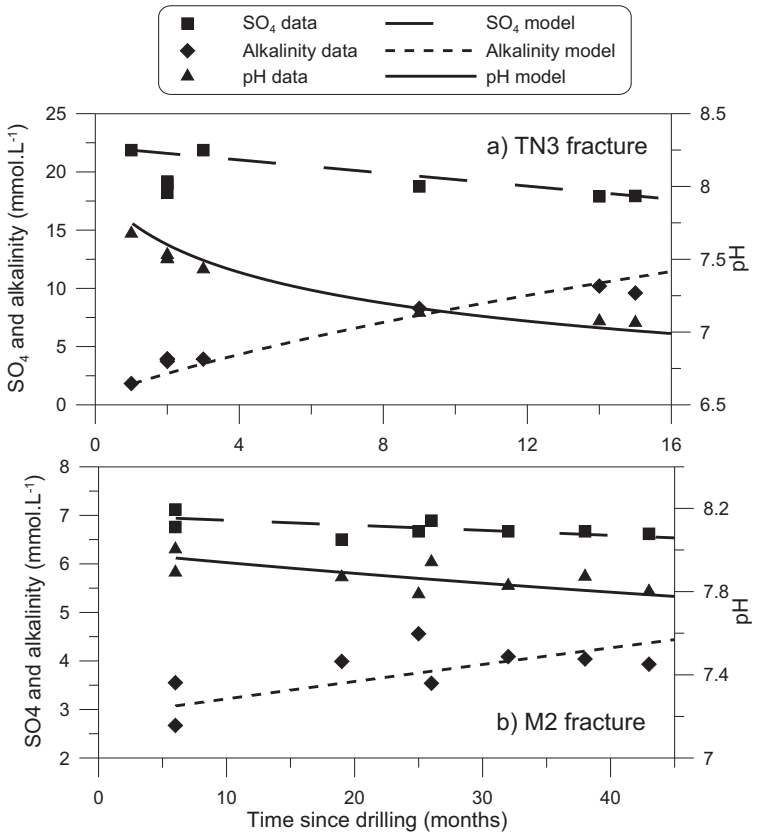

Figure 5: Data and modelled evolution of SO_4^{2-} and TIC content and pH of (a) TN3 and (b) M2 fracture waters since drilling.

Borehole	pH	Alk	SO_4	Cl	Ca	Mg	Na	K	Si	Sr
TF5	8.15	6.46	0.01	5.45	0.25	0.22	10.87	0.12	0.13	0.005
M2	7.89	5.21	6.76	3.55	1.11	0.90	18.60	0.22	0.12	0.025
TN2	7.67	8.91	10.30	4.80	1.65	1.38	26.74	0.32	0.11	0.046
TN3	7.53	10.87	18.22	3.73	3.67	2.55	37.30	0.64	0.18	0.126

Table 4: Composition of the reference waters from boreholes TF5, M2 and TN2 in the upper Toarcian and TN3 in the lower Toarcian. Contents are in mmol.L^{-1}.

3. Geochemical modelling of Tournemire clay-rock porewater

3.1. Model establishment

The purpose of this section is to establish a realistic rock–porewater interaction model for the Tournemire clay-rock porewater characterization. This model is based on the exchange intrinsic properties of the rock, directly dependent on the nature and amount of the constituting clay minerals.

Two previous models were proposed by Beaucaire et al. (2008) for the prediction of Tournemire porewater composition, but they present limitations for reproducing the monovalent cations contents, especially K^+. A good description of the potassium behaviour in the argillite–porewater system under study is particularly interesting to reach because potassium acts as a competitor to caesium, one of the radionuclide which can be released by a radioactive waste disposal. The first model is an application of Beaucaire et al. (2000) model, developed for the Boom Clay. It assumes a control of the chemical composition by dissolution and precipitation reactions with mineral phases (calcite, dolomite, quartz, kaolinite, microcline, albite and chlorite). The model validity is questionable because it considers high temperature and pressure detrital phases — feldspars — as chemical buffer in a low enthalpy system while these phases are not in equilibrium with the porewater. Indeed, as discussed by Gaucher et al. (2009), the measured K/Na ratio in fracture waters is 1.2×10^{-2} while a K/Na ratio of 2×10^{-3} is expected if K and Na contents in porewater are controlled by the solubility of microcline and albite phases. Furthermore, this model has resulted

in underestimations of K, Ca and Mg contents and overestimations of Na content and alkalinity, in comparison to fracture waters (Fig.6). The second model proposed by Beaucaire et al. (2008) considers cation exchange reactions with a one-site model to constrain Na and K contents. Cation exchange is known to control and buffer cation contents in clay-rocks porewater (Gaucher et al., 2009; Pearson et al., 2011) and predictions, including carbonates, were generally better. However, this one-site exchange model use selectivity coefficients obtained with the Gaines and Thomas (1953) relationship for Na/Ca and Na/Mg exchange (Waber and Mazurek, 1998) and with a four-sites exchange model for K exchange (Jacquier et al., 2004). Such election of model parameters was certainly made for obtaining a satisfactory reproduction of fracture water compositions but using parameters obtained with one kind of model with a model of different nature seems conceptually inadequate. The resulting K content is slightly overestimated (Beaucaire et al., 2008), even using a selectivity coefficient for K-exchange (log $K^{Na/K}$=1.5) which seems high for such a rock. One-site macroscopic selectivity coefficient (log $K^{Na/K}$), expressed following Gaines and Thomas (1953) convention, are of 1.2 to 1.35 for Tournemire clay-rock (cf. section 2.3), 0.8 for Mont-Terri Opalinus clay (Pearson et al., 2003), 0.8 to 1 for Paris basin Callovo-Oxfordian clay-rock (Tournassat et al., 2009) and slightly higher than 1 for illite pure phases (Tournassat et al., 2007). Using a lower selectivity coefficient for K-exchange will increase the over-estimation of K content in solution. A fitting of $K^{Na/K}$ can lead to the adequate concentration in solution but the model consequently loses its prediction ability (Pearson et al., 2011). This disparity between data and model results suggests a conceptual limit of K control by a one-site exchange model.

In the approach developed in this study, the contribution of the different clay minerals to cation exchange and the differences of cation behaviours with respect to these minerals are distinguished. Among the Tournemire clay-rock constituting minerals, illite and illite/smectite interstratified are the main phases implied in cation exchanges. Moreover, illite and smectite are considered respectively to cations exchange, assuming that illite/smectite mixed-layers are a mixture

of illite and smectite phases (Tournassat et al., 2009). Kaolinite implication in cation exchange is neglected as its contribution is limited in comparison to smectite or illite.

Cation exchange involving illite can be accurately represented with the multi-site model developed by Bradbury and Baeyens (2000). This macroscopic and non-electrical model considers the contribution of the different exchange site types on the illite surface as a function of the site amount and their affinities with the different cations. Introduction of sites of different affinities allows considering steric effects on bigger cations to reach lateral sites and lead to an efficient reproduction of monovalent cations interacting with illite. Such an approach has been mainly used to represent caesium uptake on illite, e.g. Baeyens and Bradbury (2004); Bradbury and Baeyens (2000); Grandia et al. (2011); Poinssot et al. (1999), but can also be used to consider the affinity and capacity influence of the different surface sites on cation behaviour in the system (Tournassat et al., 2007). The Bradbury and Baeyens (2000) model assumes three classes of surface sites for cation exchange on illite: i) the "planar sites" (Xp) associated to the fixed negative charge associated to isomorphic substitution in tetrahedral and octahedral layers. This kind of site represents 80% of the illite exchange capacity and presents a low affinity towards cations; ii) the "type-II sites" (Xii); and, iii) the "frayed edge sites", denote as FES (Xfes). Xii and Xfes classes of sites are high affinity low capacity sites and, because of steric effects, only imply monovalent cations. These exchange sites respectively represent 20% and 0.25% of the illite exchange capacity. Cation exchange reactions and their associated selectivity coefficients are summarized in Table 5.

Cation exchange reactions on the smectite phase are implemented in the model considering one low affinity high capacity surface site. Selectivity coefficients for exchange reactions in smectite surface site are determined using Tournassat et al. (2009) one-site model, allows the determining of selectivity coefficients for smectite as a function of the fractional equivalent occupancy, i.e. the exchanger composition. Model coefficients were calibrated against a large set of data and a successful reproduction of experimental selectivity coefficients was obtained

with the model. Exchange reactions and range of calculated smectite selectivity coefficients for the different measured exchangeable cation compositions are reported in Table 5.

In order to determine the amount of each sort of exchange sites, the proportion of charges associated with illite and smectite is first calculated from the rock content (in %) in illite and illite/smectite mixed-layers rich in illite. It is assumed that there is 70% of illite in the I/S mixed-layers and that the charge of smectite and illite are 0.75 and 0.2 $mmol_c.kg^{-1}$, respectively. The total amount of measured exchange sites, with the corresponding porosity and grain density, is converted in charges per mass of porewater. The amount of each sort of exchange site is then obtained by combination of the proportion of charges associated to illite and smectite, the proportion of each exchange site in illite as given in Bradbury and Baeyens (2000) model and by the sum of exchange sites. Exchanger composition is next calculated with the fractional occupancy.

Cations (Na, K, Ca, Mg and Sr) contents in porewater are thus controlled by cation exchange with the multi-site model previously presented and system description is completed considering calcite equilibrium, a Si control by quartz equilibrium and electroneutrality achievement on Na content. Concerning anions contents, Cl and SO_4 are considered as conservative, as they are not affected by precipitation/dissolution reactions due to the lack of chloride and sulphate bearing minerals and the low concentrations of these aqueous species, while C(IV) species are controlled by the CO_2 partial pressure which is fixed in the calculations. The pH is mainly controlled by calcite equilibrium and the CO_2 partial pressure fixed value. Formation reductive conditions are introduced in the model through the S(6)/S(-2) redox couple by forcing equilibrium with pyrite. Note that mineral phases considered in the model are all observed in the rock and petrologic observations indicate they are in equilibrium at in situ conditions. To summarize, the multi-site model proposed here introduces cation exchange according to the reactions presented in Table 5, thermodynamic equilibrium with calcite, quartz and pyrite mineral phases and fixed values of Cl and SO_4 contents and CO_2 partial pressure. Before performing the calculations

with this interaction model and in order to introduce an initial cation content in the range of the expected values, equilibrium between the solution and calcite, dolomite, illite, quartz, strontianite and kaolinite mineral phases is imposed. In these initial calculations, solution electroneutrality is achieved on Na concentration.

All calculations were performed with PHREEQC v2.17 (Parhurst and Appelo, 1999) geochemical calculation code, using sit.dat thermodynamic database, corresponding to the ANDRA ThermoChimie v7.b database (Duro et al., 2007).

Exchange reactions	log K	References
Illite planar site Xp		
$NaXp + K^+ = KXp + Na^+$	1.1	Bradbury and Baeyens (2000)
$2NaXp + Ca^{2+} = CaXp_2 + 2Na^+$	1.04	Baeyens and Bradbury (2004)
$2NaXp + Mg^{2+} = MgXp_2 + 2Na^+$	1.04	Baeyens and Bradbury (2004)
$2NaXp + Sr^{2+} = SrXp_2 + 2Na^+$	1.44	Missana et al. (2008)
Illite type II site Xii		
$NaXii + K^+ = KXii + Na^+$	2.1	Bradbury and Baeyens (2000)
Illite frayed-edge-site Xfes		
$NaXfes + K^+ = KXfes + Na^+$	2.4	Bradbury and Baeyens (2000)
Smectite site Z		
$NaZ + K^+ = KZ + Na^+$	0.82 - 0.88	Tournassat et al. (2009)
$2NaZ + Ca^{2+} = CaZ_2 + 2Na^+$	0.53 - 0.7	Tournassat et al. (2009)
$2NaZ + Mg^{2+} = MgZ_2 + 2Na^+$	0.47 - 0.62	Tournassat et al. (2009)
$2NaZ + Sr^{2+} = SrZ_2 + 2Na^+$	0.14 - 0.19	Tournassat et al. (2009)

Table 5: Exchange reactions for the different site classes for illite and smectite considered in the model and their associated selectivity coefficients in the Gaines and Thomas (1953) convention.

3.2. Calculations methodology

3.2.1. Comparison with experimental data and other models

The purpose of this section is to apply the multi-site model established in the previous section (3.1) to the Tournemire clay-rock and to compare the obtained results with the reference fracture water data (Table 4), considered as the best estimate of the Tournemire porewater composition. The BRGM model (Gaucher et al., 2009) is also applied to the Tournemire clay-rock and the results of the previous model based on mineral equilibrium (Beaucaire et al., 2008) are shown for comparison.

Models are applied with the clay-rock properties at the level of the URL access tunnel (Fig. 1), where 3 of the 4 fracture waters were sampled. Input parameters concern the mineralogy (with 70% of illite in the I/S mixed-layers), the cation exchange properties, the CO_2 partial pressure, the petrophysical parameters and the temperature (15 ℃). In order to compare our results with those of the Beaucaire et al. (2008) model, we have adopted the same convention for the representation of the content evolution as a function of the mobile anions sum ($[Cl^-]+2\times [SO_4^{2-}]$). The model parameters, fractional occupancy in particular, are not adjusted to salinity increase despite the frequently observed dependence of the exchanger composition to the salinity (Gaucher et al., 2006). Parameters variation with depth will be considered subsequently, for composition profile calculation.

Beaucaire et al. (2008) models for Tournemire clay-rock porewater were presented in section 3.1. Only results from model based on mineral equilibrium are represented in Fig.6. Indeed, the selectivity coefficients selection in their cation exchange model is based on expert judgement to fit the data. Consequently, the model loses its predictive ability and its comparison with the other models has little interest.

The BRGM model (Gaucher et al., 2009) considers equilibrium with the minerals identified as in equilibrium in the system conditions (quartz, calcite, siderite, pyrite, chlorite and illite) and cation exchange (Ca, Mg, Sr, and K related to

Na) on one global site for the clay-rock. The BRGM model considers that the CO_2 partial pressure value results from the mineral equilibrium. In order to apply the BRGM model to the Tournemire clay-rock, equilibrium with minerals like in Gaucher et al. (2009) reference model is considered, except for celestite (quartz, calcite, pyrite, illite-Mg and daphnite-14Å). The thermodynamic database used for these calculations is the version of the Thermoddem database (http://thermoddem.brgm.fr/index.asp) given in Gaucher et al. (2009) annex. PHREEQC v2.17 (Parhurst and Appelo, 1999) code was also used for the calculations with BRGM model. For cation exchange, the selectivity coefficients measured in the exchange experiment performed on the Tournemire clay-rock (cf. section 2.3) are considered. A-priori selectivity coefficients for one global exchange site can also be predicted for the clay-rock, considered as a mixture of illite and smectite minerals, using Tournassat et al. (2007) model to calculate illite selectivity constants and Tournassat et al. (2009) model for smectite constants. These predicted selectivity coefficients are used in the sensitivity analysis section.

3.2.2. Sensitivity analysis methodology

The sensitivity of the multi-site model is assessed to constrain and understand the model results. The sensitivity is mainly devoted to the analysis of the influence of the model parameters involved in the cation exchange and the effect of their uncertainties.

One of the uncertainties of the multi-site model concerns the proportion of sites shared by illite and smectite for cation exchange. In particular, a 70% of illite in I/S mixed-layers was considered previously, but mineralogical analysis indicate an illite proportion in I/S ranging between 50 and 90%. These two extreme values can be checked and will have an influence on the proportion of high affinity sites involved in cation exchange reactions.

Because exchangeable cations extraction experiments could present an uncertainty because of dissolution of clay-rock constituting minerals, a sensitivity analysis is performed on the exchange site composition. Variations of the K and

Na fractional occupancies (E_i) of ± 0.05 respectively to the base case are tested and their effects on porewater composition are evaluated. Changes in E_{Na} and E_K in these calculations are balanced by E_{Ca}, so that $\sum E_i = 1$.

The effects of changes in porosity are also evaluated, by using in the calculations the value of the gravimetric water content and of the total porosity and by comparing with the standard case calculations which used the anion accessible porosity. The porosity is used to convert the amount of exchange site in porewater mass (cf. section 3.1) and will consequently determine the concentration of exchange sites per volume of porewater.

Another parameter included in the sensitivity analysis on the multi-site model is the temperature. In this case, the model is applied to the whole formation where temperature varies from 24.2 to 10.7℃ from the base to the top of the Tournemire argillaceous formation. For the base case calculations the temperature was determined at 15℃, however in the present calculation case the temperature is 25℃.

The final part of this sensitivity analysis concerns the BRGM model results as a function of the cation exchange selectivity coefficients for the rock global site. Values measured on the Tournemire argillite and predicted from models and the rock content in illite and smectite are considered (Table 2).

3.2.3. Establishing the porewater composition profile

To establish the porewater composition profile across the Tournemire clayrock, the multi-site model is used considering as input data the variations in mineralogy, exchangeable cations, mobile anions content, porosity, grain density and temperature. The measured CO_2 partial pressure for lower Toarcian was used only for the lower Toarcian level. For all other levels we used the CO_2 partial pressure measured in the upper Toarcian as their proportions in carbonates minerals and organic matter are similar.

3.3. Results

3.3.1. Comparing model results with experimental data

Results obtained for the Tournemire clay-rock using the multi-site model, the BRGM model and the previous models are plotted versus the reference fracture waters in Fig.6. First of all, we can see that models based on cation exchange present a similar evolution trend for cations and carbonates content and for pH. Multi-site and BRGM models present a good agreement with the fracture waters. Their results are much better than the model only based on mineral equilibrium. In addition a slightly better agreement between model and data is obtained with the multi-site model developed here than with the BRGM model.

Potassium content evolution reproduction is improved by considering various sites associated to illite, including high affinity sites for monovalent cations. Special attention to the high affinity sites influence is paid in next section for a discussion on their importance.

The pH value also presents a dependence to the ionic strength, in both fracture waters and models results. Finally, concerning CO_2 partial content, a good agreement between BRGM model and measurements is observed. A PCO_2 value of $10^{-2.6}$ atm is obtained with the BRGM model, to compare with the $10^{-2.4}$ atm PCO_2 value measured for the Tournemire clay-rock and directly introduced in the multi-site model proposed in this study.

3.3.2. Sensitivity analysis results

The first parameter tested is this sensitivity analysis was the illite proportion in I/S mixed-layers (50%, 90% and 70% in the base case). Fig. 7 shows K content as a function of the mobile anions content for the different cases of illite proportion. It illustrates the importance of high affinity sites associated to illite for K control in the system. These calculations suggest that the proportion of illite in the Tournemire I/S mixed-layers could be higher than the selected 70% in the reference calculations. Our calculations indicate that a different proportion of illite and smectite associated sites has a very limited influence on other

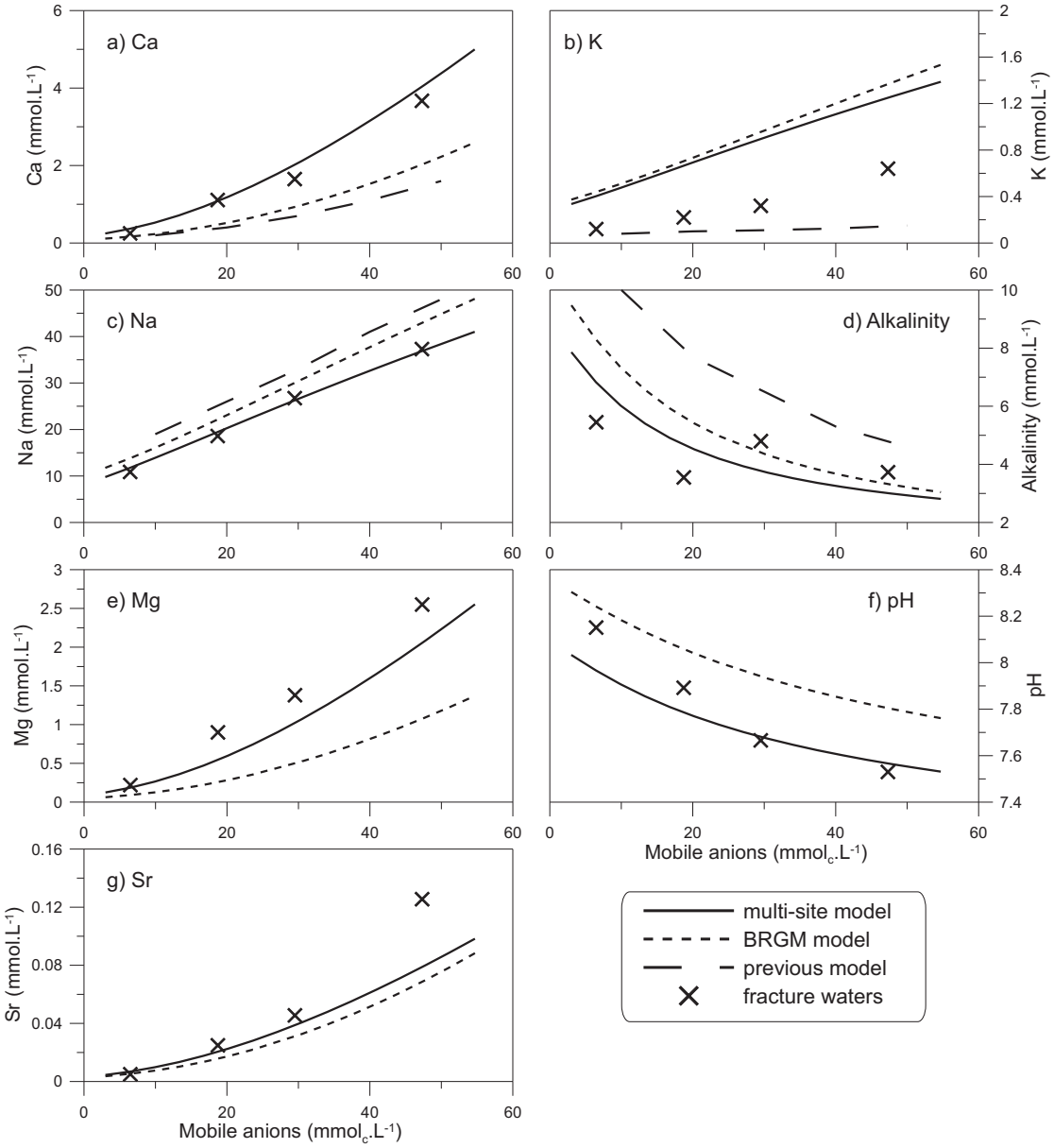

Figure 6: Models results and fracture waters for (a) Ca, (b) K, (c) Na, (d) Alkalinity, (e) Mg contents, (f) pH, and (g) Sr content evolution as a function of mobile anions content ($[Cl^-]+2\times[SO_4^{2-}]$).

porewater components.

Calculations to assess the results sensitivity to the exchanger composition were also performed. Potassium, sodium and calcium contents as a function of the mobile anions content for the ranges of fractional occupancies are represented in Fig.8. The results show that variations in the K fractional occupancy induce important changes in K content in solution and, in particular, fracture waters are better represented with a low E_K. However, E_K effect on the other components of the system, in particular for Na content, is limited. Concerning the influence of the sodium fractional occupancy, it is important for Na and Ca contents in the porewater and more restricted for K content. Changes in the concentration in Ca are related to the balance on E_{Ca} of variations of E_{Na} and E_K and consequently induce changes of the carbonate content in solution and the pH. The fractional occupancy appears to be the most sensitive parameter of the model, however the tested ranges of variation are relatively large and such variations are not observed across the argillaceous formation of Tournemire. It illustrates the importance to assess the non-perturbation of the exchangeable cations data to avoid non-negligible errors on the calculated water composition. The good representation of the experimental data with the base case conditions suggests exchangeable cations measurements are not perturbed by dissolution of Ca and Mg bearing minerals and that the measurements are representative of the in situ exchanger composition.

Very little and non significative differences are observed with porosity variations. The model is probably non-sensitive to rock/water ratio.

Regarding the sensitivity to the temperature, only carbonate content is affected by this change (Fig.7), and the pH in a limited extent.

The sensitivity of the BRGM model to the cation exchange selectivity was also investigated. The obtained porewater composition are represented in Fig. 9. Calculated Na content is higher than in the fracture waters when the measured selectivity coefficients are used and lower when the predicted coefficients are used. The opposite is observed for the Ca content calculations. Potassium content are overestimated in the two different calculation cases. Relatively im-

portant differences are found between results of the calculation cases due to large differences between measured and predicted exchange selectivity coefficients. Results obtained with the BRGM model are then in the range of the fracture water compositions but the accuracy of data reproduction seems relatively linked to the values of the selectivity coefficients. The adequate porewater composition can be obtained using a model with one global exchange site by considering selectivity coefficients calculated from the reference waters and the exchanger composition. Calculated selectivity coefficients are reported in Table 2. These values are in the range of the predicted ones for Na/Ca and Na/Mg exchanges. However, for Na/K exchange a much more higher value is found in comparison to the measured and predicted ones. The Tournemire porewater composition can then be accurately calculated (Fig. 9), once the exchange selectivity coefficients fits with in-situ experimental data.

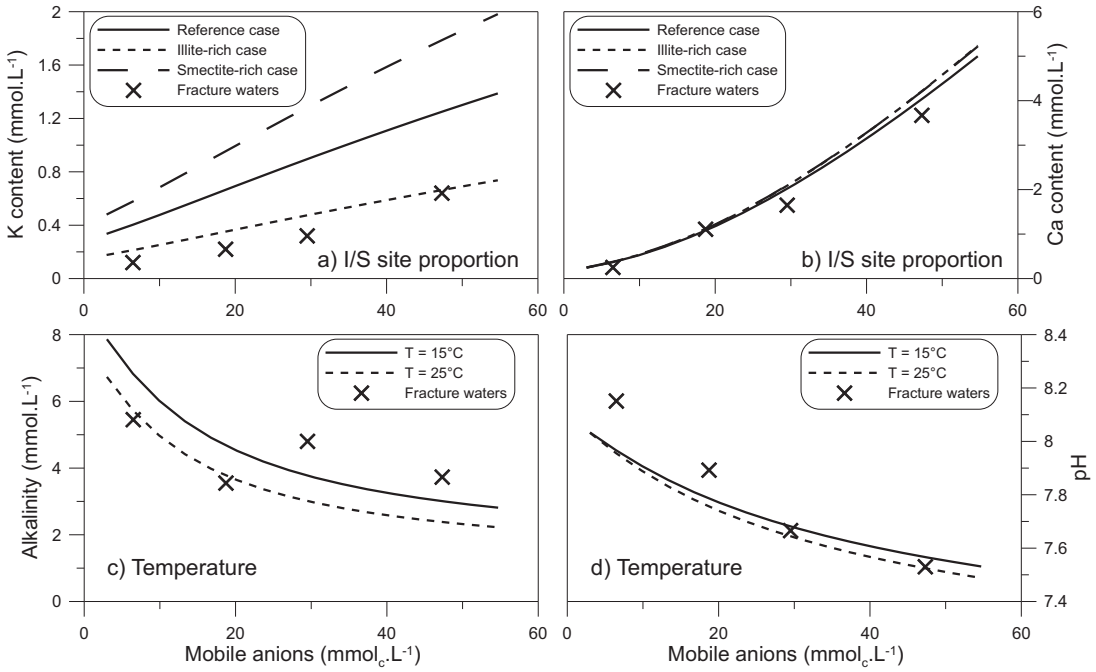

Figure 7: Sensitivity analysis results: influence of the proportion of illite in I/S mixed-layers on (a) K and (b) Ca contents; and influence of temperature on (c) alkalinity and (d) pH.

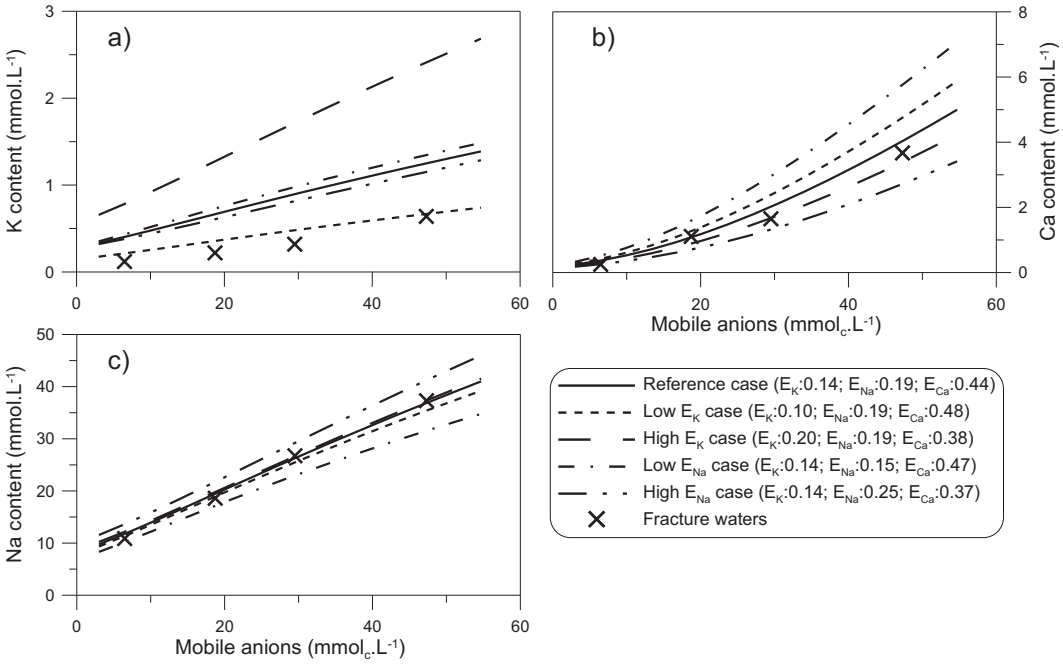

Figure 8: Results of the sensitivity analysis on the fractional occupancy of exchange sites: influence of variations in E_{Na} and E_K on the concentrations in (a) K, (b) Ca and (c) Na.

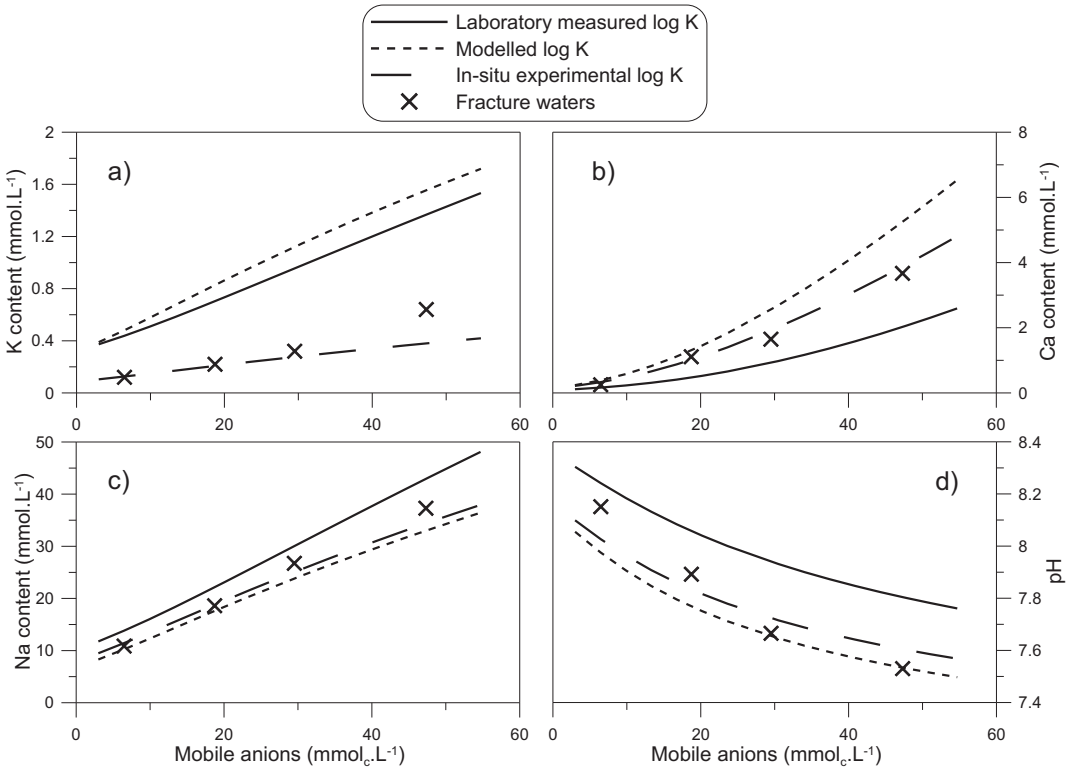

Figure 9: Results of the sensitivity analysis on the exchange selectivity coefficient in the BRGM model (see log K data in Table 2). Concentrations in (a) K, (b) Ca, (c) Na and (d) pH.

3.3.3. Obtention of the porewater composition profile

The porewater compositions calculated at different elevations across the Tournemire argillaceous formation (Table 6) allow establishing a profile (Fig.10). The composition profile follows the mobile anions and shows a bell-shape profile with a maximal concentration at the middle of the formation (salinity of 5.6 $g.L^{-1}$) and a gradual solute decrease towards the surrounding aquifers. pH varies between 7.35 and 7.9 across the formation, a typical range of values for a clay-rock porewater. The lowest pH values are observed in the Lower Toarcian, where the CO_2 partial pressure is higher.

Fracture waters were projected parallel to the stratification onto a PH4-PH5 vertical axis on Fig.10. This elevation corrections were made because of the slight inclination of the Toarcian/Domerian layer and assuming formation homogeneity in the bedding plane in order to compare the fracture water compositions with the model results. A good agreement is found between the calculated and the fracture water compositions for the same elevation. This agreement consolidates the profile obtained across the argillaceous formation with the multi-site model.

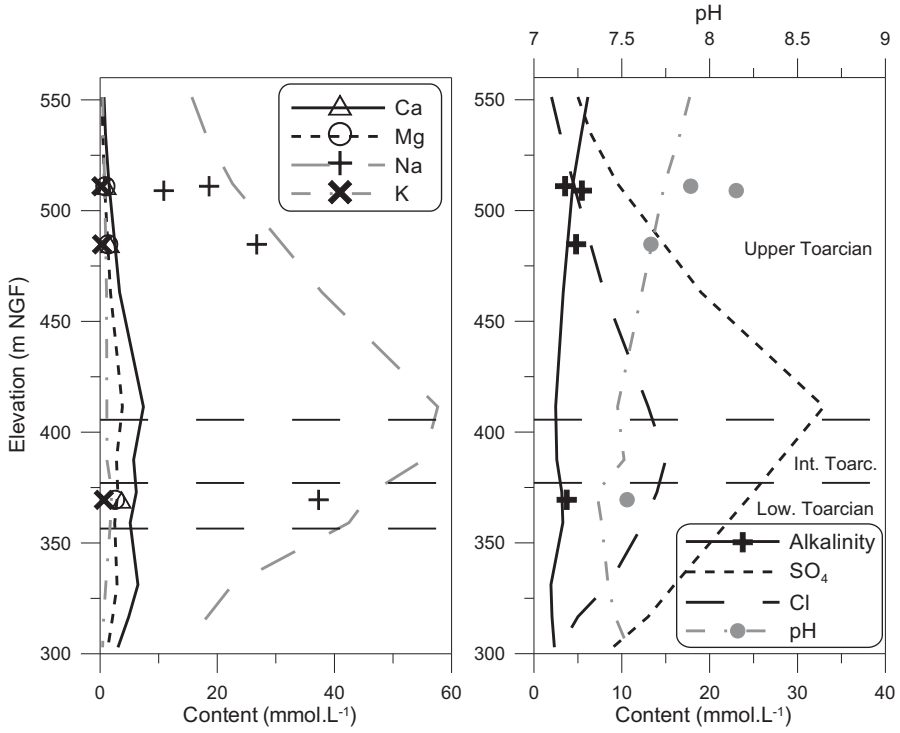

Figure 10: Porewater composition profile across the Tournemire clay-rock. Calculations were performed with the multi-site model and by using the measured clay-rock characterizing parameters. Reference fracture water compositions are also reported.

Elevation	pH	I	TDS	Alkalinity	SO_4	Cl	Ca	Mg	Na	K	Sr	Si
551.3	7.89	0.02252	1.35	6.14	5.00	2.00	0.68	0.33	15.66	0.43	0.01	0.12
534.4	7.83	0.02689	1.56	5.39	6.50	3.00	0.92	0.45	18.07	0.54	0.02	0.13
512.2	7.74	0.03548	1.99	4.43	9.50	4.50	1.50	0.75	22.60	0.77	0.03	0.13
463.1	7.61	0.06213	3.42	3.33	19.00	8.00	3.33	1.77	37.89	1.09	0.08	0.14
411.5	7.48	0.09985	5.57	2.47	33.00	13.00	7.38	3.80	57.65	1.15	0.15	0.15
387.5	7.51	0.09006	5.01	2.60	28.00	15.00	5.72	2.79	55.17	1.17	0.12	0.16
372.9	7.36	0.08233	4.59	3.17	25.00	14.00	6.18	3.01	46.36	1.99	0.22	0.16
359.1	7.38	0.07374	4.10	3.29	22.00	12.50	5.13	2.49	42.46	1.74	0.18	0.16
331.2	7.42	0.05383	2.86	1.94	16.00	8.50	6.46	2.89	22.60	0.97	0.09	0.17
316.7	7.46	0.04289	2.26	2.05	13.00	5.00	4.89	2.14	18.29	0.59	0.06	0.18
302.9	7.53	0.03086	1.62	2.33	9.00	3.00	3.04	1.33	14.09	0.42	0.04	0.18

Table 6: Composition and ionic strength (I) and salinity (TDS) profile across the Toarcian/Domerian argillaceous rock of Tournemire calculated with the multi-site model. Concentrations are in mmol.L^{-1}, the salinity in g.L^{-1} and the elevation in m NGF.

4. Discussion

The results obtained with the new model proposed for calculating the Tournemire porewater composition and based on multi-site cation exchange were compared with experimental data of the Tournemire clay-rock porewater, with a model previously developed for Tournemire clay-rock based only on mineral equilibrium (Beaucaire et al., 2008) and with an application of the BRGM model (Gaucher et al., 2009) to the Tournemire geochemical system. The best representations of the fracture waters composition are obtained with the model including a control of the cation concentration by cation exchange. Data representation is even improved when cation exchange model considers a refinement in the illite surface properties, including sites of different affinities on illite surface. Potassium control was discussed as the obtained K content was too low when controlled by a mineral phase (Beaucaire et al., 2008) and too high when controlled by cation exchange (Pearson et al., 2003), despite the studies of K/Na ratio in porewaters (Gaucher et al., 2009; Pearson et al., 2003) clearly indicate a control by cation exchange.

The uncertainty of one site cation exchange selectivity coefficients and their sensitivity towards the resulting porewater composition is most likely the main limit of this modelling approach. A complex dependence to system parameters is observed and Tournassat et al. (2009, 2007) proposed models to calculate selectivity coefficient value considering its dependence to fractional occupancy. The illite and smectite resulting selectivity coefficients were averaged and introduced as one global site in the BRGM model (Gaucher et al., 2009). One approach to achieve the representation of the cation contents, and particularly K content, is adjusting the exchange selectivity coefficient. It was done for the Tournemire argillite and a high value is obtained for Na/K exchange. In that case the model lost a large part of its prediction ability. From this analysis it can be inferred that there is no conceptual limit of K control by a one-site exchange model, as the model matches almost perfectly the data. However, the problem in this case is linked to the difficulty to define precisely the selectivity

coefficient for K on the exchanger either by generic predictive modelling or by independent experiment on clay fraction. The same holds true for Ca, Mg and Sr but in a lesser extent. It is surprising to see that even selectivity coefficient measured on the clay fraction ($< 2\mu$m) in chemical conditions similar to in situ conditions is not able to give very precise value. The $<2\mu$m fraction does not account for the whole exchange capacity of the rock, but less than 30% of the sum of exchangeable cations of the rock. This could explain for instance the slight difference observed for Ca, Mg and Sr selectivity coefficient. For K, the difference is important. The laboratory measured selectivity coefficient is in line with values reported for Callovian-Oxfordian and Mont-Terri fine clay fraction (Pearson et al., 2011; Tournassat et al., 2009) but the in-situ value (log $K^{Na/K}$=1.8) is much higher than those usually reported. The cause for this discrepancy is unknown: it could be linked to a difference between K affinity for the surface in dispersed suspension (laboratory case) and in compacted system (in situ). It has been shown that the affinity of montmorillonite for Cs increase at high compaction level (Van Loon and Glaus, 2008). However, no difference could be observed between crushed and intact Mont-Terri clay-rock material (Van Loon et al., 2009). Similarly, it would be very surprising that the difference in affinity for K between laboratory experiment and in situ determination is related to a difference of clay compaction. A second possible artefact could be due to the extractant used for cation exchange determination. While laboratory selectivity coefficients were obtained from Cobalthexamine extraction, in situ cation exchanger composition was obtained by CsCl extraction. It is possible that CsCl extraction had resulted in more efficient K removal from high energy sorption sites or that K from collapsed illite layers have been exchanged by Cs whereas it was not by CoHex.

A different modelling approach, by considering a multi-site modelling of cation exchange, was tested here. With regards to the successful data representation, it suggests the effectiveness of this approach for clay-rock porewater modelling. However it can not explain by itself the difference of global selec-

tivity coefficients obtained in situ and on Tournemire clay fraction. Additional experimental work would be needed (in particular systematic comparison of Co-Hex with CsCl extraction methods) to unravel this problem.

Sensitivity analysis performed on the multi-site model showed the robustness of the model. Interestingly, the analysis indicates not only a sensitivity to the exchanger composition but also to the proportion of illite in the illite/smectite mixed-layers. The proportion of illite in the I/S mixed-layers presents a range of uncertainty which affect the proportion of high affinity sites of illite. This effect is only noticeable on the potassium concentration and results suggest that illite proportion is perhaps higher than the average proportion indicated by the mineralogical data. The second sensitive parameter, the exchange composition, logically induces changes in the porewater composition. This sensitivity highlights the importance of using exchange cations data not affected by perturbation during their measurements. The porosity, which determines the density of exchange sites in contact with a porewater volume, has a very slight influence on the porewater composition. A limited influence was also distinguished by Wersin (2003), whereas Bradbury and Baeyens (1998) identified porosity as a sensitive parameter of their model.

The interest of the multi-site model developed in this paper is to consider cation exchange on the basis of the intrinsic properties of the clay-rock, i.e. on the exchange properties of the rock-constituting minerals, with the exchange sites proportion on illite surface and the selectivity coefficients for the mineral pure phases used in the model coming from the literature (Table 5). Exchange properties of the rock are then obtained by an average of the exchange properties of the mineral phases and the mineralogical composition. Thus, an experimental determination of the different exchange sites properties for the rock is not necessary. The interest is particularly noticeable when one wants to calculate the water composition across the formation and, then, will need a characterization of the geochemical system for the different levels of the formation. However the approach of the multi-site model introduces a dependance to the proportion of illite in the I/S mixed-layer, which can not be determined precisely. This

dependance is only significant for the K concentration, as seen in the sensitivity analysis.

Further requirements for applying the multi-site model are similar to the needs for other models for porewater composition calculation in argillaceous rocks. Sampling of water representative of the in situ conditions is made difficult by the physical constrains linked to the low permeability and high rock/porewater ratio. Appropriated methods must then be applied to obtain each data of the required data set. Non-perturbed porewater composition is also needed for model results comparison and model validation.

5. Conclusions

This paper aimed at presenting a new model to calculate the porewater composition of the Tournemire clay-rock. This model is based, among other processes, on cation exchange considering the different affinities of the exchange sites of illite and smectite rock-constituting minerals. For model application to the Tournemire clay-rock, a full data set characterizing its geochemical system was obtained. An evaluation of drilling and sampling perturbations of water from low transmissivity fractures was also performed as well as a selection of reference waters. This selection ensures comparison of the model results is made with a water composition representative of the porewater at in situ conditions. A good representation of the reference fracture waters was obtained with the multi-site model and with the BRGM model (Gaucher et al., 2009). However, the best representation was observed with the multi-site model. These results highlight the interest of considering the differences of illite exchange sites affinity (Bradbury and Baeyens, 2000). The multi-site model was next applied across the formation in agreement with the geochemical properties changes and a composition profile is obtained.

We can thus propose a porewater composition which can be directly used as a reference composition in studies dealing on interaction of engineered barrier system components with the Tournemire clay-rock. The composition profile

calculated across the Tournemire argillaceous formation will be useful in studies on transport and reactive-transport, in particular for studies on osmotic effects which required a reliable knowledge of porewater composition and its changes across the formation.

It is also worth noting that, with few modifications, the radionuclides retention capacity can be added to the model and the model can be used to study the effect of the release of radionuclides from a nuclear repository. Finally, an interesting perspective could be to test the model developed for Tournemire formation on other argillaceous formations.

References

Altmann, S., 2008. "Geo" chemical research: a key building block for nuclear waste disposal safety cases. Journal of Contaminant Hydrology 102, 174–179.

Ambert, M., Ambert, P., 1995. Karstification des plateaux et encaissement des vallées au cours du Néogène et du Quaternaire dans les Grands Causses méridionaux (Larzac, Blandas). Géologie de la France 4, 37–50.

Appelo, C.A.J., Van Loon, L.R., Wersin, P., 2010. Multicomponent diffusion of a suite of tracers (HTO, Cl, Br, I, Na, Sr, Cs) in a single sample of Opalinus Clay. Geochimica and Cosmochimica Acta 74, 1201–1219.

Arcos, D., Gimmi, T., Duro, L., Waber, H.N., 2004. Modelling of tracer behaviour and dominant reactions during the pore water chemistry (PC) experiment in the Opalinus Clay, Switzerland, in: 11th Water-Rock Interaction Congress, Saratoga Springs.

Baeyens, B., Bradbury, M.H., 2004. Cation exchange capacity measurements on illite using the sodium and cesium isotope dilution technique: Effects of the index cation, electrolyte concentration and competition: modelling. Clays and Clay minerals 52, 421–431.

Beaucaire, C., Michelot, J.L., Savoye, S., Cabrera, J., 2008. Groundwater characterisation and modelling of water-rock interaction in an argillaceous formation (Tournemire, France). Applied Geochemistry 23, 2182–2197.

Beaucaire, C., Pitsch, H., Toulhoat, P., Motellier, S., Louvat, D., 2000. Regional fluid characterisation and modelling of water-rock equilibria in the Boom clay Formation and in the Rupelian aquifer at Mol, Belgium. Applied Geochemistry 15, 667–686.

Bensenouci, F., 2010. Apport des traceurs naturels à la compréhension des transferts au sein des formations argileuses compactées. Ph.D. thesis. Université Paris-Sud 11.

Bertrand, L., Laviguerie, R., Cabrera, J., Matray, J.M., Savoye, S., 2002. Instrument for measuring pore pressure and permeability in low permeability rock, in: Clays in natural & engineered barriers for radioactive waste confinement, Andra.

Boisson, J.Y., Bertrand, L., Heitz, J.F., Moreau Le Golvan, Y., 2001. *In-situ* and laboratory investigations of fluid flow through an argillaceous formation at different scales of space and time, Tournemire tunnel, southern France. Hydrogeology Journal 9, 108–123.

Bradbury, M.H., Baeyens, B., 1998. A physicochemical characterisation and geochemical modelling approach for determining porewater chemistries in argillaceous rocks. Geochimica and Cosmochimica Acta 62, 783–795.

Bradbury, M.H., Baeyens, B., 2000. A generalised sorption model for the concentration dependent uptake of caesium by argillaceous rocks. Journal of Contaminant Hydrology 42, 141–163.

Cabrera, J., Beaucaire, C., Bruno, G., De Windt, L., Genty, A., Ramambasoa, N., Rejeb, A., Savoye, S., Volant, P., 2001. Projet Tournemire. Synthèse des programmes de recherche. Rapport DPRE/SERGD 01-19. IRSN.

Daumas, S., 2005. Caractérisation microbiologique d'eau de forages et d'argile sur le site de Tournemire. Rapport d'étude E.APR P 028306. BRGM.

De Cannière, P., Schwarzbauer, J., Höhener, P., Lorenz, G., Salah, S., Leupin, O., Wersin, P., 2011. Biogeochemical processes in a clay formation in-situ experiment: Part C–Organic contamination and leaching data. Applied Geochemistry 26, 967–979.

Delay, J., Trouiller, A., Lavanchy, J.M., 2006. Propriétés hydrodynamiques du Callovo-Oxfordien dans l'Est du bassin de Paris : comparaison des résultats obtenus selon différentes approches. C. R. Geosciences 338, 892–907.

Dohrmann, R., 2006. Cation exchange capacity methodology I: An efficient model for the detection of incorrect cation exchange capacity and exchangeable cation results. Applied Clay Science 34, 31–37.

Duro, L., Grivé, M., Domènech, C., Gaona, X., Colás, E., Montoya, V., Bruno, J., 2007. Development of the ThermoChimie thermodynamic database. ANDRA Report C.RP.0ENQ.07.0001.

ENRESA, 2008. NF-PRO Synthesis report on the chemical evolution of the barriers. Publicación técnica PT03-2008. ENRESA.

Fernandez-Garcia, D., Gomez-Hernandez, J.J., Mayor, J.C., 2007. Estimating hydraulic conductivity of the opalinus clay at the regional scale: Combined effect of desaturation and edz. Physics and Chemistry of the Earth 32, 639–645.

Gaines, G.I., Thomas, H.C., 1953. Adsorption studies on clay minerals. II. A formulation of the thermodynamics of exchange adsorption. Journal of Physical Chemistry 21, 714–718.

Gaucher, E., Blanc, P., Bardot, F., Braibant, G., Buschaert, S., Crouzet, C., Gautier, A., Girard, J.P., Jacquot, E., Lassin, A., Negrel, G., Tournassat, C., Vinsot, A., Altmann, S., 2006. Modelling the porewater chemistry of the CallovianOxfordian formation at a regional scale. Comptes Rendus Geoscience 338, 917–930.

Gaucher, E.C., Lassin, A., Lerouge, C., Fléhoc, C., Marty, N.C.M., Henry, B., Tournassat, C., Altmann, S., Vinsot, A., Buschaert, S., Matray, J.M., Leupin, O.X., De Craen, M., 2010. CO2 partial pressure in clayrocks: A general model, in: Water–Rock Interaction 13, Guanajuato (Mexico).

Gaucher, E.C., Tournassat, C., Pearson, F.J., Blanc, P., Crouzet, C., Lerouge, C., Altmann, S., 2009. A robust model for pore-water chemistry of clayrock. Geochimica et Cosmochimica Acta 73, 6470–6487.

Girard, J.P., Fléhoc, C., Gaucher, E., 2005. Stable isotope composition of CO_2 outgassed from cores of argillites: a simple method to constrain $\delta^{18}O$ of porewater and $\delta^{13}C$ of dissolved carbon in mudrocks. Applied Geochemistry 20, 713–725.

Grandia, F., Sena, C., Arcos, D., Molinero, J., Duro, L., Bruno, J., 2011. Quantitative assessment of radionuclide retention in the Quaternary sediments/granite interface of the Fennoscandian shield (Sweden). Applied Geochemistry 26, 679–687.

Horseman, S.T., Higgo, J.J.W., Alexander, J., Harrington, J.F., 1996. Water, Gas and Solute Movement Trough Argillaceous Media. Nuclear Energie Agency (NEA).

Jacquier, P., Ly, J., Beaucaire, C., 2004. The ion-exchange properties of the Tournemire argillite. I.Study of the H, Na, K, Cs, Ca and Mg behaviour. Applied Clay Science 26, 163–170.

Van der Kamp, G., Van Stempvoort, D.R., Wassenaar, L.I., 1996. The radial diffusion method-1. Using intact cores to determine isotopic composition, chemistry and effective porosities for groundwater in aquitards. Water Resources Research 35, 1815–1822.

Mathieu, R., Pagel, M., Clauer, N., De Windt, L., Cabrera, J., Boisson, J.Y., 2000. Paleocirculations in shales: a mineralogical and geochemical study of calcite veins from the Tournemire tunnel site (Aveyron, France). European Journal of Mineralogy 12, 377–390.

Matray, J.M., Savoye, S., Cabrera, J., 2007. Desaturation and structure relationships around drifts excavated in the well-compacted Tournemire's argillite (Aveyron, France). Engineering Geology 9, 1–16.

Missana, T., García-Gutiérrez, M., Alonso, U., 2008. Sorption of strontium onto illite/smectite mixed clays. Physics and Chemistry of the Earth 33, S156–S162.

Parhurst, D.L., Appelo, C.A.J., 1999. User's guide to PHREEQC (version 2) A computer program for speciation, batch-raction, one-dimensional transport, and inverse geochemical calculations. Water-Resources Investigations Report 99-4259. U.S. Geological Survey.

Patriarche, D., Ledoux, E., Michelot, J.L., Simon-Coinçon, R., Savoye, S., 2004. Diffusion as the main process for mass transport in very low water content argillites: 1. Chloride as a natural tracer for mass transport - Diffusion coefficient and concentration measurements in interstitial water. Water Resources Research 40, W01516.

Pearson, F.J., Arcos, D., Bath, A., Boisson, J.Y., Fernández, A.M., Gabler, H.E., Gaucher, E., Gaustchi, A., Griffault, L., Hernán, P., Waber, H.N., 2003. Geochemistry of water in the Opalinus Clay Formation at the Mont Terri rock laboratory. Technical Report 2003-03. Mont Terri Project.

Pearson, F.J., Tournassat, C., Gaucher, E.C., 2011. Biogeochemical processes in a clay formation in-situ experiment: Part E–Equilibrium controls on chemistry of pore water from the Opalinus Clay, Mont Terri underground research laboratory, Swisterland. Applied Geochemistry 26, 990–1008.

Poinssot, C., Baeyens, B., Bradbury, M.H., 1999. Experimental and modelling studies of caesium sorption on illite. Geochimica and Cosmochimica Acta 63, 3217–3227.

Sacchi, E., Michelot, J.L., Pitsch, H., 2000. Porewater extraction from argillaceous rocks for geochemical characterisation. Methods and interpretation. Report 66 2000 02. OCDE/NEA.

Savoye, S., Michelot, J.L., Witterbroodt, C., Altinier, M.V., 2006. Contribution of the diffusive exchange method to the characterization of pore-water in consolidated argillaceous rocks. Journal of Contaminant Hydrology 86, 87–104.

Stroes-Gascoyne, S., Sergeant, C., Schippers, A., Hamon, C.J., Nèble, S., Vesvres, M.H., Barsotti, V., Poulain, S., Le Marrec, C., 2011. Biogeochemical processes in a clay formation in-situ experiment: Part D–Microbial analyses–Synthesis of results. Applied Geochemistry 26, 980–989.

Tournassat, C., Alt-Epping, P., Gaucher, E.C., Gimmi, T., Leupin, O., Wersin, P., 2011. Biogeochemical processes in a clay formation in-situ experiment: Part F–Reactive transport modelling. Applied Geochemistry 26, 1009–1022.

Tournassat, C., Gailhanou, H., Crouzet, C., Braibant, G., Gautier, A., Gaucher, E.C., 2009. Cation exchange selectivity coefficient values on smectite and mixed-layer illite/smectite minerals. Soil Science Society of America Journal 73, 928–942.

Tournassat, C., Gailhanou, H., Crouzet, C., Braibant, G., Gautier, A., Lassin, A., Blanc, P., Gaucher, E.C., 2007. Two cation exchange models for direct and inverse modelling of solution major cation composition in equilibrium with illite surfaces. Geochimica and Cosmochimica Acta 71, 1098–1114.

Tremosa, J., 2010. Influence of osmotic processes on the excess-hydraulic head measured in the Toarcian/Domerian argillaceous formation of Tournemire. Ph.D. thesis. Université Pierre et Marie Curie, Paris 6.

Urios, L., Marsal, F., Pellegrini, D., Magot, M., 2010. Evidence and identification of microorganisms in argillite from Tournemire (France), in: 4th International meeting on Clays in natural & engineered barriers for radioactive waste confinement, Nantes (France).

Van Loon, L.R., Baeyens, B., Bradbury, M.H., 2009. The sorption behaviour of caesium on Opalinus Clay: A comparison between intact and crushed material. Applied Geochemistry 24, 999–1004.

Van Loon, L.R., Glaus, M.A., 2008. Mechanical compaction of smectite clays increases ion exchange selectivity for cesium. Environmental Science and Technology 42, 1600–1604.

Waber, H.N., Mazurek, M., 1998. Tournemire shale pore water composition: derivation from geochemical modeling. Technical Report. University of Bern.

Wersin, P., 2003. Geochemical modelling of bentonite porewater in high-level waste repositories. Journal of Contaminant Hydrology 61, 405–422.

Witterbroodt, C., Savoye, S., Jacquier, P., Beaucaire, C., Bensenouci, F., Pitsch, H., Gouze, P., Michelot, J.L., 2007. Comparison between radial diffusion and leaching for determining chloride and sulphate in Tournemire argillite porewater, in: 3rd International meeting on Clays in natural & engineered barriers for radioactive waste confinement, Lille (France).

List of Figures

List of Tables

Part IV

Characterization of osmotic processes in clay-rocks: Case study of Tournemire

Chapter 4

Chemical osmosis

4.1 Introduction

Chemical osmosis is a type of fluid flow already observed in natural shales with properties similar to those of the Tournemire argillite properties. Owing to its small pore-size, its clay minerals content and its moderate porewater salinity, a chemo-osmotic flow is expected to develop in the Tournemire clay-rock when submitted to a salinity gradient. The ability of a material to conduct a chemical osmotic flow is described through the chemo-osmotic efficiency, i.e. the coupling coefficient linking the chemical potential gradient to the fluid flow. On top of depending on the studied rock, the osmotic coefficient also depend on the medium conditions, mainly the solution composition.
Two complementary ways were proceeded for determining the chemical osmotic efficiency of the Tournemire clay-rock : by numerical reproduction of the anionic exclusion in the shale porosity, i.e. the mechanism responsible of chemical osmosis; and by experiments.
The first method, presented in section 4.2, consists in calculating the interactions between the charged solid surface and solutes in porewater using a triple-layer electrical model taking into account the interacting diffuse layers and solutions with complex compositions, i.e. with mono- and divalent counter-ions. This approach especially allows considering the effects of Ca^{2+} ions on the osmotic efficiency and to establish a profile of the chemo-osmotic efficiency across the Tournemire argillaceous formation.
Chemo-osmotic parameters were also determined by off-site experiments conducted on Tournemire argillite samples (section 4.3). The chemo-osmotic efficiency was estimated during measurements of an osmotic fluid flow induced by a chemical concentration gradient through a clay-rock sample.

Experiments allow determining if a chemo-osmotic flow can develop in the studied shale and also measuring an osmotic efficiency for specific conditions of pore-size and solution composition. Predicted chemo-osmotic efficiencies present the advantage to account for the petrophysical parameters and solution composition variations across the formation. Thus, we can dispose of a chemical osmosis efficiency profile, useful for, next, calculating the resulting osmotic flow in the overall Tournemire argillaceous formation.

4.2 Predictive calculations of the chemo-osmotic efficiency coefficient

4.2.1 Introduction

The physical explanation of the specific behaviour of clays systems mainly lies in surface processes, related to large specific area, small size of particles and pores and complex interactions between the clay surface, the water molecules and the solutes. In particular, understanding transport processes in natural argillaceous media requires considering the interactions between clay minerals and the pore solution [69, 103]. Isomorphic substitutions in the tetrahedral (Si^{4+} by Al^{3+}) and the octahedral (Al^{3+} by a divalent cation) layers and protonation/deprotonation reactions of surface groups induce an electrical charge at the clay mineral surface. This surface charge is generally negative [143], and leads to the development of an electric field. The ions distribution in the pore space consequently results from two opposite effects: the counterions attraction by the surface charge and their diffusion from the ion accumulation zone at the surface vicinity towards the pore center [103]. Models are developed to estimate the incidence of these surface processes on transport processes, by the calculations of the coefficients relating a flux to a driving force. They are complementary to experiments in the characterization of coupled-flow in a charged porous media. Two kinds of models can be used for obtaining the coupling coefficients: phenomenological models, based on the thermodynamic of irreversible processes [22, 76]; and mechanical models, which homogenize coupled-flow equation at the pore scale to the REV (Representative Elementary Volume) scale [64, 107, 130].
The goals of this chapter are to investigate the influence of a complex solution with both monovalent and divalent counterions on osmotic efficiency and to calculate theoretical values of the osmotic efficiency for the Tournemire argillaceous formation. To reach this goal, an electrical triple-layer-model (TLM) including interaction between diffuse layers was improved to consider multi-ionic solutes and non-symmetric solutions.

4.2.2 Expression of the coefficient of chemical osmosis

Chemical osmosis occurs in clay-rocks because of anion exclusion and disequilibrium of the internal pressure of the solution by salinity changes [46, 69, 81]. Anion exclusion of clays lies on ionic transport restrictions by size and/or by electrical effects (and salinity, consequently). Anion exclusion will be particularly efficient when a clayrock is highly compacted and the adjacent electrical diffuse layers overlap. Thus, pore size and salinity will control the membrane behaviour of the clay and its osmotic efficiency coefficient. A simple relation for the osmotic efficiency, ε, can then be proposed, related to the proportion of the concentration of anions in the porosity, $\overline{C-}$, and in bulk water, C_f [22, 27, 83]:

$$\varepsilon = 1 - \frac{< \overline{C-} >}{C_f} \tag{4.1}$$

where $< \overline{C-} >$ is the mean concentration of anions in the porosity. The osmotic efficiency coefficient is calculated in the triple-layer-model developed in next section according to the expression developed by Bolt *et al.* [22] (see also Rousseau-Gueutin [135]). This expression is obtained from the resolution of the Navier-Stokes's equation integrating the chemical force [22], for a porous medium with a parallel plane geometry:

$$\varepsilon = \frac{\int_0^b (1 - \frac{\overline{C-}(x)}{C_f})(2bx - x^2)dx}{\frac{2b^3}{3}} \tag{4.2}$$

where $\overline{C-}(x)$ is the anion concentration at a distance x from the clay surface and $2b$ is the pore size. Note that Eq.(4.1) is a simplification of Eq.(4.2) if $\overline{C-}$ is set to its average and constant value. It is worth noting that anion exclusion expression is applicable for both symmetric and non-symmetric solutions [22].

Pore size, $2b$, appears to be a crucial parameter for the chemical osmotic efficiency determination (Eq. 4.2) and, then, in the TLM calculations. It is determined using a mass balance [58, 110, 116]. For clay-rocks, the mass balance is established for a plane-parallel geometry:

$$b = \frac{\omega}{\rho_s A_s (1 - \omega)} \tag{4.3}$$

where b is the half-pore size (m), ω is the total porosity, ρ_s is the grain density (g m^{-3}) and A_s is the specific surface area (m^2 g^{-1}).

4.2.3 A triple-layer-model with interacting diffuse layers including multi-ionic counterions distribution

The electrical model developed here to describe the ions distribution in the porosity of a clay-rock is an improvement of the Avena and De Pauli [10] double-layer-model (DLM) and Leroy and Revil [89] triple-layer-model (TLM), modified by Gonçalvès *et al.* [59]. The DLM is based on the Gouy-Chapman theory, where the counterions are distributed in the vicinity of the charge surface as a diffuse layer, according to a Boltzmann distribution. The TLM is based on the Stern-Grahame theory, which introduced a compacted layer of bound counterions between the surface and the diffuse layer, the Stern layer. Treatment of ions as particles of finite size in Stern-Grahame theory, rather than point charges in the Gouy-Chapman theory, allows considering high ion concentration near the surface [69]. TLM modification by Gonçalvès *et al.* [59] consists in considering the interaction of adjacent diffuse layers, by a truncation of these layers, because of the weak pore size in such rocks. It appears particularly important to consider the interaction of diffuse layers in complexation models for osmotic efficiency determination as osmosis results from diffuse layers overlapping. Gonçalvès *et al.* [59] truncated TLM considers a symmetric solution (e.g., NaCl), but natural waters present more complex compositions with various cations and anions of different valences. Such solutions can now be considered by following Leroy *et al.* [90] approach which allows exchange of diverse cations on surface sites. Let's detail the resulting model.

A schematic view of solid surface–solution interactions in case of diffuse layers overlap is depicted in Fig. 4.1. It allows identifing two compact layers, limited by the Inner and the Outer Helmoltz Plane (IHP and OHP), corresponding to the Stern layer and are constituted by ions strongly sorbed at the mineral surface. Diffuse layer starts at the OHP and is limited by the interaction with the diffuse layer of another clay mineral particle. The diffuse layers overlapping is essential to explain processes such as chemical osmosis [27] or disjoining pressure [39].
Model considers the surface sites linked to the permanent negative charge due to isomorphic substitutions and the variable charge hydroxyl surface sites of protonation/deprotonation. Permanent exchange surface sites are represented here as X sites and each site carries one negative charge X^-. The exchange half-reactions with their respective reaction constant involving Na^+, Ca^{2+} and H^+ are:

$$XNa = X^- + Na^+, K_{Na} \tag{4.4}$$

$$X_2Ca = 2\,X^- + Ca^{2+}, K_{Ca} \tag{4.5}$$

$$XH = X^- + H^+, K_H \tag{4.6}$$

The surface site density Γ_i^0 (in sites.m^{-2}) for each species i is expressed from the reaction constant expressions, using the Gaines and Thomas [49] convention:

$$\Gamma^0_{XH} = \frac{\Gamma^0_{X^-} a_{H^+}}{K_H} \tag{4.7}$$

$$\Gamma^0_{XNa} = \frac{\Gamma^0_{X^-} a_{Na^+}}{K_{Na}} \tag{4.8}$$

$$\Gamma^0_{X_2Ca} = \frac{(\Gamma^0_{X^-})^2\, a_{Ca^{2+}}}{K_{Ca}} \tag{4.9}$$

where a_i is the activity of species i. The $\Gamma^0_{X^-}$ expression is obtained using the total surface site density of the X sites, Γ^0_3, by the Newton method:

$$\Gamma^0_3 = \Gamma^0_{X^-} + \Gamma^0_{XH} + \Gamma^0_{XNa} + \Gamma^0_{X_2Ca} \tag{4.10}$$

Γ^0_1 and Γ^0_2 correspond to the total surface site density of aluminol and silanol hydroxyl sites, obtained from the following complexation reactions:

$$AlOH_2^{1/2+} = AlOH^{1/2-} + H^+, K_1 \tag{4.11}$$

$$SiOH_2^{1/2+} = SiOH^{1/2-} + H^+, K_2 \tag{4.12}$$

The surface charge density of the clay minerals Q_0 (C m^{-2}) is obtained, using the surface site density, by the following equation:

$$Q_0 = -e[\frac{1}{2}(\Gamma^0_{AlOH_2^{1/2+}} - \Gamma^0_{AlOH^{1/2-}} + \Gamma^0_{SiOH_2^{1/2+}} - \Gamma^0_{SiOH^{1/2-}}) - \Gamma^0_3] \tag{4.13}$$

The charge density in the Stern layer Q_β can be expressed as:

$$Q_\beta = e(\Gamma^0_{XNa} + 2\Gamma^0_{X_2Ca} + \Gamma^0_{XH}) \tag{4.14}$$

Potentials in the IHP and the OHP drop linearly and are related to the charge densities by the relationships:

$$\varphi_0 - \varphi_\beta = Q_0/C_1 \tag{4.15}$$

$$\varphi_\beta - \varphi_d = Q_S/C_2 \tag{4.16}$$

where φ_0, φ_β and φ_d are, respectively, the electrical potentials (V) at the surface, at the β plane and the d plane (see Fig. 4.1 for variables). C_1 and C_2 are the capacities (F m^{-2}) between the surface and the IHP and between

the IHP and the OHP, respectively.
In the diffuse layer, the electrical potential and the ions concentration are obtained by the Poisson-Boltzmann equation. The charge density in the diffuse layer Q_S is written as follows, for a solution with N species i and a distance from the mineral surface x_d to b, i.e. from the OHP to the truncation plane:

$$Q_S = \int_{x_d}^{b} \sum_{i=1}^{N} \frac{C_i^f \gamma_i^f}{\gamma_i} \, e \, z_i \, exp\Big(- \frac{z_i e \varphi}{k_B T} \Big) dx \tag{4.17}$$

where e is the elementary charge (1.6×10^{-19} C), k_B is the Boltzmann constant (1.38×10^{-23} J K^{-1}), T is the temperature (K), z_i is the valence of the ion i and C_i^f is the concentration of species i in the equilibrium solution (ions m^{-3}, related to mol L^{-1} by the Avogadro number). This concentration C_i^f is the concentration in the porous media out of the electrostatic field influence and corresponds to the concentration obtained by a classical geochemical model; e.g., Gaucher *et al.* [53]. γ_i^f and γ_i are the activity coefficients, calculated with the Davies [37]'s equation, in the equilibrium solution and in the diffuse layer, respectively. Davies [37]'s equation can be used for solutions with salinity lower than 0.7 M [87], i.e. up to seawater salinity.
The last equation of the TLM is a global electroneutrality equation:

$$Q_0 + Q_\beta + Q_S = 0 \tag{4.18}$$

Once the TLM equations are established, a selection of parameters has to be performed, by estimation and calibration versus experimental data. This selection is made for natural clay-rocks, for which smectite and illite minerals mainly control the surface processes. Contribution of other minerals to surface processes is neglected.
The first parameters are the surface site densities Γ_1^0, Γ_2^0 and Γ_3^0. The surface site density of aluminol sites, Γ_1^0, is here set to 0, as these sites are encountered in kaolinite but are absent in 2:1 clay minerals. The surface site density with permanent charge Γ_3^0 is obtained from the CEC (mol$_c$ kg^{-1} and the specific surface area, A_s (m^2 g^{-1}) [10]:

$$\Gamma_3^0 = \frac{CEC \cdot F}{A_s \cdot e} \tag{4.19}$$

where, F is the Faraday number.
Hydroxyl groups represent between 5 and 20% of the surface groups on smectite [10, 23, 147] and, thus, the Γ_2^0 value is set between 5 and 20% of Γ_3^0 value.

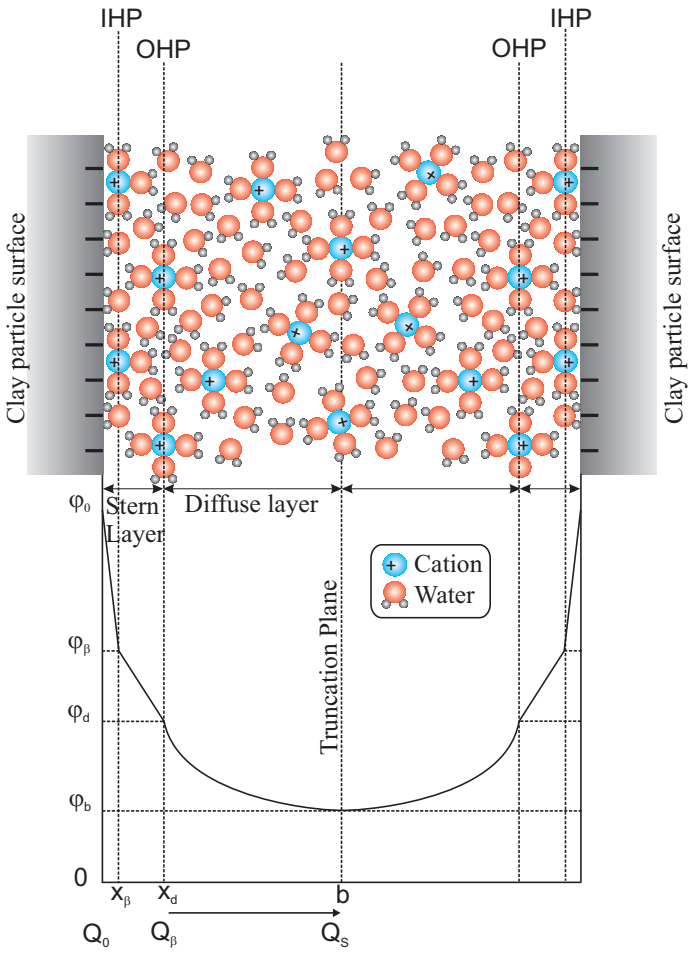

Figure 4.1: Schematic representation of solution - mineral surface interaction and associated electrochemical variables (electrical potentials φ_i and surface charges Q_i) in the TLM with interacting diffuse layers [58].

Exchange and protonation/deprotonation reactions constants are also introduced in the calculations, using available values from the literature [9, 52, 59, 89].
Last parameters need in the TLM are the capacities C_1 and C_2, which are calibrated in the range of expected values. Capacities are physically constrained by the inner and outer Stern layers thickness, by the relationships:

$$x_\beta = \frac{\epsilon_0 \epsilon_D^1}{C_1}, x_d - x_\beta = \frac{\epsilon_0 \epsilon_D^2}{C_2} \tag{4.20}$$

where, x_β and $x_d - x_\beta$ are the thickness of the inner and outer Stern layers, respectively (see Fig. 4.1), ϵ_0 is the vacuum permittivity (8.85×10^{-12} F m^{-1}) and ϵ_D^1 and ϵ_D^2 are, respectively, the dielectric constants for the inner and outer Stern layers. Stern layer thickness is about 1 nm and x_d^1 about 0.35 nm [67, 103]. Dielectric constants present some variations in the literature: ϵ_D^1 is found equal to 6 by Hiemstra and Van Riemsdijk [67], ranges between 6 and 30, according to Elimenech *et al.* [44], or between 10 and 15 [57]. ϵ_D^2 is found to range between 50 and 78 [57] or between 6 and 78 [67]. Taking into consideration the uncertainty on the dielectric constants and the limitations imposed by the Stern layer thickness [67], capacities C_1 and C_2 are calibrated against experimental data.

The TLM for multi-ionic solutions with interacting diffuse layers allows calculating the osmotic efficiency using Eq.(4.2. TLM predictions are calibrated against osmotic efficiency data of various natural clay-rocks in a NaCl-clay system (Fig. 4.2). Resulting parameters are listed in Table 4.1. As observed by Gonçalvès *et al.* [59], the most sensitive parameters are K_{Na} and C_2. It is also worth noting that the model does not converge for high salinity and calculations are thus limited to a range of concentratios, which, nevertheless, covers most of the natural waters.

4.2.4 Effect of mixed Na^+/Ca^{2+} solutions on the osmotic efficiency

Theoretical and experimental studies of chemical osmosis in pure clays and argillaceous rocks found in the literature (e.g., Bresler [27]; Neuzil and Provost [110]) are made for a pure NaCl-clay or $CaCl_2$-clay system, but not for complex solutions with both monovalent and divalent solutes, like in natural waters. Osmotic efficiency ought to be strongly dependent on this variable composition. The osmotic efficiency coefficient is observed to be lower with Ca^{2+} than with Na^+ [27], but the evolution trend of the

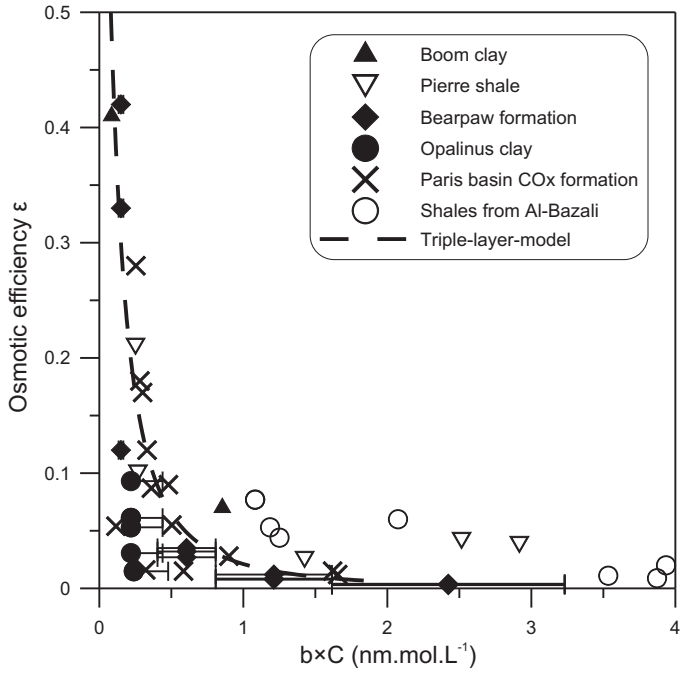

Figure 4.2: Model and data from several argillaceous formations of chemo-osmotic efficiency coefficient in function of $b \times C$ for a NaCl-clay system. Data references: Oligocene Boom clay [51], Cretaceous Pierre shale [1, 50, 116], Cretaceous Bearpaw formation [32, 66], Jurassic Opalinus clay [19, 68], Paris basin Callovo-Oxfordian (COx) formation [136, 137] and shales from Al-Bazali [1, 110].

Parameters	Natural clay-rocks values
Γ_1^0 (sites nm^{-2})	0
Γ_2^0 (sites nm^{-2})	0.52
Γ_3^0 (sites nm^{-2})	2.58
K_1	—
K_2	1.3×10^{-6}
K_H	1×10^{-2}
K_{Na}	1.3×10^{-1}
K_{Ca}	5×10^{-3}
C_1 (F m^{-2})	1
C_2 (F m^{-2})	0.2

Table 4.1: TLM parameters for natural clay-rocks.

osmotic efficiency coefficient of a clay-rock from a Na^+ end-member solution to a Ca^{2+} end-member solution is unknown. Indeed, no experimental data describing the osmotic efficiency for mixed Na^+ / Ca^{2+} solutions are available in the literature.

In order to investigate the evolution of the coefficient of chemical osmotic efficiency for various mixed Na^+ / Ca^{2+} solutions, calculations of the osmotic efficiency are performed for different solution compositions with the TLM developed in the previous section. Changes in solution composition are introduced according to a molal ratio $2\times Ca^{2+}$ / (Na^+ + $2\times Ca^{2+}$) which varies between 0, for a pure Na^+ solution, to 1, for a pure Ca^{2+} solution. Figure 4.3 shows osmotic efficiency values as a function of the ratio $2\times Ca^{2+}$ / (Na^+ + $2\times Ca^{2+}$) and of the product $b \times C$ of the half pore size, b (in nm), and the concentration in chloride in the bulk solution, C (in mol L^{-1}). This graph illustrates the osmotic efficiency drop when salinity and pore size increase and when counterions are Ca^{2+} and not Na^+. It corresponds to the commonly reported osmotic efficiency evolution. At large pore size anionic exclusion is weak and at high bulk concentration, the electrical double layer collapses yielding again a weak anion exclusion. According to our calculations, clay-rock osmotic efficiency strongly decreases for mixed Na^+ / Ca^{2+} solutions even at low content in Ca^{2+} in comparison to purely Na^+ solutions. Furthermore, elevate osmotic efficiency, i.e. ε close to 1, can not be reached for high Ca^{2+} contents in solution. These observations suggest that introduction of Ca^{2+}, even at low amounts, in a Na-clay system will induce a dramatic decrease of osmotic efficiency and a weakening of the clay membrane behaviour. It also implies that an osmotic efficiency experimentally determined with NaCl solutions will probably overestimate the osmotic

efficiency involved in fluxes in natural conditions.

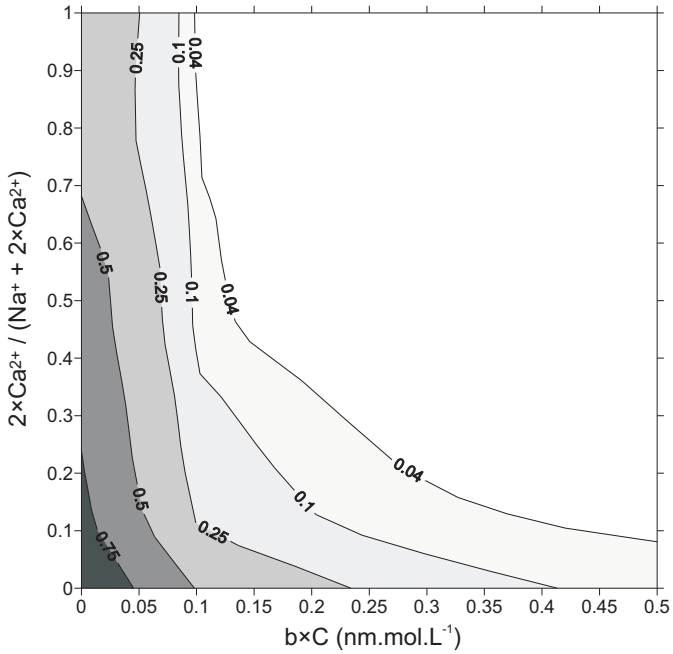

Figure 4.3: Evolution of chemo-osmotic efficiency coefficient calculated with the TLM as a function of $2\times Ca^{2+}/(Na^{+} + 2\times Ca^{2+})$ and $b \times C$.

4.2.5 Predictive calculations of chemo-osmotic efficiency for the Tournemire clayrock

The TLM is now applied to the Tournemire argillaceous rock for obtaining an osmotic efficiency profile. For these predictive calculations, the profiles in the z-axis direction of porewater composition and pore size are necessary.

The porewater composition profile was obtained in Chapter 3 by geochemical modelling of the clayrock–porewater interactions. It included cation exchange considering the different proportions and affinities of the exchange sites of the rock-constituting minerals and equilibrium with some mineral phases and with the measured in situ $CO_2(g)$ partial pressure. The identification of the porewater composition profile also required a full characterization of the Tournemire clayrock geochemical system. The porewater composition obtained with such a geochemical model corresponds to the equilibrium solution composition used in an electrical model, i.e. the water not affected by the electrical field influence of the charged surface of

clay minerals.
In the calculations of the osmotic efficiency of Tournemire clayrock, for the sake of simplicity and to avoid introducing even more uncertainties in the TLM, the equilibrium solution is assumed to be only composed of Cl^-, Na^+ and Ca^{2+} solutes. All monovalent cations being considered as Na^+ and divalent cations as Ca^{2+}. Solution electroneutrality is achieved on Cl^-. The resulting input composition is reported in Table 4.3, as well as the $2\times Ca^{2+}$ / ($Na^+ + 2\times Ca^{2+}$) ratio.

The pore size is calculated using Eq.(4.3), from the porosity, the grain density and the specific surface area. These parameters were determined on samples from PH4 and PH5 boreholes, at the Tournemire URL during the boreholes drilling for the porosity, at IRSN and Etudes Recherches Matériaux (ERM) facilities in Fontenay-aux-Roses and Poitiers, respectively, for the grain density and at ERM facilities for the specific surface area.
The total porosity is defined as the ratio of the pore volume to apparent volume and is determined by the method reported in Matray *et al.* [98] based on measurements of water content and volume. The grain density is obtained by helium pycnometry, which consists in measuring the He gas volume displaced by a dried mass of clayrock. The specific surface area is determined by the Brunauer, Emmett and Teller (BET) method from the linear part of the nitrogen adsorption isotherm. It consists in measuring the adsorbed volume of nitrogen as a function of the gas relative pressure in a pressure range of 0.05 to 0.25 at liquid nitrogen temperature (77K), corresponding to the domain in which one monolayer of nitrogen molecule is adsorbed [28].
These parameters values — an average from various samples for the porosity and the grain density — for different levels in the Toarcian and the Domerian are reported in Table 4.2. The resulting pore size is also reported. It is homogeneous across the formation, except for the lower Toarcian that exhibits higher values.

The porewater composition and the pore size are thus introduced as input parameters in the TLM previously developed to account for multi-ionic counterions and interacting diffuse layers and calibrated versus osmotic efficiency of natural argillaceous rocks (see section 4.2.3 and Table 4.1).
A profile of osmotic efficiency is calculated and reported in Table 4.3. The calculated osmotic efficiency presents variations across the Tournemire argillaceous formation with lower values (less than 0.1) in the lower Toarcian and higher values (around 0.5) in the more elevated part of the upper Toarcian. The effect of the concentration on the osmotic efficiency seems to be the most

important since the osmotic efficiency profile globally follows the concentration profile. Indeed, ε exhibits higher values for the lower concentrations and lower values for the higher concentrations. However the effect of the pore size also act as the lower osmotic efficiency is obtained for the lower Toarcian which shows the higher pore size. Finally, the effect of the third recognized parameter of influence on the osmotic efficiency, i.e. the ratio of the content of divalent to monovalent cations, is also observed. The ratio $2\times Ca^{2+}$ / (Na^{+} + $2\times Ca^{2+}$) increases with depth from 0.1 to 0.4 thus explaining why the osmotic efficiency is higher in the upper Toarcian than in the Domerian despite the similar porewater concentrations and pore sizes.

Formation unit	Elevation	ω_{tot}	ρ_s	A_s	b
upper Toarcian	551.3	0.111	2.732	28	1.64
upper Toarcian	534.4	0.111	2.721	25	1.84
upper Toarcian	512.2	0.111	2.723	24	1.91
upper Toarcian	463.1	0.096	2.709	23	1.71
upper Toarcian	411.5	0.084	2.735	22	1.52
intermediate Toarcian	387.5	0.100	2.734	25	1.63
lower Toarcian	372.9	0.047	2.424	5	4.06
lower Toarcian	359.1	0.027	2.385	5	2.32
Domerian	331.2	0.082	2.740	22	1.48
Domerian	316.7	0.077	2.733	23	1.34
Domerian	302.9	0.085	2.737	26	1.30

Table 4.2: Calculation of the half-pore size b (nm) from petrophysical parameters. ω_{tot} is the total porosity, ρ_s is the grain density (g cm^{-3}) and A_s is the specific surface area (m^2 g^{-1}). Elevation is in m NGF.

Formation unit	Elevation	C^f_{Cl}	C^f_{Na}	C^f_{Ca}	$\frac{2\times Ca^{2+}}{Na^{+}+2\times Ca^{2+}}$	b	ε
upper Toarcian	551.3	1.83E-02	1.61E-02	1.13E-03	0.12	1.64	0.513
upper Toarcian	534.4	2.15E-02	1.86E-02	1.50E-03	0.14	1.84	0.425
upper Toarcian	512.2	2.81E-02	2.34E-02	2.38E-03	0.17	1.91	0.323
upper Toarcian	463.1	4.95E-02	3.90E-02	5.23E-03	0.21	1.71	0.204
upper Toarcian	411.5	8.16E-02	5.88E-02	1.13E-02	0.28	1.52	0.104
int. Toarcian	387.5	7.37E-02	5.63E-02	8.67E-03	0.24	1.63	0.129
lower Toarcian	372.9	6.74E-02	4.84E-02	9.35E-03	0.28	4.06	0.025
lower Toarcian	359.1	6.00E-02	4.42E-02	7.78E-03	0.26	2.32	0.085
Domerian	331.2	4.26E-02	2.36E-02	9.52E-03	0.45	1.48	0.127
Domerian	316.7	3.32E-02	1.89E-02	7.21E-03	0.43	1.34	0.206
Domerian	302.9	2.34E-02	1.45E-02	4.55E-03	0.39	1.30	0.317

Table 4.3: Establishment of the profile of osmotic efficiency ε with the multi-ionic TLM. The input parameters are the equilibrium concentration in Cl^-, Na^+ and Ca^{2+} (C^f_i, in mol L^{-1}) and the half-pore size (b, in nm). The elevation is expressed in m NGF.

4.2.6 Conclusion

This chapter aimed at predicting the osmotic efficiency of the Toarcian / Domerian argillaceous formation of Tournemire considering the natural factors of influence on the osmotic efficiency. An electrical triple-layer-model (TLM) [59, 89] describing interactions between the charged surface of clay minerals and a solution with electrolytes was improved to account for multi-ionic solutions and study the effects of monovalent and divalent cations on the osmotic efficiency of natural clay-rocks.
Upon calibration, the model was tested as a function of the proportion of divalent and monovalent cations in the solution, the salinity and the pore size. The influence of the salinity and the pore size, the two well established influent parameters on the osmotic efficiency, was recognized in our results. Furthermore, a decrease of the osmotic efficiency was predicted with the introduction of Ca^{2+} in a Na^{+}–clay system. This decrease is observed even at low proportions of divalent cations. This loss of efficiency of clay membranes with divalent cations appears particularly important for calculations of osmotic flows in natural clayrocks since porewaters are constituted of both monovalent and divalent cations in shales. This effect and its implication on abnormal pressures is studied in chapter 6. It is also worth that experimental constraints on the electrical interactions in clays with mixed monovalent/divalent solutions and their macroscopic effects would be crucial, since only theoretical models are available in the literature, so far.
Finally, the TLM was applied to the Tournemire argillaceous formation and a profile of osmotic efficiency was obtained from the composition profile predicted in chapter 3 and petrophysical parameters. The osmotic efficiency profile results from the variations in concentration, composition and pore-size observed in the formation. This profile will be useful for the abnormal pressures interpretation in the Tournemire clayrock, issue of the chapter 7.

4.3 Experiments of chemical osmosis on Tournemire clay-rock

4.3.1 Introduction

Chemical osmosis is the best characterized osmotic process though experiments were mainly performed on artificial argillaceous materials, such as pure clays, bentonite or remoulded soils or rocks. Until recently, only one chemo-osmosis experiment was made on natural shales [155]. However, since chemical osmosis ability to generate a significant fluid flow at the formation

scale was demonstrated [116], some experiments were performed on different mudstones [32, 51, 68, 116, 136, 137].

The aim of the experiments presented in this section is characterizing the chemical osmosis process in the Tournemire clay-rock by an experimental determination of the chemo-osmotic efficiency.
Several attempts were performed, at the laboratory on samples in flow-through and radial geometries and in situ in equipped boreholes, but alone the successful experiments conducted on the flow-through cells are reported here.
First attempts of off-site laboratory experiments were performed on air-cored samples having a radial geometry. A measurement chamber was drilled lengthwise in a cylindrical sample and the sample confinement was ensured by epoxy resin in one configuration and by a vertical load in a second configuration. Confinement was apparently not enough and micro-cracks were observed to open in the argillite sample, at the chamber drilling or delayed in time, leading to capillarity conditions in the measurement chamber. The in situ experiments were performed at the Tournemire URL in two 7 m deep equipped boreholes but these boreholes were installed in a zone where pressures were affected by the hydromechanical response consecutive to gallery excavation. This pressure evolution was higher than the pressure variation linked to the chemical osmosis response induced by the salinity gradient between the borehole and the formation porewater. In both experiments, a statement on the chemical osmotic ability of the Tournemire clay-rock was impeded and another experimental configuration was required.

The chemical osmosis experiments presented here were performed in collaboration with Pr. Skoczylas of the Ecole Centrale de Lille. These experiments were carried out in flow-through geometry, i.e. by inducing a flow across a Toarcian clay-rock sample from Tournemire installed between two isolated reservoirs. The sample and the reservoirs were installed in an uniaxial confining cell ensuring the mechanical integrity of the sample.
Different salinity gradients were tested for assessing the sensitivity of the osmotic response to salinity.

4.3.2 Sample characteristics

Tournemire clay-rock sample used in these experiments come from the PH4 borehole, a 250 m length borehole air-drilled during Autumn 2006. It was drilled vertically and directed downward from the Tournemire URL tunnel

(PM 840). It provided samples of 65 mm of diameter, drilled normal to the bedding. This borehole was dedicated to the acquisition of the flow and diffusion characteristics across the formation. It particularly enabled the identification of profiles of the petrophysical parameters (porosity, density, specific surface area, cation exchange capacity), the mineralogy, the natural tracers (water isotopes, helium, chloride [15]), the porewater composition and the fluid pressure. Rock properties are thus well constrained along this profile, which is interesting for a critical discussion of the measured chemical osmotic properties.

The selected sample is 20 cm length and was obtained at 47.1 m depth in PH4 borehole, corresponding to a NGF elevation of 471.9 m and to the center of the upper Toarcian formation. Mineralogy obtained on a sample at 55.35 m depth in PH4 borehole indicates a composition dominated by clay phases (30 % of illite/smectite mixed-layers rich in illite, 16 % of illite and micas, 17 % of kaolinite and 3 % of chlorite). The rock is also composed by 13 % of quartz, 13 % of calcite and dolomite, 3 % of feldspars, 2 % of pyrite and 2 % of accessory minerals (see Chapter 3). An organic matter content of about 1 % is also found in the upper Toarcian layer [30].
The total porosity was determined by measurement of water content and volume with the method presented in Matray *et al.* [98] on the PH4 47.3 m depth sample and presents a value of 9.1 $\pm$ 0.06 %. Accessible porosity to water isotopes and chloride was determined by the radial diffusion method on the 50.6 m depth PH4 sample [15]. The values obtained were, respectively, 10.77 and 4.04 % and the corresponding effective diffusion coefficients are 7.8×10^{-12} and 1.2×10^{-12} m^2 s^{-1}. A grain density of 2.7054 g cm^{-3} was determined by helium pycnometry on 48.6 m depth PH4 sample. A specific surface area of 23 $\pm$ 2 m^2 g^{-1} was obtained by the BET method on 55.35 m depth PH4 sample. Bulk rock cation exchange capacity (CEC) was calculated on the 55.35 m depth PH4 sample to 5.52 $mmol_c$ 100 g^{-1} using the <100 μm fraction CEC and the clay phases content (see section 5.2.2).

Just after the drilling, the sample used in these experiments was conditioned in a triaxial cell, with the in situ lithostatic pressure applied as vertical load. At the end of January 2010, the sample was withdrawn from the triaxial cell and sliced in the bedding plane in 1 $\pm$ 0.1 cm disks with a diamond wire saw. Saw tracks on both surfaces were then polished.
The absence of fissuration in the clay-rock sample was noted before using it for the experiment.

4.3.3 Experimental device

The experimental device for chemical osmosis experiments (Fig. 4.4) was designed to be able to generate a salinity gradient between two reservoirs separated by a clay-rock sample, but not a pressure gradient. The sample is installed horizontally inside a Viton jaket in an uniaxial confining cell which avoids micro-cracks opening in the rock and filtration between the two reservoirs except through the clay-rock porosity. The reservoirs are in contact with the sample through a porous steel disk allowing a mechanical constrain of the sample, avoiding swelling in particular, as well as fluid flow through the whole sample surface (3.32×10^{-3} m^2). Reservoirs volumes were chosen to be large enough so that water composition in the reservoirs is not modified by solutes diffusion through the sample during the experiment duration. The reservoirs present a volume of 0.15 L, to which the volume of the tubes (diameter of 2.4 mm) are to be added. Reservoirs can be connected through a capillary tube (diameter of 0.5 mm) allowing a pressure equilibrium with a weak volume movement between the reservoirs.
Note that the experimental device, i.e. the confining cell, the reservoirs, the tubes, the valves and the porous disks, are made with stainless steel (Z2 CN17-12 steel for the reservoirs and tubes) in order to avoid corrosion and, then, perturbations on the sample and the water salinity during the experiments.

Monitoring of the water movements was chosen to be done by the pressure change in the two reservoirs. Indeed, because of the small water volumes displaced during such chemical osmosis experiments, a direct measurement of the water volume changes, e.g. in a capillary tube, was not appropriate. Both reservoirs were equipped by a high precision (2.5 mbars) Kobold SEN 3231 pressure sensor allowing measurements in the range 0 - 25 bars.
The experiments were performed in isothermal conditions as the device was installed in a thermostatic test chamber where temperature and relative humidity were constant, at 30 ℃ and 50 % RH, respectively. It allows avoiding pressure measurement perturbations due to its variations with temperature changes [136].
During the experiment, pressure modification had to be done in the reservoirs for the reservoir calibration, permeability measurements on the sample and water change in the reservoir for inducing a salinity gradient. Operations were made using a Gilson Inc. 307 piston pump allowing a flow rate from 10 μL min^{-1} to 10 mL min^{-1}.

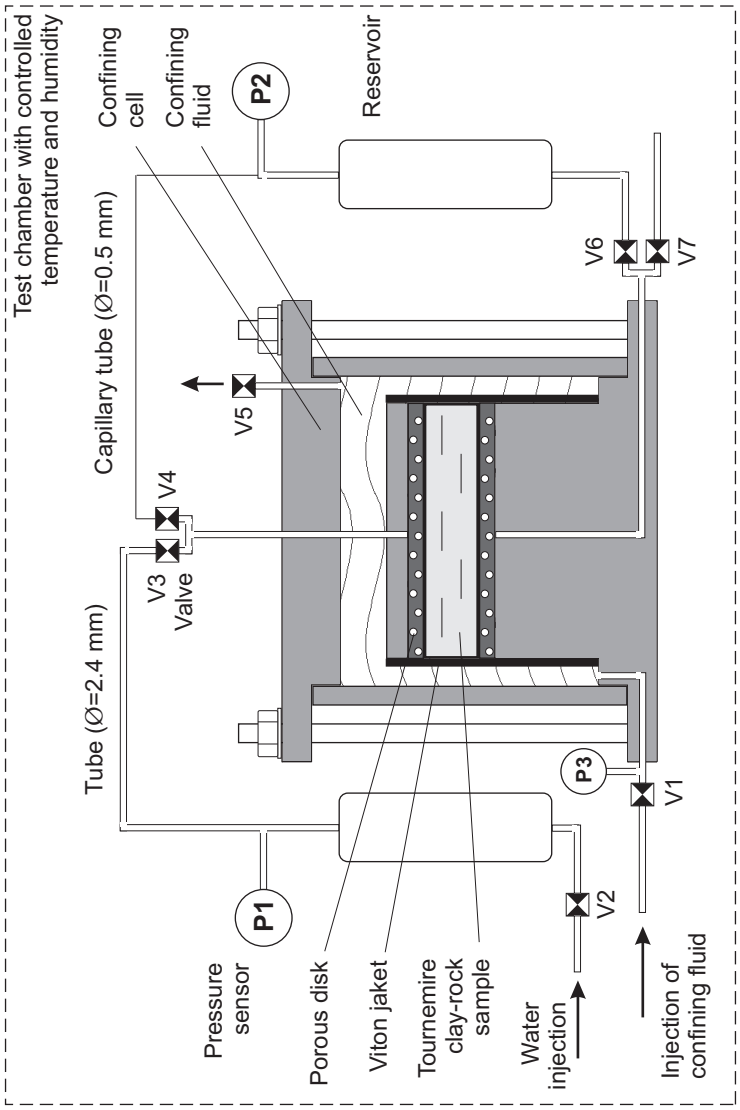

Figure 4.4: Scheme of the experimental device used for the chemical osmosis experiments on Tournemire Toarcian clay-rock disks.

4.3.4 Experimental protocol

The purpose of this study is to estimate the chemical osmotic efficiency of the Tournemire argillite accounting for the effect of salinity. The experiment consists in substituting the water of one reservoir by a more concentrated solution which consequently leads to the development of a salinity gradient. If a chemical osmotic flow develops through the clay-rock, pressures are expected to increase in the reservoir with higher salinity and to decrease in the reservoir filled with the fresher water resulting from a fluid flow towards the more salty reservoir.

In a preliminary stage, the clay-rock disk shaped sample was installed in the confining cell, separating the two reservoirs, as shown in Fig. 4.4. A confinement was applied through the confining fluid to a value P3 of 80 MPa. This high confinement value allowed ensuring that no flow can filtrate at the jaket - clay-rock interface. The confining pressure was observed to be stable during the different tests and confinement was readjusted before inducing a new concentration gradient. The reservoirs and tubes were then filled with water and the absence of fluid losses in the circuit was ensured. The reference water was that of the Tournemire Aalenian aquifer and presents a concentration of 0.015 mol L^{-1} and is equilibrated with carbonates phases. This water composition, in mol L^{-1}, is: [Na] = 7.6×10^{-4}, [Ca]=3.05×10^{-3}, [Mg] = 1.87×10^{-3}, [K] = 3.7×10^{-5}, [Sr] = 4×10^{-6}, [Cl] = 1.05×10^{-3}, [HCO_3] = 5.3×10^{-3}, [SO_4] = 2.5×10^{-3} and [NO_3] = 7.5×10^{-4}.

During sample preparation, a desaturation of the clay-rock was possible and the sample had to be resaturated before performing the chemical osmotic experiments. Sample saturation was made by advection, applying a pressure gradient between the two reservoirs. During resaturation piston pump flow rate decreases, corresponding to a water volume retained in the rock porosity. Saturation was reached when the pump flow rate stabilized after approximately one month.

Different concentration gradients were applied between the two reservoirs to induce a chemical osmotic flow. Both experiments were performed in the same way. First, valve V3 (see Fig. 4.4) is closed and the upper reservoir is disconnected at the level of the valve V3 to be drained off, outside of the test chamber. The reservoir is next rinsed and filled with the new solution to test. The upper reservoir is then reconnected to the confinement cell at the valve V3 location, ensuring the reservoir and tubes volume are totally filled with water. The reservoir and its filling solution were next kept some hours to equilibrate with the test chamber temperature, to avoid a thermal perturbation on the measured pressures or a thermo-osmotic flow. After thermal equilibration, valve V3 was reopened and, using the piston pump

connected to valve V2, pressure in the upper reservoir (P1) was imposed to a similar value than that of the pressure in the lower reservoir (P2). Valve V2 was closed and pressures in both reservoirs wers equilibrated to a same value (around 10 MPa) by opening some seconds the valve V4, allowing the reservoirs to be linked through the capillary tube. The system is next free to evolve and an osmotic flow to develop through the clay-rock sample, driven by the salinity gradient between the reservoirs. System evolution is followed by the pressure measurement in both reservoirs.
Various salinity gradients were successively applied on the same clay-rock sample and without replacing the water in the lower reservoir but only the water in the upper reservoir. Three concentrated solutions were prepared for the upper reservoir by adding NaCl salt to the reference water, used in the saturation phase and which always fills the lower reservoir. The first solution was made with 1.15 g of NaCl added to 500 mg of reference water water (0.072 mol L^{-1}), the second water with 3.25 g of NaCl in 500 mg of reference water (0.144 mol L^{-1}) and the third one with 7.5 g of NaCl in 500 mg of reference water (0.272 mol L^{-1}).
Chronologically, two tests with a solution at 0.072 mol L^{-1} were performed, followed by one test with a solution at 0.144 mol L^{-1} and, finally, one test with a solution at 0.272 mol L^{-1}. Note that between the two tests using a solution with a salinity 0.072 mol L^{-1}, solution was not replaced but only the reservoirs pressures were re-equilibrated. This set of chemical concentration gradients applied to this Toarcian clay-rock sample with solutions mainly composed of Na^+ as counterion was performed from mid April 2010 to the end of September 2010 and the tests lasted after 10 days to one month.

At the end of chemical osmosis experiments, a permeability measurement was performed on the clay-rock sample by two approaches. A pressure gradient is imposed between the two reservoirs and the inversion of pressure evolution allows obtaining the intrinsic permeability value. In addition to the pressure gradient, the piston pump is connected on valve V2 to the upper reservoir with a low set point value of 20×10^5 Pa. Then, the pump injected water when pressure in the upper reservoir became lower than the set point value, allowing a direct measurement of the flow rate.
The reservoirs compressibility was also determined by following the pressure difference induced by a water volume injected in the reservoir. Experimental device configuration allows the compressibility determination for the whole device (lower and upper reservoirs and the pump connection tube), for the upper reservoir and for the pump connection pump. Reservoir compressibility of each reservoir was deduced from these measurements. Reservoir compressibility is a crucial parameter for the interpretation of the pressure

evolution in the reservoir as fluid flow in the rock, during the chemo-osmotic experiments [117].

4.3.5 Numerical model

The pressure evolution in the reservoirs during the chemical osmotic experiments was interpreted through a numerical model using finite differences in a 1D vertical geometry (Fig. 4.5), with a 1 mm grid spacing. Flow in the horizontal plane of the clay-rock sample were neglected because of the Viton jaket constraining the sample (see Fig. 4.4) and impeding fluid flow and mass transport at the lateral boundaries of the sample.

Model consists in reproducing the fluid flow and the Fick's diffusion in the clay-rock sample and its consequences on the pressures in the reservoirs. For fluid flow and mass transport, both equations for the porous medium and the measurement reservoirs have to be considered.

For the porous medium, the continuity equation describes the fluid pressure evolution [38]:

$$\frac{\partial}{\partial z}\left(\rho_f\, q\right) = -\frac{S_s}{g}\frac{\partial p}{\partial t} \tag{4.21}$$

where q is the specific discharge (m s^{-1}), ρ_f is the fluid density (kg m^{-3}), S_s is the specific storage coefficient (m^{-1}), g is the acceleration due to the gravity (m s^{-2}), p is the pressure in the porous medium (Pa), t is the time (s) and z is the vertical axis directed upward.
Accounting for the Darcy's flow and the chemical osmosis, the specific discharge writes:

$$q = -\frac{k}{\eta}\left(\nabla p + \rho_f\, g \nabla z\right) + \varepsilon\frac{k}{\eta}\nabla\Pi \tag{4.22}$$

where k is the intrinsic permeability (m^2), η is the fluid viscosity (Pa s), ε is the chemo-osmotic efficiency and Π is the osmotic pressure (Pa).
The osmotic pressure gradient is related to the chemical concentration gradient by the Van't Hoff relation, valid for concentrations lower than 1 mol L^{-1}:

$$\nabla\Pi = \nu\, R\, T\, \nabla c \tag{4.23}$$

where ν is the number of dissociated ions of the salt, i.e. 2 for NaCl, R is the gas constant (8.314×10^3 m^3 Pa K^{-1} mol^{-1}), T is the temperature (K) and c is the concentration in the porous media (mol L^{-1}).

The pressure behaviour in the reservoirs is described by the mass balance equation [26]:

$$\frac{\partial P}{\partial t} = \frac{q_r\, S_r}{\beta_r V_r} \tag{4.24}$$

where P is the pressure in the reservoir (Pa), q_r is the specific discharge across the clay-rock sample - reservoir interface (m s^{-1}) counted positive when directed towards the reservoir, S_r is the surface of this interface (m^2), β_r is the reservoir compressibility (Pa^{-1}) and V_r is the reservoir volume (m^3). The reservoirs compressibility and volume were not experimentally determined individually but the product of both was obtained during the reservoir calibration, where a pressure variation dP is followed as a function of a volume variation dV_r and writes [111]:

$$\beta_r\, V_r = \frac{dV_r}{dP} \tag{4.25}$$

The mass transport in the porous medium is described by the Fick's law:

$$\nabla(D_e\, \nabla c) = \omega \frac{\partial c}{\partial t} \tag{4.26}$$

where D_e is the effective diffusion coefficient (m^2 s^{-1}), c is the concentration in the porous medium (mol L^{-1}) and ω is the porosity.
For the reservoir, the mass balance equation describing concentration evolution writes [137]:

$$S_r\, J_r^d = V_r \frac{\partial C}{\partial t} \tag{4.27}$$

where C is the concentration in the reservoir and J_r^d is the diffusive flux across the surface of the clay-rock sample - reservoir interface (mol m^{-2} s^{-1}), determined using the Fick's law (counted positive when directed towards the reservoir):

$$J_r^d = -D_e \nabla c \tag{4.28}$$

The boundary conditions at the clay-rock sample - reservoir interface (Γ_r) state that the pressure and concentration at the upper and lower boundaries of the porous medium equal the pressure and concentration in the upper and the lower reservoir, respectively. They write:

$$p|_{Z(z)\,\epsilon\,\Gamma_r}(t) = P(t), \tag{4.29}$$

and

$$c|_{Z(z)\,\epsilon\,\Gamma_r}(t) = C(t). \tag{4.30}$$

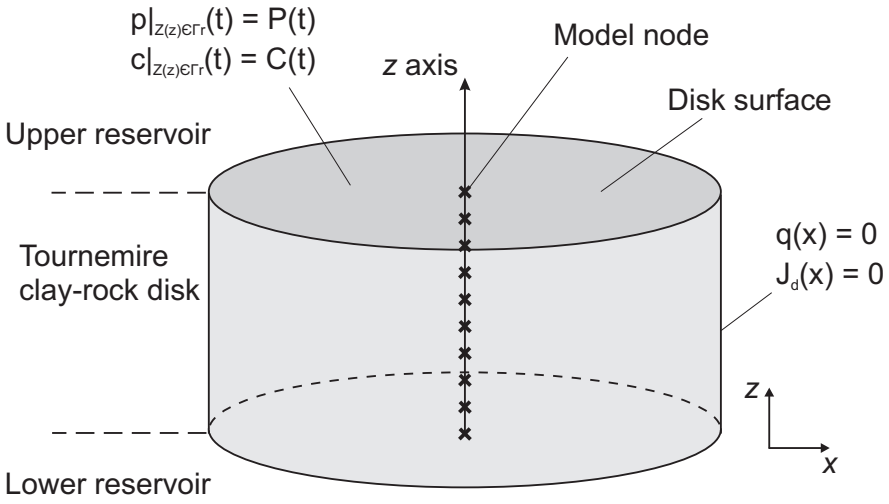

Figure 4.5: Scheme of the 1D modelled domain for the interpretation of the chemical osmosis experiments on clay-rock disk shape sample.

4.3.6 Results and interpretation

Reservoirs compressibility determination

First results presented in this section are the reservoirs compressibility determination. These values are needed for the interpretation of the intrinsic permeability and chemical osmosis coefficient.
Product of both reservoir compressibility and volume was determined by measurement of the pressure change as a function of a water volume variation (Eq. 4.25). These compressibility measurements were made on the whole device βV_{device}, i.e. upper and lower reservoirs and the pump connection tube, (Fig. 4.6.a); on the upper reservoir and the pump connection tube $\beta V_{meas.\,upp.}$ (Fig. 4.6.b); and on the pump connection tube βV_{pump} (Fig. 4.6.c). For the modelling of the hydraulic and osmotic tests, the compressibility of the upper, $\beta_r V_{r\,(upp.\,res)}$, and lower $\beta_r V_{r\,(low.\,res)}$ reservoirs are required. They can be determined as follows:

$$\beta_r V_{r\,(upp.\,res)} = \beta V_{meas.\,upp.} - \beta V_{pump} \tag{4.31}$$

$$\beta_r V_{r\,(low.\,res)} = \beta V_{device} - \beta V_{meas.\,upp.} \tag{4.32}$$

Average values and ranges of measured compressibilities are given in Table 4.4. Compressibility of the whole device is higher at low pressures. In Table 4.4, it is given for the pressure range 5 to 20 $\times$ 10^5 Pa, while chemical osmosis experiments were made at pressures between 6 and 12 $\times$ 10^5 Pa. Compressibility of the upper reservoir $\beta_r V_{r\,(upp.\,res)}$ presents an average value

of 9.33×10^{-14} m^3 Pa^{-1} in a range between 9.26×10^{-14} and 9.39×10^{-14} m^3 Pa^{-1}. The average compressibility of the lower reservoir $\beta_r V_{r\,(low.res)}$ is 1.09×10^{-13} m^3 Pa^{-1}, with values ranging between 9.73×10^{-14} and 1.30×10^{-13} m^3 Pa^{-1}. Product of the compressibility and volume of the lower reservoir is most likely slightly higher than the upper reservoir one because of a higher volume.

	average value	lower value	higher value
βV_{device}	2.24×10^{-13}	2.13×10^{-13}	2.44×10^{-13}
$\beta V_{meas.\,upp.}$	1.15×10^{-13}	1.14×10^{-13}	1.15×10^{-13}
βV_{pump}	2.16×10^{-14}	2.14×10^{-14}	2.18×10^{-14}

Table 4.4: Average value and range of value for βV determined during the compressibility measurements on different part of the sample. Data are expressed in m^3 Pa^{-1}.

Intrinsic permeability measurements

Results of the clay-rock sample permeability measurements are now presented. Two approaches were carried out for intrinsic permeability determination: a direct measurement of the flow rate injected by the piston pump when pressure in the upper reservoir reaches a low set point value; and a permeability determination by the inversion of the pressure evolution in the reservoirs during a period when no water is injected by the pump.
Permeability test lasted 5 days and 0.145 mL of water were injected during this time span (Fig. 4.7) by the pump programmed at set point value of 20 bars. After a little less than 3 days, 0.108 mL were injected. The intrinsic permeability was estimated using the Darcy's law:

$$Q = S_r \frac{k}{\eta} \frac{\Delta P}{L} \tag{4.33}$$

where Q is the flow rate given by the measured injected volume during the test duration, ΔP is the pressure gradient assumed constant at the pump set point pressure value and L is the sample thickness. An intrinsic permeability of 5.1×10^{-22} m^2 is obtained by this method for the entire test duration. Permeability for the first 3 days is found to be 6.5×10^{-22} m^2. This direct method only provides an estimation of the intrinsic permeability because of the uncertainties on the time when pump set point value was reached and fluid injected and because of the hypothesis of a constant pressure gradient.

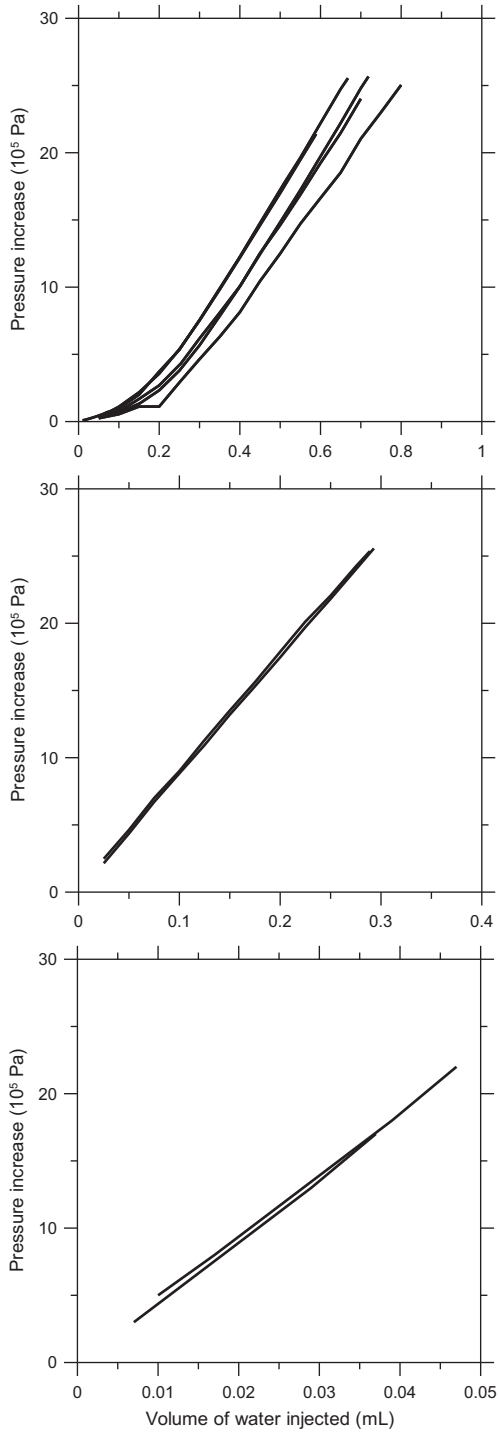

Figure 4.6: Reservoir compressibility determination by measurements of the pressure increase induced by an injected water volume. a) whole device; b) upper reservoir ; and c) pump connection tube.

A finest estimation of the sample intrinsic permeability can be achieved by the inversion of the pressure evolution monitored in the upper and lower reservoirs. Pressure transient evolution can be reproduced using the model previously presented (section 4.3.5). The pressure gradient initially measured between the reservoirs is considered as initial calculations conditions and no concentration differences are introduced. The pressure inversion can be made for a constant water volume in the system, i.e. for a period of time during which no water is injected by the pump. Two pressure evolution periods can then be reproduced (Fig. 4.7): from day 0 to day 0.3 and from day 2.9 to day 4.3. Experimental and modelled pressure evolution, for the intrinsic permeability achieving the best data reproduction, are represented in Fig. 4.8 for the first test period and in Fig. 4.9 for the second test period. Intrinsic permeabilities of 8×10^{-22} m^2 and 7×10^{-22} m^2 from day 0 to day 0.3 and from day 2.9 to day 4.3, respectively, were obtained using an a priori specific storage coefficient S_s value of 10^{-6} m^{-1}. These values are in the same range of the intrinsic permeabilities determined by direct measurement of the flow rate. Intrinsic permeabilities determined on this sample are in the range of the values previously for the Tournemire clay-rock (see section 1.3.2), in the lower part of the values range.

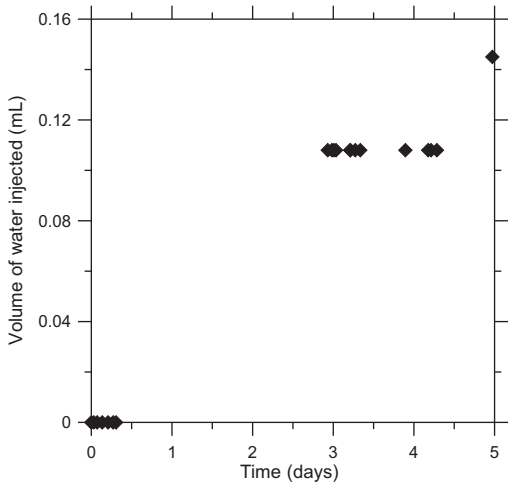

Figure 4.7: Water volume injected during the permeability test in the upper reservoir by the piston pump programmed at a set point value of 20×10^5 Pa.

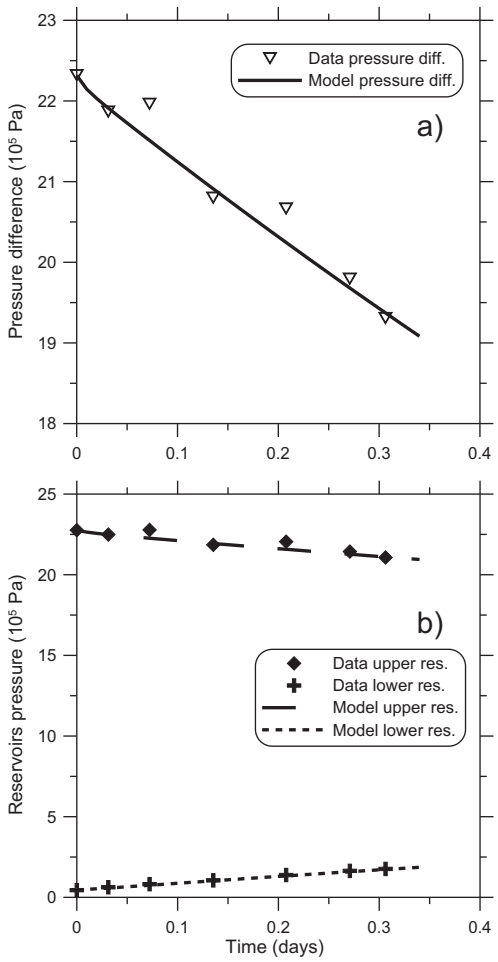

Figure 4.8: Data and model results for the pressure evolution during the permeability determination test from day 0 to day 0.3. a) pressure difference between the reservoirs ; and b) absolute pressure in the upper and lower reservoirs.

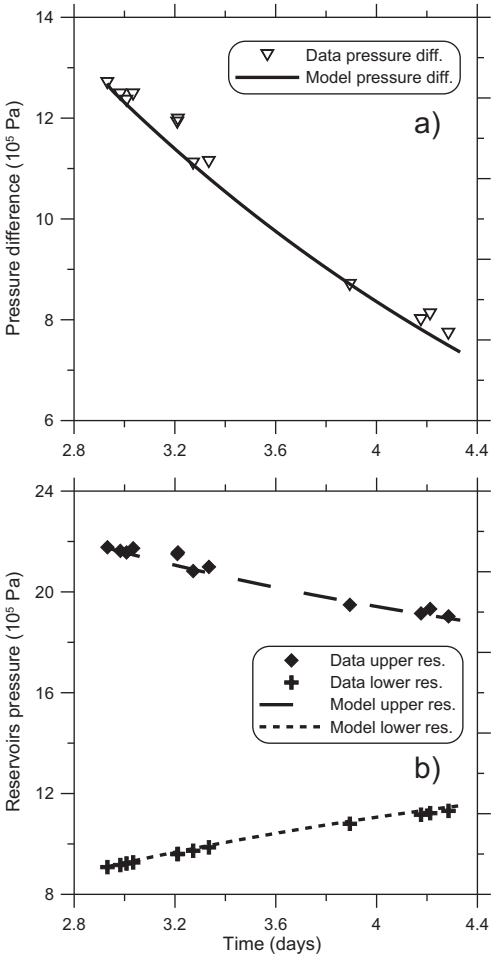

Figure 4.9: Data and model results for the pressure evolution during the permeability determination test from day 2.9 to day 4.3. a) pressure difference between the reservoirs ; and b) absolute pressure in the upper and lower reservoirs.

Chemo-osmotic efficiency measurements

Once determined the compressibility of the reservoirs and the intrinsic permeability of the upper Toarcian sample, the results of the chemo-osmotic experiments are now detailed. The experiments have consisted in replacing the solution filling the upper reservoir by more salted solutions. After equilibrating the pressures in the two reservoirs, pressures are free to evolve and flow interpretation lies on this evolution.
After performing the water replacement, the pressure difference between the upper and the lower reservoirs showed an increase until reaching a plateau (Fig. 4.10). This increase of the pressure difference corresponds to an osmotic flow occurring across the clay-rock from the reservoir with fresher water towards the more salted reservoir. The pressure difference presented a small extent, i.e. some tens of kPa, so that a data dispersion was observed and the pressure evolution in only one reservoir did not clearly indicate the osmotic flow occurrence. Consequently, pressure evolutions are represented here as the pressure difference between the two reservoirs. Moreover, this representation allows a filtering of pressure perturbations linked to environmental conditions (temperature or atmospheric pressure) and the device (e.g., little changes in the confinement pressure).
The osmotic flow identified by the increase of pressure difference can be reproduced for each test. The calculation code developed in section 4.3.5 is used for this goal, assuming the imposed concentration difference and the same pressure value as initial conditions in the reservoirs. Other parameters used in these calculations are summarized in Table 4.5. A range of chemical osmotic efficiency bordering the data is obtained in each chemical osmosis test by fitting of the pressure evolution. Model results are presented together with the measurements of the pressure difference evolution in Fig. 4.10. For the first chemical osmotic experiment, reservoirs contained solutions at 0.015 mol L^{-1} and 0.072 mol L^{-1}, i.e. 4.7 times higher in the upper reservoir than in the lower one. Two water replacements were made at this salinity providing osmotic efficiencies ranging between 0.20 and 0.31 for the first test and between 0.175 and 0.19 for the second test. A more accurate determination of the osmotic efficiency can be made in this second test thanks to a lower data dispersion. During the second concentration gradient applied through the sample, reservoirs were filled with solutions at 0.015 mol L^{-1} and 0.144 mol L^{-1}, i.e. 9.4 times higher in the upper reservoir than in the lower one. Lower chemo-osmotic efficiencies ranging between 0.027 and 0.043 were obtained in this case. Solution concentration were 0.015 mol L^{-1} in the lower reservoir and 0.272 mol L^{-1} in the upper reservoir during the fourth chemical osmotic test, corresponding to a concentration 18.1 times higher

in the upper than in the lower reservoir. Chemical osmotic efficiencies were found to range between 0.014 and 0.018 in this last test. The reproduction of the pressure difference evolution is unperfect, in particular for the test with a solution salinity of 0.144 mol L^{-1} in the upper reservoir, suggesting that pressure difference stabilization is longer to reach than modelled.
Note that during the tests, the concentration in the two reservoirs did not vary significantly. Considering an effective diffusion coefficient of 1.2×10^{-12} m^2 s^{-1} for Cl^-, during the first test, concentration increases of 0.003 % in the less concentrated reservoir and decreases of 0.02 % in the more concentrated reservoir, + 0.01 % and - 0.03% during the second test, + 0.13 % and - 0.05 % during the third test and + 0.08 % and - 0.04 % during the fourth test.

k	8×10^{-22} m^2
S_s	10^{-6} m^{-1}
ρ_f	10^3 kg m^{-3}
η	10^{-3} Pa s
ω	0.091
D_e	1.2×10^{-12} m^2 s^{-1}
$\beta_r V_{r\,(upp.res)}$	9.3×10^{-14} m^3 Pa^{-1}
$\beta_r V_{r\,(low.res)}$	1.1×10^{-13} m^3 Pa^{-1}

Table 4.5: Parameters used in the model for chemo-osmotic experiments results inversion.

4.3.7 Discussion and conclusions

Chemical osmosis experiments were performed by inducing a concentration gradient, using NaCl in salted solutions, across a clay-rock sample from the upper Toarcian level, installed in an isotropic confinement cell. These experiments allow observing the development of a chemo-osmotic flow in the Tournemire argillite and, thus, to confirm that the Toarcian clay-rock exhibits a membrane behaviour. The chemo-osmotic efficiency ε of the rock was determined by a phenomenological approach, i.e. so that its value can represent the fluid flow related with a concentration gradient. A range of osmotic efficiency was obtained, between 0.014 and 0.31. Variations are associated to concentration changes, lower ε values being obtained for the higher salinities.
These experimental results can be compared with the osmotic efficiency data measured on other natural shales and already presented (Fig. 4.2) and with the triple-layer-model results (see section 4.2.3). The Toarcian sample half-pore size is calculated at 1.61 nm from the petrophysical properties of the

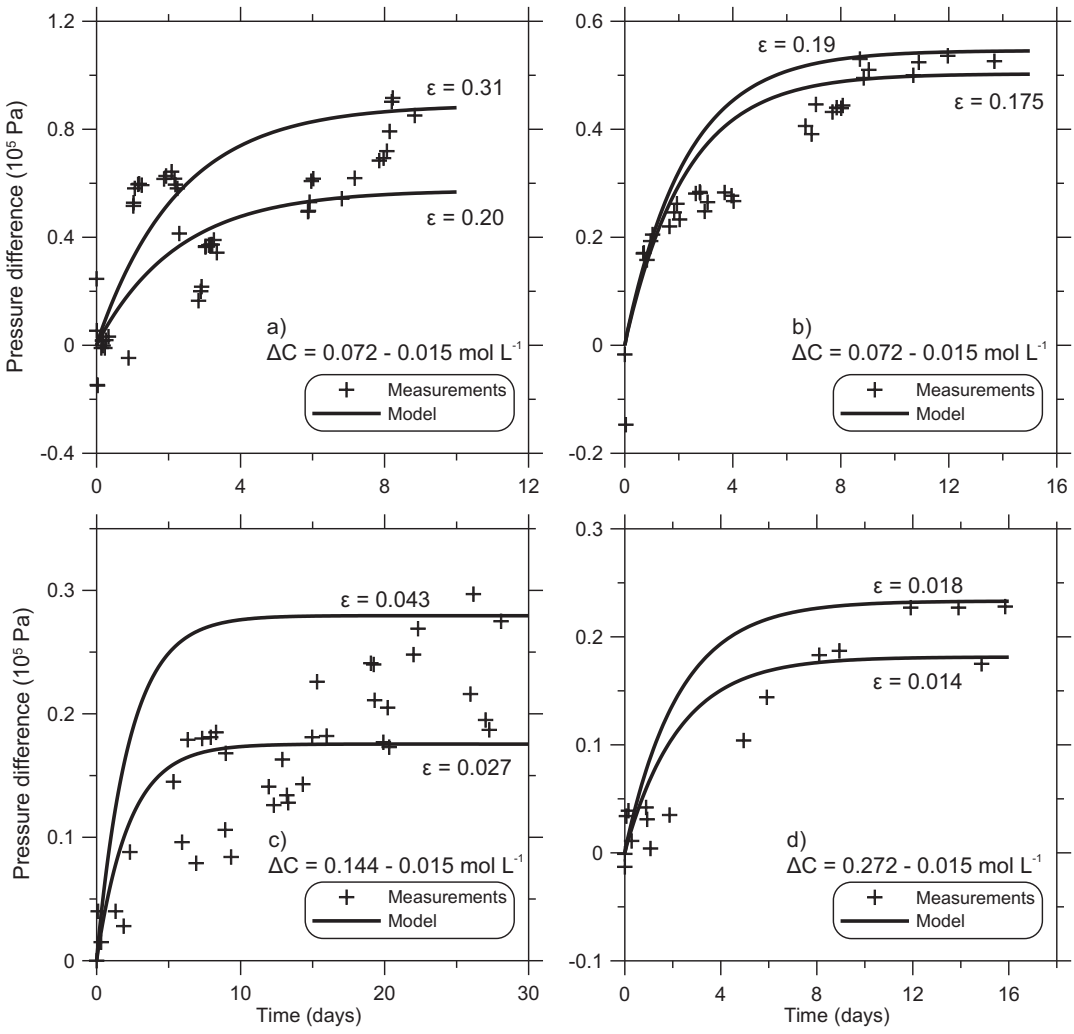

Figure 4.10: Evolution of the pressure difference between the two reservoirs during chemical osmosis experiments: measurements and modelling. a) first test with concentrations of 0.015 and 0.072 mol L^{-1} in the reservoirs; b) second test with concentrations of 0.015 and 0.072 mol L^{-1} in the reservoirs; c) concentrations of 0.015 and 0.144 mol L^{-1} in the reservoirs; and d) concentrations of 0.015 and 0.272 mol L^{-1} in the reservoirs.

sample (section 4.3.2) and using Eq.(4.3). Comparison is made in Fig. 4.11 and it is observed that Toarcian clay-rock presents the lower $b \times C$ values while its osmotic efficiency coefficients are in the range of the ε measured on other natural shales. Tournemire measured ε seem lower than the other ε and than the model prediction for a same $b \times C$ value. It is most likely due to its very low pore size which tends to minimize the effect of the salinity on the osmotic efficiency value in the selected representation.
A new set of chemical osmosis experiments is planned on the Tournemire clay-rock, but using Ca^{2+}. Indeed, it appears interesting to experimentally observe on a natural compacted shale the effect on the osmotic efficiency of divalent counterions and not monovalent ions as commonly used.

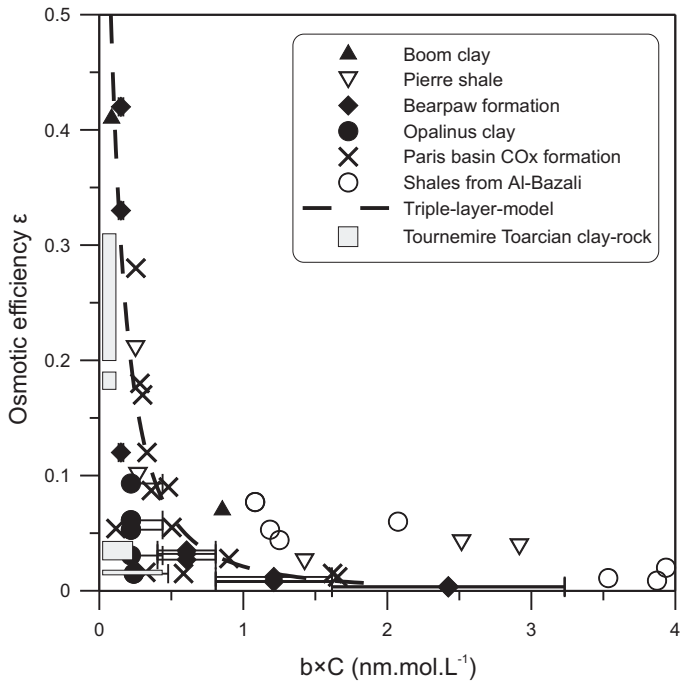

Figure 4.11: Comparison of the osmotic efficiencies experimentally obtained on the Tournemire argillaceous formation with other data determined on shales (see Fig. 4.2) and with the TLM results (see section 4.2.3). Grey areas for Toarcian clay-rock correspond to the ε and $b \times C$ ranges.

4.4 Conclusions

This chapter presented the work performed during this PhD thesis dealing with the characterization of the chemical osmotic process in the Tournemire clay-rock. An electrical model for the prediction of the osmotic efficiency was improved to represent the interactions between the charged solid surface and the solution in conditions close to those occurring in natural shales. Low pore size in such compacted rocks was considered through the overlapping of the diffuse layers [59] and the possibility of multi-ionic composition of the solution was now introduced in the model. It results in a noteworthy decrease of the chemo-osmotic efficiency in presence of divalent cations, compared with a clay - water system with only monovalent cations. Calculations and discussions on the consequences of this effect on the abnormal pressures in shales are addressed in Chapter 6. This predictive model was applied to the Toarcian/Domerian formation to obtain a profile of the chemo-osmotic efficiency across the formation. Predicted osmotic efficiency coefficients present variations across the profile between 0.025 and 0.513 as a function of the pore size, the salinity and the proportion of monovalent and divalent cations in the solution. The knowledge of the variations of the osmotic efficiency is required to interpret the pressure profile at Tournemire (see Chapter 7).
The second part of this work on chemical osmosis has consisted in performing experiments on the Toarcian clay-rock of Tournemire to characterize the osmotic properties of this shale. Experiments were made on an upper Toarcian sample, maintained in an isotropic confinement cell and surrounded by two reservoirs. Concentration differences were applied between the two reservoirs and the pressure evolution successive to these replacements was followed. Experimental results showed that a chemo-osmotic flow can develop in the sample and thus that Tournemire clay-rock presents a membrane behaviour. A range of osmotic efficiency was measured between 0.014 and 0.31, in the range of the chemo-osmotic efficiencies previously observed on natural shales. A comparison between predicted and experimentally determined osmotic efficiencies for the Tournemire argillite can be made and indicates an agreement between the ranges of osmotic efficiency. However, differences between both are also observed most likely because of model simplifications (e.g., on the Bresler's expression, the hypothesis of plane parallel clay platelets, the consideration of only one anion) and experimental artefacts.

Chapter 5

Thermo-osmosis

5.1 Introduction

Thermo-osmosis, a flow of water driven by a temperature gradient, is a poorly understood process in argillaceous media. Indeed, this process has been neglected, so far, despite several warnings on its possible importance in transport in clay-rocks [31, 141]. While substantial research was made on the two other osmotic processes, i.e. chemo- and electro-osmosis, thermo-osmosis remains largely disregarded.

This chapter presents the different contributions to thermo-osmosis characterization performed during this thesis. Two predictive models were developed for estimating the thermo-osmotic permeability in argillaceous media (section 5.2). The second model, which presents a better predictive ability, was then applied to the Tournemire argillaceous formation in order to obtain a profile of the thermo-osmotic permeability.
The second part of this chapter (see section 5.3) is dedicated to in situ experimental determination of the thermo-osmotic permeability of the Tournemire clay-rock.

5.2 Models for the prediction of thermo-osmotic phenomena in clays

5.2.1 Thermo-osmosis predictive models

Theoretical estimation of the thermo-osmotic permeability was made in two steps by the development of two models and are presented in two papers. The first one is published in Journal of Colloid and Interface Science and

the second one has been submitted to Earth and Planetary Science Letters. The aim of both models was the obtention of a macroscopic model for the thermo-osmotic permeability. Upscaling of a microscopic expression for the thermo-osmotic flow at the pore scale [39] gives a macroscopic expression for the thermo-osmotic permeability. The obtained expression indicates that the thermo-osmotic permeability is proportional to the intrinsic permeability and proportional to the excess of specific enthalpy of the fluid in the pores compared with the bulk fluid.

The first paper estimates this excess of specific enthalpy through the excess Gibbs energy of the fluid. The excess Gibbs energy of the fluid is itself obtained using the disjoining pressure. The model requires, in particular, the determination of the structural component of the disjoining pressure, since thermo-osmotic process is attributed by Derjaguin *et al.* [39] to structural changes of the water. Due to the uncertainties on this structural component, a fully satisfying quantitative prediction cannot be achieved.
The discussions of one anonymous reviewer of this paper highlighted the interest of understanding the real physical causes of such structural disruption of water molecules at the charged clay surface vicinity. Following this discussion, a second model exploring partly the molecular scale was developed. The excess of specific enthalpy was related to: i) the disruption of the hydrogen bounds around ions and ii) the antagonistic , i.e. the presence of water molecules more strongly hydrogen bonded at the clay surface.
This second attempt to estimate the thermo-osmotic permeability of argillaceous media, with molecular considerations, led to a fully predictive model requiring only petrophysical parameters of the porous medium, concentration and temperature conditions as input parameters. Interestingly this second model suggests a lower dependence to temperature than the pioneering theory proposed by Derjaguin *et al.* [39] and used in our first model. Derjaguin *et al.*'s conjecture was that thermo-osmosis vanishes with increasing temperature and disappears at temperature higher than 70 ℃.
In the second paper, submitted to Earth and Planetary Science Letters, a discussion of the impact of thermo-osmosis on the fluid flow and pressure field in argillaceous formations is addressed, especially for the formations studied for nuclear wastes repository purposes. In particular, a reevaluation of the interpretation of the excess-head measured in the Callovo-Oxfordian formation of the Paris basin was proposed.

Journal of Colloid and Interface Science 342 (2010) 166–174

Contents lists available at ScienceDirect

Journal of Colloid and Interface Science

www.elsevier.com/locate/jcis

Estimating thermo-osmotic coefficients in clay-rocks: I. Theoretical insights

J. Gonçalvès [a,b,*], J. Trémosa [a,c]

[a] UPMC Univ. Paris 06, UMR-7619 SISYPHE, 4 Pl. Jussieu, F-75252 Paris, France
[b] CNRS, UMR 6635 CEREGE, F-13100 Aix en Provence, France
[c] Institut de Radioprotection et de Sûreté Nucléaire/DEI/SARG/LR2S, BP 17, F-92262 Fontenay-aux-Roses, France

ARTICLE INFO

Article history:
Received 17 July 2009
Accepted 28 September 2009
Available online 9 October 2009

Keywords:
Coupled flow
Thermal gradients
Disjoining pressure
Structural energy

ABSTRACT

The conditions to obtain a macroscopic model for the thermo-osmotic coupling coefficient which is needed for practical calculations of fluid flow in clay-rocks subjected to temperature gradients are investigated in this paper. A theoretical expression for the thermo-osmotic coupling coefficient proportional to the hydraulic conductivity was obtained. The theoretical expression of the thermo-osmotic conductivity involves the excess Gibbs energy of the fluid between adjacent charged surfaces. The interaction energy was calculated using disjoining pressure data. Our calculations suggest a crucial role of the so-called hydration or structural energy of interaction to explain the thermo-osmotic process. The mean pore size, i.e. the mean interparticle spacing, the concentration of the equilibrium solution and the temperature are determinant variables in this process. Some exploratory comparisons between the model and the available data for pure clays are proposed.

1. Introduction

The electrical properties of clay minerals yield severe alterations of the transport equation in consolidated clays. In such media, the occurrence of the so-called coupled fluxes is well known [1–5]. The conjugated driving forces appearing in the classical transport laws (e.g. the pressure gradient for fluid flow) are not sufficient to describe the fluxes. Other forces termed non-conjugated such as the concentration, electrical potential or temperature gradients have to be considered [1,2]. Therefore, the coupled fluxes correspond to fluid, solute, heat fluxes or current density which share the same driving forces. The resolution of these fluxes coupled with balance equations allows the identification of the distribution of the variables and thus their gradients. Consequently, these fluxes should be calculated simultaneously whence the notion of coupling. Here, we will focus on the fluid and heat fluxes. For fluid flow, the non-conjugated terms, i.e. those which are not proportional to the pressure are referred to as osmotic flows. In coupled flow theories, the fluid velocity is linearly proportional to the driving forces. The coefficient of proportionality are the so-called coupling coefficients. For clay materials, a large amount of studies aimed at characterizing the chemical or electro-osmotic coefficients (see e.g. [5–18]). Whether theoretical or experimental, these studies have been often carried out under isothermal conditions. Consequently, theoretical expression for the chemical osmotic coefficient [2,5,7] or for the electro-osmotic coefficient [2,5,12] are available. To our knowledge, the same cannot be said for the thermo-osmotic coefficient. Thermo-osmotic flow which is defined as a fluid flow under thermal gradients was measured by Derjaguin and Sidorenkov (reference in [19]) for porous glasses. On the basis of such experiments, Derjaguin and co-workers built the only available theory on thermo-osmosis. Interestingly, the experimental conditions of the experiment by Derjaguin and Sidorenkov but not the existence of such process were largely questioned by Hutchison et al. [20] who argued that the volume flux measured by these authors was mostly due to the thermal expansion of the fluid. Careful experiments have been subsequently conducted to identify a rigorous thermo-osmotic behavior in different materials. Some of these studies were carried out on compacted clays such as the work by Dirksen [21], Srivastava and Avasthi [22,23] or more recently by Rosanne et al. [18]. But it must be pointed out that this process has not been as widely studied as the chemical osmosis in clays for instance. Therefore, and despite the presence of high temperature gradients across natural shale layers in sedimentary basins due to the low thermal conductivity of clays, this process has attracted weak attention. Although a theoretical basis for the prediction of the thermo-osmostic coefficients has been provided by Derjaguin et al. [19], a clear and convenient expression for this parameter is missing. In the present paper, we investigate the conditions to obtain such an expression.

2. Theory on thermo-osmosis

2.1. Water-interface interaction

As will be seen in the following section, Derjaguin et al. [19] invoked the major alteration of the structure of the water adjacent to

* Corresponding author. Address: UPMC Univ. Paris 06, UMR-7619 SISYPHE, 4 Pl. Jussieu, F-75252 Paris, France.
E-mail address: julio.goncalves@upmc.fr (J. Gonçalvès).

0021-9797/$ - see front matter © 2009 Published by Elsevier Inc.
doi:10.1016/j.jcis.2009.09.056

a solid surface to explain the mechano-caloric and related thermo-osmotic process. For this reason, we start with a brief description of such interaction.

Isomorphic substitutions in the clay minerals lattice such as the substitution of Si^{4+} by Al^{3+} in tetrahedral-Si sheets or that of Al^{3+} by Fe^{2+} and/or Mg^{2+} octahedral-Al sheets yields a net permanent negative charge of the basal surfaces at natural pH values. For minerals such as kaolinite or illite, hydroxyl groups at the edges contributes by hydroxylation reactions to the overall charge of the mineral. In smectite type clays, these edge surfaces are negligible (see e.g. [24]). The negative charge is balanced by an accumulation of ions close to the surface, and an electrical double layer develops [3,25]. The distribution of the counterions can be accurately described by the Stern–Grahamme model. In this model, it is assumed that a substantial part of the negative surface charge is balanced by ions adsorbed on the surface (hydrated or not) forming the well-known Stern layer [26]. This adsorption to the clay minerals surface involves the formation of two types of complexes, i.e. inner and outer sphere complexes (Fig. 1). Inner sphere complexes correspond to ions directly bound to the surface and thus partially or fully dehydrated while outer sphere complexes are hydrated ions electrostatically bound to the surface. The remaining unbalanced surface charge is balanced by the ions in the diffuse layer. Therefore, in the Stern–Grahamme view of surface interactions, two layers are considered, the Stern layer involving one or two planes (inner and outer Helmholtz planes in Fig. 1) containing the ions closely packed to the surface, and the so-called Gouy–Chapman or diffuse layer made of more dispersed ions weakly attracted by the surface [25]. The consequence of these electrochemical interactions is the presence of an electric field normal to the clay mineral surfaces. If the adjacent diffuse layers overlap, the whole interplatelet space is subjected to an electric field. This contributes to a major alteration of the structure of the fluid at the solid surface. This alteration is schematically depicted in Fig. 1, where oriented water dipoles at the surface and in the hydration spheres of ions are shown. This change in water structure (hydrogen-bond network) takes two forms: (i) an ordering of water molecules associated with the solvation of the counterions and (ii) a preferential orientation of the water dipoles close to the surface. The layer of specifically structured water associated with interface interaction could extend to several nanometers from the surface [19,27].

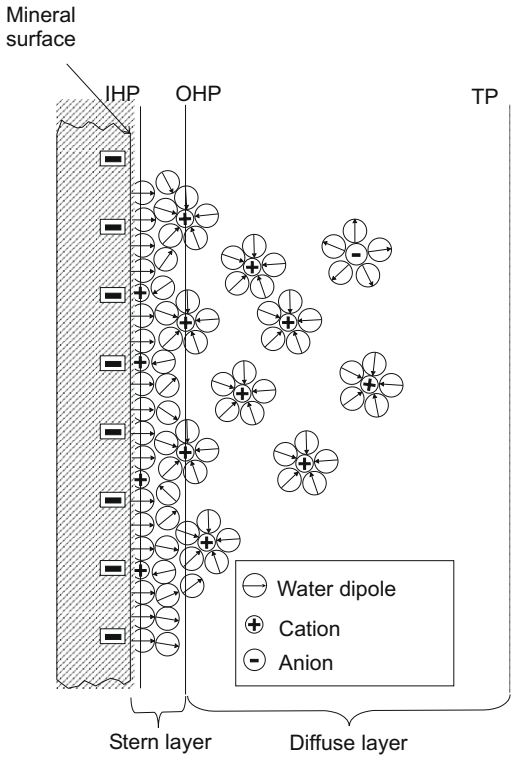

Fig. 1. Schematic view of solution–mineral interactions. OHP and IHP stand for Outer Helmholtz Plane and Inner Helmholtz Plane respectively. TP stands for Truncation Plane.

2.2. From Derjaguin's theory to macroscopic coupling coefficients

The only fully comprehensive theoretical model that was developed for the thermo-osmotic flow was due to Derjaguin et al. [19]. The authors use non-equilibrium thermodynamics concepts and considered the reciprocal process, i.e. the mechano-caloric process to identify a theoretical expression for the thermo-osmotic coupling coefficient at the pore scale. The interaction between a solid surface and the electrolyte at the contact with this surface yields a substantial alteration of the water structure in terms of hydrogen-bond network. This causes an alteration of the specific enthalpy of the solution in the pore space of a clay for instance. Let H (J m^{-3}) denote the specific enthalpy of the bulk solution (the solution in a reservoir in thermodynamic equilibrium with the clay), the specific enthalpy of the water film in the pores is then $H + \Delta H$, where ΔH is the mean "excess" specific enthalpy due to surface interactions. An isothermal fluid flow across the porous media would thus produce an "excess" heat flow and a related temperature gradient. This is the well-known mechano-caloric effect. Non-equilibrium thermodynamics requires that the reciprocal processes, i.e. a fluid flow due to a temperature gradient must exist. Let's consider a volume of clay-rock characterized by a membrane behavior separating two reservoirs so that pressure or temperature differences Δp (Pa) or ΔT (K) can be applied between the reservoirs. For a single pore representative of the porous media and idealized as a parallel plate slit (see Fig. 2) subjected only to pressure or temperature differences, the non-equilibrium thermodynamics approach yields [1,19]

$$j_V = l_{11}\Delta p + l_{12}\frac{\Delta T}{T}, \tag{1}$$

$$j_Q - j_V h = l_{21}\Delta p + l_{22}\frac{\Delta T}{T}, \tag{2}$$

where j_Q is the total heat flux (J s^{-1}), j_V (m^3 s^{-1}) is the volumetric flow rate and h (J m^{-3}) is the microscopic specific enthalpy of the bulk ($\rho_f C_f T$, ρ_f is the fluid density in kg m^{-3}, C_f the specific heat of the fluid in J kg^{-1} K^{-1}). The coefficient l_{11} and l_{22} refer to the well known direct flows. The coefficients l_{12} and l_{21} are the thermo-osmotic and mechano-caloric coefficients respectively. For a single plate-parallel pore, Derjaguin et al. [19] identify indirectly the thermo-osmotic coefficient using the Onsager reciprocity principle $l_{12} = l_{21}$ and establishing the theoretical expression of the mechano-caloric coefficient. For a single pore, the authors write the net heat flux transferred from one side to the opposite side during an isothermal fluid flow. Taking into account the effect of the pore walls on the specific heat of the film of fluid between the solid surfaces, the authors obtained

$$(j_Q - j_V h)_{\Delta T=0} = L\int_{-b}^{b}\Delta h(z)\,v(z)dz, \tag{3}$$

where $v(z)$ is the local fluid velocity (m s^{-1}) and z (m) is a local coordinate associated with each pore. For a practical use at the scale of interest, i.e. the macroscopic scale, an upscaling method must be used to obtain some expressions for the coupling coefficients such as

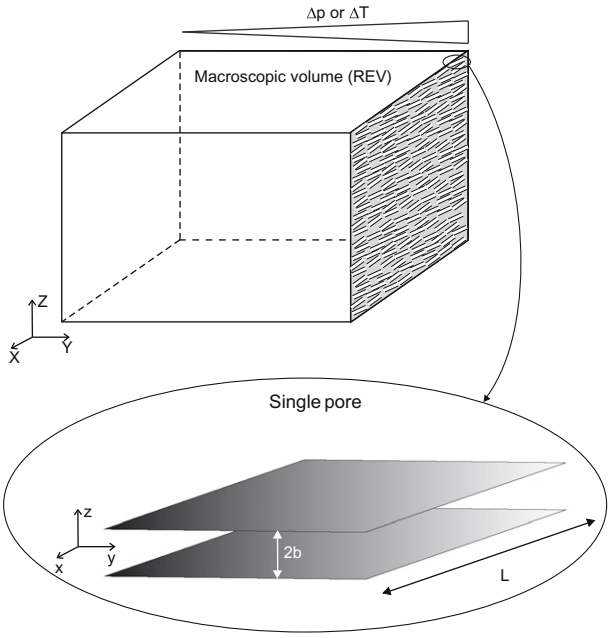

Fig. 2. Sketch of the geometrical framework for the development of a macroscopic thermo-osmotic coupling coefficient.

$$\begin{bmatrix} U \\ Q - UH \end{bmatrix} = \begin{bmatrix} L_{11} & L_{12} \\ L_{21} & L_{22} \end{bmatrix} \begin{bmatrix} \nabla p \\ \frac{\nabla T}{T} \end{bmatrix}. \tag{4}$$

where U is the specific discharge ($\mathrm{m\,s^{-1}}$), Q is the total heat flux ($\mathrm{J\,m^{-2}\,s^{-1}}$). It is reminded here that the macroscopic Darcy's velocity corresponds in fact to the fluid flow ($\mathrm{m^3\,s^{-1}}$) per unit porous surface ($\mathrm{m^2}$, solid plus pores). It is thus more rigorously a specific discharge. The same convention is used for the other fluxes like e.g. the heat flux Q (see below). To move to a macroscopic volume of porous media we shall use the notion of Representative Elementary Volume (REV). The REV is the volume over which the mean properties such as the porosity or the hydraulic conductivity can be defined. According to Marsily [28], this volume should be sufficiently large to contain a great number of pores and to ensure a mean global estimate of a given property. However, it must be sufficiently small so that a description of the variability of the parameters over a domain of interest is possible. According to this author, the REV can be trivially assimilated to a sample used to measure some physical properties. Consider here a macroscopic volume of clay-rock (REV) submitted to a pressure difference alone. At the macroscopic scale, the mean real velocity u ($\mathrm{m\,s^{-1}}$) of the fluid in the pores of the REV is given by [28]

$$u = \frac{U}{\omega}, \tag{5}$$

where ω is the dimensionless porosity assumed constant. This mean velocity u which is also termed the mean pore velocity can also be identified by returning to the definition of this velocity, i.e. a volume average of the mean fluid velocity in each individual pore of the REV. The mean velocity in an individual pore which pore size is $2b$ (see Fig. 2) is

$$\langle v \rangle = \frac{1}{2b} \int_{-b}^{b} v(z)dz. \tag{6}$$

The volume averaging over all the pores contained in a volume V_p ($\mathrm{m^3}$) of porous medium yields

$$u = \frac{1}{V_p} \int_{V_p} \langle v \rangle dV. \tag{7}$$

Introducing Eq. (7) into Eq. (5) and considering Darcy's law yields

$$U = -\frac{k}{\eta_f} \nabla p = \frac{\omega}{V_p} \int_{V_p} \langle v \rangle dV, \tag{8}$$

where k is the intrinsic hydraulic conductivity ($\mathrm{m^2}$) and η_f is the dynamic viscosity of the fluid (Pa s). Let's now consider the heat flux across a macroscopic sample subjected to a pressure gradient. According to Derjaguin et al. [19], under this condition the heat flux for a single pore is given by Eq. (3). Dividing this equation by the surface of one pore of width L (see Fig. 2) yields the following expression for the heat flux per unit surface of pore perpendicular to the advective flow direction

$$\frac{j_Q - j_V h}{2bL} = \frac{1}{2b} \int_{-b}^{b} \Delta h(z)\, v(z) dz. \tag{9}$$

The macroscopic heat transport in porous media should be expressed in joule per unit surface of the porous medium and per unit time [28]. If S denotes the macroscopic surface of the porous medium perpendicular to the flux, then the total surface corresponding to the pores can be approximated by ωS [28]. Writing the volume average of the heat flux over the REV yields

$$J_Q - j_V H = \frac{1}{V_p} \int_{V_p} \omega S \left(\frac{1}{2b} \int_{-b}^{b} \Delta h(z)\, v(z) dz \right) dV. \tag{10}$$

Dividing the left hand side of Eq. (10) by the porous surface S, noting that by definition $U = J_V/S$ and $Q = J_Q/S$ and introducing the simplifying assumption of a macroscopic constant mean value of the excess enthalpy $\Delta H(\sim \Delta h)$ as suggested by Derjaguin et al. [19] yields

$$Q - UH = \frac{\omega \Delta H}{V_p} \int_{V_p} \left(\frac{1}{2b} \int_{-b}^{b} v(z) dz \right) dV. \tag{11}$$

Using Eqs. (6) and (8), we obtain

$$Q - UH = -\frac{k \Delta H}{\eta_f} \nabla p. \tag{12}$$

Finally, the Onsager reciprocity principle yields

$$L_{12} = L_{21} = -\frac{k \Delta H}{\eta_f}. \tag{13}$$

The other coefficient are the well known Darcy's law coefficient $L_{11} = -k/\eta_f$ and according to de Groot and Mazur [1] or Revil and Leroy [5] $L_{22} = T\lambda$, where λ is the thermal conductivity of the porous medium ($\mathrm{W\,m^{-1}\,K^{-1}}$). The final form of the macroscopic equations are

$$U = -\frac{k}{\eta_f} \nabla p - \frac{k}{\eta_f} \frac{\Delta H}{T} \nabla T, \tag{14}$$

$$Q - UH = -\frac{k \Delta H}{\eta_f} \nabla p - \lambda \nabla T. \tag{15}$$

Note that gravity effects neglected so far could be readily introduced in Eq. (14) yielding

$$U = -\frac{k}{\eta_f} (\nabla p + \rho_f g \nabla z) - \frac{k}{\eta_f} \frac{\Delta H}{T} \nabla T, \tag{16}$$

where ρ_f ($\mathrm{kg\,m^{-3}}$) is the density of the fluid and g ($\mathrm{m\,s^{-2}}$) is the acceleration due to gravity. If no cross-coefficient is considered in Eq. (15), i.e. $L_{12} = L_{21} = 0$, this heat flow equation takes the classical form used to solve transport problems in porous media except for the so-called dispersion term which is not accounted for here.

Interestingly, the thermo-osmotic term in Eq. (14) is very similar to the expression obtained for the chemical osmosis in isothermal conditions, i.e.

$$U = -\frac{k}{\eta_f}\nabla p + \varepsilon_c \frac{k}{\eta_f}\nabla \pi, \tag{17}$$

where π and ε_c are the osmotic pressure (Pa) and the dimensionless osmotic efficiency (see e.g. [2,5,7]). By analogy with Eq. (17), we can define a coefficient ε_T so that

$$\varepsilon_T = \frac{L_{12}}{L_{11}} = \frac{\Delta H}{T}, \tag{18}$$

thus defining a thermo-osmotic conductivity k_T ($m^2\,K^{-1}\,s^{-1}$) such as

$$k_T = \varepsilon_T \frac{k}{\eta_f}. \tag{19}$$

According to Eq. (14), a positive value of ΔH results in a thermo-osmotic flux oriented from the warm to the cold side of a sample. This is the flow direction which was mostly identified for compact clay samples. The opposite flow direction (from cold to warm) is however possible, although rare, as noted by Dirksen [21]. The author reported an inversion of the fluid flow direction for high values of the porosity in illite samples. According to Eq. (19), a direct relation between the thermo-osmotic conductivity and the hydraulic conductivity is expected. This possible relation was studied here using a data set which is presented in Table 1. A nearly linear log-log relation is illustrated for $k \geqslant 1\times10^{-19}$ m^2 in Fig. 3a which shows the available data of k_T for clay materials listed in Table 1. However, the values of k_T obtained by Zheng and Samper [29] for bentonite and by Trémosa et al. [30] in a companion paper for Toarcien argilites at Tournemire, France, suggest that it would be hazardous to suppose a direct Log-linear proportionality between these two parameters. A more reliable relation is shown in Fig. 3b which strongly suggests that this proportionality coefficient, i.e. $\Delta H/T\eta_f$ and thus the excess enthalpy ΔH is highly dependent on the pore size $2b$. Whenever the porosity was known, the mean pore size was estimated using the simple mass balance equation valid for a parallel plate conceptual model for the pores and which writes [9]

$$\omega = (1-\omega)A_S\rho_S b, \tag{20}$$

where A_S is the specific surface ($m^2\,g^{-1}$), ρ_S is the density of the solid ($kg\,m^{-3}$) and b (m) stands here for the mean half pore size over the REV. The values of the specific surfaces used to identify the pore size are listed in the legend of Table 1. When the porosity ω was unknown, approximate values were obtained using the relationship between porosity and hydraulic conductivity for pure clays established experimentally by Mesri and Olson [31]. Fig. 3b shows an increase of the parameter ε_T when the pore size decreases. This figure

Table 1
Porosity values in italic were calculated using the hydraulic conductivity (see text). The specific surfaces used in Eq. (20) to calculate the half-pore size b are: for bentonite $A_S = 750$[a,b], 725[c] $m^2\,g^{-1}$, for kaolinite $A_S = 30$[a,d] $m^2\,g^{-1}$, for Orly silt (mostly kaolinite) $A_S = 30$ $m^2\,g^{-1}$ and for Callovo-oxfordian formation $A_S = 36$ m^2 [6]. The pore size for Toarcian formation is from Ref. [30].

Material	ω (−)	b (nm)	k (m^2)	k_T ($m^2\,s^{-1}\,K^{-1}$)
Bentonite[a]	*0.92*	5.9	1.77×10^{-18}	3.05×10^{-13}
Bentonite[a]	*0.92*	5.9	8.80×10^{-19}	1.60×10^{-13}
Bentonite[a]	*0.92*	5.9	1.87×10^{-18}	3.20×10^{-13}
Bentonite[b]	*0.96*	13.20	1.13×10^{-16}	1.30×10^{-10}
Bentonite[c]	0.42	0.37	3.50×10^{-21}	3.62×10^{-12}
Kaolinite[a]	0.56	16.50	1.22×10^{-17}	9.70×10^{-14}
Kaolinite[a]	0.51	13.45	6.10×10^{-18}	6.70×10^{-14}
Kaolinite[a]	0.45	10.40	2.00×10^{-18}	6.60×10^{-14}
Kaolinite[a]	0.42	9.32	1.30×10^{-18}	3.90×10^{-14}
Kaolinite[a]	0.29	5.11	1.74×10^{-19}	1.17×10^{-14}
Kaolinite[a]	0.56	16.51	1.20×10^{-17}	1.60×10^{-13}
Kaolinite[a]	0.56	16.51	1.25×10^{-17}	1.64×10^{-13}
Kaolinite[d]	0.30	8.25	3.20×10^{-17}	2.50×10^{-10}
Callovo-oxfordian formation[e]	0.3	5.50	5.00×10^{-18}	1.00×10^{-12}
Callovo-oxfordian formation[e]	0.3	5.50	5.00×10^{-18}	1.00×10^{-13}
Orly silt[f]	0.37	11.50	5.00×10^{-17}	1.50×10^{-11}
Orly silt[f]	0.37	11.50	5.00×10^{-17}	2.36×10^{-11}
Orly silt[f]	0.37	11.50	5.00×10^{-17}	2.20×10^{-11}
Toarcian formation[g]	0.07	1.25	1.00×10^{-21}	6.20×10^{-12}
Toarcian formation[g]	0.07	1.25	1.00×10^{-21}	2.00×10^{-10}

[a] Ref. [21].
[b] Ref. [23].
[c] Ref. [29].
[d] Ref. [22].
[e] Ref. [18].
[f] Ref. [57].
[g] Ref. [30].

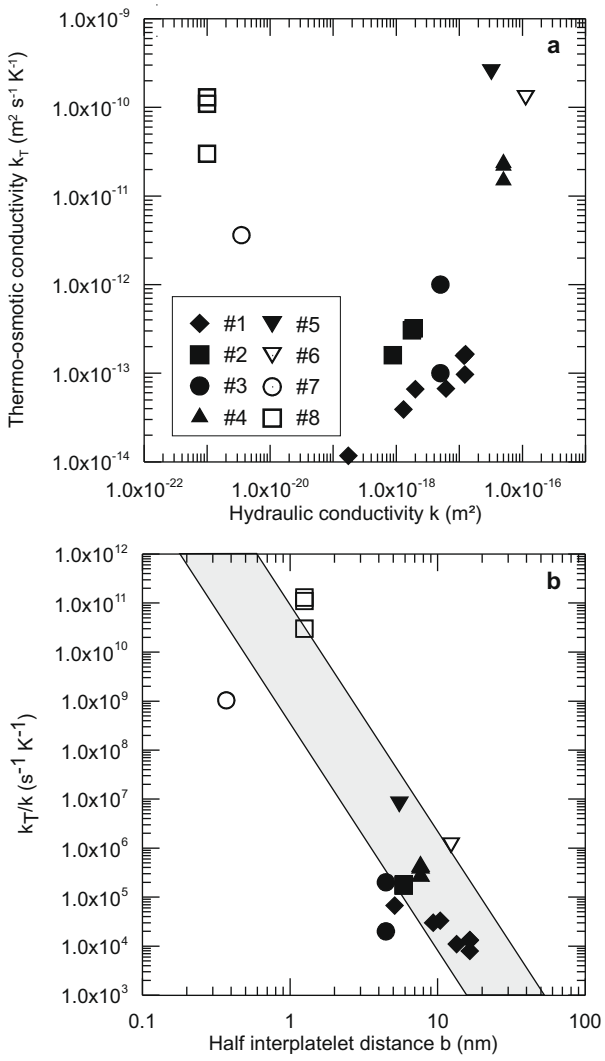

Fig. 3. (a) Experimental values of the thermo-osmotic permeability $k_T = \frac{k}{\eta_f}\frac{\Delta H}{T}$ plotted as a function of the hydraulic conductivity k. Data are #1 kaolinite [21], #2 bentonite [21], #3 remolded natural Callovo-oxfordian shale, France [18], #4 Orly silt (kaolinite) [57], #5 and #6 kaolinite and bentonite respectively [22,23], #7 bentonite [29] and #8 Toarcian clay formation at Tournemire, France (b) ratio k_T/k as a function of the mean half pore size (see text for its determination).

could be used to obtain a first estimate of the thermo-osmotic coupling coefficient as a function of the pore size within almost one order of magnitude (gray zone in the figure). It must be noted here that a theoretical expression for the thermo-osmotic coefficient was obtained by Revil and Leroy [5] without considering the microscopic theoretical framework proposed by Derjaguin et al. [19]. These authors obtained a ratio $k_T/k = \rho_f C_f/T\eta$. This suggests an almost constant value of this ratio if the specific heat of water C_f is taken to be equal to its bulk value while up to eight orders of magnitude variations are measured (Fig. 3b). It could be argued that interfacial interactions modifies the specific heat but no clear view of how this alteration could be modeled is proposed by the authors. The dispersion of the values illustrated by the gray area in Fig. 3b could be due to temperature effects. Indeed, in addition to the pore size, the temperature could influence the thermo-osmotic conductivity. So far, only the study by Dirksen [21] allowed an exploratory and almost qualitative discussion on this influence. The author made a sensitivity analysis on the mean temperature during thermo-osmotic experiments on a sodium bentonite. Almost constant ratios k_T/k were measured for this material at increasing temperature suggesting that ΔH varies as $T\eta_f$, i.e. weakly. This is in total contradiction with the idea of a thermo-osmotic effect related to a special water structure since this later vanishes at high temperature (see Section 4.1). Therefore, a dramatic decrease of the thermo-osmotic coefficient should be expected at increasing temperatures. The new experimental work presented in the companion paper [30] supports this view. Variations as high as one order of magnitude of the thermo-osmotic conductivity were found for a temperature variation of 9 °C. To summarize, the present simple analysis based on the available data suggests a strong dependence of the excess specific enthalpy ΔH on the pore size. It is interesting to note here that significant thermo-osmotic coefficients were measured for weak interparticle distances (low pore size) for which an interaction of adjacent modified structure water is plausible. This is consistent with the interpretation of Derjaguin and co-workers. The temperature effect could also be very important. This point is discussed in Section 4.1. Therefore, the pore geometry and the temperature would be, a priori, the main descriptive variables for the thermo-osmotic conductivity. The mean excess enthalpy associated with the solid–pore fluid interaction is a crucial quantity to characterize the thermo-osmotic process. Its identification is thus a prerequisite in order to obtain a quantitative model of the thermo-osmotic coefficient.

3. Towards a quantitative model for thermo-osmotic flow

According to e.g. Lyklema [32], the excess Gibbs energy of the film of fluid (in joule per unit surface of the solid) subjected to interfacial interactions is given by

$$\Delta g = -\int_{\infty}^{B} \pi_D(B')dB', \tag{21}$$

where π_D is the disjoining pressure and $B = 2b$ is the interparticle distance. The desired estimate of the excess specific enthalpy can be obtained using the Gibbs–Helmholtz relation. The notion of disjoining pressure was introduced by Langmuir [33] and Derjaguin and Kussakov [34] (cited in [19]) at the end of the 1930s. This pressure corresponds to the difference between the pressure in a water film between two interfaces (e.g. solid surfaces) and the hydrostatic pressure of the fluid in the reservoir in contact and equilibrium with the interfaces. This pressure difference which exists only when interfacial zones (e.g. the diffuse layer) overlap is caused by the presence of surface forces, e.g. of electrostatic or molecular origin. The following theoretical expression of the electrostatic component of the disjoining pressure π_D^e is obtained by Derjaguin et al. [19]

$$\pi_D^e = -\int_0^{\varphi_b} \rho d\varphi, \tag{22}$$

where φ_b is the electrical potential at the midplane (V) and ρ is the volumetric charge density (C m^{-3}). For a symmetric and monovalent salt, one finds the classical result

$$\pi_D^e = 2k_B T c_f \left(\cosh\left(\frac{e\varphi_b}{k_B T}\right) - 1\right), \tag{23}$$

where k_B is the Boltzmann's constant (1.38×10^{-23} J K^{-1}), c_f (ions m^{-3}) is the equilibrium solution concentration and e is the elementary charge (1.6×10^{-19} C). Besides the electrostatic component of the disjoining pressure, additional components were identified. A positive component corresponds to a repulsive force, and conversely a negative (traction) component corresponds to an attractive force between surfaces. The second component of the disjoining pressure introduced by Derjaguin et al. [19] is an attractive Van der Waals term corresponding to weak attraction between the molecules of the adjacent surfaces. This short range (less than 1 nm) term can be accounted for by using the relationship

$$\pi_D^{vdw} = -\frac{A}{6\pi(2b)^3}, \tag{24}$$

where A is the Hamaker constant dependent on the mineralogic nature of the surface. For mica and water films a value of 2.2×10^{-20} J was reported [19]. The electrostatic and molecular components are used in the DLVO (Derjaguin–Landau–Verview–Overbek) theory of the stability of colloidal suspensions. The DLVO theory cannot explain certain experimental data as claimed by e.g. McBride [35] and previously recognized by one of the authors of this theory [19]. For instance, higher surface forces than those predicted by the DLVO theory were measured at small interparticle distance (few nanometers). Consequently, an additional repulsive term to the DLVO disjoining pressure was proposed, the "structural" or "hydration" component. This component is often identified as the difference between experimental results for the disjoining pressure and the values predicted by the DLVO theory. In fact, the real origin of this component is still debated. However, two main explanations emerged: (i) the hydration of ions at the solid surface and (ii) a specific structure of the water at the interface. Certain authors invoked the counterions dehydration at the solid surface whence the notion of hydration forces [36]. Indeed, when the surfaces are brought to close vicinity, the ions located at the solid surfaces must dehydrate partially which is energetically unfavorable yielding an additional repulsive force. This view points to a length scale for this repulsive force in the order of a hydrated ionic diameter while larger length scales were obtained (up to 4 nm, [37]). According to Derjaguin et al. [19], this non-DLVO additional repulsive force is related to the presence of a layer of water molecules characterized by a modified structure, i.e. an alteration of their hydrogen-bond network in comparison to the equilibrium solution. Although this view was challenged by Israelachvili and Wennerstrom [27] who advocated the influence of the solid surface to explain the non-DLVO forces (e.g. protruding surface groups shifting the electrostatic repulsion outwards), the structural forces were continuously considered highly plausible. The existence of the specific structure water at water–mineral interfaces has long been reported in the literature through the observation of the alteration of the density or the viscosity of the water bound by clay surfaces (see e.g. [38,4]) and confirmed by molecular dynamics modeling [39,40]. When the interparticle distance is small, the two adjacent layers of structurally specific water overlap and, an additional repulsive term comes into play. This term was referred to as the structural component of the disjoining pressure π_D^s by Derjaguin et al. [19]. In accordance with Rabinovich and Derjaguin[37] or Derjaguin et al. [19], this ambiguous hydration component should be the combination of

several terms including ions hydration (short range) and hydrogen-bond network rearrangement (larger range) and should be termed the structural component. In their pioneering work, Marcelja and Radic [41] proposed a theoretical framework, although not predictive, to interpret the structural forces. From this initial study, some attempts using molecular dynamics concepts or electrostatic mean field calculations were made to understand the structural force (see e.g. [42–45]). But, to our knowledge, a fully predictive and convenient model is still awaited to emerge. Nevertheless, despite the uncertainties concerning their origin, a special attention was paid to the structural component here since the thermo-osmotic process was attributed by Derjaguin et al. [19] to structural changes of the water. This component can be accounted for using an exponential relation which writes [19,41]

$$\pi_D^s = \kappa \exp\left(-\frac{2b}{\lambda}\right) \tag{25}$$

where κ and λ are coefficients which have to be determined experimentally. Parameter λ represents a decay length of the structural forces. An alternative bi-exponential decay was also proposed by Pashley [46] based on experimentations on mica sheets. The bi-exponential expression could be interpreted as a consequence of a double origin for the surface forces, i.e. a short range term related to ions hydration and a long range force associated with a special structure of the water. The more general bi-exponential expression is considered in the following. Once identified, a linear additivity of the different components of the disjoining pressure is assumed by the authors yielding

$$\pi_D = \pi_D^e + \pi_D^{vdw} + \pi_D^s. \tag{26}$$

The disjoining pressure, which is a microscopic concept, is highly dependent on the interparticle distance. It also depends on other variables such as the temperature and the concentration of the equilibrium solution (see below).

Although its decomposition into different terms is still debated, the existence of the disjoining pressure was confirmed by numerous experimental studies, some of which were reviewed by Derjaguin et al. [19]. A classical experiment consists in placing a sample, for instance an oriented gel of clay minerals aligned in the horizontal direction, in contact with a reservoir and maintained in mechanical equilibrium by a piston exerting a vertical stress. This vertical stress which is necessary to maintain the volume of the sample and thus the mean distance between clay particles corresponds to the disjoining pressure. This experimental definition applies also to the well-known swelling pressure for the clay-rich materials. Such experiments, which provide direct values of the disjoining pressure, were made by e.g. Viani [47] or Callaghan and Ottwill [48]. Israelachvili [49,50] developed a surface force apparatus (SFA) which allows the measurement, at the microscopic scale, of the force F (N) between particles placed on the surface of two cross-oriented cylinders of radius R (m) and immersed in electrolytes. Numerous experiments were carried out by Pashley, Quirk and co-authors notably on mica using such apparatus (see e.g. [36,51]). SFA experiments provide values of the ratio F/R as a function of the surface spacing. More recently, an atomic force microscope (AFM) was used to measure the interaction force F between microscopic spherical probes of radius R in electrolytic solutions [52]. While the first apparatus provides direct estimates of the disjoining pressure, the two other ones (SFA and AFM) require some algebraic treatment in order to obtain an equivalent disjoining pressure for a plane-parallel geometry. In the case of F/R data obtained using a SFA, the following approximation by Derjaguin et al. [19, p. 49]

$$\frac{F}{R} = 2\pi \int_B^\infty \pi_D(B)dB, \tag{27}$$

can be used. Noting that the relation between the disjoining pressure and the interparticle distance B corresponds to a power law or an exponential decay, the derivative of Eq. (27) relative to B is defined and yields

$$\pi_D(B) = -\frac{1}{2\pi}\frac{d\left(\frac{F}{R}\right)}{dB}. \tag{28}$$

Similarly, the ratio F/R obtained with the AFM can be interpreted in terms of disjoining pressure using the approximation by [19, p. 49] for two interacting spheres. This yields

$$\pi_D(B) = -\frac{1}{\pi}\frac{d\left(\frac{F}{R}\right)}{dB}. \tag{29}$$

For the scale of interest, i.e. the REV, a mean value of the excess Gibbs energy ΔG can be obtained using an average value of the disjoining pressure over the REV in Eq. (21). The average value is in fact the swelling pressure Π_D. In a simplified averaging approach, the value of the microscopic π_D for the mean pore size $\langle 2b\rangle$ characterizing the REV calculated using Eq. (20) can be considered an estimate of Π_D, i.e. $\Pi_D = \pi_D(\langle 2b\rangle)$. In the following, we shall dispense with the mean sign '$\langle\rangle$' but note that b now and in Eq. (20) stands for the mean pore size over the REV. Noting that a unit volume of porous media corresponds to a total solid surface of $(1-\omega)\rho_S A_S$ and to a fluid volume of ω and making use of the Gibbs–Helmholtz relation yield the following expression for the macroscopic excess specific enthalpy ΔH (J m^{-3})

$$\Delta H = \frac{(1-\omega)\rho_S A_S}{\omega}\left[\Delta G - T\frac{\partial(\Delta G)}{\partial T}\right]. \tag{30}$$

Using Eqs. (20) and (30) becomes

$$\Delta H = \frac{1}{b}\left[\Delta G - T\frac{\partial(\Delta G)}{\partial T}\right]. \tag{31}$$

If the different components of the disjoining pressure are known, the same decomposition applied to π_D can be used for the excess specific enthalpy. Indeed, introducing Eq. (26), where mean values for the different components of the disjoining pressure are considered into Eq. (30) gives the following expression for the macroscopic excess specific enthalpy of the pore fluid

$$\Delta H = \Delta H^e + \Delta H^{vdw} + \Delta H^s, \tag{32}$$

where each term ΔH^i represents the excess enthalpy associated with the electrostatic, molecular and structural interactions corresponding to '$i = e$, vdw or s' respectively and writes

$$\Delta H^i = -\frac{1}{b}\left[\int_\infty^B \Pi_D^i(B') - T\frac{\partial \Pi_D^i(B')}{\partial T}dB'\right]. \tag{33}$$

In the following section, the analysis of the relative importance of each component is made for smectite which has been widely studied and the approach is applied, after some simplifications, to kaolinite.

4. Application to clay systems

4.1. Assessing the structural component and its dependence to temperature

Thermo-osmotic coefficient were measured mostly in smectite and kaolinite pure materials. We thus focus our study on these clays. Eqs. (32) and (33) are based on the assumption that each component of the disjoining pressure can be individually identified. In fact, the different experimental approaches described in Section 3 allow the determination of the total surface force or disjoining pressure. The most challenging issue is to identify the structural component and its temperature dependence. Due to

the absence of a fully satisfactory and predictive theory for structural forces, this component is conveniently obtained by subtracting the disjoining pressure calculated using the DLVO theory to the measured one. For this purpose, electrical models can be used to calculate the electrostatic component (see e.g. [53]) and the molecular component can be determined using Eq. (24), where the Hamaker constant is identified from measurements or models (see e.g. [54]). The main criticism concerning this decomposition approach stems from the combined uncertainties of both the measurements and the models. Whatever the material, the developments in Section 3 require to identify the temperature dependence of the different components of the disjoining pressure. According to Derjaguin et al. [19, Chapter 7], the electrostatic and molecular components are weakly dependent on temperature while the structural component shows a strong dependence. Indeed, the authors reported some experimental evidences pointing to a dramatic effect of the temperature on the boundary layer with modified water structure. At a temperature of about 70 °C, the specific structure of water is destroyed restoring the normal properties of water (notably viscosity, permittivity). The structural repulsive component π_D^s stems (at least partly) from the existence of this layer, a collapse of this component at a temperature of 70 °C can thus be expected. The theoretical calculations for undifferentiated materials by Boinovich and Emelyanenko [43] support the idea of a rapid decline of the structural forces with increasing temperatures. The temperature dependence of π_D^s for clay minerals is not clearly established. For the sake of simplicity and in order to obtain first estimates of the thermo-osmotic coupling coefficient for such materials, a linear decrease of the structural component with the temperature was assumed in the following, i.e. $T\frac{\partial \Pi_D^s}{\partial T} \approx -T\frac{\Pi_D^s(T=298K)}{\delta T}$, with $\delta T = 45$ K. The dependence to temperature of the two other components are more readily obtained (see below). This approach also necessitates a large data set for the disjoining pressure in order to capture its dependence on the salinity of the bulk solution and the pore size (and thus the mean interplatelet spacing). For some clays such as kaolinite, to our knowledge, these large data set is missing. Despite the critical points raised above, this decomposition is possible for the most studied clay material, i.e. montmorillonite. A simplified approach is also proposed to interpret the thermo-osmotic behavior identified for kaolinite materials in Section 4.3.

4.2. Smectite clays

The disjoining pressure data of Callaghan and Ottwill [48] were used here. The authors measured by the mechanical approach the total disjoining pressure for a Na–montmorillonite at different concentrations of the equilibrium (bulk) solution (10^{-1}, 10^{-2}, 10^{-3} and 10^{-4} mol L^{-1}) and at $T = 298$ K. The data can be used to examine the relative importance of the different excess specific enthalpy terms in Eq. (32). Once the excess specific enthalpy is characterized, the value of the thermo-osmotic coefficient k_T can be calculated. The excess specific enthalpy related to structural forces requires the identification of an expression for the structural component of the disjoining pressure. Fig. 4 shows the disjoining pressure measured by Callaghan and Ottwill [48] for a bulk solution at 10^{-4} mol L^{-1} and the theoretical DLVO curve. A Hamaker constant of 2.2×10^{-20} (J) consistent with that used by Garcìa-Garcìa et al. [54] for bentonite was used in the calculations. The electrical model required to calculate the electrostatic term (Eq. (23)) is the triple layer model developed by Leroy and Revil [55] and subsequently modified by Gonçalvès et al. [53,56] to account for double layer overlap. This model was already used to calculated the electrostatic component of the disjoining pressure for Na–montmorillonite [53]. The structural component was obtained by subtracting the

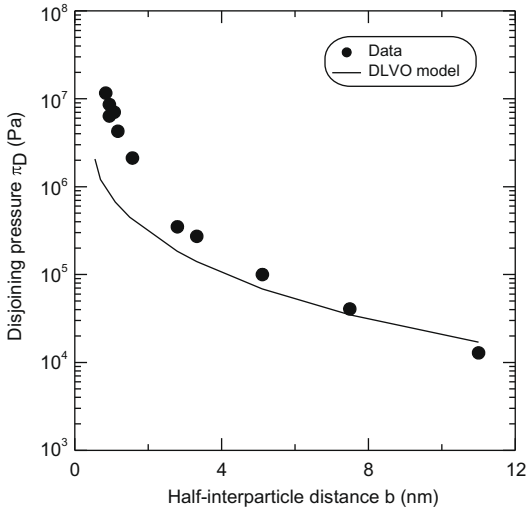

Fig. 4. Measured disjoining pressure and DLVO calculation for a smectite at 10^{-4} mol L^{-1}. Data from [48].

DLVO disjoining pressure to the measurements. Fig. 5 shows the results obtained for the different concentrations of the bulk solution. At high concentrations, the structural term is described by a single exponential decay while a bi-exponential decay better describes this term for dilute solutions. Indeed, at dilute solution (here 10^{-4} mol L^{-1}), the long range behavior of structural forces is enhanced. Conversely, high concentrations for the bulk solution would promote short range structural forces. This could be related to the collapse of the electrical double layer at elevated concentrations yielding a layer of counterions closer to the mineral surface. The parameters for the two limiting curves describing the behavior at 10^{-1} and 10^{-4} mol L^{-1} are given in the legend of Fig. 5. Interestingly, the same longer range behavior at dilute bulk solutions was obtained by Rabinovich and Derjaguin [37] for quartz flat surfaces.

The different components of the disjoining pressure were used to calculate the excess specific enthalpy terms involved in Eq. (32). According to Derjaguin et al. [19], the Van der Waals component is almost insensitive to temperature. This was verified in a recent

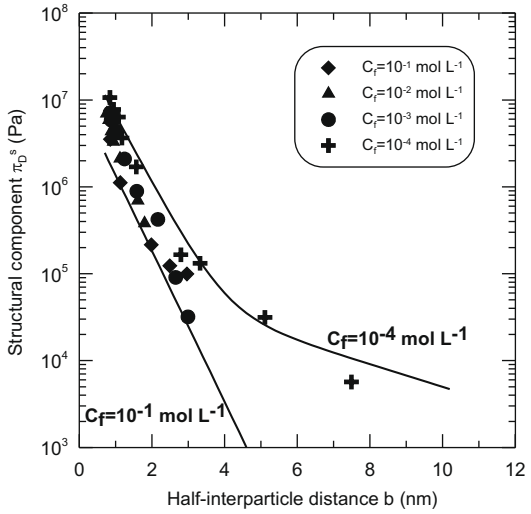

Fig. 5. Structural component of the disjoining pressure inferred from the difference between the DLVO theory and the data of Callaghan and Ottwill [48] for smectite. Bi-exponential curves $\pi_D^s = \kappa_1 \exp(-B/\lambda_1) + \kappa_2 \exp(-B/\lambda_2)$ are considered. At 10^{-1} mol L^{-1}, $\kappa_1 = 10^7$ Pa and $\lambda_1 = 1$ nm and $\kappa_2 = 0$ (no long range behavior). At 10^{-4} mol L^{-1}, $\kappa_1 = 4 \times 10^7$ Pa, $\lambda_1 = 1.1$ nm, $\kappa_2 = 10^5$ Pa and $\lambda_2 = 6.70$ nm.

study on bentonites by García-García et al. [54]. Therefore, introducing the expression for Π_D^{vdw} into Eq. (33) and neglecting the second term leads to a trivial expression for the molecular excess enthalpy term ΔH^{vdw}. This expression yields negligible contributions to the total excess specific enthalpy. Consequently, it is not considered hereafter. The electrostatic term for the excess specific enthalpy was calculated using the electrical model mentioned above. The temperature dependence for the electrostatic component of the disjoining pressure was identified using a perturbation method. These calculations yielded negative values of ΔH^e which are depicted in Fig. 6. The same result was obtained by Derjaguin et al. [19, Chapter 11] for a single plane-parallel slit. Consequently, if electrostatic interactions are considered alone, a positive thermo-osmotic coupling coefficient would be predicted when mostly negative value were measured for clay materials. Positive values of the structural excess specific enthalpy were obtained using the structural component of the disjoining pressure determined above and the simple temperature relation presented in Section 4.1 (see Fig. 6). Fig. 6 also shows the few available data for bentonite in dilute solutions but unknown equilibrium solution concentration. The calculations suggest that whatever the concentration of the bulk solution, the structural excess specific enthalpy generally outweighs the electrostatic one. However, due to the uncertainty on the disjoining pressure decomposition, a prominent electrostatic component at large pore size explaining some (although rare) positive value of the thermo-osmotic coefficient reported by Dirksen [21] is possible. Therefore, the significant and negative values of the thermo-osmotic coupling coefficients obtained for smectitic clays can only be explained by a generally prominent structural term ΔH^s. These results support the interpretation of Derjaguin et al. [19] that the thermo-osmotic process is related to the presence of specific structure water in interfacial zones. The results points to a fundamental role of temperature in explaining at least qualitatively the relation between thermo-osmotic coefficients and pore size.

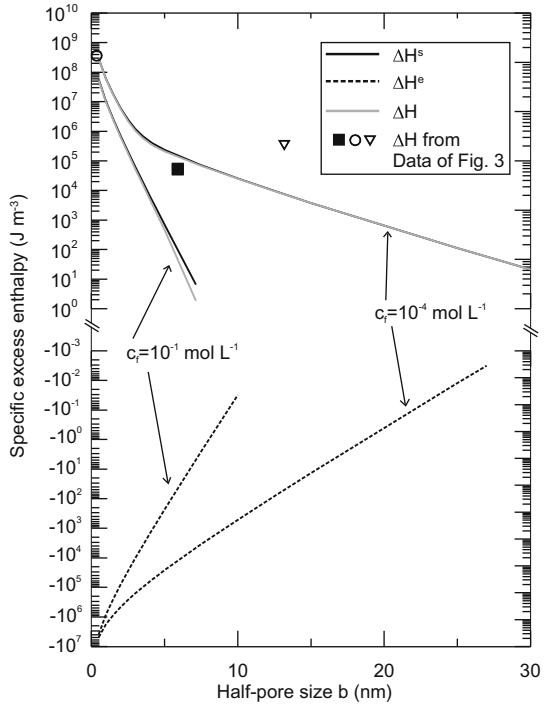

Fig. 6. Excess specific enthalpy components and total values for smectite. The values from the data (same symbols than in Fig. 3) are computed using $k_T/kT\eta_f = \Delta H$.

4.3. Kaolinite

Some valuable thermo-osmotic coefficient data for kaolinite were obtained by Dirksen [21]. Despite the small amount of disjoining pressure data for kaolinite, an attempt is made here to apply the approach described in Section 3. In a simplified manner, since the analysis carried out in the previous section suggests the dominance of the structural specific excess enthalpy ΔH^s, this later was considered alone. The only reliable surface force data for kaolinite is from Li et al. [52]. The authors used AFM measurements to identify the total surface force between two spherical probes covered with kaolinite in a KCl solution at 10^{-3} mol L^{-1}. A measured value of -35 mV for the zeta potential was used as a boundary condition to solve numerically the Poisson–Boltzmann equation and to

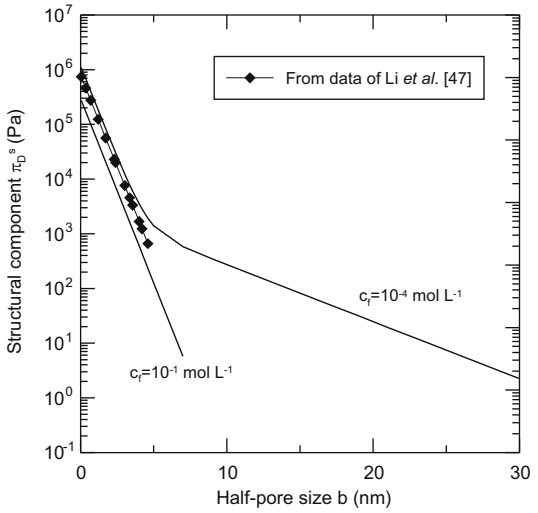

Fig. 7. Structural component of the disjoining pressure inferred from the difference between the DLVO theory and the data of Li et al. [52] for kaolinite. The figure also show the curves postulated by similarity with the results obtained in Section 4.2 for smectite. Bi-exponential curves $\pi_D^s = \kappa_1 \exp(-B/\lambda_1) + \kappa_2 \exp(-B/\lambda_2)$ are considered. At 10^{-1} mol L^{-1}, $\kappa_1 = 2.95 \times 10^5$ Pa, $\lambda_1 = 1.30$ nm and $\kappa_2 = 0$ (no long range behavior). At 10^{-4} mol L^{-1}, $\kappa_1 = 1.2 \times 10^6$ Pa, $\lambda_1 = 1.30$ nm, $\kappa_2 = 3 \times 10^3$ Pa and $\lambda_2 = 8.30$ nm.

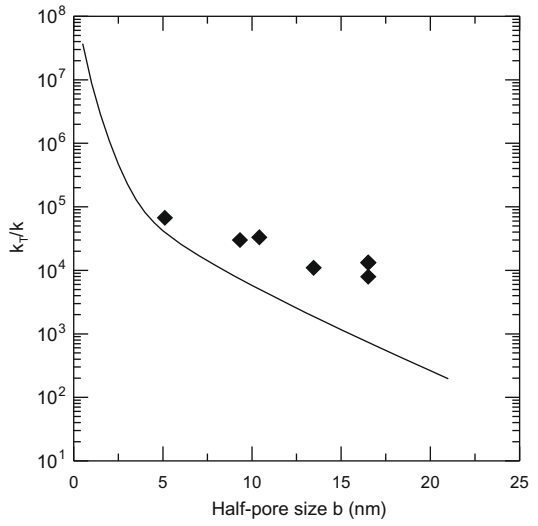

Fig. 8. Calculated ratio $k_T/k = \Delta H/\eta_f T$ using the expression of the structural component of the disjoining pressure of Fig. 7at $c_f = 10^{-4}$ mol L^{-1} alone to estimate ΔH and measurements of Dirksen [21] for kaolinite.

calculate the electrostatic component of the DLVO surface force. In addition, the molecular surface force was calculated using Eq. (25) with a Hamaker constant of 2×10^{-20} (J). A substantial structural force was inferred from the comparison between DLVO calculations and measurements. The data of Li et al. [52] together with Eq. (29) was used to determine the structural component of the disjoining pressure at 10^{-3} mol L^{-1}. The result is shown in Fig. 7. Fig. 8 also shows the dependence of the structural component π_D^s on the concentration assumed here by similarity with the results obtained for smectite in this study or for quartz by Rabinovich and Derjaguin [37]. These curves are used to calculate the structural excess specific enthalpy. The results are shown in Fig. 8 together with the values of the ratio k_T/k measured by Dirksen [21]. This figure shows that the measured values of the ratio k_T/k are found to be close to the calculated curve for dilute solutions. Although the equilibrium solution concentration for the experiments carried out by Dirksen [21] is unknown, such dilute solutions were used by the author during the thermo-osmotic experiments suggesting an appreciable consistency within one order of magnitude between the data and the model.

5. Concluding statements

The pioneering theoretical work on thermo-osmosis of Derjaguin et al. [19, and references herein] for a single plane-parallel pore was extended at the macroscopic scale using a simple volume averaging approach. This original theory seems to capture at least qualitatively the behavior of the thermo-osmotic coefficient k_T which shows a rapid decrease with increasing pore size. The model requires the identification of the mean excess specific enthalpy associated with interfacial interactions. This latter was calculated using the relation between the disjoining pressure and the excess Gibbs energy of the interfacial fluid and applying the Gibbs–Helmholtz relationship. In accordance with Derjaguin's view, a prominent role of the structural part of the excess specific enthalpy ΔH^s associated with the presence of a specific water structure at the mineral–water interface was identified. In this context, the temperature is an important variable since the layer of specific water structure is destroyed at temperatures above 70 °C. The model is based on a decomposition of the disjoining pressure yielding some expressions of the structural component π_D^s. A simple but plausible temperature dependence for the structural component of the disjoining pressure was considered. The enhanced long range of structural forces at low bulk concentration obtained for smectite and assumed for kaolinite yielded a better agreement with the thermo-osmotic data. Despite the simplifications and uncertainties on the disjoining pressure decomposition, encouraging results were obtained. Additional surface force measurements (notably for kaolinite) and most expectedly a fully predictive model for the structural surface forces are desirable in order to improve the model. Provided that a better description of the structural component of the disjoining pressure of pure clays is available, an interesting prospect would be to extend this analysis to natural media. In the absence of such developments and in a pragmatic view, the empirical results shown in Fig. 3b can be used to obtain first estimates of the thermo-osmotic conductivity for natural formations.

Acknowledgments

The French Institut de Radioprotection et de Sûreté Nucléaire (IRSN) is acknowledged for his support. The two anonymous reviewers are acknowledged for their relevant comments which allowed a substantial improvement of the manuscript.

References

[1] D.V. de Groot, P. Mazur, Non-Equilibrium Thermodynamics, Dover, New York, 1984.
[2] G.H. Bolt, Soil Chemistry, B: Physicochemical Models, Elsevier, Amsterdam, 1979.
[3] S.T. Horseman, J.J.W. Higgo, J. Alexander, J.F. Harrington, Water, Gas and Solute Movement Trough Argillaceous Media, Nuclear Energie Agency Rep. CC-96/1, OECD, Paris, 1996.
[4] J.K. Mitchell, Fundamentals of Soil Behavior, John Wiley & Sons, New York, 1993.
[5] A. Revil, P. Leroy, J. Geophys. Res. 109 (2004) B03208, doi:10.1029/2003JB002755.
[6] P. Rousseau-Gueutin, J. Gonçalvès, S. Violette, Phys. Chem. Earth 33 (2008) S106.
[7] E. Bresler, Soil Sci. Soc. Am. Proc. 37 (5) (1973) 663.
[8] B.D. Cey, S.L. Barbour, M.J. Hendry, Can. Geotech. J. 38 (5) (2001) 1025.
[9] C.E. Neuzil, Nature 403 (2000) 182.
[10] D. Coelho, M. Shapiro, J.F. Thovert, P.M. Adler, J. Colloid Interface Sci. 181 (1996) 169.
[11] A.M. Garavito, I. De Cannire, H. Kooi, Phys. Chem. Earth 32 (2007) 421.
[12] A. Gupta, D. Coelho, P.M. Adler, J. Colloid Interface Sci. 319 (2008) 549.
[13] T.J.S. Keijzer, J.P.G. Loch, Soil Sci. Soc. Am. J. 65 (2001) 1045.
[14] W.D. Kemper, J.B. Rollins, Soil Sci. Soc. Am. Proc. 30 (5) (1966) 529.
[15] M.A. Malusis, C.D. Shackelford, H.W. Olsen, Eng. Geol. 70 (2003) 235.
[16] C. Moyne, M. Murad, Int. J. Solids Struct. 39 (2002) 6159.
[17] M. Rosanne, M. Pastzkuta, J.-F. Thovert, P.M. Adler, Geophys. Res. Lett. 31 (2004) L18614, doi:10.1029/2004GL020770.
[18] M. Rosanne, M. Paszkuta, P.M. Adler, J. Colloid Interface Sci. 297 (2006) 353.
[19] B.V. Derjaguin, N.V. Churaev, V.M. Muller, Surface Forces, Plenum Press, New York, 1987.
[20] H.P. Hutchison, I.S. Nixon, K.G. Denbigh, Discuss. Faraday Soc. 3 (1948) 86.
[21] C. Dirksen, Soil Sci. Soc. Am. Proc. 33 (1969) 821.
[22] R.C. Srivastava, P.K. Avasthi, J. Hydrol. 24 (1975) 111.
[23] R.C. Srivastava, A.K. Jain, Indian J. Chem. 12 (1974) 1276.
[24] C. Tournassat, E. Ferrage, C. Poinsignon, L. Charlet, J. Colloid Interface Sci. 273 (2004) 234.
[25] H. Van Olphen, An Introduction to Clay Colloid Chemistry for Clay Technologists, Geologists and Soil Scientists, John Wiley & sons, New York, 1977.
[26] G. Sposito, N.T. Skipper, R. Sutton, S.-H. Park, A.K. Soper, J.A. Greathouse, Proc. Natl. Acad. Sci. USA 96 (1999) 3358.
[27] J. Israelachvili, H. Wennerstrom, Nature 379 (1996) 219–225.
[28] G. de Marsily, Quantitative Hydrogeology, Groundwater Hydrology for Engineers, Academic Press, New York, 1986.
[29] L. Zheng, J. Samper, Phys. Chem. Earth 33 (2008) S486.
[30] J. Trémosa, J. Gonçalvès, J.-M. Matray, S. Violette, J. Colloid Interface Sci., (2009), doi:10.1016/j.jcis.2009.09.055.
[31] G. Mesri, R.E. Olson, Clays Clay Miner. 19 (1971) 151.
[32] H. Lyklema, Fundamentals of Interface and Colloid Science, Elsevier, Amsterdam, 1991. Vol. I.
[33] I. Langmuir, J. Chem. Phys. 6 (1938) 873.
[34] B.V. Derjaguin, M.M. Kussakov, Acta Physicochim. URSS 10 (1939) 153.
[35] M.B. McBride, Clays Clay Miner. 45 (1997) 598.
[36] R.M. Pashley, J. Colloid Interface Sci. 80 (1981) 153.
[37] Y.I. Rabinovich, B.V. Derjaguin, Langmuir 3 (1987) 625.
[38] S. Martin, Clays Clay Miner. 9 (1960) 28.
[39] J. Wang, A.G. Kalinichev, R.J. Kirkpatrick, Geochim. Cosmochim. Acta 70 (2006) 562.
[40] M.R. Warne, N.L. Allan, T. Cosgrove, Phys. Chem. Chem. Phys. 2 (2000) 3663.
[41] S. Marcelja, N. Radic, Chem. Phys. Lett. 42 (1976) 129.
[42] M.L. Berkowitz, K. Raghavan, Langmuir 7 (1991) 1042.
[43] L.B. Boinovich, A.M. Emelyanenko, Adv. Colloid Interface Sci. 96 (2002) 37.
[44] J. Faraudo, F. Bresme, Phys. Rev. Lett. 94 (2005) 077802.
[45] V.M. Paunov, R.I. Dimova, P.A. Kralchevsky, G. Broze, A.J. Mehreteab, J. Colloid Interface Sci. 182 (1996) 239.
[46] R.M. Pashley, Adv. Colloid Interface Sci. 16 (1982) 57.
[47] B. Viani, P. Low, C. Roth, J. Colloid Interface Sci. 96 (1) (1983) 229.
[48] I.C. Callaghan, R.H. Ottwill, Discuss. Faraday Soc. 57 (1974) 110.
[49] J.N. Israelachvili, G.E. Adams, J. Chem. Soc., Faraday Trans. I 74 (1978) 975.
[50] J.N. Israelachvili, Proc. Natl. Acad. Sci. USA 84 (1987) 4722.
[51] J.I. Quirk, R.M. Pashley, Aust. J. Soil Res. 29 (1991) 209.
[52] H. Li, J. Long, Z. Xu, J.H. Masliyah, AIChE J. 53 (2007) 479.
[53] J. Gonçalvès, P. Rousseau-Gueutin, A. Revil, J. Colloid Interface Sci. 316 (2007) 92.
[54] S. García-García, M. Jonsson, S. Wold, J. Colloid Interface Sci. 298 (2006) 694705.
[55] P. Leroy, A. Revil, J. Colloid Interface Sci. 270 (2004) 371.
[56] J. Gonçalvès, P. Rousseau-Gueutin, J. Colloid Interface Sci. 320 (2008) 590.
[57] P. Habib, F. Soeiro, Migrations d'eau dans les sols provoquées par une difference de température, in: International Congres of Soil Mechanics, Proceedings, 1957, p. 40.

Importance of thermo-osmosis for fluid flow and transport in clay formations hosting a nuclear waste repository

Julio Gonçalvès[a,b], Ghislain de Marsily[c], Joachim Tremosa[c,d]

[a] *Aix-Marseille Univ., CEREGE, UMR 6635, 13545 Aix en Provence cedex 4, France*
[b] *CNRS, CEREGE, UMR 6635, 13545 Aix en Provence cedex 4, France*
[c] *UPMC Univ. Paris 6, UMR-7619 SISYPHE, 4 place Jussieu, 75252 Paris cedex 05, France*
[d] *Institut de Radioprotection et de Sûreté Nucléaire, IRSN/DEI/SARG/LR2S, BP 17, 92262 Fontenay-aux-Roses, France*

Abstract

Three osmotic processes have been identified in clay-rich media. Electro- and chemo-osmosis -flows of water caused by salinity and electrical potential gradients - have so far attracted almost exclusive attention. But, despite the recurring concern about the importance of thermo-osmosis - a flow of water driven by a temperature gradient - in argillaceous media, it remains largely neglected. Here we propose a new formalism for estimating the thermo-osmotic permeability based on a theoretical analysis at the molecular and pore scale, then upscaled. We show that the thermo-osmotic permeability, poorly predicted so far, can be estimated only from surface-charge density, temperature, pore size and salinity. The prominent role of thermo-osmosis in compacted shale layers with a temperature gradient is then exemplified. This first general estimate of the thermo-osmotic permeability can be used to improve our understanding of the influence on fluid flow and pressure fields of the natural geothermal gradient in sedimentary basins, which is required

e.g. for safety assessments of nuclear-waste repositories in shale layers.

Keywords: Transport processes, Thermo-osmosis, clay materials, Nuclear safety

---

1. Introduction

Electro- and chemo-osmosis have been described and quantified since the 19th century (Mitchell, 1993; Neuzil, 2000). The physical principles of thermo-osmosis, at the molecular and pore scales, were established more than 70 years ago by Derjaguin and coworkers (Derjaguin and Sidorenkov, 1941; Churaev, 2000) as the so-called mechano-calloric effect, but its importance in argillaceous media has only recently been emphasized (Carnahan, 1986; Soler, 2001); the link was missing between the physical and chemical properties of the medium and the magnitude of the thermo-osmotic permeability for practical applications. When a quasi-isothermal pressure gradient is prescribed through a porous membrane, the fluid flow causes a temperature gradient build-up (see Fig. 1). This heat flux is attributed to a specific enthalpy of the fluid film in the pores which differs by a quantity $\triangle h$ (J m^{-3}) at the pore scale from that of the bulk fluid (Derjaguin and Sidorenkov, 1941; Churaev, 2000). This difference is associated with an alteration of the hydrogen bond (HB) network of the water molecules and thus of the intermolecular bond energy due to fluid-solid interactions. If the hydrogen bonding is weakened by these interactions, i.e. the HB concentration decreases, heat absorption occurs when the fluid enters into the pore space (Churaev, 2000). Conversely, heat is released at the outlet generating the temperature gradient depicted in Fig. 1. The counterpart of the mechano-caloric effect outlined above,

i.e. thermo-osmosis, derives from Onsager's reciprocity principle. This thermodynamic principle requires that the reciprocal process exists, i.e., a fluid flow caused by a temperature gradient. Such a thermo-osmotic process has been observed in clay-rich materials (see e.g., Gonçalvès and Tremosa, 2010; Tremosa *et al.*, 2010). The alteration of the HB network in the pore space of clay-rocks is due to two main antagonistic mechanisms. First, the negative surface charge of clay minerals at natural pH is balanced by counterions (cations, Mitchell, 1993; Sposito *et al.*, 1999) and forms together with the mineral surface the electrical double-layer. But, solvated ions cause some disruption of HB especially in the first hydration shells (Guàrdia *et al.*, 2005). For instance, the calculated average number of hydrogen bonds per water molecule in the first hydration shell of Na^+ is 2.27 while it is 3.5 for bulk water (Guàrdia *et al.*, 2005). In addition, molecular dynamics simulations (Wang *et al.*, 2004; Guàrdia *et al.*, 2005; Marry *et al.*, 2008) have shown that the first two or three mono-layers of water molecules at the clay surface are more strongly hydrogen bonded than the bulk water. This results in an average number of hydrogen bonds per water molecule of between 3.5 and 4 (Wang *et al.*, 2004; Marry *et al.*, 2008). Beyond this thickness, the water is ordered like bulk water except in the hydration shells of ions.

However, although the molecular concepts supporting this thermo-osmotic flow are part of fundamental physics, a macroscopic law for practical thermo-osmosis calculations in geological media is needed. We used a simple volume-averaging approach which yields (Gonçalvès and Tremosa, 2010) :

$$q = -\frac{k}{\eta}(\nabla p + \rho g \nabla z) - \frac{k \triangle H}{\eta T} \nabla T, \tag{1}$$

where q is the pore fluid specific discharge (m s^{-1}), k is the classical Darcy

permeability (m^2), η is the dynamic viscosity (Pa s), p is the pressure (Pa), ρ is the fluid density (kg m^{-3}) g is the acceleration due to gravity (m s^{-2}), ∇z is (0,0,1) if the z axis is vertical upwards, T is the temperature (K) and $\triangle H$ is the macroscopic volume-averaged excess specific enthalpy due to fluid-solid interactions (J m^{-3}). According to Eq. (1), the thermo-osmotic permeability is $k_T = k\triangle H/T$ (Pa m^2 K^{-1}). In most observed cases, $\triangle H$ >0, and fluid flow occurs from the warm to the cold side of a clay sample. A theoretical expression for k_T/k had been developed (Tasaka and Nagasawa, 1978) by introducing several molecular parameters, which must however be calibrated on thermo-osmotic experiments, thus weakening its a priori predictability. A macroscopic expression was also developed by Revil and Leroy (2004) but some of its limitations were discussed by Gonçalvès and Tremosa (2010). Therefore, fully predictive theoretical expressions for k_T are lacking so far. Here, we developed such an expression by directly formalizing the enthalpy change $\triangle H$ due to hydrogen bonding modifications at the macro-scale.

2. Mathematical model

The theoretical model is described here for a 1:1 salt like NaCl. Following the thermodynamic interpretation by Derjaguin and Sidorenkov (1941), the required $\triangle H$ value can be heuristically obtained with:

$$\triangle H = (C^b_{HB} - C_{HB})\triangle H_{HB} \tag{2}$$

where C^b_{HB} and C_{HB} are the HB concentrations in the bulk (mol m^{-3}) and the pore fluid and $\triangle H_{HB}$ (J mol^{-1} of HB) is the energy to break one mole of HB. Estimated values of $\triangle H_{HB}$ between 6 and 23 kJ mol^{-1} are reported

(Hakem *et al.*, 2007). Let C_w and N_{HB} be the water concentration (mol m^{-3}) and the mean number of hydrogen bonds per water molecule, respectively. Taking into account the 1/2 bind order (Hakem *et al.*, 2007) of a HB, the HB concentration C_{HB} is $C_w 1/2 N_{HB}$. Consequently, the hydrogen-bond concentrations are calculated with :

$$\begin{aligned} C_{HB} =& N_w^+ C_+ 1/2 N_{HB}^+ + N_w^- C_- 1/2 N_{HB}^- \\ &+ (C_w - N_w^+ C_+ - N_w^- C_-)(\frac{b - b_s}{b} N_{HB}^b + \frac{b_s}{b} N_{HB}^s) 1/2 \end{aligned} \tag{3}$$

and,

$$\begin{aligned} C_{HB}^b =& N_w^+ c_b 1/2 N_{HB}^+ + N_w^- c_b 1/2 N_{HB}^- \\ &+ (C_w - N_w^+ c_b + -N_w^- c_b) N_{HB}^b 1/2 \end{aligned} \tag{4}$$

where C_w, C_+ and C_- are the water, cation and anion concentrations (mol m^{-3}) in the pore space, N_w^+ and N_w^- are the number of water molecules in the first hydration shell of the cation and the anion, N_{HB}^+ and N_{HB}^- are the mean number of HB per water molecule in the first hydration shells, b and b_s are the mean half pore-size and the half thickness of highly ordered water (m), N_{HB}^b and N_{HB}^s are the mean number of HB per water molecule of bulk and highly ordered water. The sum of the two first terms on the right-hand side of Eq. (3) is the number of HB per unit volume of pore fluid affected by ionic disruption while the third term is the complementary part for water molecules outside the influence of ions. For the latter, $\frac{b-b_s}{b} N_{HB}^b + \frac{b_s}{b} N_{HB}^s$ represents the mean number of HB per water molecule accounting for the highly ordered water at the solid surface. C_w is calculated with the conservation equation

(see e.g., Revil and Leroy, 2004; Gonçalvès and Rousseau-Gueutin, 2008):

$$\nu_w C_w + \nu_+ C_+ + \nu_- C_- = 1 \tag{5}$$

where ν_w, ν_+ and, ν_- are the molar volumes of the water, cation and anion, respectively. In the bulk water, Eq. (3) with $C_+ = C_- = c_b$ is used to calculate C_w. In the pore space, C_+ and C_- are identified using the Donnan equilibrium equation. The Donnan equilibrium model (Mitchell, 1993) allows the identification of the average concentrations of counterions and co-ions in the porosity of the charged porous medium, which are

$$C_+ = \sqrt{\frac{Q_V^2}{4N_a^2 e^2} + c_b^2} + \frac{Q_V}{2N_a e}, C_- = \sqrt{\frac{Q_V^2}{4N_a^2 e^2} + c_b^2} - \frac{Q_V}{2N_a e}, \tag{6}$$

where c_b is the concentration of the cation and the anion in the bulk solution, e is the elementary charge (1.6 10^{-19} C), N_a is Avogadro's constant (6.02 10^{23} mol^{-1}) and Q_V is the excess charge per unit pore volume (C m^{-3}) to be compensated by counterions. Note that in Eq. (6), concentrations are in mol m^{-3}. Q_V is obtained by dividing the excess charge (C) in a unit volume of porous medium (1-ω)$\rho_s CEC \times 96.3$ by the associated water volume ω yielding

$$Q_V = \frac{(1-\omega)\rho_s CEC \times 96.3}{\omega}, \tag{7}$$

where ω is the porosity, ρ_s is the density of the solid (kg m^{-3}) and CEC is the cation exchange capacity (meq g^{-1}). For the practical use of this model, the half-pore size b has to be calculated. the half-pore size b can be calculated by equating $A_s b$ (m^3 per kg of solid) with A_s (m^2 g^{-1} the specific surface area (SSA) to the water content per kg of solid $\omega/(1-\omega)\rho_s$ considering a plane-parallel conceptual geometry for the porous medium (Neuzil, 2000)

yielding:

$$b = \frac{\omega}{(1-\omega)\rho_s A_s}. \tag{8}$$

Note that introducing Eq.(8) into Eq. (7) yields $Q_V = CEC \times 96.3/A_s b = \sigma/b$ where $\sigma = CEC \times 96.3/A_s$ (C m^{-2}) is the solid surface-charge density. Eq. (4) was obtained by setting $C_+ = C_- = c_b$ and b_s=0 in Eq. (3) leading to the expression for C^b_{HB} to be used in Eq. (2). Equations (2) to (8) form a model whose main inputs are a few petrophysical parameters and molecular properties of solutions. The main advantage of this model is the use of petrophysical parameters currently measured in clay-rocks together with molecular parameters that are well constrained notably through molecular dynamics simulations. For the molecular parameters, values from the literature (Guàrdia *et al.*, 2005; Hakem *et al.*, 2007; Marry *et al.*, 2008; Gonçalvès and Rousseau-Gueutin, 2008) were used: N^+_w=N^-_w=6, N^+_{HB}=2.27, N^-_{HB}=2.65, N^b_{HB}=3.5, ν_+, ν_- and ν_w, are 23.80, 17.40 and 18.00 10^{-6} m^3 mol^{-1} except for N^s_{HB} and $\triangle H_{HB}$ where average values of 3.75 and 14.5 kJ mol^{-1} were used. A mean value of 1 nm for b_s was used (Mitchell, 1993). A similar state of hydration of ions in the pore space and in the bulk solution was postulated. This is supported by recent molecular dynamics simulations for clay-solution systems (Marry and Turq, 2003). Besides the $1/T$ coefficient appearing in the theoretical expression of k_T, a weak temperature effect can be expected. For instance, the quantities most sensitive to the temperature, i.e. the number of hydrogen bonds in the bulk and the $\triangle H_{HB}$, are weakly variable with temperature. Indeed, the mean number of HB per water molecule varies by less than 15% between 273 K and 373 K (Suresh and Naik, 2000). In addition, $\triangle H_{HB}$ can be identified for instance by dividing the enthalpy of vaporization

by $1/2N_{HB}$. But this enthalpy varies from 45 to 40 kJ mol^{-1} between 273 and 373 K. This is in complete contradiction with the unsupported assertion by Derjaguin (see Tremosa *et al.*, 2010, and references therein) that the thermo-osmotic process should disappear at about 343 K.

3. Results and discussion

3.1. Model vs data

We assembled the best quality data on thermo-osmosis available in the literature for clay-rocks, including some exhaustive petrophysical descriptions i.e. porosity ω, permeability k, SSA A_s , CEC, density of the solid ρ_s and variables such as the concentration of the bulk solution c_b (mole L^{-1}) and the temperature T. These data (64) are listed in Table 1. Some studies provide directly k_T/k values (Dirksen, 1969; Rosanne *et al.*, 2006; Zheng and Samper, 2008; Tremosa *et al.*, 2010) while others present $\triangle p/\triangle T|_{q=0}$ measured at steady state in horizontal thermo-osmotic flow experiments (see Fig. 1; Habib and Soeiro, 1957; Taylor and Cary, 1960; Cary, 1966; Gray, 1966). $\triangle p$ and $\triangle T$ are the pressure and temperature differences across a clay-rich sample. If the higher values of p and T are on the same side of the sample, this ratio is positive. Most often in clay materials, $\triangle p/\triangle T|_{q=0} < 0$ i.e. water flows from the warm to the cold side and pressure rises on the latter. Recalling the fluid-flow equation:

$$q = -\frac{k}{\eta}(\nabla p + \rho g \nabla z) - \frac{k_T}{\eta}\nabla T, \tag{9}$$

one can see that$\triangle p/\triangle T|_{q=0} = -k_T/k$.

For shale C1 (Al-Bazali, 2005), k_T/k was inferred from chemo- and thermo-osmotic fluxes at constant temperature and concentration differences across

a sample. At equilibrium, $q = -k/\eta\nabla p + k\varepsilon/\eta\nabla\pi - k_T/\eta\nabla T = 0$ yielding $k_T/k = (\varepsilon\triangle\pi - \triangle p)/\triangle T$ where ε, $\triangle p$, $\triangle\pi$ and $\triangle T$ are the measured chemical osmotic efficiency, the measured pressure difference across the shale sample at equilibrium and the imposed osmotic pressure and temperature differences, respectively. The thermo-osmotic permeability k_T is identified only if k has been estimated independently. Pore size which is a crucial parameter for predictive models of transport coefficients in clay-rich porous media (see e.g., Mitchell, 1993; Neuzil, 2000) was calculated for each clay-rock in Table 1. Only pores efficient for conducting fluid flow i.e., those in contact with the external surfaces of clay aggregates, have to be considered for hydrodynamic calculations. This excludes the interlayer space i.e., the pores between basic clay layers (interlayer distance as low as 1 nm or less) where fluid is almost immobile (Mitchell, 1993). Consequently, only petrophysical properties related to external surfaces are used hereafter. From this standpoint, a porosity measurement by mercury porosimetry which does not explore pores below 3 nm of interparticle distance satisfies the above-mentioned constraint. In addition, external and total (including interlayer space) SSA can be estimated by BET and EGME measurements. Once external SSA is estimated for each material, the use of "external" porosity ω and SSA in Eq. (8) provides an estimate of the required representative pore size $2b$, thus in contact with external surfaces. Besides the pore size, the surface charge density σ (C m^{-2}) which can be obtained by $\sigma = CEC(\text{meq g}^{-1})/A_s(\text{m}^2\ \text{g}^{-1})\times 96.3(\text{C meq}^{-1})$ is the other key parameter to calculate the thermo-osmotic permeability. For consistency reasons, external σ should be estimated in clay-rocks by dividing an "external" CEC by the external (BET) SSA. This calculation is straight-

forward when the clay fraction is composed of illite and kaolinite due to the absence of interlayer space and/or weakly exchangeable interlayer cations. Therefore, the measured CEC and external SSA can be used directly to compute σ. The situation is rather different if smectite is present in the clay-rock since the interlayer surfaces of this mineral contribute significantly to the measured CEC. Consequently, some corrections which basically consist in subtracting the contribution of the interlayer surfaces, must be introduced to compute the required "external" CEC reported in Table 1. Such corrections as well as the data set analysis are presented in Appendix A.

A rapid statistical analysis of these data shows that k_T/k is strongly correlated to the solid surface-charge density σ - the excess of negative charge per surface area of solid - confirming an electrochemical control of thermo-osmosis (Carr and Sollner, 1962). In addition, the theoretical dependence of k_T/k to the total ionic content $C_+ + C_- = (Q_V^2/4Na^2e^2 + c_b^2)^{1/2}$ of the porous medium predicted by the model was verified with the available data (see Fig. 2). Values of $k_T/k = \triangle H/T$ calculated with our model as functions of σ, the salinity c_b (mol L^{-1}) and bT where $2b$ is the estimated mean representative pore-size (nm) and T is the temperature (K) are shown in Fig. 3. Use of variable bT allows an exhaustive representation without substantial accuracy loss since the predicted influence of temperature is low (see section 2). With highly plausible values for the parameters described in the previous section, a fairly good agreement (order of magnitude and sign) with the data is found. This is a noteworthy improvement since, so far, an empirical range of 10^{-13}-10^{-17} Pa m^2 K^{-1} for k_T has been used in natural media (Soler, 2001). For positive k_T, i.e. at small pore-sizes and potentially significant thermo-

osmotic permeabilities, the data are reproduced within about one order of magnitude. Less agreement is found for negative k_T (when flow occurs from the cold to the warm side) but this concerns large-pore materials with weak thermo-osmotic properties. Higher uncertainty on pore-size calculations may be the reason. Fig. 3 also shows the prominent role of σ the surface charge density. Indeed, when σ is large, k_T/k is almost independent of c_b. Our model provides a simple theoretical justification of an empirically observed (Carr and Sollner, 1962) dependence of the thermo-osmotic permeability on the surface-charge, the bulk fluid concentration, the type of counterion (here through the solvation number and its HB disruption properties), the pore size and the temperature.

3.2. Thermo-osmosis in sedimentary basins

We applied our model to an illitic shale in a sedimentary basin containing a c_b=10^{-1} mol L^{-1} NaCl solution. Considering that fluid flow is mostly vertical across shale layers (Marsily, 1986), we computed the thermo-osmotic to hydraulic flow ratio $q_T/q_p = \frac{k_T}{\eta}\frac{\partial T}{\partial z}/\frac{k}{\eta}\frac{\partial p}{\partial z}$ as a function of depth. Plausible pressure and temperature gradients, constant across the shale layer, were prescribed, ($\frac{\partial p}{\partial z} = -\rho g - 10^3$ Pa m^{-1}, e.g. 10 m of hydraulic head loss across a 100 m thick shale layer and $\frac{\partial T}{\partial z} = -G_T$ with G_T ≈0.033 K m^{-1} the usual natural geothermal gradient). In this case the Darcy and the thermo-osmotic flows are both directed vertically upward. $k_T/k = \triangle H/T$ at depth z^* was calculated with our model for σ=0.29 C m^{-2} which corresponds to a specific surface area A_s of 50 m^2 g^{-1} and a cation exchange capacity CEC of 0.15 meq g^{-1} (Mitchell, 1993). The mean half pore-size b at depth z^* was computed using A_s, the solid-grain density ρ_s=2600 kg

m^{-3} and the shale porosity ω (see section 2, Eq. (8)). ω at depth z^* resulting from the basin history (compaction, erosion) including a possible erosion thickness z_e^* explaining overconsolidation (lower porosity than expected at a given depth) was calculated with an exponentially decreasing porosity-depth function (Sclater and Christie, 1980): $\omega = \omega_0 exp(-c(z^* - z_e^*))$; z^* (m) is the depth, $\omega_0 = \omega(z^* = z_e^* = 0)$ is the initial (uncompacted) porosity and z_e^* is an erosion thickness. For shales, the coefficient c equals 5.1 10^{-4} m^{-1} and ω_0=0.63 (Sclater and Christie, 1980). The temperature was calculated with $T(z^*) = T_0 + G_T z^*$ and T_0=285 K as average surface temperature. Fig. 4 shows that for standard shale and conditions, the thermo-osmotic flow can be up to 10 times larger than the classical Darcy flow due to the pressure gradient. Furthermore, thermo-osmotic flow can be enhanced if the low thermal conductivity of clays is taken into account, leading to a higher than 0.033 K m^{-1} geothermal gradient. This situation could be even more pronounced if heat-emitting nuclear wastes were stored in deep shale layers creating higher temperature gradients though limited to the duration of the heat-emitting phase of the waste storage.

3.3. Implications for nuclear safety calculations

Thermo-osmosis might contribute to convective transport of unsorbed radionuclides in the context of nuclear waste confinement in argillaceous media. In general, to insure nuclear safety, the waste packages are designed in order to delay the radionuclide release beyond the maximum heat period and no radionuclides are expected to reach the boundaries of a confining shale unit in less than 100 ky (Marsily *et al.*, 1977). Considering that the major heat-emitting phase will last only about 10 ky, and therefore that

its effect will not last long enough to have any great effect, even if during this phase the thermo-osmotic velocity can be much higher than in natural conditions, we calculated the migration distance after 100 ky of thermo-osmotic convection only, as driven by the natural geothermal gradient. This distance which must not exceed the half-thickness of the shale layer (usually 50 m) is thus a minimum in the context of a heat-emitting nuclear waste repository. The thermo-osmotic travel distance $\triangle z$ after $\triangle t$=100 ka is $\triangle z = q_T/\omega \times \triangle t = k_T G_T \triangle t/\eta\omega$, where $-G_T = \partial T/\partial z$ is the natural geothermal gradient. k_T/k were calculated for different couples (b, σ) and two representative values of external SSA A_s using our model for c_b=10^{-1} mol L^{-1} and T=298K. The requested k_T value is then obtained from k which is calculated using a plane-parallel Poiseuille type law $k = b^2/3F$, where F is the formation factor accounting for the tortuosity of porous media. F was calculated using (Mitchell, 1993; Revil and Leroy, 2004) $F = \omega^{-m}$ where m is the cementation factor and $1< m <3$, taken here as 2. The porosity is calculated from b, A_s and ρ_s=2600 kg m^{-3} (see Eq. 8, section 2). For natural shale (of Underground Research Laboratories, URL), corrected external σ were calculated following the methodology described in Appendix A, since an interlayer contribution to CEC associated with the presence of smectite layers (mostly mixed illite/smectite, I/S) can be expected. Indeed, average values of 22% and 9% by weight of I/S for the Callovo-Oxfordian shale and the Opalinus Clay with 35-55% and 30% of smectite in I/S are respectively reported (Gaucher *et al.*, 2004; Boisson, 2005; Tournassat *et al.*, 2009). This yields weight fractions of smectite f_w^{sm} of 7.7-12% and 2.7% for the Callovo-Oxfordian shale and the Opalinus Clay. For the Boom clay, the

approximate expression (Eq. (A.1)) calculated from total and external SSA (44 and 200 m^2 g^{-1}, Boisson, 2005) gives f_w^{sm}=19.5 %. Using these f_w^{sm} values, average CEC and external SSA for the Callovo-Oxfordian shale, the Opalinus Clay and the Boom clay (0.175, 0.11, 0.24 meq g^{-1} and, 30, 30, 44 m^2 g^{-1}) yields the external σ values 0.25-0.36, 0.28 and 0.18 C m^{-2}, respectively. For the Toarcian shale, the smectite fraction is negligible and no correction was made. The values of σ and b are taken from Table 1. For the Wakkanai formation, the 16% and 10% weight fractions (Tachi *et al.*, 2009) of smectite and illite, respectively, are consistent with the measured CEC of 0.2 C m^{-2}. This mineralogical composition yields an estimated external (BET) SSA of 23 m^2 g^{-1} (using Eq. (A.2))which is used to compute σ (0.30 C m^{-2}) and b (9.8 nm with a porosity of 0.37, Tachi *et al.* (2009)). Computed distances and the position of various underground storage levels in argillaceous formations are plotted in Fig. 5. For some storage levels, migration distances of 10 m are obtained. Since average parameters and simplified conditions are used, this study demonstrates the necessity for more exhaustive nuclear safety calculations accounting for all transport processes including thermo-osmosis. Moreover, such calculations could benefit from additional thermo-osmosis experiments in shales.

3.4. Influence of thermo-osmosis on pressure fields

In natural environments, osmotic flows modify both velocity and pressure fields (Neuzil, 2000; Rousseau-Gueutin *et al.*, 2009). Transient (chemical) osmotic flows have been considered plausible causes of anomalous pressures in shales (Neuzil, 2000) i.e., non-hydrostatic pressure distributions. Thermo-osmosis could be another reason for such anomalies. Considering that fluid

flow in shales is mostly vertical and introducing the excess pressure p^* so that $\frac{\partial p^*}{\partial z} = \frac{\partial p}{\partial z} + \rho g$ ($\frac{\partial p^*}{\partial z} = 0$ for hydrostatic variations of p), the steady-state flow regime writes:

$$\frac{\partial}{\partial z}\left(\frac{k}{\eta}\frac{\partial p^*}{\partial z} + \frac{k_T}{\eta}\frac{\partial T}{\partial z}\right) = 0 \tag{10}$$

Assuming p^*=0 at the top and bottom of a shale layer in contact with aquifers on both sides, non-hydrostatic pressures can be obtained if k_T and/or $\frac{\partial T}{\partial z}$ depend on z. To illustrate this, we solved Eq. (10) for the Callovo-Oxfordian formation in north-eastern France, currently considered for a potential nuclear waste repository. The steady-state calculations require that the temperature profile be known. No continuous temperature profile is available at the Bure URL where the excess pressures were measured. But a continuous temperature profile was recently obtained in the transposition zone (less than 10 km away from the URL, Andra, pers. communication), i.e. an area with the same transport and mineralogical characteristics for the Callovo-Oxfordian formation as at the URL. These new data depicted in Fig. 6a show a change in the slope of the temperature-depth evolution which is consistent with weaker clay content in the upper third of the shale layer than in the rest of the layer. Due to the weaker thermal conductivity of clay minerals, this results in a higher thermal gradient at the bottom of the layer. Moreover, the above-mentioned clay content variation is accompanied by mineralogical transitions which affect the petrophysical characteristics of the shale (Gaucher *et al.*, 2004). Therefore, the mean values of ω, CEC, external SSA A_s, fraction of I/S and smectite fraction in I/S are 0.125, 0.1 meq g^{-1}, 16 m^2 g^{-1}, 15% and, 55% in the upper third of the shale (Gaucher *et al.*, 2004). The corresponding values for the lower part are 0.14, 0.175

meq g^{-1}, 34 m^2 g^{-1}, 26% and, 35%. Using these data and correcting for the smectite interlayer (see section 2 and Appendix A) yields σ of 0.20 and 0.29 C m^{-2} in the upper and lower part of the shale, respectively. Note that the uncorrected value of σ is about 0.5 C m^{-2}. Similarly, introducing the porosity and the external SSA values in Eq. (8) yields corresponding b values of 3.5 and 1.9 nm. These values for b and σ together with the mean concentrations of 5×10^{-2} and 10^{-1} mol L^{-1} yield k_T/k of 6.4×10^4 and 2.7×10^5 Pa K^{-1} for the upper and lower part of the clay formation. The excess-pressure values were calculated for a constant k and compared to those calculated with the measured hydraulic head values (Delay *et al.*, 2007). The pressure in the Dogger reservoir was taken as the reference to calculate excess pressures. Fig. 6b shows that excess-pressures of up to 3.6×10^5 Pa occurring at about two-thirds of the thickness of the shale layer could be explained by steady-state thermo-osmosis. Temperature-gradient and thermo-osmotic permeability variations contribute half of this value each. By superposing the steady-state thermo-osmotic effect and the previously calculated chemo-osmosis one (Rousseau-Gueutin *et al.*, 2009), a value of excess pressure of 4.8×10^5 Pa is obtained. This value is close to the maximum observed (Gonçalvès *et al.*, 2004) steady-state excess-pressure of 5.3×10^5 Pa, not fully explained so far.

4. Conclusions

Based on the physical molecular theory for thermo-osmosis, we developed a mathematical expression for the thermo-osmotic permeability. With this new theoretical expression, the thermo-osmotic permeability of argillaceous media can be estimated from their standard physical and chemical properties,

providing both the sign and the order of magnitude of this permeability; this new expression substantially improves the estimation of this permeability, which varies over four orders of magnitude. This new theoretical framework allows the development of a similar model for more complex solutions than the 1:1 electrolyte studied here, using e.g. an electrical model to calculate the mean concentrations in the porosity. Moreover, this approach can be extended to other fields exploring the transport properties of membranes (e.g. mineral, biological, industrial). We demonstrate that thermo-osmosis may prevail over the classical Darcy flow driven by pressure gradients, in clay-rich formations under natural or artificial thermal gradients. Furthermore, this flow can greatly contribute to convective transport of dissolved species. It is thus fundamental to take into account thermo-osmosis to understand and explain the pressure distribution and flow in shale layers, but even more when predicting transport phenomena in such media, particularly for nuclear-waste storage projects.

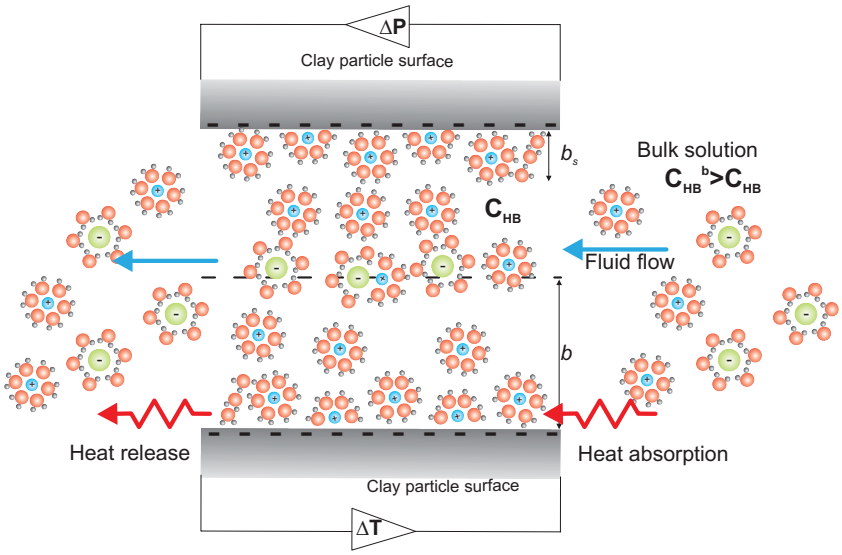

Figure 1: Schematic view of clay surface-pore fluid interactions. The negative surface charge of clay minerals is balanced by counterions. In blue and green, the cations and the anions with their first solvation shell; in red and grey, water molecules. Water molecules outside the first solvation shells are not represented. C^b_{HB} and C_{HB} are the hydrogen bond (HB) concentrations in the bulk solution and in the pore fluid, b and b_s the half interparticle distance and half-thickness of highly structured water. $\triangle p$ and $\triangle T$ are the pressure and temperature gradients. The situation considered is when a pressure gradient $\triangle p$ is instantaneously imposed. If the HB concentration in the pore space is lower than in the bulk fluid due to solid-fluid interactions, heat absorption (breaking of HB) occurs when fluid enters the pore. Conversely heat is released at the outlet. This causes the temperature gradient $\triangle T$. This is the so-called mechano-caloric effect. A thermo-osmotic flow can then balance the Darcy flow and an equilibrium is attained ($q = -\frac{k}{\eta}\nabla p - \frac{k_T}{\eta}\nabla T$)=0

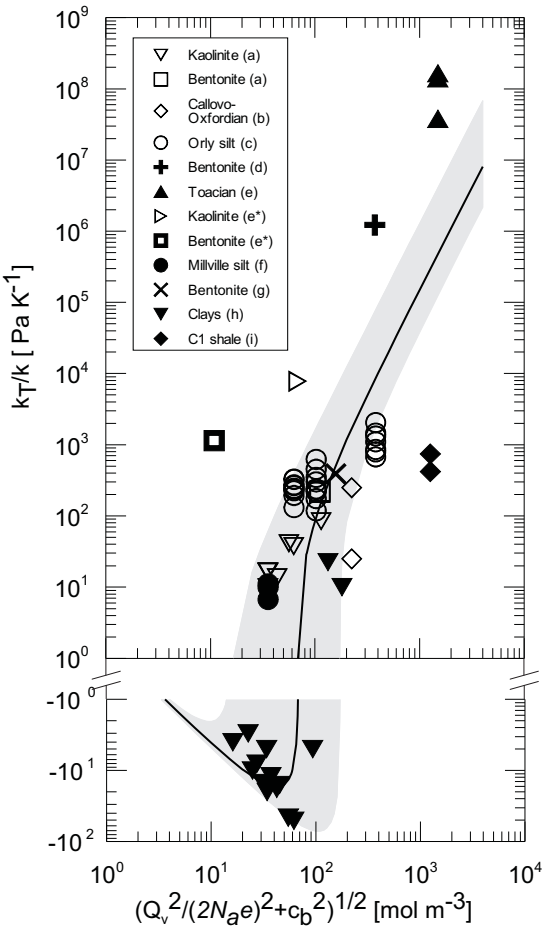

Figure 2: Relation between measured k_T/k and $C_+ + C_- = (Q_V^2/4Na^2e^2 + c_b^2)^{1/2}$. The same labels ('a' to 'i') as in Table 1 are used for the reference. Note that Q_V can be directly calculated from the petrophysical parameters since $Q_V = (1-\omega)\rho_s CEC \times 96.3/\omega$ where the CEC is the value corrected for the contribution of smectite (see section 2 and Appendix A). The dark line is the best fit to the data while the grey area contains 85% of the data.

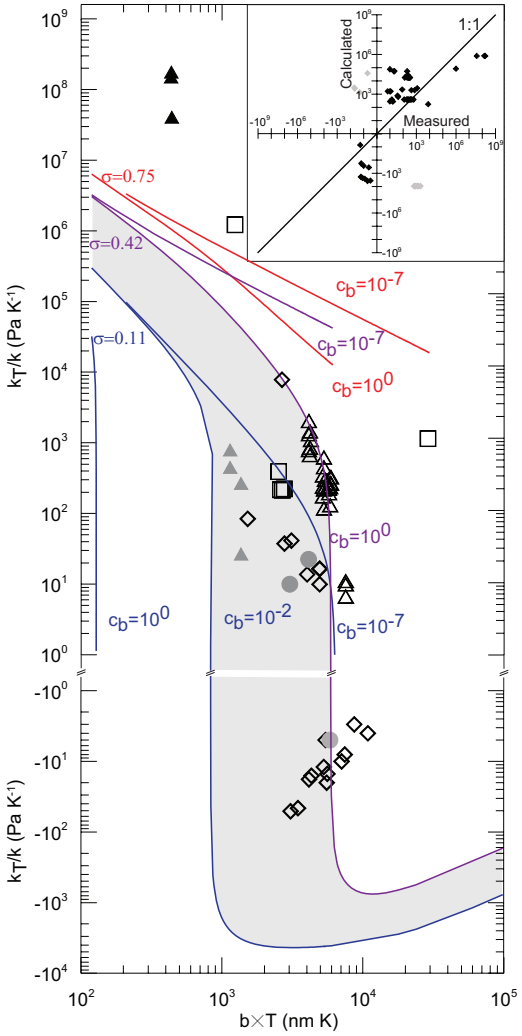

Figure 3: Available k_T/k data (ratio of osmotic permeability to classical permeability) and results of the model as functions of bT (half-pore thickness times temperature). c_b (concentration) and σ (surface charge) are in mol L^{-1} NaCl and C m^{-2} (see text for the molecular parameters). Triangle: natural clay-rich materials; diamonds: kaolinite; circles: illite; squares: smectite. Open, solid grey and solid dark symbols for low, intermediate and high intrinsic surface-charge density materials, respectively. The grey area corresponds to the most natural conditions and contains a large part of the data. In the inset, comparison between measured and computed k_T/k. Grey symbols refer to data for which neither the sign nor the order of magnitude are reproduced (15%). The poor agreement for the few high surface-charge data may be explained by a combination of model simplifications and in-situ experimental interpretation uncertainties (Tremosa *et al.*, 2010).

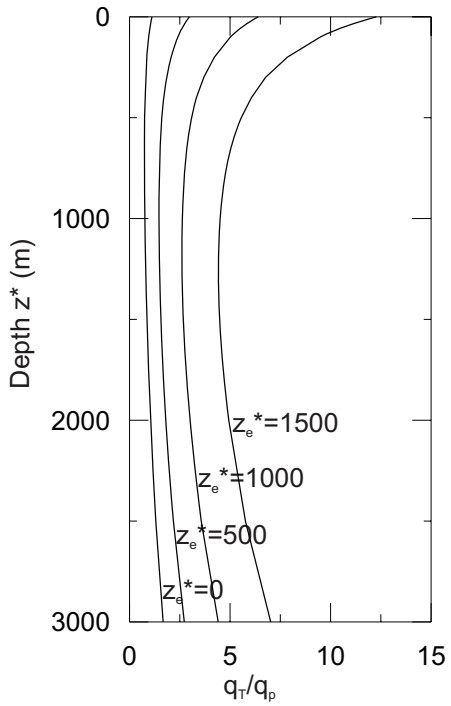

Figure 4: Computed ratio of thermo-osmotic to hydraulic specific discharge q_T/q_p in natural conditions for an illitic shale at c_b=10^{-1} mol L^{-1} NaCl as a function of the depth below the topographic surface z^* and for different values of the erosion thickness z_e^*. A ratio of up to ten is obtained highlighting the plausibility of a prominent role of thermo-osmosis in natural shale layers.

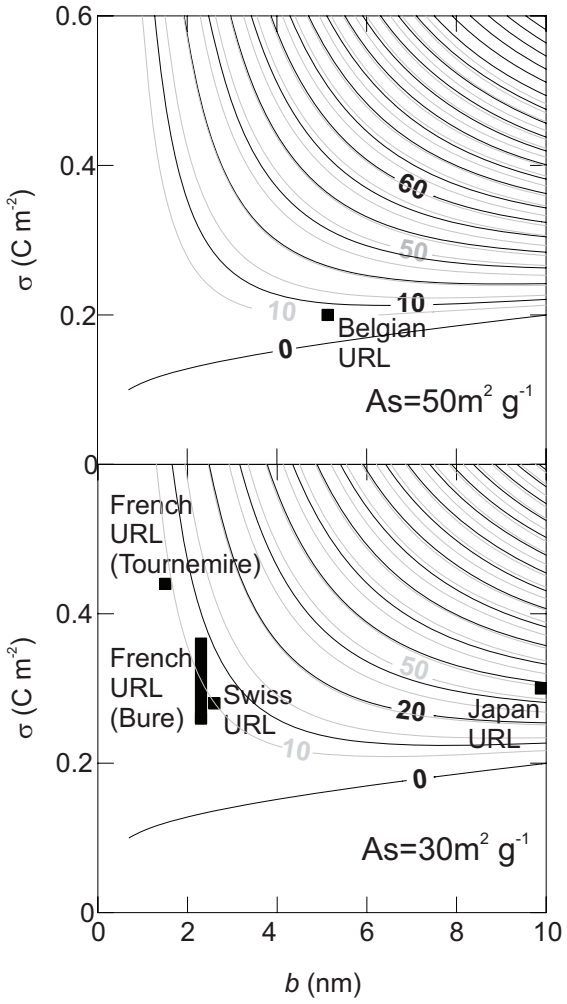

Figure 5: Calculated convective migration distances after 100 ky due to thermo-osmosis under the natural geothermal gradient G_T as a function of the half-pore size b and the surface charge density σ. Black lines for G_T=0.033 K m^{-1} and grey line for G_T=0.05 K m^{-1}. The positions, according to the mean values of σ and b of the shales (see section 3.3 for evaluation details) of various potential storage levels (or underground research laboratories) are also depicted: Boom Clay at Mole (Belgium), Opalinus Clay at Mont Terri (Switzerland), Callovo-Oxfordian formation at Bure (France), Toarcian shale at Tournemire (France), Wakkanai mudstone at Horonobe (Japan). The shale thicknesses are 100 m, 140 m, 130 m, 200 m and 500 m, respectively.

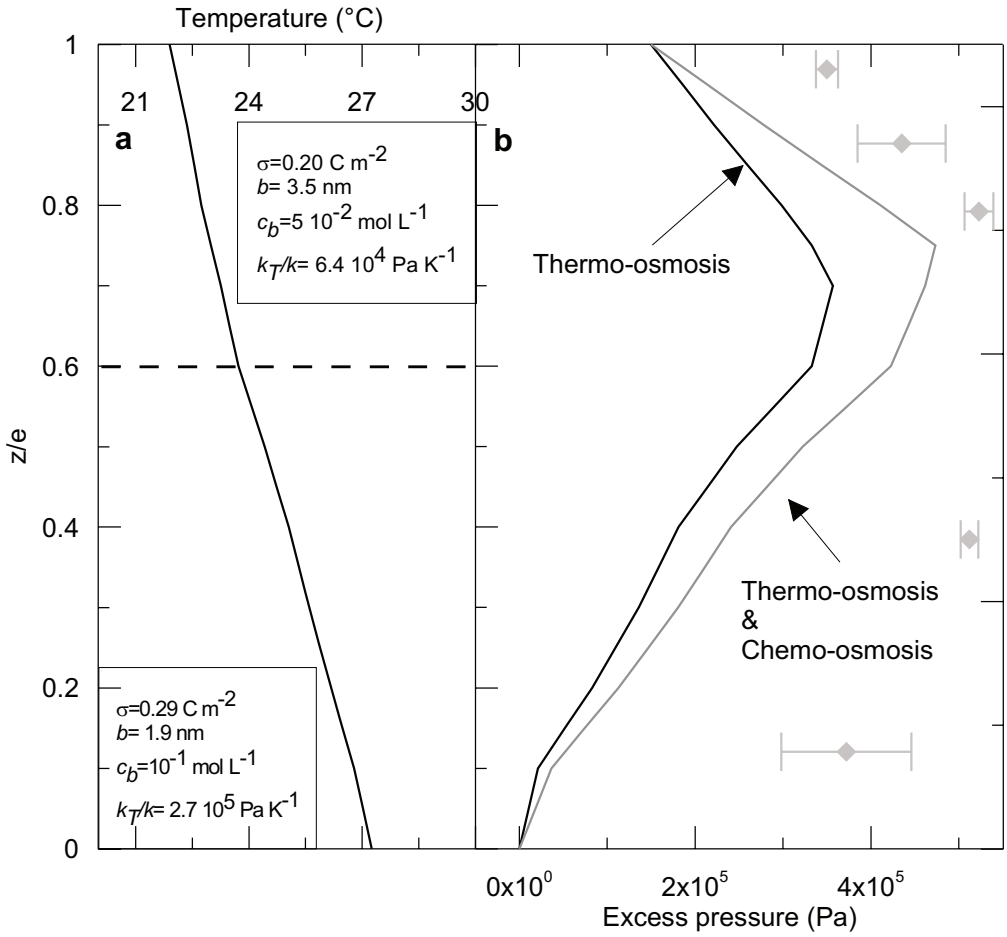

Figure 6: a) Continuous steady-state temperature profile measured in a borehole less than 10 km from the French URL at Bure, in the Callovo-Oxfordian and petrophysical parameters (see section 3.4). z is the vertical axis with its origin z=0 at the lower boundary of the shale and e is the thickness of the layer. These recent data strongly suggest a change in slope of the temperature profiles at z/e=0.6 which is consistent with a higher clay content (lower thermal conductivity) below this depth (see section 3.4) and b) computed steady-state thermo-osmotic excess-pressure profile in the Callovo-Oxfordian shale. The reference p^*=0 was taken at the top of the underlying aquifer (Dogger limestone). Previous calculations of steady-state chemo-osmotic excess-pressures (Rousseau-Gueutin *et al.*, 2009) are added to the thermo-osmotic ones. Grey diamonds represent the steady-state excess-pressures measured in the Callovo-Oxfordian at the URL. These data are indicative since no temperature profile is available at the URL. However, assuming homogeneity of the formation transport properties and mineralogy between the two locations, 10 km apart, a similar temperature profile is expected at the URL.

Appendix A. Data set analysis

For clay-rocks containing smectite, some corrections were introduced to compute the required "external" CEC. Considering the proportion (by weight) of smectite f_w^{sm} in the clay-rock and the interlayer CEC of pure smectite (80% of the charge i.e. 0.8 meq g^{-1}, Jury and Horton, 2004), the correction consists in subtracting $f_w^{sm} \times 0.80$ from the measured CEC. In the absence of any precise mineralogical data providing f_w^{sm}, the latter can be approximated by

$$f_w^{sm} \approx (A_s^{tot} - A_s^{ext})/A_s^{sm}, \tag{A.1}$$

where A_s^{tot}, A_s^{ext} and A_s^{sm}=800 m^2 g^{-1} are the total, external SSA of the clay-rock and internal SSA of the pure smectite. Indeed, $(A_s^{tot} - A_s^{ext})$ is the amount of internal surfaces per gram of the whole rock and, dividing by A_s^{sm} yields the required quantity (gram of smectite per gram of rock). When the required petrophysical parameters (thus relative to external surfaces) were missing, typical values from the literature (Mitchell, 1993; Revil and Leroy, 2004) for pure clays (illite, smectite, kaolinite) together with the mineralogical composition were considered. Indeed, if S is a surface property (e.g. SSA, CEC), and f_w^{sm}, f_w^{ill},f_w^k and S^{sm}, S^{ill}, S^k are the weight fractions and the S values of pure smectite, illite and kaolinite, respectively, the bulk rock property is:

$$S = f_w^{sm} \times S^{sm} + f_w^{ill} \times S^{ill} + f_w^k \times S^k. \tag{A.2}$$

This was done for pure clay samples (kaolinite, bentonite) but also for natural materials. Hence, the external SSA for the clay materials in (Gray, 1966) were calculated using the given mineralogical composition. In addition, for those materials containing smectite (bentonite, Callovo-Oxfordian

shale, Orly and Millville silts, and C1 shale), the above mentioned correction to obtain the external CEC was made. For bentonite (except that of Zheng and Samper, 2008), besides the 100 $m^2\ g^{-1}$ of mean external SSA estimate, it was considered that 20% of the surface charge was located on the external surface (Jury and Horton, 2004) corresponding to a mean value of 0.2 meq g^{-1} used to compute σ. For the Callovo-Oxfordian shale, the external CEC was computed using the measured CEC and a 12% weight fraction of smectite (see section 4.3). For the Orly silt, A_s and CEC were calculated using the mineralogical composition. A clay weight fraction of 15% was obtained using a clear relation (Audric, 1973) between some geotechnical characteristics of Orly silts (provided by Habib and Soeiro, 1957) and the clay content. In addition, we used a clay fraction composition (Cabane, 2005) of 50% smectite, 35% Illite and 15% kaolinite. For the Millville silt, external A_s and CEC were calculated from the mineralogical composition inferred from the total SSA. The 16% clay fraction (Or and Ghezzehei, 2002) of the Millville silt is composed of smectite and kaolinite. Using the reported total SSA of 73 $m^2\ g^{-1}$(Or and Ghezzehei, 2002), a total SSA of 800 and 30 $m^2\ g^{-1}$ for pure smectite and kaolinite in Eq. (A.2), respectively with $f_w^{sm} + f_w^k$=0.16, yields 8.8% and 7.2% for the weight fractions of smectite and kaolinite, respectively. The required value of the external SSA not provided for shale C1 was estimated from the measured CEC (0.21 meq g^{-1}) of the shale and mineralogical considerations. Assuming that besides the reported kaolinite content (29%), the clay fraction (76% by weight) is also composed of illite and smectite, $CEC = f_w^{sm} \times CEC^{sm} + f_w^{ill} \times CEC^{ill} + f_w^k \times CEC^k$ where f_w^{sm}, f_w^{ill},f_w^k and CEC^{sm}, CEC^{ill}, CEC^k are the weight fractions and the CEC of pure

smectite, illite and kaolinite, respectively. Noting that $f_w^{sm} + f_w^{ill} + f_w^k$=0.76, f_w^k=0.296 and, CEC^{sm}, CEC^{ill}, CEC^k are in the range 0.8 to 1.2, 0.1 to 0.4 and 0.03 to 0.05 meq g^{-1}, respectively (Mitchell, 1993), multiple simulations using randomly selected values of the above CEC values allows estimating f_w^{sm} and f_w^{ill}. Once estimated, the external SSA A_s of the shale was calculated using Eq.(A.2) and, A_s^{sm}=100, A_s^{ill}=75, A_s^k=30 m^2 g^{-1} the mean values of the external SSA of pure smectite, illite and kaolinite, respectively (Mitchell, 1993). A value of 43 m^2 g^{-1} consistent with other natural shale was found. Although this introduces some undesirable uncertainty, the use of the same parameters for the data treatment and model calculations insures consistency of comparisons. For instance, the mean half pore-size b involves the same parameter values as the model. Once external SSA and CEC were identified for all the materials, σ values were calculated. Most data were characterized by low to moderate surface charge, between 0.11 and 0.40 C m^{-2} while values of σ between 0.1 and 0.75 C m^{-2} were reported for clays (Jury and Horton, 2004). Together with the pore size, the most sensitive parameter for k_T/k is the surface-charge density σ. This supports the idea of a HB disruption caused by the counterions since their distribution is controlled by σ. The net intrinsic negative charge of clay minerals is -σ which is balanced by an atmosphere of counterions close to the surface.

Acknowledgments This study was supported by Institut de Radioprotection et de Sûreté Nucléaire (IRSN), AMPHOS XXI and, the French National Center for Scientific Research (CNRS) through the GNR FORPRO II. The French National Agency for Radioactive Waste Management (Andra) is acknowledged for providing data. We appreciated comments from Pr.

Pierre Turq (University Paris VI) and from Dr. Coelho (Andra) on an earlier version of this paper.

References

Al-Bazali, T.M., 2005. Experimental study of the membrane behavior of shale during interaction with water-based and oil-based muds. Ph.D. thesis, University of Texas, Austin (USA), 304 pp.

Audric, T., 1973. Etude géologique et géotechnique des limons de plateaux de la région parisienne. B. Int. Assoc. Eng. Geol. 8, 49-59.

Boisson, J.Y., 2005. Catalogue of Characteristics of Argillaceous Rocks Studied with Respect to Radioactive Waste Disposal Issues, OECD/NEA, Report 4436, Paris (France).

Cabane, N., 2005. Sols traités à la chaux et aux liants hydrauliques: Contribution l'identification et l'analyse des éléments perturbateurs de la stabilisation. Ph.D. thesis, Ecole Nationale Suprieure des Mines de St-Etienne, St-Etienne (France), 189 pp.

Carnahan, C.L., 1986. Thermal osmosis near a buried heat source. Int. Com. Heat Mass Transfer 13, 659-664.

Carr, C.W., Sollner, K., 1962. New experiments on thermoosmosis. J. Electrochem. Soc. 109, 616-622.

Cary, J.W., 1966. Soil moisture transport due to thermal gradients: practical aspects. Soil Sci. Am. Proc. 30, 428-433.

Churaev, N.V., 2000. Liquid and Vapour Flows in Porous Bodies: Surface Phenomena. Taylor & Francis, London.

Delay, J., Distinguin, M., Dewonck, S., 2007. Characterization of a clay-rich rock through development and installation of specific hydrogeological and diffusion test equipment in deep boreholes. Phys. Chem. Earth 32, 393-407.

Derjaguin, B.V., Sidorenkov, G.P., 1941. On thermo-osmosis of liquid in porous glass. C.R. Acad. Sci., U.R.S.S. 32, 622-626.

Dirksen, C., 1969. Thermo-osmosis through compacted saturated clay membranes. Soil Sci. Soc. Am. Proc. 33: 821-826.

Gaucher, E., Robelin, C., Matray, J.M., Négrel, G., Gros, Y., Heitz, J.F., Vinsot, A., Rebours, H., Cassagnabre, A., Bouchet, A., 2004. ANDRA underground research laboratory: interpretation of the mineralogical and geochemical data acquired in the CallovianOxfordian formation by investigative drilling. Phys. Chem. Earth 29, 55-77.

Gonçalvès, J., Violette, S., Wendling, J., 2004. Analytical and numerical solutions for alternative overpressuring processes: Application to the Callovo-Oxfordian sedimentary sequence in the Paris basin, France. J. Geophys. Res. 109, B02110.1-B02110.14.

Gonçalvès, J., Rousseau-Gueutin, P., 2008. Molecular-scale model for the mass density of electrolyte solutions bound by clay surfaces: Application to bentonites. J. Colloid Interface Sci. 320, 590-598.

Gonçalvès, J., Tremosa, J., 2010. Thermo-osmosis in clay-rocks: I Theoretical insights. J. Colloid Interface Sci. 342, 166-174.

Gray, D.H., 1966. Coupled flow in clay-water systems. Ph.D. thesis, University of California, Berkeley (USA), 170 pp.

Guàrdia, E., Martí, J., García-Tarrés, L., Laria, D.A., 2005. Molecular dynamics simulation study of hydrogen bonding in aqueous ionic solutions. J. Mol Liq. 117, 63-67.

Habib,. P., Soeiro, F., 1957. Water movement in soils promoted by a thermal gradient. Int. Cong. Soil Mech., Proc. 4th, 40-43.

Hakem, I.F., Boussaid, A., Benchouk-Taleb, H., Bockstaller, M.R., 2007. Temperature, pressure, and isotope effects on the structure and properties of liquid water: A lattice approach. J. Chem. Phys. 127, 224106(1-10).

Jury, A., Horton, R., 2004. Soil physics, 6th Ed. John Wiley & Sons, New York)

Marry, V., Turq, P., 2003. Microscopic Simulations of Interlayer Structure and Dynamics in Bihydrated Heteroionic Montmorillonites. J. Phys. Chem. B 107, 1832-1839.

Marry, V., Rotenberg, M., Turq, P., 2008. Structure and dynamics of water at a clay surface from molecular dynamics simulation. Phys. Chem. Chem. Phys. 10, 4802-4813.

Marsily, G. de, Ledoux, E., Barbreau, A., Margat, J., 1977. Nuclear Waste Disposal: Can the Geologist Guarantee Isolation? Science 197, 519-527.

Marsily, G. de, 1986. Quantitative hydrogeology, Academic Press, London.

Mitchell, J.K., 1993. Fundamentals of Soil Behavior. John Wiley & Sons, New-York.

Neuzil, C.E., 2000. Osmotic generation of 'anomalous' fluid pressures in geological environments. Nature. 403, 182-184.

Or, D., Ghezzehei, T.A., 2002. Modeling post-tillage soil structural dynamics: a review. Soil Till. Res. 64, 41-59.

Revil, A., Leroy, P., 2004. Constitutive equations for ionic transport in porous shales. J. Geophys. Res. 109, B03208, doi:10.1029/2003JB002755.6.

Rosanne, M., Paszkuta, M., Adler, P.M., 2006. Electrokinetic phenomena in satured compact clays. J. Colloid Interface Sci. 297, 353-364.

Rousseau-Gueutin, P., Greef, V. de, Gonçalvès, J., Violette, S., Chanchole, S., 2009. Experimental device for chemical osmosis measurement on natural clay-rock samples maintained at in situ conditions. Implications for formation pressure interpretations. J. Colloid Interface Sci. 337, 106-116.

Sclater, J.G., Christie, P.A.F., 1980. Continental stretching: An explanation of post-mid-Cretaceous subsidence of the central North Sea Basin. J. Geophys. Res. B 85, 3711-3739.

Soler, J.M., 2001. The effect of coupled transport phenomena in the Opalinus Clay and implications for radionuclide transport. J. Contam. Hydrol. 53, 63-84.

Sposito, G., Skipper, N.T., Sutton, R., Park, S.-H., Soper, A.K., Greathouse,

J.A., 1999. Surface geochemistry of the clay minerals. Proc. Natl. Acad. Sci. USA 96, 3358-3364.

Suresh, S.J., Naik, V.M, 2000. Hydrogen bond thermodynamic properties of water from dielectric constant data. J. Chem. Phys. 113, 9727-9732.

Tachi, Y., Seida, Y., Doi, R., Xia, X., Yui, M., 2009. Sorption and diffusion of Cs in Horonobe-URL's sedimentary rock: comparison and model prediction of retardation parameters from sorption and diffusion experiments. Proceedings, Materials Research Society Symposium, Warrendale, USA, Scientific basis for nuclear waste management XXXII, 573-579.

Tasaka, M., Nagasawa, M., 1978. Thermoosmosis through charged membranes. Theoretical analysis of concentration dependence. Biophys. Chem. 8, 111-116.

Taylor, S.A., Cary, J.W., 1960. Analysis of the simultaneous flow of water and heat or electricity with the thermodynamics of irreversible processes. Int. Congr. Soil Sci. Trans. 7th (Madison, Wis.), I, 80-90.

Tournassat, C., Gailhanou, H., Crouzet, C., Braibant, G., Gautier, A., Gaucher, E.C., 2009. Cation Exchange selectivity coefficient values on smectite and mixed-layer illite/smectite minerals. Soil Sci. Soc. Am. J. 73, 928-942.

Tremosa, J., Gonçalvès, J., Matray, J-M., Violette, S., 2010. Thermo-osmosis in clay-rocks: II In-situ experimental approach. J. Colloid Interface Sci. 342,175-184.

Wang, J., Kalinichev, A.G., Kirkpatrick, R.J., 2004. Molecular modeling of water structure in nano-pores between brucite (001) surfaces. Geochim. Cosm. Acta 68, 3351-3365.

Zheng, L., Samper, J., 2008. A coupled THMC model of FEBEX Mock-up test. Phys. Chem. Earth, 33, S486-S498.

Table A.1: Table 1: Data and electrochemical properties: a (Dirksen, 1969), b (Rosanne *et al.*, 2006), c (Habib and Soeiro, 1957), d (Zheng and Samper, 2008), e (Tremosa *et al.*, 2010), f (Taylor and Cary, 1960), g (Cary, 1966), h (Gray, 1966), i (Al-Bazali, 2005). A_s is in m^2 g^{-1}, ρ in kg m^{-3}, CEC in meq g^{-1} and σ in C m^{-2}. c_b values of 1.00 10^{-7} and 1.00 10^{-2} mol L^{-1} are used for distilled water (Dirksen, 1969; Habib and Soeiro, 1957), (Tremosa *et al.*, 2010)* and water (Taylor and Cary, 1960), respectively. The values within brackets refer to the total values including smectite interlayer contribution. The symbol '*' refers to data from Ref. (22) and (23) in (Tremosa *et al.*, 2010).

ω (-)	b (nm)	k (m^2)	c_b (mol l^{-1})	T (K)	k_T/k
Kaolinite[a,e*]		A_S = 30	ρ_S= 2600	CEC= 0.035	σ= 0.11
0.56	16.52	1.22×10^{-17}	1.00×10^{-7}	298	9.93×10^{0}
0.51	13.45	6.10×10^{-18}	1.00×10^{-7}	298	1.37×10^{1}
0.45	10.41	2.00×10^{-18}	1.00×10^{-7}	298	4.12×10^{1}
0.42	10.41	1.30×10^{-18}	1.00×10^{-7}	298	3.75×10^{1}
0.29	5.11	1.74×10^{-19}	1.00×10^{-7}	298	8.40×10^{1}
0.56	16.52	$1.19,1.25\times10^{-17}$	1.00×10^{-7}	298	$1.66,1.64\times10^{1}$
*0.40	85.50	3.20×10^{-17}	1.00×10^{-7}	311	7.81×10^{3}
Bentonite[a,e*]		A_S = 100 (750)	ρ_S= 2600	CEC= 0.2 (1.00)	σ= 0.19
0.70	1.20	1.77×10^{-18}	1.00×10^{-7}	289	2.18×10^{2}
0.70	1.20	8.80×10^{-19}	1.00×10^{-7}	308	2.23×10^{2}
0.70	1.20	1.87×10^{-18}	1.00×10^{-7}	298	2.13×10^{2}
*0.96	92.30	1.13×10^{-16}	1.00×10^{-7}	313	1.15×10^{3}
Callovo-oxfordian[b]		A_S = 36	ρ_S= 2600	CEC= 0.08(0.17)	σ= 0.20
0.30	4.58	5.00×10^{-18}	1.00×10^{-3}	298	2.5-25.0$\times10^{1}$
Orly silt[c]		A_S = 12	ρ_S= 2600	CEC= 0.03(0.09)	σ= 0.23
0.37	2.87	5.00×10^{-17}	1.00×10^{-7}	313	2.66×10^{2}
0.37	2.87	5.00×10^{-17}	1.00×10^{-7}	313	3.27×10^{2}
0.37	2.87	5.00×10^{-17}	1.00×10^{-7}	308	2.37×10^{2}
0.37	2.87	5.00×10^{-17}	1.00×10^{-7}	308	1.31×10^{2}
0.37	2.87	5.00×10^{-17}	1.00×10^{-7}	308	3.29×10^{2}
0.37	2.87	5.00×10^{-17}	1.00×10^{-7}	308	2.72×10^{2}
0.37	2.87	5.00×10^{-17}	1.00×10^{-7}	303	1.94×10^{2}
0.37	2.87	5.00×10^{-17}	1.00×10^{-7}	303	2.26×10^{2}
0.37	2.87	5.00×10^{-17}	1.00×10^{-7}	303	2.45×10^{2}
0.30	2.06	5.00×10^{-17}	3.70×10^{-1}	313	1.10×10^{3}
0.30	2.06	5.00×10^{-17}	3.70×10^{-1}	308	6.75×10^{2}
0.30	2.06	5.00×10^{-17}	3.70×10^{-1}	308	1.46×10^{3}
0.30	2.06	5.00×10^{-17}	3.70×10^{-1}	308	8.59×10^{2}
0.30	2.06	5.00×10^{-17}	3.70×10^{-1}	303	1.33×10^{3}
0.30	2.06	5.00×10^{-17}	3.70×10^{-1}	303	2.05×10^{3}
0.30	2.06	5.00×10^{-17}	3.70×10^{-1}	303	7.95×10^{2}
0.35	2.59	5.00×10^{-17}	7.50×10^{-2}	313	2.35×10^{2}
0.35	2.59	5.00×10^{-17}	7.50×10^{-2}	313	3.00×10^{2}
0.35	2.59	5.00×10^{-17}	7.50×10^{-2}	308	1.18×10^{2}
0.35	2.59	5.00×10^{-17}	7.50×10^{-2}	308	2.20×10^{2}
0.35	2.59	5.00×10^{-17}	7.50×10^{-2}	308	6.24×10^{2}
0.35	2.59	5.00×10^{-17}	7.50×10^{-2}	308	4.52×10^{2}
0.35	2.59	5.00×10^{-17}	7.50×10^{-2}	303	1.75×10^{2}
0.35	2.59	5.00×10^{-17}	7.50×10^{-2}	303	2.40×10^{2}
0.35	2.59	5.00×10^{-17}	7.50×10^{-2}	303	3.47×10^{2}
Bentonite[d]		A_S = 75 (725)	ρ_S= 2780	CEC= 0.2 (1.00)	σ= 0.25
0.42	0.37	3.50×10^{-21}	1.00×10^{-1}	333	1.22×10^{6}
Toarcian Shale[e]		A_S = 22	ρ_S= 2600	CEC= 0.1	σ= 0.44
0.08	1.50	1.00×10^{-21}	1.00×10^{-2}	289	3.80×10^{7}
0.08	1.50	1.00×10^{-21}	1.00×10^{-2}	287	1.65×10^{8}
0.08	1.50	1.00×10^{-21}	1.00×10^{-2}	286	1.40×10^{8}
Millville Silt[f]		A_S = 11	ρ_S= 2600	CEC= 0.02(0.09)	σ= 0.16
0.69	25.30	-	1.00×10^{-2}	298	0.67,1.0,1.1$\times10^{1}$
Bentonite[g]		A_S = 100(750)	ρ_S= 2600	CEC= 0.2(1.00)	σ= 0.19
0.68	8.17	-	1.00×10^{-1}	308	3.92×10^{2}
Illitic clay[h]		A_S = 46	ρ_S= 2780	CEC= 0.17	σ= 0.35
0.62	12.80	2.70×10^{-17}	1.00×10^{-3}	299	2.24×10^{1}
0.55	9.46	7.00×10^{-18}	1.00×10^{-3}	299	9.97×10^{0}
0.7	18.30	1.27×10^{-16}	1.00×10^{-3}	299	-5.00$\times10^{0}$
Kaolinite[h]		A_S = 30	ρ_S= 2630	CEC= 0.04	σ= 0.12
0.60	18.51	2.91×10^{-16}	1.00×10^{-3}	299	-2.00$\times10^{1}$
0.47	11.60	3.40×10^{-17}	1.00×10^{-3}	299	-4.60$\times10^{1}$
0.44	10.25	2.60×10^{-17}	1.00×10^{-3}	300	-5.10$\times10^{1}$
0.66	24.85	9.70×10^{-16}	1.00×10^{-2}	299	-8.00$\times10^{0}$
0.58	17.60	1.52×10^{-16}	1.00×10^{-2}	299	-1.20$\times10^{1}$
0.53	14.40	8.30×10^{-17}	1.00×10^{-2}	299	-1.60$\times10^{0}$
Silt[h]		A_S = 18	ρ_S= 2650	CEC= 0.021	σ= 0.11
0.63	42.67	-	1.00×10^{-3}	299	-4.00$\times10^{0}$
0.52	27.80	3.71×10^{-16}	1.00×10^{-3}	299	-1.00$\times10^{1}$
0.46	22.00	1.81×10^{-16}	1.00×10^{-3}	300	-1.50$\times10^{1}$
0.39	16.27	4.40×10^{-17}	1.00×10^{-3}	300	-1.80$\times10^{1}$
0.57	34.00	1.16×10^{-15}	1.00×10^{-2}	300	-3.00$\times10^{0}$
0.46	21.27	2.31×10^{-16}	1.00×10^{-2}	300	-5.00$\times10^{0}$
C1 Shale[i]		A_S = 43	ρ_S= 2600	CEC=0.12(0.21)	σ= 0.27
0.28	3.40	2.96×10^{-21}	1.20×10^{0}	330	7.5×10^{2}
0.28	3.40	2.96×10^{-21}	1.20×10^{0}	330	4.2×10^{2}

5.2.2 Predictive calculations of the thermo-osmotic coefficient for the Tournemire clay-rock

For the prediction of the thermo-osmotic coefficient for the Tournemire clay-rock, the second model developed and presented in the previous section, based on the consideration of enthalpy changes by hydrogen bounding modifications, is know applied. As seen in the model presentation, k_T/k, where k_T is the thermo-osmotic permeability (m^2 s^{-1} K^{-1}) and k the intrinsic permeability (m^2), can be predicted by our model from a few petrophysical and chemical parameters: the cation exchange capacity CEC, the surface specific area A_s, the half-pore size b and the concentrations of anions and cations in the bulk solution.

The obtention of these parameters was already detailed in the section 4.2.5 for the specific surface area and the pore size and in the chapter 3 for the CEC and the solutes concentrations in porewater. Nevertheless, a correction on the CEC determined in chapter 3 for the fraction <100 μm by the proportion of clay minerals content is applied to obtain the bulk rock CEC. A simplification is also made on the bulk solution composition, which is considered in the present calculations as only composed by Na^+ and Cl^- solutes.

The predictive model for thermo-osmotic coefficients is then applied at different levels in the argillaceous formation for the establishment of a profile. The input parameters are reported in Table 5.1, with the results of the model. Note that the model gives the macroscopic volume-averaged excess specific enthalpy due to fluid-solid interactions ΔH and that k_T/k is calculated by the relation $k_T/k = \Delta H/T$ with the temperature given by the temperature profile obtained in section 2.3.
The resulting k_T/k profile shows variations of a little less than one order of magnitude across the formation. The higher values are computed for the lower Toarcian, because of the high surface-charge density, $\sigma = CEC$ ($mmol_c$ g^{-1}) $/A_s$ (m^2 g^{-1}) $\times$ 96.3 (C $mmol_c$ g^{-1}), obtained with the corresponding parameters for this level. σ for the lower Toarcian (around 0.75) is in the high range of σ values reported for clays, between 0.1 and 0.75 C m^{-2} [75]. Its effect on k_T/k is related to the strong positive relationship between σ and k_T/k, previously noted. Lowest k_T/k values are calculated for the upper Toarcian, which presents a σ of about 0.2 C m^{-2}.

Formation unit	Elevation	C^f	b	A_s	$CEC_{bulkrock}$	σ	ΔH	k_T/k
upper Toarcian	551.3	1.83E-02	1.64	28	6.02	0.208	5.91E+07	2.08E+05
upper Toarcian	534.4	2.15E-02	1.84	25	5.29	0.204	4.91E+07	1.72E+05
upper Toarcian	512.2	2.81E-02	1.91	24	5.27	0.212	4.97E+07	1.74E+05
upper Toarcian	463.1	4.95E-02	1.71	23	5.52	0.232	6.53E+07	2.26E+05
upper Toarcian	411.5	8.16E-02	1.52	22	5.54	0.243	7.84E+07	2.69E+05
int. Toarcian	387.5	7.37E-02	1.63	25	7.36	0.284	9.71E+07	3.32E+05
lower Toarcian	372.9	6.74E-02	4.06	5	3.85	0.744	1.33E+08	4.54E+05
lower Toarcian	359.1	6.00E-02	2.32	5	3.93	0.758	2.54E+08	8.63E+05
Domerian	331.2	4.26E-02	1.48	22	6.28	0.275	1.07E+08	3.63E+05
Domerian	316.7	3.32E-02	1.34	23	6.10	0.256	1.09E+08	3.68E+05
Domerian	302.9	2.34E-02	1.30	26	6.47	0.240	1.02E+08	3.42E+05

Table 5.1: Establishment of the profile of the thermo-osmotic coefficient. The input parameters are the equilibrium concentration (C^f, in mol L^{-1}), the half-pore size (b, in nm), the specific surface area (A_s, in m^2 g^{-1}) and the bulk rock CEC (in $mmol_c$ $100g^{-1}$). Calculations results are the surface-charge density (σ, in C m^{-2}), the macroscopic excess specific enthalpy (ΔH, in J m^{-3}) and k_T/k (in s^{-1} K^{-1}). The elevation is expressed in m NGF.

5.3 Thermo-osmotic experiments on Tournemire clay-rock

This section presents the thermo-osmotic experiments performed at the Tournemire URL, in an equipped borehole. It consisted in the first thermo-osmotic experiments carried out on natural and thus non-remoulded shales. During these experiments a temperature gradient was imposed between the test interval of the borehole and the clay-rock by changes of the water filling the test interval with a warmer one, at constant pressure and salinity. The pressure evolution consecutive to the water changes was monitored and its interpretation was made using a numerical code including the thermo-hydromechanical behaviour of porewater and the porous medium and coupled flow of fluid, i.e. Darcy's flow and thermo-osmosis, and heat. These experiments have allowed identifying the occurrence of a thermo-osmotic flow in the Tournemire argillite when submitted to a temperature gradient and a range of thermo-osmotic permeability was determined by inversion of the measured pressure evolution.

A paper on these experiments and their interpretation was published in Journal of Colloid and Interface Science and is inserted below.

ERRATUM: Please note that a mistake was made on the left y-axis of Figures 2, 3 and 5. The unity of the pressure evolution is "10^5 Pa" and no "hPa" as indicated in the paper.

Journal of Colloid and Interface Science 342 (2010) 175–184

Contents lists available at ScienceDirect

Journal of Colloid and Interface Science

www.elsevier.com/locate/jcis

Estimating thermo-osmotic coefficients in clay-rocks: II. In situ experimental approach

J. Trémosa [a,b,*], J. Gonçalvès [b,c], J.M. Matray [a], S. Violette [b,d]

[a] Institut de Radioprotection et de Sûreté Nucléaire, IRSN/DEI/SARG/LR2S, BP 17, F-92262 Fontenay-aux-Roses, France
[b] UPMC Univ. Paris 06, UMR-7619 SISYPHE, 4 place Jussieu, F-75252 Paris, France
[c] CNRS, UMR-6635 CEREGE, F-13100 Aix en Provence, France
[d] CNRS, UMR-7619 SISYPHE, 4 Pl. Jussieu, F-75252 Paris, France

ARTICLE INFO

Article history:
Received 17 July 2009
Accepted 28 September 2009
Available online 8 October 2009

Keywords:
Coupled-flow
Thermo-osmosis
Thermal gradient
Tournemire argillite

ABSTRACT

Water flow in compacted shales is expected to be modified by thermo-osmosis when a thermal gradient exists. However this coupled-flow process is poorly characterized since no experiments on non-remoulded clay-rocks are found in the literature. This paper presents a set of thermo-osmosis experiments carried out in an equipped borehole installed in the Liassic argillite at the Institut for Radiological protection and Nuclear Safety (IRSN) underground research laboratory (URL) of Tournemire (southeastern France). A numerical model – including coupled-flow equations, mass conservation laws, thermal expansion and changes of water properties with temperature – was developed for the interpretation of these experiments. A thermo-osmotic response was deduced from the pressure evolution in the test interval after temperature pulses (+2.5, +5.1, and +9 °C). The values of thermo-osmotic permeability determined during the experiments range between 6×10^{-12} and 2×10^{-10} m^2 K^{-1} s^{-1}, depending on the pulse temperature and uncertainties on the model parameters. A sensitivity analysis on several model parameters was performed to constrain these uncertainties.

1. Introduction

In the framework of studies on clay-rocks confinement abilities, a special attention has been paid on coupled-flux processes, i.e. a flow driven by a non-conjugated force. Among non-Darcian flows in low permeability argillaceous formations, chemical osmosis is the best characterized phenomenon. But other coupled-flux processes, like thermo-osmosis [1–4], can also affect water flow in these media. Thermo-osmosis consists in a flow of water driven by a temperature gradient and, in clay-rocks, it usually occurs from the warmer towards the colder zone. It is a process related to the small pore size of consolidated clay-rocks and to surface forces associated with the surface charge of clay minerals [5]. Clay minerals are characterized by a negative surface charge under natural pH values. Because of isomorphic substitutions in tetrahedral and octahedral layers, clay minerals present surface charge, which induces a non-uniform distribution of anions and cations in the pore space and an electric field, e.g. described by diffuse double-layer or triple-layer models. These surface forces could affect water molecules enough to change their structure and properties from the bulk liquid phase [5,6]. According to Derjaguin et al. [5] (and references inside), thermo-osmosis develops because specific enthalpy of liquid water differs by ΔH in the boundary layer from its bulk value. Experimental observations show that an isothermal flow of liquid layers in the clay-rock porosity caused by a pressure gradient produces an excess heat flux, i.e. isothermal heat transfer, leading to a temperature gradient in the flow direction. This process is know as the mechanocaloric effect. By the reciprocal principle of Onsager [7,8], the reverse effect, i.e. the flow of a liquid due to a temperature gradient, must also exist.

Derjaguin et al. [5] proposed that thermo-osmosis results from the alteration of water properties close to the solid surface. The importance of these effects depends on: (i) the surface hydrophilicity, (ii) the temperature, as the special structure of boundary layers is destroyed by increasing temperatures, and (iii) the pore size, thermo-osmosis conductivity being larger in narrow pores. The authors [5] provide basis for estimating thermo-osmotic conductivity for a single plane-parallel pore but a convenient expression at macroscale is missing. To overcome this difficulty the theory is formalized and upscaled in a companion paper [9].

Studying coupled-flux processes in clay-rocks could be particulary relevant for safety evaluation of high-level nuclear waste (HLNW) geological repositories. First, because clay-rocks are considered in some countries as possible host-rocks for a HLNW geological repository and a bentonite engineered barrier is sometimes proposed in the repository design. Second, because temperature gradient is the driving force of thermo-osmosis and, in a HLNW

* Corresponding author. Address: UPMC Univ. Paris 06, UMR-7619 SISYPHE, 4 place Jussieu, F-75252 Paris, France.
E-mail address: joachim.tremosa@irsn.fr (J. Trémosa).

0021-9797/$ - see front matter © 2009 Elsevier Inc. All rights reserved.
doi:10.1016/j.jcis.2009.09.055

geological repository, three kinds of temperature gradients could be considered: (i) at the basin scale, due to the regional geothermal gradient, which is in the range 0.02–0.03 K m^{-1} in a sedimentary basin [3]. Note that the geothermal gradient is higher in shale layers as a consequence of the low thermal conductivity of clay minerals; (ii) at the repository scale, due to the heat generated by decay of radioactive matters in waste canisters. According to the french national agency for radioactive wastes management (ANDRA) [10], temperature is expected to reach a maximum (about 70 °C) few years after the repository closure and the temperature gradient in the bentonite buffer and the host-rock could be of some K m^{-1} in the near-field of wastes. After 100 years, calculations indicate that the temperature gradient should be smaller than 1 K m^{-1} and 0.1 K m^{-1} at the contact with radioactive wastes and a few meters from the repository drifts, respectively; and (iii) also at the repository scale, due to the gallery excavation.

Thermo-osmosis phenomenon is poorly constrained since few thermo-osmosis experiments on saturated clay-rocks are reported in the literature [11–16]. These experiments have been performed on remoulded materials, using powdered clay-rock or industrial bentonite. To our knowledge, no in situ nor laboratory experiments on natural clay-rocks of thermo-osmosis have been done, so far. In spite of being unperfect to quantify thermo-osmosis process in a natural clay-rock, these experiments give a range of expected thermo-osmosis permeabilities. They are summarized in Table 1.

In this paper, a set of thermo-osmotic tests is presented and interpreted. For this purpose, a model based on coupled-flow equations and mass conservation laws was developed. In a first section, the model is described and a priori exploratory simulations of thermo-osmotic experiments are presented. Then, the in situ thermo-osmotic experiments in a packer equipped borehole installed in the Liassic argillite studied at IRSN URL at Tournemire (southeastern France) are detailed and interpreted using the numerical model.

2. A priori simulations of in situ thermo-osmotic experiments

In low-permeability geological media, simultaneous flows of different types are observed even when only one gradient (e.g. pressure) is present. Conversely, each flux may be the result of several driving forces. Quantification of the different flows as a function of the acting driving forces has to be done by solving simultaneously the flows, whence the notion of coupled flows. Two different ways may be considered to obtain the set of equations linking flows to driving forces: the first approach is based on the principles of irreversible thermodynamics leading to the so-called phenomenological equations (see e.g. [18–20]); and the second approach refers to the continuum equations at the local scale (mechanical models) (e.g. [9,21]). Phenomenological models establish a linear proportionality between flows and driving forces, via coupling coefficients measured or assumed using the Onsager reciprocal relations [7,8]. Mechanical models consist in upscaling local continuum equations to obtain coupling equations at the Representative Elementary Volume (REV) scale (e.g. a core sample). These equations are expressed as functions of petrophysical and electrochemical parameters of the rock.

The numerical model given hereafter is derived from a previous model developed for the interpretation of a chemo-osmotic response subsequent to a chemical pulse [22,23]. Couplings associated with temperature were implemented in this model. The numerical model was developed for the geometry of a shut-in chamber in a borehole within a geological formation (Fig. 1). Consequently, a set of equations for the chamber and another one for the porous medium were considered. The model is based on a 2D horizontal finite-differences scheme expressed in cartesian coordinates (x,y). Equations are solved on a square-nested grid centered onto the chamber. The mesh is refined around the chamber to obtain a better accuracy at this location. The model geometry allows to adapt the shut-in chamber orientation, i.e. in a vertical or in an horizontal borehole, keeping the fluid flow along the bedding (see Section 4). This geometry has been chosen assuming that the fluid flow occurs along the bedding, sub-horizontal in a sedimentary basin. This assumption is based on the anisotropy of permeability in clay-rocks, where the stratification induces a much higher horizontal, parallel to the bedding, permeability than in the vertical direction [24]. The same assumption was made for the heat flow considering an anisotropy of the thermal conductivity [25].

2.1. Mathematical formulation

2.1.1. Porous medium formalism

In the porous medium, the continuity equation is combined with a generalized Darcy's law to obtain the pressure diffusion equation. In the continuity equation

Table 1
Summary of the previous thermo-osmotic experiments performed on saturated argillaceous materials.

Reference	Material	Experimental conditions	Thermo-osmotic permeability
Habib and Soeiro [11]	Saturated silt from Orly (France)	A temperature gradient of +0.5 to +3 °C m^{-1} is applied to a silt sample for various mean temperatures (30, 35, and 40 °C)	1.50×10^{-11}–2.36×10^{-11} m^2 K^{-1} s^{-1}
Dirksen [12]	Saturated Na-kaolinite and Wyoming Na-bentonite	Experiments were conducted for several temperature differences (from +2 to +30 °C), average temperature (15, 25, and 35 °C) and compaction pressure (resulting in water contents of 80% for the Na-bentonite and ranging from 48.9% to 15.1% for the Na-kaolinite	9.7×10^{-14}–1.64×10^{-13} m^2 K^{-1} s^{-1} for Na-kaolinite and 1.60×10^{-13}–3.25×10^{-13} m^2 K^{-1} s^{-1} for Na-bentonite
Srivastava and Jain [14] and Srivastava and Avasthi [15]	Saturated and compacted bentonite and kaolinite	Thermo-osmotic flow measurements were performed at 38.4 °C for several temperature differences (from +1.2 to +29.1 °C) and at various temperature (31.9, 38.4, 43.8, and 51.3 °C) with a temperature difference of +2.7 °C	1.5×10^{-10} m^2 K^{-1} s^{-1} for the bentonite and 2.5×10^{-10} m^2 K^{-1} s^{-1} for the kaolinite
Rosanne et al. [13]	Callovo-Oxfordian argillite of the Paris basin crushed to powder and recompacted to a porosity of 30%	Thermo-osmotic permeability was determined during a thermo-diffusion experiment carried at 25 °C for various solute concentrations in water and temperature differences of about −15 to +15 °C	10^{-13} to 10^{-12} m^2 K^{-1} s^{-1}
Zheng and Samper [16]	Ca–Mg bentonite from Serrata de Níjar (southeastern Spain)	FEBEX *mock-up* test [17], consisting in a long term simultaneous heating and hydration experiment	3.62×10^{-12} m^2 K^{-1} s^{-1}

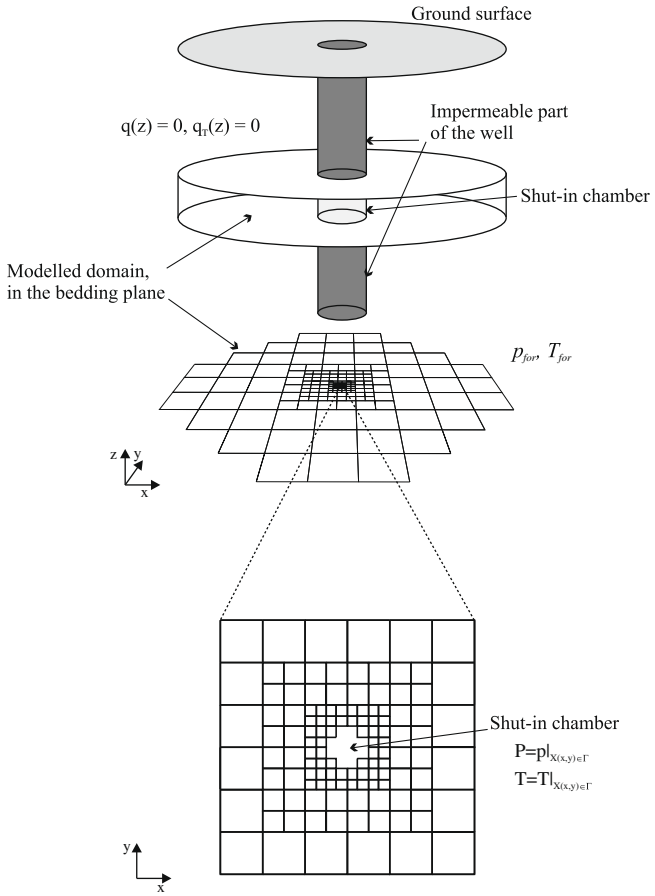

Fig. 1. Geometry of the modeled domain in a vertical borehole. In this figure, $q(z)$ and $q_T(z)$ stand for the vertical components of the fluid and heat fluxes.

$$\nabla \cdot (\rho_f q) = -\frac{S_s}{g}\frac{\partial p}{\partial t} + \chi_T \rho_f \omega \frac{\partial T}{\partial t}, \tag{1}$$

the left hand side corresponds to the mass flux in the porous medium and the right hand side represents the mechanical changes in the porous medium [24], ρ_f is the fluid density (kg m^{-3}), q is the specific discharge (m s^{-1}), S_s is the specific storage coefficient associated with the hydro-mechanical coupling (m^{-1}), g is the acceleration due to gravity (m s^{-2}), p is the pore pressure in the porous medium (Pa), t is the time (s), χ_T is the coefficient of thermal volumetric expansion of the fluid (K^{-1}), ω is the connected porosity, T is the temperature in the porous medium (K), k is the intrinsic permeability (m^2), η is the dynamic viscosity of the water (Pa s). The first term in the right hand side of Eq. (1) takes in account the deformation of the porous medium with varying pore pressure while the second term accounts for the "volume production" due to the thermal expansion of water. This term was obtained using a simplification of a more general thermo-poroelastic analysis for highly compacted materials [23]. Indeed, Rousseau-Gueutin et al. [23] showed that in a highly compacted medium, the thermal expansion of the solid and of the porous medium compensate and only the thermal expansion of water is to be considered, whence the simplified expression of the mass balance Eq. (1). The same approximation was made by Luo and Vasseur [26]. The fluid flow is described by

$$q = -\frac{k}{\eta}\nabla p - k_T \nabla T, \tag{2}$$

for which flow is driven by pressure and temperature gradients. In Eq. (2), k_T is the coefficient of thermo-osmotic permeability (m^2 K^{-1} s^{-1}) and, the gravity term ($-\rho g \frac{k}{\eta}\nabla z$ with z the vertical axis directed upward) is neglected since horizontal flow is assumed.

Combining Eqs. (1) and (2), leads to the pressure diffusion equation [24]

$$\nabla \cdot \left[\rho_f \left(-\frac{k}{\eta}\nabla p - k_T \nabla T\right)\right] = -\frac{S_s}{g}\frac{\partial p}{\partial t} + \chi_T \rho_f \omega \frac{\partial T}{\partial t}. \tag{3}$$

Neglecting the advective contribution due to the very low permeability of the medium, the heat equation in a porous medium is given by the expression [24]

$$\nabla \cdot (\lambda \nabla T) = \rho' C' \frac{\partial T}{\partial t}, \tag{4}$$

where $\rho' C'$ is the mass per unit volume and the specific heat of the porous medium (solid and fluid) and λ is the thermal conductivity of the water-saturated porous shale. The term $\rho' C'$ corresponds to

$$\rho' C' = \omega \rho_f C_f + (1-\omega)\rho_s C_s, \tag{5}$$

where C_f, C_s and ρ_f, ρ_s are the specific mass heat (J kg^{-1} K^{-1}) and the density (kg m^{-3}) of the fluid and the solid, respectively. The thermal conductivity λ (W m^{-1} K^{-1}) is estimated by a geometric mean, which is found to give good estimates of the equivalent thermal conductivity [27]

$$\lambda = \lambda_f^{\omega} \lambda_s^{1-\omega}, \tag{6}$$

where λ_s and λ_f are the thermal conductivities of the solid and fluid, respectively. Note that a thermal equilibrium between the solid and the fluid is assumed. For the porous medium, Eq. (3) in a variational form (see below) and (4) are solved numerically using a finite-difference scheme and boundary conditions which are detailed in Section 2.2.

2.1.2. Shut-in chamber formulation

The expression of a pressure variation in the shut-in chamber given by Bredehoeft and Papadopoulos [28] is modified to account for the internal "volume production" of fluid caused by its thermal expansion. The expression now writes

$$\frac{\partial P}{\partial t} = \frac{q_c S_c}{\beta_c V_c} + \frac{\chi_T}{\beta_c}\frac{\partial T}{\partial t}. \tag{7}$$

Eq. (7) comes from the mechanical, $dV_c = q_c S_c dt$, and the thermal, $dV_c = V_c \chi_T dT$, contributions to the internal "volume production" and by combination with Eq. (8) [23,29]

$$\frac{dV_c}{V_c} = \beta_c dP, \tag{8}$$

where P is the pressure in the chamber (Pa), q_c is the filtration rate (given by Eq. (2)) across the cylindrical chamber's wall (m s^{-1}), S_c is the wall surface of the chamber (m^2), V_c is the volume of the chamber including the tubing (m^3), β_c is the compressibility of the chamber and tubing (Pa^{-1}), T is the temperature in the chamber (K), dV_c is the volume of water injected in or withdrawn from the chamber (m^3) and dP is the pressure difference induced by the dV_c. According to Neuzil [29], the compressibility of the chamber must be used instead of the water compressibility to take into account the compressibility of the whole chamber device (including the tubing and the packers). The parameter β_c was determined before the temperature pulse, during hydraulic pulses, with Eq. (8).

The heat-transfer equation in the chamber is obtained by writing the heat transfer balance across the wall of the chamber

$$S_c H_c = (\rho_w C_w V_c + \rho_{st} C_{st} V_{st})\frac{\partial T}{\partial t}, \tag{9}$$

where $H_c = -\lambda \nabla T|_{X(x,y)\in\Gamma}$ is the heat flux across the wall of the chamber (Γ) calculated in the porous medium at the interface with the chamber and $\rho_w C_w V_c$ and $\rho_{st} C_{st} V_{st}$ correspond to the heat

stored by the water in the chamber and in the stainless steel borehole completion, respectively. Heat dissipation along the completion can be neglected because, in spite of its thermal conductivity higher than the porous medium one (about 20 times), the available area for heat dissipation is much lower than the chamber wall area (about 50 times), as the borehole completion consists in a rod of few mm thick.

Eq. (7) in a variational form and (9) are solved numerically using a finite-difference scheme for the flow terms.

2.1.3. Changes of water properties with temperature

The changes of water properties with temperature were taken into account, as these changes can affect the water flow in the clay-rock. These changes are considered in both the porous medium and the shut-in chamber. The first effect, i.e. the thermal expansion of water, was already introduced in Eqs. (1) and (7). The following expression was used, graphically determined from the data in [24] for $T \leqslant 40$ °C.

$$\chi_T = 7 \times 10^{-6} T + 3 \times 10^{-5}, \tag{10}$$

where T, the temperature, and χ_T, the coefficient of thermal expansion, are expressed in K and K^{-1}, respectively. Eq. (10) is valid for free and pure water while the thermal properties of adsorbed water on mineral phases in the clay-rock could slightly differ [3]. Nevertheless, Rousseau-Gueutin et al. [23] obtained accurate simulations of thermal effects during chemical osmotic experiments using bulk properties for the mobile pore water in shales. The thermal properties for free water were thus used in the following. Changes of water density with pressure are already accounted for (in the specific storage coefficient) but, introducing temperature changes in the system requires to consider density changes with temperature, according to the relation

$$\rho_f(T) = \rho_{f0} \exp(-\chi_T (T - T_0)), \tag{11}$$

where $\rho_f(T)$ is the water density (kg m^{-3}) for temperature T (K) and ρ_{f0} is the water density for the reference temperature T_0. Changes in water density are expected to induce a vertical flux, since they modify the gravity term in the continuity flow equation. However, for the maximum applied temperature change ($\Delta T = 10$ °C), water density changes only by 1.5‰. Using a simulation in the (x,z) plane, it was verified that the contribution of the gravity term due to temperature variation is weak under the experimental conditions. Thereby the density variation is not able to alter significantly the flow anisotropy in the clay-rocks, thus the modeling assumption of considering only the flow along the bedding remains valid. Water viscosity also depends on temperature. In the range 0–300 °C, Mercer et al. [30] proposed the following formulation

$$\frac{1}{\eta} = (5.38 + 3.8A - 0.26A^3) \times 10^3, \tag{12}$$

where

$$A = \frac{(T - 150)}{100}, \tag{13}$$

with T, the temperature, expressed in °C. Expressions (10)–(12) were taken into account in the model.

2.2. Theoretical analysis of a temperature pulse

2.2.1. Behavior of the water–clay-rock system during a temperature pulse

In the following, theoretical simulations of a temperature pulse in a shut-in chamber in order to study the behavior of the water–clay-rock system are proposed. Let's consider a vertical borehole (Fig. 1), normal to the bedding, with no vertical fluxes as upper and lower boundary conditions. At the chamber's wall the continuity of the pressure and the temperature, i.e.

$$P = p|_{(x,y)\in\Gamma}, \quad T = T|_{(x,y)\in\Gamma}, \tag{14}$$

where Γ is the location (x,y) of the wall surface, holds. At a distance L from the chamber location, the following external boundary conditions are considered

$$p = p_{for}, \tag{15}$$

$$T = T_{for}, \tag{16}$$

where p_{for} and T_{for} are the pressure and the temperature of the formation, assumed constants. The distance L is chosen to ensure constant boundary conditions as the pressure perturbation induced by the hydraulic or temperature pulse does not reach this limit during the experiment duration. The extent of the perturbation can be obtained via the determination of the characteristic time and the distance L chosen larger than the perturbation extent. With, the characteristic time $\tau = L^2/D_h$ and the diffusivity coefficient $D_h = \rho g k/\eta S_s$. Using parameters from Table 2, a characteristic time τ of 10^8 s is obtained, i.e. an hydraulic perturbation will reach 1 m in about 3 years. A modelled domain size of 8 m × 8 m has been considered.

In natural media, the initial pore pressure distribution is often poorly constrained. In order to overcome this difficulty, a convenient variational formulation which is independent from the initial state $P_0(x,y)$ was used. This formulation is made possible by the linearity of the mathematical operators involved in the pressure diffusion equation and holds true for a steady or a transient state [24]. The variational formulation, $\delta P = P - P_0$ and $\delta p = p - p_0$ – where P_0 and p_0 are the initial pressure (dependent on the location) and P and p the pressure after temperature variation – allows analyzing the propagation of the perturbation, independently of the initial pressure. Flow Eqs. (1) and (7) become

$$\nabla \cdot \left[\rho_w \left(-\frac{k}{\eta}\nabla(\delta p) - k_T \nabla T\right)\right] = -\frac{S_s}{g}\frac{\partial(\delta p)}{\partial t} + \chi_T \rho_w \omega \frac{\partial T}{\partial t} \tag{17}$$

$$\frac{\partial(\delta P)}{\partial t} = \frac{q_c S_c}{\beta_c V_c} + \frac{\chi_T}{\beta_c}\frac{\partial T}{\partial t} \tag{18}$$

At the chamber wall location, $P_0 = p_0$ and $P = p$, so $\delta P = \delta p$.

Hydraulic, petrophysical and thermal parameters of the clay-rock and the chamber used in this theoretical temperature pulse are presented in Table 2. Clay-rock parameters are average values for the Tournemire argillite (see Section 3.1), located in southeastern France.

A temperature pulse consists in applying at a time t an excess temperature in the chamber, without changing the pressure. In this case, a temperature 5 °C warmer in the chamber than in the porous medium was applied. Water–clay-rock system evolution subsequent to the temperature pulse after 5 and 100 days is depicted in Fig. 2. Temperature evolution and pressure evolution, with ther-

Table 2
Hydraulic, petrophysical and thermal parameters for standard case calculation.

Hydraulic parameters	
k_T	10^{-11} m^2 s^{-1} K^{-1}
k	10^{-21} m^2
S_s	10^{-6} m^{-1}
β_c	510^{-8} Pa^{-1}
Petrophysical parameters	
ω	0.1
ρ_s	2.7 g cm^{-3}
Thermal parameters	
λ_s	1.8 W m^{-1} K^{-1}
C_s	700 J kg^{-1} K^{-1}

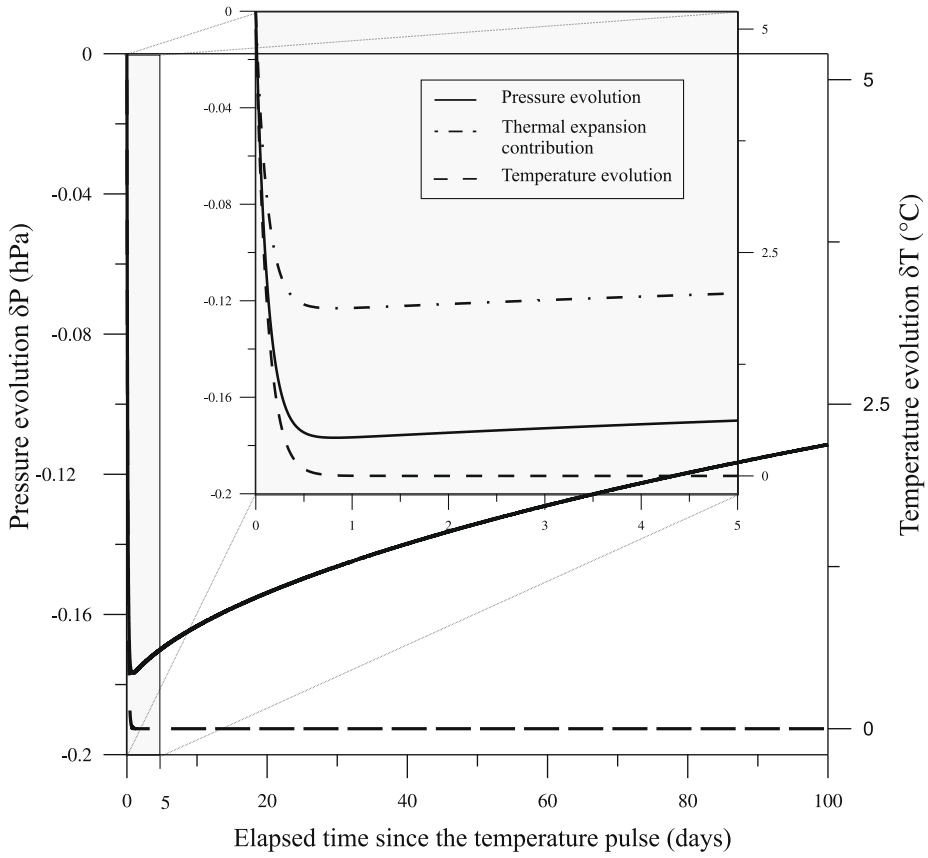

Fig. 2. Pressure and temperature evolution in the chamber after a temperature pulse during 100 and 5 days.

mal expansion and changes of water properties and with thermo-osmosis added, are shown together in this figure. It allows to highlight the thermo-osmotic and the thermal expansion respective contributions. Three stages can be identified in the pressure evolution: (i) immediately after the temperature pulse, the pressure decreases as a consequence of the temperature dissipation in the system. This decrease is due to a diverging water flow from the chamber towards the argillite (thermo-osmosis) and to a subsequent reduction of the water volume in the chamber because of the temperature decrease. During this stage thermo-osmosis phenomenon, driven by the temperature difference between the chamber and the clay-rock, represents the major contribution to pressure decrease; (ii) when the temperature gradient vanishes, thermo-osmotic flux stops and the pressure reaches a minimum; and (iii) during the last stage, a Darcian flux develops due to the pressure gradient established between the formation and the chamber and its neighboring area. This flux is directed in the opposite direction of the thermo-osmotic flux and pressure raises in the chamber. It tends to recover the initial pressure, before the temperature perturbation.

2.2.2. Sensitivity analysis on the different parameters

A sensitivity analysis on the different parameters of the model was performed in order to have a critical view on the osmotic response and to evaluate the ability of the model to estimate thermo-osmotic coefficients from a temperature pulse experiment in a clay-rock. Four parameters were considered: the thermo-osmotic permeability, the intrinsic permeability, the specific storage coefficient and the compressibility of the chamber. Standard parameters values as well as the maximum and the minimum values used in the sensitivity analysis are listed in Table 3.

Table 3
Parameters used in the sensitivity analysis.

Parameters	Low value	Standard value	High value
k_T(m^2 s^{-1} K^{-1})	10^{-12}	10^{-11}	10^{-10}
k(m^2)	10^{-22}	10^{-21}	10^{-20}
S_s(m^{-1})	10^{-7}	10^{-6}	10^{-5}
β_c(Pa^{-1})	10^{-8}	5×10^{-8}	10^{-7}

Sensitivity analysis results are shown in Fig. 3, where the pressure evolution is reported for the different cases. The thermo-osmotic permeability coefficient (k_T) (Fig. 3a) has a direct influence on the pressure decrease since an higher coefficient causes a more important thermo-osmotic flow towards the formation. The differences in pressure minimum as a function of the k_T value are enough to constrain the corresponding k_T with this experiment design and this model, provided that the chamber compressibility and thermal expansion are well constrained. The intrinsic permeability (k) (Fig. 3b) and the specific storage coefficient (S_s) (Fig. 3c) influence the minimum pressure reached because higher Darcian flux is more efficient to counterbalance the thermo-osmotic one. Those parameters also condition the pressure rise once the thermal gradient is null. Since k and S_s are inverse in the hydraulic diffusivity, they have an opposite influence on the flow and the pressure. By the shape of the pressure rise and by hydraulic tests prior to the temperature pulses, k and S_s can be well constrained during the pressure interpretation. The compressibility of the chamber (β_c) determines the "volume production" caused by a pressure variation in the chamber (Eq. (7)). The model shows a strong sensitivity to the chamber compressibility β_c (Fig. 3d), to such an extent that, depending on its value, pressure signal can

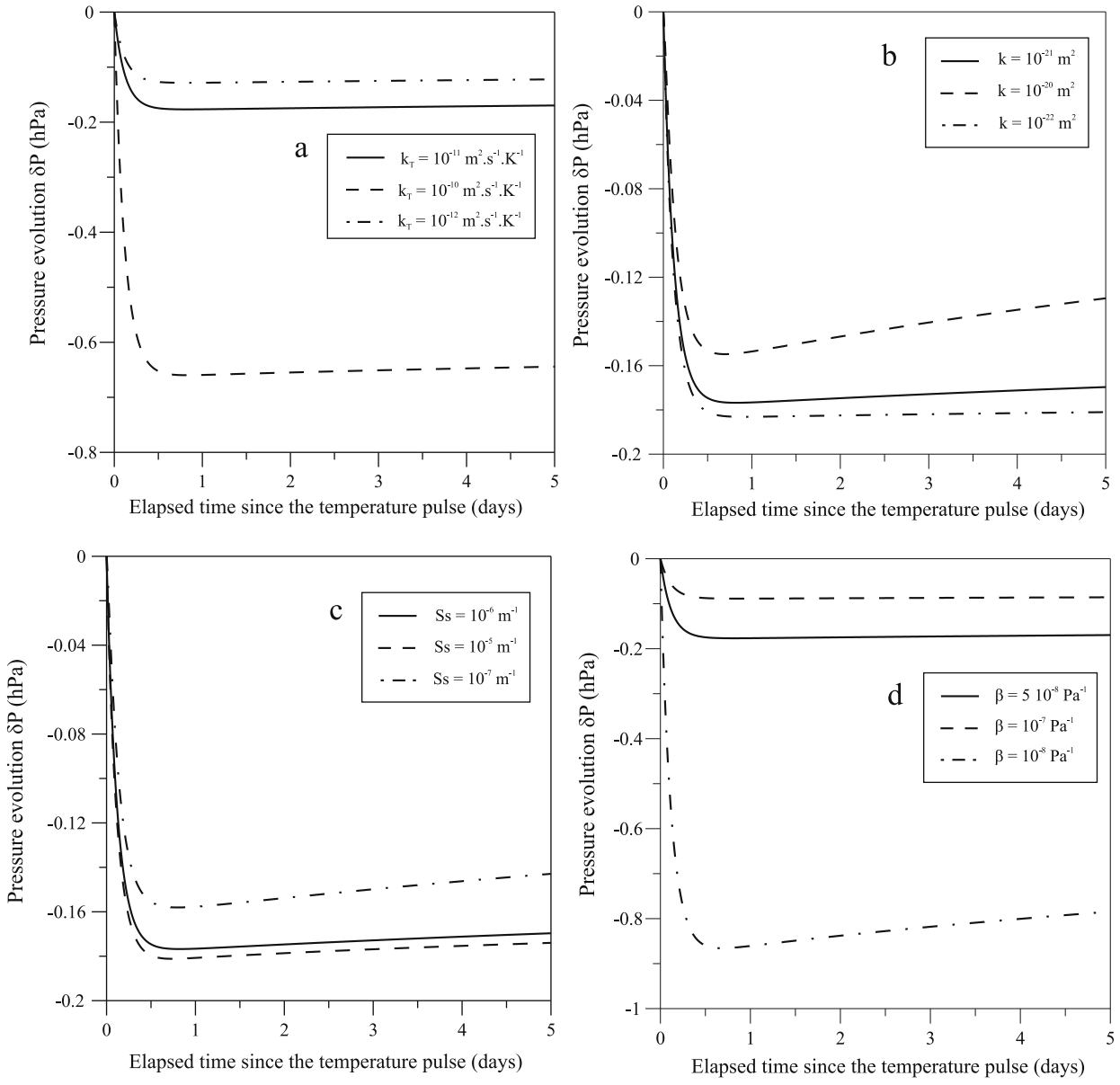

Fig. 3. Sensitivity analysis on the pressure evolution after a temperature pulse. Sensitivity on: (a) the coefficient of thermo-osmotic permeability; (b) the intrinsic permeability; (c) the specific storage coefficient; and (d) the compressibility of the chamber.

be only explained with thermal expansion. This parameter needs a precise characterization by multiplying measurements to reduce the uncertainty due to β_c.

3. Experimental design

3.1. Characteristics of the Tournemire Liassic argillite

Thermo-osmosis experiments were performed at IRSN URL located at Tournemire (southeastern France). This URL consists in a century-old tunnel crossing the Liassic argillite and more recent galleries excavated from the tunnel. The Liassic argillite of Tournemire forms part of the *Grands Causses* Mesozoic basin. It is 250 m thick at the URL location and is surrounded by two limestone formations. The Tournemire argillite is composed by clay minerals (about 50%wt, mainly illite and illite-smectite mixed layers rich in illite and also kaolinite and mica), carbonates (mainly calcite), quartz and secondary minerals [31,32]. The shale presents a very low natural water content, around 3–4%wt, a porosity in the range 6–9% and a mean pore size of 2.5 nm [31]. In the non-perturbed or non-fractured zone, the Tournemire argillite has an intrinsic permeability of 10^{-22}–10^{-21} m^2 and a specific storage coefficient between 10^{-6} and 10^{-5} m^{-1}. Permeability measurements parallel and normal to the bedding suggest an anisotropy [31,33,34]. Tritiated water diffusion in Tournemire argillite also indicates an anisotropy: a 1/3 ratio is observed between the HTO effective diffusion normal to the bedding and the one parallel to the bedding [35]. The Tournemire argillite presents clay-rock typical thermal characteristic values: a thermal conductivity of 1.6–1.8 W m^{-1} K^{-1} and a specific heat of about 700 J kg^{-1} K^{-1} [32].

3.2. Borehole and equipment characteristics

Experiments were carried out in a 5 m depth horizontal air-drilled borehole with a diameter of 65 mm, located in the 1996 East gallery of the Tournemire URL. This borehole was equipped

with a multi-packer device, made with steel, to individualize 5 chambers of 0.1 m length. Pressure in each chamber is measured in its corresponding hydraulic line by a Keller 33× type pressure transducer (0–10 hPa range, 0.25% accuracy). Chamber 2 was used in the experiments because it presented the best pressure equilibrium and no perturbation was induced in the other chambers to avoid by-pass between chambers. Chamber 2 is located at 4 m from the borehole head. It has a volume V_c (including tubing) of 2.25×10^{-4} m^3 and the surface of the external cylindrical wall of the chamber S_c is 2.14×10^{-2} m^2.

3.3. Experimental protocol

Just after the drilling, equipment was installed in the borehole and chambers were saturated. A set of vacuum–CO_2(g) flushes was made in the chambers to avoid air trapping. Next, chambers were saturated with a water of similar composition than the formation water and the pressure in the chambers tend to equilibrate with the formation pressure. Once pressure was stabilized, hydraulic pulses were performed in each chamber. However, permeability and storage coefficient obtained from these pulses seemed overestimated. This is probably due to the short time between equipment installation and the pulses (1 month) which did not allow to perform the pulses in steady state conditions and due to desaturation in the three closest chambers from the gallery wall.

The temperature pulse has consisted in changing the water filling the chamber by a warmer water. This change was performed via the circulation circuit presented in Fig. 4. Before the circulation, the test interval was isolated, with valves B and C closed, and the pressure in the interval was recorded by sensor P1. It was first needed to prepare the water change. The test water used in the experiment was a water with the same composition as the water in the chamber. The test water was put in the flow-through sealed reservoir installed in the thermostatic bath and the water was heated till the required temperature. Once the desired temperature was reached and stabilized, a circulation in the external circuit has been induced using the peristaltic pump, valves B and C staying closed, to saturate the circuit and to equilibrate it at the test water temperature. Temperature in the circuit was measured with sensors P,T3 and T4. However sensor P,T3 temperature was not representative of that of the circuit since the sensor was installed at the end of an hydraulic line. The sensor T4 is considered to be indicator of the test water temperature. During the experiments, temperature differences between water formation, measured by T7 sensor at the feet of the borehole completion ($T_{for} = 11.8$ °C), and test water were: +2.5, +5.1 and +9 °C. In this circulation preparation phase, pressure sensors P2 and P,T3 were also calibrated and the pressure in the circuit was adjusted to the pressure in the interval (P1) via the manometer P6 to avoid a pressure disturbance during the water change.

Then the water change was performed, opening valves B and C to the test interval. It induced a pressure record during the circulation into the interval with sensors P2 and P,T3 and no longer with P1. Water change lasted about 10 min at a constant flow rate of 100 mL min^{-1}, allowing to change about four times the water in the interval. At the end of the water change and in order to control temperature behavior, valves A and E of the flow-through sealed reservoir were closed. Thus, water circulated in a closed circuit, without water or temperature supply, between the test interval and the external sensors. Note that the external hydraulic lines were thermally insulated. Once the temperature in the circuit recovered the formation temperature, valves B and C were closed and the circulation ceased to isolate the test interval and let the pressure evolve (again recorded with pressure sensor P1).

Several temperature pulses via water changes were performed during winter and spring 2008 at the Tournemire URL in the same chamber, with ΔT of +5.1, +9 and +2.5 °C, successively. Various hydraulic pulses were performed to obtained the compressibility of the chamber, applying Eq. (9). Obtained β_c parameter values are 2.59×10^{-8} Pa^{-1}, measured after borehole device installation, 7.15×10^{-8} Pa^{-1}, measured after the test at +9 °C and before the test at +2.5 °C and 4.47×10^{-8} Pa^{-1}, measured after the test at +2.5 °C, giving an average β_c of 4.73×10^{-8} Pa^{-1}.

4. Experimental results and interpretation

After the temperature pulses, pressure decreases rapidly and reaches a minimum then it increases slowly. The evolution of measured pressures after temperature pulses of +2.5, +5.1 and +9 °C are shown in Fig. 5. The shape of the pressure evolutions are consistent with the theoretical evolution simulated in Section 2.2. Pressure decrease corresponds to the effect of temperature dissipation from the chamber to the argillite and, when the temperature gradient vanishes, pressure reaches a minimum (second term in the right hand side of Eq. (2) is null). The pressure response must be interpreted in order to identify the relative contributions of thermal expansion and thermo-osmosis to the pressure decrease. This interpretation involves numerical simulations of the temperature pulses using the model presented in Section 2 in its variational form. Firstly, the model geometry needs to be adapted to the

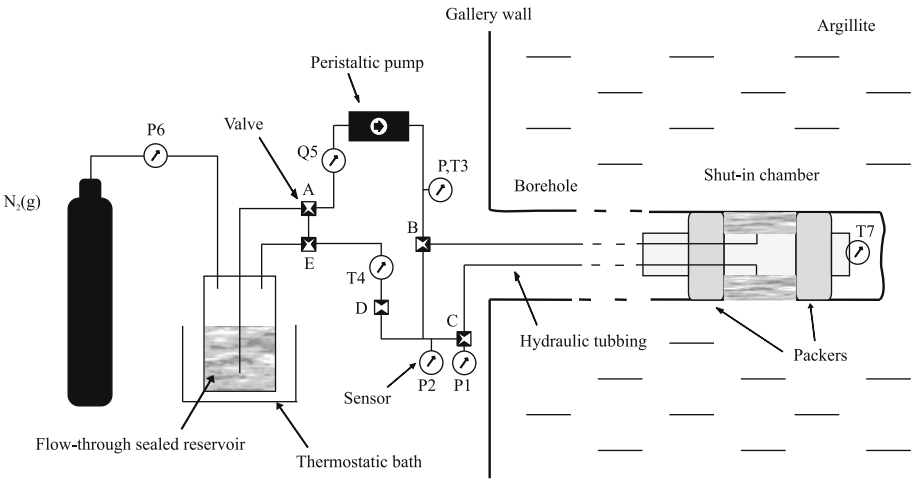

Fig. 4. Schematic sketch of the equipped borehole and the water change device.

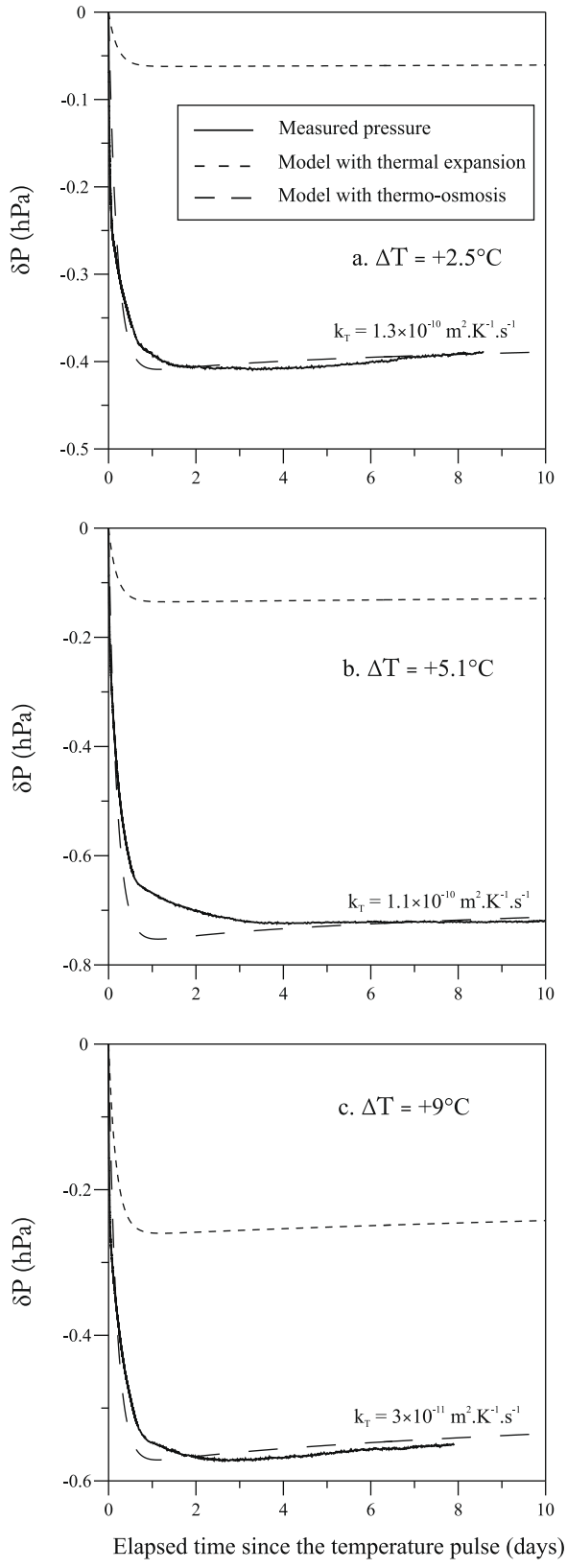

Fig. 5. Measured and modelled pressure evolution after a temperature pulse of: (a) +2.5 °C; (b) +5.1 °C; and (c) +9 °C. Two model cases are considered: only with thermal expansion and changes of water properties with temperature; and with thermo-osmosis added.

experiment geometry: experiments were performed in a horizontal borehole drilled in the direction of the bedding, equipped with a packers system. Because fluxes occur mainly in the bedding direction, a modeled domain in the plane of the borehole (Fig. 6) and not normal to the borehole (see previous theoretical calculations and Fig. 1) is required. In this configuration, the chamber is represented by a rectangular zone in the center of the grid (Fig. 6). Mesh refinement around the chamber by a square-nested grid is maintained to obtain a better accuracy. As fluxes occur across the wall chamber and not at the chamber–packer boundary, a no-flow condition is imposed between the chamber and the lateral cells corresponding to the packers (lateral meshes on the right and on the left in Fig. 6). The chamber properties as given in Section 3.2, and the properties of the Tournemire argillite (see Section 3.1) are introduced in the simulations.

In a first calculation step, the temperature pulses at +2.5, +5.1 and +9 °C were simulated by considering only thermal expansion of water and changes of water properties with temperature but no thermo-osmosis. The resulting pressure evolutions for the different temperature pulses are represented in Fig. 5. In the three cases the thermal expansion and the changes of water properties with temperature do not completely explain the pressure evolution recorded in the experiments. It is also readily noted that the pressure decrease is more important when higher temperature difference is imposed. Nevertheless, the calculated pressure decrease is not sufficient to reproduce the measured pressure evolution. This suggests that another process, namely thermo-osmosis, has to be accounted for in our calculations. When thermo-osmosis, thermal expansion and changes of water properties with temperature are introduced in the model, simulations better reproduce the temperature pulses. The coefficient of thermo-osmotic permeability k_T is determined by inversion, i.e. by fitting graphically the calculated evolution for a k_T to the measured pressure evolution. Best fits of the model to the measured pressure are shown in Fig. 5 for the different temperature pulses. As seen in the analysis of a theoretical temperature pulse (Section 2.2), the model presents a significant sensitivity on the chamber compressibility β_c. In the calculations presented here, the average chamber compressibility is used but modeling of the temperature pulses are also performed for the range of β_c experimentally determined. Thus, for each temperature pulse, a range of thermo-osmotic permeabilities are obtained. The results are shown in Table 4. These values vary within one order of magnitude for a temperature pulse.

The results suggests a decrease of the thermo-osmotic permeability when the temperature pulse ΔT increases. This observation is in agreement with the theory of Derjaguin et al. [5] which states that thermo-osmosis is less efficient at high temperature. This might be due to a destruction of the liquid boundary layer at the charged surface of clay minerals when temperature increases.

In the theoretical analysis of a temperature pulse (Section 2.2), it was shown that the pressure rise subsequent to temperature perturbation dissipation is dependent on the hydraulic parameters k and S_s. In the inversion of the experimental temperature pulses, an intrinsic permeability k of 10^{-21} m^2 and a specific storage coefficient S_s of 10^{-6} m^{-1} are needed. These values are typical values of the Tournemire argillite (see Section 3.1) and, despite the difficulties for obtaining k and S_s during the preliminary pulse (Section 3.3), these parameters are constrained by the pressure recovery shape.

Although almost satisfying simulations of the temperature pulses were obtained, some little discrepancies between simulations and measurements have to be recognized. Some aspects not taken into account in the model could explained these differences. Negligible vertical fluxes were assumed due to permeability anisotropy in layered clay-rocks. Although presumably weak, vertical fluxes could participate to the pressure evolution in the chamber. The observed deviations between the model and the measurements could also be the result of a thermal perturbation

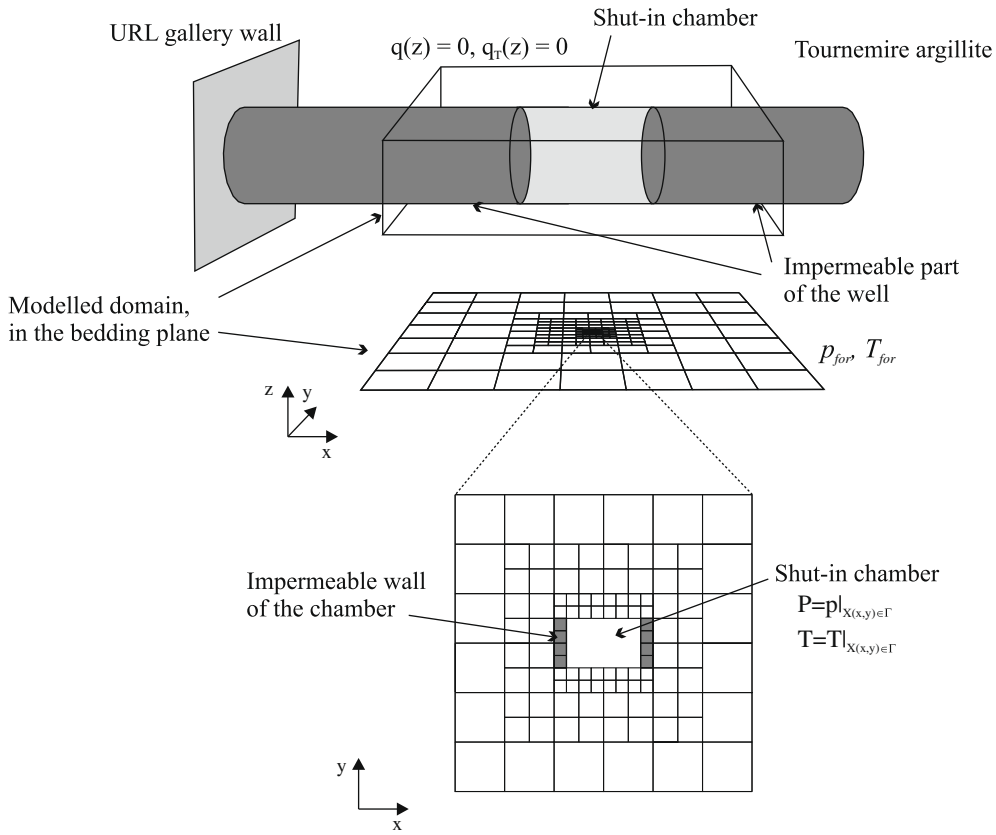

Fig. 6. Geometry of the modelled domain in an horizontal borehole. In this figure, $q(z)$ and $q_T(z)$ stand for the vertical components of the fluid and heat fluxes.

Table 4
Coefficients of thermo-osmotic permeability k_T obtained for each temperature pulse for the measured range of chamber compressibility β_c.

β_c (Pa^{-1})		2.59×10^{-8}	4.73×10^{-8}	7.15×10^{-8}
k_T (m^2 s^{-1} K^{-1})	+2.5 °C	6×10^{-11}	1.3×10^{-10}	2×10^{-10}
	+5.1 °C	5×10^{-11}	1.1×10^{-10}	1.8×10^{-10}
	+9 °C	6×10^{-12}	3×10^{-11}	6×10^{-11}

during the temperature dissipation stage. Two perturbations of this kind can be envisaged: the hypothesis of no heat dissipation along the borehole completion is perhaps partially not verified and the completion could contribute in heat dissipation from the chamber; and, the water circulation between the chamber and the external circuit, maintained after the water change in order to record temperature evolution, could has perturbed the temperature dissipation, in spite of the circuit thermal insulation.

5. Discussion and conclusions

In this paper, a set of thermo-osmosis experiments performed in the Tournemire Liassic argillite were presented. To our knowledge it is the first in situ thermo-osmosis experiments performed on a non-remoulded clay-rock. It provides first estimates for thermo-osmotic permeability in a natural material. The range of thermo-osmotic permeabilities obtained in this study is in the high range of thermo-osmotic permeabilities previously determined on argillaceous materials (Table 1). This could be explained by the low pore size of the Toarcian clay-rock (2.5 nm) and by the low formation temperature (around 12 °C) at the IRSN URL. Indeed, according to the developments presented in the companion paper [9], thermo-osmotic permeability increases as pore size or temperature decreases. During the experiments, a decrease of the thermo-osmotic permeability at increasing imposed temperature difference was observed. The pulses interpretation with the model is satisfactory, however little differences between the measured and modeled evolutions remain. The sensitivity analysis indicated that the thermo-osmotic permeability can be properly constrained with the model. The shape of the pressure response allows an acceptable inversion of the hydraulic parameters of the argillite. The highest source of uncertainty on the thermo-osmotic coefficient is the chamber compressibility, which has to be accurately determined.

Although, the thermo-osmotic model developed in the companion paper [9] was applied exclusively to pure materials (Na-smectite and kaolinite), a semi-quantitative comparison with values obtained here for a natural material can be made. Indeed, the values of k_T/k for smectite and kaolinite calculated by the model could represent, respectively, the higher and lower bounds for a natural clay-rock. For the Tournemire argillite pore size, the model [9] yields k_T/k values of 1.25×10^8 and 1.90×10^7 s^{-1} K^{-1} for smectite and kaolinite, respectively, while experimental values at Tournemire range from 6×10^9 to 2×10^{11} s^{-1} K^{-1}, depending on experiment temperature and uncertainties on chamber compressibility. Part of these two orders of magnitude difference might be due to temperature effects. Indeed, the model calculations [9] are based on a temperature of 298 K, while the mean temperature at Tournemire for the experiments was 285 K. Since k_T decreases with increasing temperature, these effects could explain almost one order of magnitude difference between the experiments and the range given by the model. The combined uncertainties on both the model and the experiments could explain partly or totally the remaining difference. The experimental thermo-osmosis

permeability can also be compared with the expression proposed by Revil and Leroy [21] $k_T = k\rho_f C_f/\eta$. Using the hydraulic conductivity of the Tournemire argillite yields a k_T of 4.2×10^{-12} m^2 s^{-1}K^{-1}, in the order of magnitude of the experimentally determined k_T. However, as seen in the companion paper [9], it seems that the model of Revil and Leroy [21] does not reproduce the various orders of magnitude variations of the k_T/k ratio with the poresize shown by the available data.

These first results on thermo-osmosis on natural clay-rocks have to be confirm by laboratory experiments upon which experimental conditions are better constrained. It also seems interesting to perform a new set of in situ experiments, but in a vertical borehole to better constrain the uncertainty due to a possible non-anisotropy of the fluxes.

The goal of this study on thermo-osmosis, by theoretical [9] and experimental approaches, was to assess the importance of this process for water flow calculations in a clay-rock. The results suggest that thermo-osmosis can significantly affect the water flow and could partly explain overpressures in such impervious rocks. Indeed, the non-linearity of k_T (temperature dependence) can cause overpressures, i.e. pressure above the hydrostatic equilibrium even at steady state. Such feature was discussed for the chemical osmosis by Rousseau-Gueutin et al. [23]. In future work, it seems that this process should be considered in fluid flow calculations in clay-rocks, especially when, like in the HLNW geological repository case, a significant temperature gradient is expected to develop.

Acknowledgments

The two anonymous reviewers are acknowledged for their relevant comments which allowed a substantial improvement of the manuscript. The IRSN and the Tournemire URL staff are also acknowledged for their support.

References

[1] C.L. Carnahan, Int. Commun. Heat Mass Transfer 13 (1986) 659.
[2] A. Ghassemi, A. Diek, J. Pet. Sci. Eng. 34 (2002) 123.
[3] S.T. Horseman, T.J. McEwen, Eng. Geol. 41 (1996) 5.
[4] J.M. Soler, J. Contam. Hydrol. 53 (2001) 63.
[5] B.V. Derjaguin, N.V. Churaev, V.M. Muller, in: J.A. Kitchener (Ed.), Surface Forces, first ed., Consultants Bureau, New York, 1987.
[6] G. Sposito, The Surface Chemistry of Soils, Oxford University Press, 1984.
[7] L. Onsager, Phys. Rev. 37 (1931) 405.
[8] L. Onsager, Phys. Rev. 38 (1931) 2265.
[9] J. Gonçalvès, J. Trémosa, J. Colloid Interface Sci. (2009), doi:10.1016/j.jcis.2009.09.056.
[10] ANDRA, Dossier 2005. Référentiel du Site Meuse/Haute Marne - Tome 2: Caractérisation comportementale du milieu géologique sous perturbation., C.RP.ADS.04.0022/A, ANDRA, Châtenay-Malabry, France, 2005.
[11] P. Habib, F. Soeiro, in: Proceedings 4th International Congress of Soil Mechanics, 1957, p. 40.
[12] C. Dirksen, Soil Sci. Soc. Am. Proc. 33 (1969) 821.
[13] M. Rosanne, M. Paszkuta, P. Adler, J. Colloid Interface Sci. 299 (2006) 797.
[14] R. Srivastava, A. Jain, Indian J. Chem. 12 (1974) 1276.
[15] R. Srivastava, P. Avasthi, J. Hydrol. 24 (1975) 111.
[16] L. Zheng, J. Samper, Phys. Chem. Earth 33 (2008) S486.
[17] J.L. Martín, J.M. Barcala, Eng. Geol. 81 (2005) 298.
[18] A. Katchalsky, P.F. Curran, Nonequilibrium Thermodynamics in Biophysics, Harvard University Press, Cambridge, Massachusetts, 1967.
[19] J.K. Mitchell, K. Soga, Fundamentals of Soil Behavior, John Wiley & Sons, New-York, 2005.
[20] J.R. Philip, D.A. De Vries, Trans. Am. Geophys. Union 38 (2) (1957) 222.
[21] A. Revil, P. Leroy, J. Geophys. Res. 109 (2004) B03208, doi:10.1029/2003JB002755.
[22] J. Gonçalvès, S. Violette, J. Wending, J. Geophys. Res. 109 (2004) B02110, doi:10.1029/2002JB002278.
[23] P. Rousseau-Gueutin, V. de Greef, J. Gonçalvès, S. Violette, S. Chanchole, J. Colloid Interface Sci. 337 (2009) 106.
[24] G.d. Marsily, Quantitative Hydrogeology, Groundwater Hydrology for Engineers, Academic Press, New-York, 1986.
[25] D. Jougnot, A. Revil, Hydrol. Earth Syst. Sci. Discuss. 5 (2008) 2409.
[26] X. Luo, G. Vasseur, Am. Assoc. Pet. Geol. Bull. 76 (10) (1992) 1550.
[27] L. Demongodin, B. Pinoteau, G. Vasseur, R. Gable, Geophys. J. Int. 105 (1991) 675.
[28] J.D. Bredehoeft, S.S. Papadopulos, Water Resour. Res. 16 (1) (1980) 233.
[29] C.E. Neuzil, Water Resour. Res. 18 (2) (1982) 439.
[30] J.W. Mercer, G.F. Pinder, I.G. Donalson, J. Geophys. Res. 80 (1975) 2608.
[31] J.Y. Boisson, L. Bertrand, J.F. Heitz, Y. Moreau Le Golvan, Hydrogeol. J. 9 (2001) 108.
[32] B. Bonin, J. Contam. Hydrol. 35 (1998) 315.
[33] L. Bertrand, R. Laviguerie, J. Cabrera, J.M. Matray, S. Savoye, in: Clays in Natural & Engineered Barriers for Radioactive Waste Confinement, Andra, 2002.
[34] J.-M. Matray, S. Savoye, J. Cabrera, Eng. Geol. 9 (2007) 1.
[35] S. Motellier, I. Devol-Brown, S. Savoye, D. Thoby, J.-C. Alberto, J. Contam. Hydrol. 94 (2007) 99.

5.4 Conclusion

In this chapter, dealing with the characterization of thermo-osmosis in argillaceous media and particularly in the Tournemire argillite, two predictive models were presented as well as a set of in situ experiments.
Thermo-osmosis was suspected to have a non negligible role in the fluid flow and pressure fields in the Callovo-Oxfordian formation [135]. However this process was poorly understood and a large uncertainty on the thermo-osmotic permeability [141] prevented any conclusive statement on the process relevancy.

Through the observations on the thermo-osmotic permeability dependency on petrophysical parameters (pore size, surface charge density) and medium conditions (salinity, temperature), the establishment of predictive models and some thermo-osmotic experiments on the Tournemire Toarcian clay-rock in natural conditions, our contribution leads to an improvement of the knowledge on thermo-osmosis.
However, as seen in the paper in preparation Gonçalvès *et al.*, Fig. 1, the measured thermo-osmotic permeability for the Tournemire argillite presents an important deviation compared with the predictive model. A better agreement is found between model and data for other thermo-osmotic experiments on non natural argillaceous materials. This discrepancy could be due to experimental artefacts, to errors introduced in the experiments interpretation or to limitations in the predictive model. Indeed, predictive calculations were done for Na^+ ions as counterions but the solutions used in the experiments also contained Ca^{2+} and Ca is expected to induce a higher disruption in the hydrogen bonding and, consequently, higher excess specific enthalpy and thermo-osmotic permeability. We can not presently state on this difference between data and model results but it illustrates the need for further studies on thermo-osmosis, both experimental and theoretical.

Part V

Interpretation of the pressure fields in argillaceous formations

Chapter 6

Influence of chemical osmosis on the pressure fields

In this Chapter, some causes of attenuation of the chemo-osmotically induced overpressures are discussed. It aims at contributing to the discussion on the ability of shales to generate significant abnormal pressures. Indeed, a recent recompilation and analysis of available chemo-osmotic experiments performed on compacted shales [110] suggests that large overpressures can be presumably found in argillaceous layers of sedimentary basins. However, such overpressures are not observed and osmotically induced overpressures are even rare in subsurface. In our study we show that the consideration of divalent counterions or mixed monovalent and divalent ions, like in natural waters, instead of monovalent counterions, as commonly used in experiments, tends to drastically decrease the osmotic efficiency value, as already seen in section 4.2. This decrease in the osmotic efficiency induces an important weakening of the generated overpressures in the shale formations. In the second part of the chapter, the ability of argillaceous layers to generate abnormal pressures in equilibrated basins, i.e. with linear concentration profiles, is studied. The spatial variations of the chemical osmotic efficiency as a function of the concentration or porosity changes have a crucial role in this abnormal pressures generation.
The constraints on abnormal pressures presented in this discussion are illustrated in the next chapter on the interpretation of the pressure field in the Tournemire formation, where osmotic efficiency profile account for the effects on monovalent and divalent counterions and a special attention is paid on the variations of the flow coefficients across the formation.

This chapter is presented as a paper submitted to Water Resources Research.

Natural conditions for more limited osmotic abnormal fluid pressures in sedimentary basins

Joachim Tremosa[1,2], Julio Gonçalves[3,4], Jean-Michel Matray[2]

[1]UPMC Univ. Paris 06, UMR-7619

SISYPHE, 4 place Jussieu, F-75252 Paris,

France.

[2]IRSN, DEI/SARG/LR2S, BP 17,

F-92262 Fontenay-aux-Roses, France.

[3]Aix-Marseille Univ., CEREGE,

UMR-6635, 13545 Aix en Provence cedex 4,

France.

[4]CNRS, CEREGE, UMR-6635, 13545 Aix

en Provence cedex 4, France.

Abstract. Chemical osmosis is considered a plausible cause of abnormal pressures in shale formations of sedimentary basins. A set of experimental data on chemical osmosis was recently obtained for different shales, mainly in the framework of studies on radioactive waste repositories in deep argillaceous formations. These data were analyzed by *Neuzil and Provost* [2009] who predicted large osmotically induced overpressures when required conditions are available. However, such large overpressures have not been found in sedimentary basins and the reasons for this disparity between predictions and observations need to be clarified. Here, two natural causes for lower than expected osmotic pressure are investigated: i) the effect of the complex composition of natural waters, including both monovalent and divalent cations, on the osmotic efficiency and the resulting abnormal pressures; and ii) the presence of steady-state rather than transient-state salinity distributions. For this purpose, a triple-layer electrical model accounting for multi-ionic solutions is developed and used to calculate the osmotic efficiency at different proportions of monovalent and divalent cations. The calculated decrease of the osmotic efficiency when Ca^{2+} is introduced in a Na^{+} - clay system yields a noticeable decrease in the ability of the shale to generate overpressures. In the second part of the paper, a discussion addresses the generation of abnormal pressures at steady-state conditions found in sedimentary basins, i.e. with a linear distribution of the concentration across the formation. The persistence of moderate overpressures is predicted due to the non-linearity associated with the dependence of the chemo-osmotic efficiency on the concen-

tration and the porosity. Finally, a case-study of the moderate excess-hydraulic head measured in the Toarcian/Domerian argillaceous formation of Tournemire (SE of France) is investigated. Our analysis indicates an osmotic origin for the excess-head and illustrates the influence of the porewater composition.

1. Introduction

Abnormal fluid pressures, which can be defined as a variation of fluid pressure from the hydrostatic pressure, are frequently encountered in subsurface environments, in a wide range of depths and geological settings [*Chilingar et al.*, 2002]. One of the motivation for studying abnormal pressures is provided by the hydrodynamic information on the fluid flows occurring in the studied formation we can obtain from the interpretation of the abnormal pressures origin [*Neuzil*, 1995]. Osmosis, or fluid flow driven by a chemical potential gradient, is considered a plausible cause of abnormal or non-hydrostatic fluid pressures in sedimentary basins when favorable conditions are encountered [*Marine and Fritz*, 1981; *Neuzil*, 2000; *Gonçalvès et al.*, 2004; *Rousseau-Gueutin et al.*, 2009; *Neuzil and Provost*, 2009]. However, the debate concerning this osmotic origin of abnormal pressure continues and the concept is controversial, since few examples are reported and the nature of the process is not well established [*Neuzil and Provost*, 2009].

Overpressures in many basins are not caused by osmosis but rather by a forcing, such as when a portion of the mechanical stress is transferred to fluids [*Neuzil*, 1995, 2003; *Chilingar et al.*, 2002]. Therefore, a careful characterization of the geological environment and its related flow and transport processes, coupled to an hydromechanical study is needed to assess the osmotic origin of observed overpressures. However abnormal fluid pressures due to a physical forcing tend to dissipate quickly in a geological sense and these overpressures are most common in young basins [*Lee and Deming*, 2002; *Gonçalvès et al.*, 2004]. Osmotic origin of abnormal pressures can be envisaged in specific geological environments: in clay-rich and highly compacted formations where a chemical concentra-

tion gradient exists and when overpressures persist in old basins [*Marine and Fritz*, 1981; *Neuzil and Provost*, 2009]. A situation presenting a maximum concentration at the center of the formation, with transient-state conditions for solute transport and water flow, is most often required for inducing an excess pressure [*Neuzil and Provost*, 2009].

Osmosis is related to the anionic exclusion caused by the negative electrical charges at the clay mineral surface. It confers to the clay-rock a membrane behaviour, partially impeding the solutes crossing the membrane but not the water molecules. The osmotic efficiency of a clay-rock is expressed through the osmotic efficiency coefficient, ε, which ranges between 0 for a non-membrane material behaviour and 1 for a perfect membrane, where solute flux is totally impeded. This coefficient can be determined by experiments, performed in-situ in boreholes [*Neuzil*, 2000; *Garavito et al.*, 2007; *Rousseau-Gueutin et al.*, 2010] or on samples in the laboratory [*Cey et al.*, 2001; *Horseman et al.*, 2007; *Rousseau-Gueutin et al.*, 2009; *Tremosa*, 2010]. The osmotic efficiency can also be computed in a predictive sense using theoretical models which consider the electrical interactions between the solution and the charged surface together with the petrophysical properties of the porous media [*Bresler*, 1973; *Fritz*, 1986; *Revil and Leroy*, 2004; *Gonçalvès et al.*, 2007]. Chemo-osmotic fluid flow is considered in a generalized Darcy's law as follows:

$$q = -\frac{k}{\eta}\left(\nabla P + \rho_f g \nabla z\right) + \varepsilon(b, C)\frac{k}{\eta}\nabla \Pi, \tag{1}$$

where q is the specific discharge (m s^{-1}), k is the intrinsic permeability (m^2), η is the dynamic viscosity of water (Pa s), P is the pore pressure (Pa), ρ_f is the fluid density (kg m^{-3}), g is the acceleration due to the gravity (m s^{-2}), ∇z is (0,0,1) if z axis is directed upwards, $\varepsilon(b, C)$ is the osmotic efficiency dependent on the half-pore size, b (m), and on

the concentration C (mol L^{-1}), and Π is the osmotic pressure (Pa).

Until recently, few measurements of osmotic efficiency coefficients on natural argillaceous formation were available [*Young and Low*, 1965], leading to a general skepticism on overpressures generation by osmosis. Some experiments have, however, been performed this last decade [*Neuzil*, 2000; *Cey et al.*, 2001; *Al-Bazali*, 2005; *Garavito et al.*, 2007; *Horseman et al.*, 2007; *Rousseau-Gueutin et al.*, 2009, 2010], leading to a better characterization of chemo-osmotic properties of argillaceous rocks. In particular, these studies clearly show that a chemo-osmotic flow exists in such rocks.

In their analysis of these experiments, *Neuzil and Provost* [2009] predicted overpressures of few bars up to tens of MPa, depending on the petrophysical properties of the clay-rock and on the concentration difference across the clay-rock. However, such large overpressures attributed to chemical osmosis have not been observed in sedimentary basins. For example, a 1 MPa overpressure that appears to be caused by chemical osmosis has been documented in the Dunbarton basin [*Marine and Fritz*, 1981] and an osmosis contribution of 0.1 to 0.15 MPa to the total overpressure ranging between 0.5 and 0.6 MPa has been calculated for the Callovo-Oxfordian of the Paris basin [*Rousseau-Gueutin et al.*, 2009]. Different explanations of this disparity were analyzed by *Neuzil and Provost* [2009]: i) shales are less osmotically efficient than suggested and the *Bresler* [1973] predictive model, commonly used, is perhaps conceptually flawed, though it was fitted mostly on experimental data. However, *Neuzil and Provost* [2009] argued that this is likely not the real cause of disparity since large pressures were generated by osmosis in laboratory test; ii) argillaceous formations are ineffective membranes at large scale and the osmotic efficien-

cies measured at small scale on samples and in boreholes can not been upscaled at the formation scale. In particular, this statement is supported by the fact that osmotic efficiency is expected to vanish when a connected fractures network is present in the clay-rock [*Swarbrick and Osborne*, 1998; *Chilingar et al.*, 2002]. However, similar hydraulic permeabilities are found at both small and large scale, indicating an absence of short-circuiting [*Neuzil*, 1994]; iii) the conditions for the generation of overpressures by osmosis are rare; and iv) osmotic overpressures are not systematically studied when an abnormal pressure is encountered in a basin.

Other natural causes for lower than expected osmotic overpressures, not accounted for in the works by *Neuzil and Provost* [2009], are examined in this paper. In the first part, the effect of a more complex porewater composition than the simple NaCl solution typically considered, i.e. including both monovalent and divalent solutes, is analyzed. In the second part, the basin salinity distribution is examined at quasi-equilibrium (steady-state fluxes) and no more at transient-state, which is commonly invoked. The resulting pressure fields are identified. Finally, the results of an investigation of the origin of the moderate excess-hydraulic head measured in a Toarcian/Domerian argillaceous formation, studied at the Tournemire IRSN underground research laboratory (SE of France). Chemical osmosis is addressed as a cause and the influence of porewater composition on the osmotic process in the formation is analyzed.

2. Effect of mixed Ca/Na solutions on the osmotic efficiency and abnormal pressures

Theoretical and experimental studies of chemical osmosis in pure clays and argillaceous rocks typically have been conducted using pure NaCl or $CaCl_2$ solutions (see compilations by *Bresler* [1973] and *Neuzil and Provost* [2009]), rather than more complex solutions containing both monovalent and divalent solutes. The osmotic efficiency coefficient is significantly lower with Ca^{2+} than with Na^+ solutions [*Bresler*, 1973]. In particular, *Shackelford and Lee* [2003] measured a destruction of the membrane potential of a Na-bentonite induced by the replacement of the Na^+ interlayer cations by Ca^{2+}. However, the osmotic efficiency coefficient of clay-rocks with a mix of Na^+ and Ca^{2+} solutions is unknown. Because natural waters present complex compositions, the osmotic efficiency is expected to be affected according to such compositions. Such effects on abnormal fluid pressure are evaluated in the following discourse.

2.1. Model for osmotic efficiency calculations with mixed Ca/Na solutions

Chemical osmosis occurs in clay-rocks because of anion exclusion, which results from ionic transport restrictions due to size and/or electrical effects (and salinity, consequently). Anion exclusion and, thus, osmotic efficiency is particularly efficient when clay is highly compacted and the electrical diffuse layers overlap [*Bolt*, 1979]. Calculations of the osmotic efficiency will consequently depend on the mean content of anions in the clay pores, $< \overline{C-} >$, and on the anion content in the bulk water, C_f. A simplified relationship expressing these factors is [*Kemper and Rollins*, 1966; *Bresler*, 1973; *Bolt*, 1979]:

$$\varepsilon = 1 - \frac{< \overline{C-} >}{C_f}. \tag{2}$$

A more complex expression, obtained by the resolution of the Navier-Stockes equation integrating the chemical force is presented in Appendix A (Eq. A16). This expression

requires knowledge of the ion distribution in the pores related to the clay surface and its dependence on the pore size, which can be calculated using an electrical triple-layer-model (TLM). In Appendix A, a TLM which accounts for multi-ionic solutions and interacting adjacent diffuse layers (compacted clay-rocks with low pore size) is developed.

The TLM is calibrated against osmotic experimental data from experiments on natural clay-rocks [*Neuzil*, 2000; *Cey et al.*, 2001; *Al-Bazali*, 2005; *Garavito et al.*, 2006, 2007; *Horseman et al.*, 2007; *Rousseau-Gueutin et al.*, 2009, 2010]. Comparison of predicted osmotic efficiencies using the TLM with measured osmotic efficiencies for NaCl – clay systems is shown in Fig. 1, as a function of the product of the half pore size and the concentration in chloride in the bulk solution $b \times C_f$, where b (in nm) is the half pore size and C_f (in mol L^{-1}) is the chloride concentration in the bulk solution. This representation was elected because it illustrates the combined effect of the pore size and the salinity, which modify the electrical potentials and lead to transport restrictions. Similar representation was used by previous authors (e.g., *Bresler* [1973]; *Gonçalvès et al.* [2007]). A fairly good agreement is observed between the TLM results and the data for natural clay-rocks. Reported osmotic efficiency measurements show a dispersion for the lowest measured osmotic efficiencies, i.e., for ε lower than 0.08. Moreover, some data present an important uncertainty regarding their $b \times C_f$ value, because of the range of concentration imposed to the sample during the experiment. Thus, the TLM can provide a relatively good estimation of osmotic efficiency in porewater – clay-rock systems presenting low $b \times C_f$ values but the estimation is less accurate for systems with high $b \times C_f$ values. The main uncertainty on the use of the TLM stems from the absence of osmotic experiments performed on natural clay-rocks with Ca^{2+} pure solution or Na^{+}/Ca^{2+} mixed solutions

to validate the osmotic efficiencies calculated for solutions different than Na^+ solutions. Most of natural waters concentrations and compositions can be considered in the TLM accounting for diffuse layers truncation and multi-ionic solutions. For high salinity, diffuse layers in the pores collapse and membrane behavior of the clay-rock almost vanishes [*Mitchell and Soga*, 2005]. Positive electrical potentials are, therefore, calculated by the TLM in this situation at the limit of validity of the model since it can only consider negatively charged surfaces.

The pore size, $2b$, is a critical parameter for TLM calculations and the chemical osmotic efficiency determinations. The half pore size, b (m), is determined, for clay-rocks, by a mass balance equation based on a plane-parallel geometry assumption, as follows [*Neuzil*, 2000; *Neuzil and Provost*, 2009; *Gonçalvès et al.*, 2010]:

$$b = \frac{\omega}{\rho_s A_s (1-\omega)}, \tag{3}$$

where ω is the porosity, ρ_s is the grain density (g m^{-3}) and A_s is the specific surface area (m^2 g^{-1}).

2.2. Effect of mixed Ca/Na solutions on the osmotic efficiency

In order to determine the chemical osmotic efficiency for mixed Na^+/Ca^{2+} solutions, calculations are performed for varying solution composition with the TLM presented in Appendix A. Changes in solution composition are introduced according to a ratio $2\times Ca^{2+}/(Na^+ + 2\times Ca^{2+})$, expressed in molal units, which varies between 0 for a pure Na solution, to 1 for a pure Ca solution. This ratio is denoted hereafter as the Calcium Index. It presents the advantage to express the relative contents in Na^+ and Ca^{2+} in

a simple way, ranging between 0 and 1 independently of the solution salinity. Figure 2 shows the osmotic efficiency as a function of the Calcium Index and of $b \times C_f$. Figure 2 illustrates that the osmotic efficiency drops when the salinity or the pore size increases and when the counterions are Ca^{2+} versus Na^{+}. At large pore size and at high bulk concentration, the electrical double layer collapses yielding a weak anionic exclusion. According to our calculations, clay-rock osmotic efficiency strongly decreases for mixed Na^{+}/Ca^{2+} solutions even at low proportions in Ca^{2+} in comparison to purely Na^{+} solutions. Indeed, the osmotic efficiency calculated for a Calcium Index of 0.1 (which corresponds to a Na to Ca ratio of 18:1, in molar units) is approximately the half than the efficiency for a Calcium Index of 0. Furthermore, large osmotic efficiency values, i.e. ε close to 1, can not be reached for Calcium Indices higher than 0.25, corresponding to a Na to Ca ratio of 6:1. For a pure $CaCl_2$ solution the higher calculated osmotic efficiency are slightly lower than 0.5 when very low pore sizes and low-salinity waters are considered. These observations suggest that introduction of Ca^{2+}, even at low amounts, in a Na-clay system will induce a dramatic decrease of osmotic efficiency and a weakening of the clay membrane behaviour. Consequently, an osmotic efficiency determined experimentally using NaCl solutions will probably overestimate the osmotic efficiency under natural conditions.

2.3. Implications of mixed Ca/Na solutions for overpressures

Generation of abnormal pressures in a sedimentary basin by osmosis can only occur in low permeability or hydraulically isolated layers [*Chilingar et al.*, 2002]. Furthermore, in presence of permeable connections, such as fracture networks, abnormal pressure generation will be impossible, because of the weakness of osmotic flow with respect to the hydraulic flow. The situation encountered in sedimentary basins illustrated in Fig. 3 is

particularly favorable to generate overpressures by osmosis. It consists in an argillaceous layer surrounded by two aquifer layers, with the porosity initially filled by a connate seawater entrapped during sedimentation. During basin evolution and especially during aquifer outcropping, saline porewater in the aquifers is flushed by freshwater, but not the clay-rock porewater because of the conductive flow inefficiency. A salinity gradient between the argillaceous formation and the aquifers is thus established and tends to equilibrate with time by diffusion, e.g. *Pearson et al.* [2003]; *Patriarche et al.* [2004]; *Neuzil and Provost* [2009]; *Mazurek et al.* [2011]. If the argillaceous formation exhibits membrane properties, the salinity gradient causes an osmotic flow directed towards the formation with higher salinity, i.e. towards the center of the clay-rock upward from the lower aquifer and downward from the upper aquifer. This osmotic flow generates a pressure buildup in the clay-rock to a quasi-equilibrium, corresponding to $q \simeq 0$ in Eq.(1).

Let's consider a horizontal argillaceous formation surrounded by two aquifer layers, with only vertical fluid flow in the shale layer and a salinity gradient in the argillaceous formation. According to the scenario previously presented (Fig. 3), C_{max} and C_{min} are the concentrations (mol L^{-1}) at the center of the shale layer and at the aquifer-shale boundaries, respectively. The resulting abnormal pressure is calculated in a similar way as *Neuzil and Provost* [2009], accounting for osmotic efficiency dependence to concentration. Assuming a constant pore size, an expression of the abnormal pressure, P_0 (Pa), is obtained, dependent on the concentration difference through $\varepsilon(C)$ but not on the formation thickness [*Neuzil and Provost*, 2009]:

$$P_0 = \int_{C_{max}}^{C_{min}} \varepsilon(C) \frac{d\Pi}{dC} dC. \quad (4)$$

227 P_0 corresponds to the non-hydrostatic pressure such that P_0=0 for hydrostatic pressures
228 and is positive for overpressures and negative for abnormal low pressures. Osmotic pres-
229 sure is expressed according to the Van't Hoff relation, $\Pi = \nu RTC$, which holds for
230 solutions with concentration lower than 1 mol L^{-1} [*Fritz*, 1986], where ν is the number
231 of ionic species, R is the Universal Gas Constant (8.314 m^3 Pa K^{-1} mol^{-1}) and T is the
232 absolute temperature (K).

233

234 In order to evaluate the influence of natural solutions with both monovalent and divalent
235 cations on osmotically generated abnormal pressures, P_0 is calculated for solutions with
236 various proportions of Ca^{2+} and Na^+ , as a function of the concentration gradient and the
237 half-pore size. The TLM accounting for multi-ionic solutions, described in Appendix A,
238 is used for the calculations of the osmotic efficiency as a function of the salinity, solution
239 composition and pore size. Results for a concentration ratio C_{max}/C_{min} of 10 and a
240 Calcium Index ($2\times Ca^{2+}/(Na^+ + 2\times Ca^{2+})$ ratio) of 0, 0.1, 0.2, 0.5 and 1 are depicted in
241 Fig. 4. The half pore size range of 1 to 10 nm used in Fig. 4 corresponds to a porosity
242 ranging between 0.1 and 0.5, using Eq.(3) and average values of the specific surface area
243 and grain density for compacted clay-rocks of 40 m^2 g^{-1} and 2700 kg m^{-3} respectively
244 [*Boisson*, 2005].
245 In the case of a pure NaCl solution (Fig. 4.a), moderate overpressures are generated
246 by osmosis, ranging between some tens of kPa to 1 MPa, as a function of the pore size
247 and the salinity difference. The highest overpressure is obtained for a half-pore size close
248 to 1 nm and, conversely, P_0 values lower than 0.1 MPa are obtained for a half-pore
249 size higher than 5 nm. Introducing a dependence on the concentration to the osmotic

efficiency allows observing opposite effects on the abnormal fluid pressures. With a salinity increase, the osmotic flow and its related overpressure tends to increase because of the concentration difference increase but, inversely, ε decreases with the salinity increase and tends to lower the osmotic flow. This explains why, for a same pore size, the overpressure first increases with an increasing concentration difference then, the calculated overpressure slightly decreases when higher concentrations are considered.

Comparison of the calculated overpressures for various Calcium Indices (Fig. 4) indicates a strong decrease of P_0 with increasing Ca^{2+} concentration compared to Na^+. This decrease is observed even for solutions with a low Calcium Index (0.1) and P_0 decreases further as the Ca^{2+} proportion increases. The highest P_0 of 1 MPa occurs for a Calcium Index of 0 and P_0 decreases to 0.8 MPa for a Calcium Index of 0.1 , to 0.4 MPa for an index of 0.2, to 0.1 MPa for an index of 0.5 and only to 0.015 MPa for a Calcium Index of 1. These results suggest that osmotic phenomena will be nearly unable to generate significant overpressures with pure Ca^{2+} solutions. For mixed Ca/Na solutions, overpressures are expected to be more moderate than for pure Na^+ solutions.

2.4. Discussion

The interactions between the charged surface of the clay and the porewater were represented using a TLM accounting for diffuse layers overlapping and multi-ionic solutions. It revealed a decrease of the osmotic efficiency with increasing Ca^{2+} in solution compared to Na^+ solutions, even with low proportions of Ca^{2+}. Since the Calcium Index in porewater of natural shales is around 0.1 and 0.2 [*Pearson et al.*, 2003; *Vinsot et al.*, 2008], the ability of natural buildup of large overpressures by osmosis appears consequently reduced by the osmotic efficiency degradation with the porewater composition. This reduction

of the osmotic efficiency may explain the scarcity of observed overpressures linked to osmosis. However, uncertainties in the predictive model make it difficult to state if it is the only cause of apparent discrepancy. The fact remains that the effect of mixed monovalent/divalent solutions appears important for the interpretation of abnormal pressures generated by osmosis in a clay-rock.

3. Abnormal fluid pressures generation at steady-state

Abnormal fluid pressures generated by osmosis have been so far associated exclusively to transient salinity distributions, where the abnormal pressures will evolve with the salinity profile across the argillaceous formation, e.g. by solutes diffusion towards the surrounding aquifers (Fig. 3). However, due to the osmotic efficiency dependence on the concentration and the pore size, i.e. the non-linearity of the osmotic efficiency, any variations, including linear variations, in the argillaceous formation of the concentration or the porosity will change the osmotic efficiency value. These changes in ε can lead to abnormal pressures, even when the salinity gradient is at steady-state and the basin at equilibrium. The abnormal pressure profile merely fulfils constant fluid flow by balancing the osmotic and hydraulic components of the fluid flow.

As an illustration, abnormal fluid pressure is calculated by solving the continuity equation at steady-state, considering that fluid flow is entirely vertical across a shale:

$$\frac{\partial}{\partial z}\left(\rho_f \frac{k}{\eta}\left(\frac{\partial P}{\partial z}+\rho_f g\right)-\rho_f \varepsilon(b,C)\frac{k}{\eta}\frac{\partial \Pi}{\partial z}\right)=0. \quad (5)$$

. The resolution of this equation requires determining relevant hydraulic parameters. Intrinsic permeability is obtained using a Poiseuille law for a plane parallel pore geometry

292 [*Walsh and Brace*, 1984]:

293 $$k = \frac{b^2}{3\,\omega^{-m}}, \tag{6}$$

294 with b the half-pore size (m), ω the porosity and m the cementation factor, estimated at
295 2.3 for natural shales [*Tremosa*, 2010]. Fluid density ρ_f and dynamic viscosity η are con-
296 sidered constant across the formation at values of 1000 kg m^{-3} and 10^{-3} Pa s, respectively.

297

298 Two scenarios for abnormal pressure calculations at steady state were tested using
299 plausible salinity and pore-size variations across a 100-m-thick argillaceous formation,
300 considering a linear hydrostatic pressure gradient. The first case (Fig. 5) considers a
301 formation with a linear concentration profile (between 10^{-1} and 10^{-3} mol L^{-1} of pure
302 NaCl solution) with higher concentrations in the deeper part, as salinity generally in-
303 creases with depth in sedimentary basins [*de Marsily*, 1986], and a constant porosity
304 of 0.2. Salinity profiles are generally transient in argillaceous sequences in sedimentary
305 basins [*Mazurek et al.*, 2011], but linear salinity profile with steady-state diffusion process
306 are also sometimes observed, like in the Boom Clay at Essen in Belgium [*Mazurek et al.*,
307 2011]. Considering a linear salinity profile allows identifying the individual effect of the
308 salinity variations on the osmotic flow and associated pressures. Pore size is calculated
309 using Eq.(3), a constant specific surface area of 40 m^2 g^{-1} and a grain density of 2700 kg
310 m^{-3}, average values for compacted clay-rocks [*Boisson*, 2005], yielding a 2.3 nm half-pore
311 size. The osmotic efficiency is calculated as a function of the concentration and pore size
312 using the TLM presented in Appendix A for pure NaCl solutions.
313 According to the concentration variation across the formation, osmotic efficiency is higher
314 at the upper part of the formation. It induces differences in osmotic flow in the forma-

315 tion leading to a limited pressure buildup of 0.04 MPa (Fig. 5). The resulting overall
316 flow in the argillaceous formation, calculated using Eq.(1), is directed downward and is
317 dominated by osmotic flow in comparison to purely hydraulic flow.
318 In the second case (Fig. 6), in addition to the previous linear concentration profile a linear
319 porosity variation (between 0.15 and 0.2), with a lower value in the deeper part because of
320 a higher compaction, was considered. This porosity variation corresponds to the maximal
321 vertical porosity variations for a 100-m-thick shale layer predicted by porosity – depth
322 functions [*Magara*, 1980]. Porosity range corresponds to a half-pore size ranging from
323 1.6 to 2.3 nm. The resulting osmotic efficiency variations across the formation is more
324 complex because ε increases with decreasing concentration, but it also decreases when the
325 pore size increases. These changes lead to a pressure buildup higher than in the previous
326 case with concentration variations only. Therefore, an overpressure of about 0.075 MPa
327 is obtained, at steady-state. This overpressure is slightly lower than the overpressure
328 predicted at transient state (Fig. 4) for similar pore size and concentration gradient. The
329 overall flow is, like in the previous case, directed downward. The influence of the intrinsic
330 permeability variations related to porosity changes across the formation was also evalu-
331 ated by calculating the pressure build-up considering a constant permeability instead of
332 a variable one. In such conditions, a more limited overpressure of about 0.025 MPa is
333 obtained (Fig. 6), illustrating the influence of both osmotic efficiency and intrinsic per-
334 meability in the osmotic flow term in Eq.(1).

335

336 Though limited, osmosis can generate overpressure at steady-state, i.e. in basins at
337 equilibrium, contrarily to the commonly accepted idea that osmotic overpressure can only

develop at transient-state because of the osmotic efficiency non-linearity. With only variations of concentration, a weak overpressure is calculated. This overpressure is almost undetectable in an argillaceous layer, because of the pressure measurement difficulties in such rocks. With both concentration and pore-size variations, a more noticeable overpressure is obtained though slightly lower than the overpressures obtained at transient-state. Fairly important differences in the calculated overpressures are observed when limited variations of concentration and flow coefficients (k and ε), through porosity, are considered across the shale layer. Identifying these variations in concentration and porosity and considering the non-linearity of the osmotic efficiency (and other flow coefficients) are thus crucial for overpressures understanding.

4. Influence of chemical osmosis on the excess-hydraulic head measured in the Toarcian/Domerian argillaceous formation of Tournemire (France)

An illustration of the effect of porewater composition on osmotically partly-induced pressure-profile can be made by considering the pressure field measured in the Toarcian/Domerian argillaceous formation of Tournemire (SE of France), studied at the IRSN underground research laboratory (URL). For this purpose we extended the notion of excess-pressure expressed in terms of excess-head. Indeed, an excess-head in the argillaceous sequence is considered herein as a hydraulic head which derives from the linear head profile given by the heads measured in two aquifers surrounding the sequence when purely hydraulic flow at steady-state with constant permeability is considered.

The Toarcian/Domerian argillaceous formation of Tournemire is part of the Mesozoic Grands Causses basin and presents a thickness of 250 m of shales and marls at the URL location. The shale is surrounded by two karstic limestones aquifers of Carixian and

Aaleanian ages. Since sedimentation ceased in the basin at the end of the Jurassic, the basin evolved under subaerial conditions leading to the erosion of 800 to 1600 m of material during the Cretaceous [*Peyaud et al.*, 2005] and karst development in limestones layers [*Ambert and Ambert*, 1995; *Simon-Coinçon and Schmitt*, 1999]. Major uplifts occurred during the Pyrenean orogenesis in the Eocene and canyon incision mainly occurred during Miocene.

The identification of the hydraulic head profile across the formation (Fig. 8) was made by a careful selection of pressure measurements in equipped boreholes [*Tremosa*, 2010]. These measurements were selected outside of the depressed zone induced by the URL [*Matray et al.*, 2007] and such as they are constant during a sufficiently long time period to be representative of the formation fluid pressure. A moderate excess-hydraulic head of about 30 m is observed (between 20 and 40 m depending on the boreholes; Fig. 8), compared to the linear profile bounded by the aquifers heads characterizing purely hydraulic flow at steady-state conditions using a constant permeability. This excess-head is moderate so that the head in the shale layer does not exceed the head in the overlying aquifer and thus cannot be strictly considered as an overpressure. However, because of its non-linear shape, crucial hydrodynamic information can be obtained by the study of the non-linear profile.

Causes of excess-head linked to the basin history, such as compaction disequilibrium, tectonic compression, visco-plastic behaviour of clays or changes in hydraulic boundary conditions for explaining the Tournemire excess-head can be discarded. Indeed, because of the basin evolution and valley incision age and because of the massif actual exhumation, these processes are not relevant for the actual pressure profile interpretation [*Tremosa*,

2010]. Conversely, chemical osmosis was suspected to be a plausible cause of excess-head because the clay-rich content and low porosity of the Toarcian/Domerian shale confers a membrane behaviour to the formation and because of the observed concentration profile in the formation with a higher salinity in its center (Fig. 7).

In the Toarcian/Domerian argillaceous formation of Tournemire, the intrinsic permeability measurements considered as representative of the undisturbed rock [*Boisson et al.*, 2001; *Bertrand et al.*, 2002] range between 10^{-21} and 10^{-20} m^2. In such an impervious rock, it is difficult to measure the permeability with an accuracy lower to the order of magnitude [*Neuzil*, 1994]. However, permeability variations are suggested by the easy-measurable porosity profile. Porosity mean value is 9 % and ranges between 2.7 % in the lower Toarcian and 11.1 % in the upper part of the upper Toarcian. Porosity, measured and calculated permeability variations across the formation are depicted in Fig. 7. Intrinsic permeability is calculated using Eq.(6), where the poresize was estimated using Eq.(3). The porosity was determined by measurements of water content and volume [*Matray et al.*, 2007], the grain density by helium pycnometry and the specific surface area by the BET method. Parameter profiles are listed in Table 1.

The membrane behaviour of the Toarcian/Domerian clay-rock of Tournemire has been demonstrated by a set of laboratory experiments on samples using NaCl solutions [*Tremosa*, 2010]. Chemo-osmotic efficiencies were measured to range between 0.014 and 0.31 for salinity gradients ranging between 5 and 18, using the formation salinity as reference salinity in these experiments. However, measurements at only one elevation were carried out which impedes establishing the osmotic efficiency profile from these measurements. The osmotic efficiency profile was then calculated using the TLM presented in

Appendix A, using pore size and porewater composition as input parameters. The porewater composition profile was calculated by a thermodynamic geochemical model which aims at reproducing the rock – porewater interactions [*Tremosa et al.*, submitted]. This geochemical model requires the measured Cl and SO_4 mobile anion profiles, which give the porewater salinity, and calculates the cations content as a function of the interactions with the rock (mineral saturation and cation exchange). For the sake of simplicity, monovalent cations are here considered as Na^+ ions, divalent cations as Ca^{2+} and anions as Cl^- (Fig. 7). The TLM developed in this study can account for multi-ionic solution and the osmotic efficiency is thus calculated as a function of the solution composition (Table 1).

The hydraulic head profile in the Toarcian/Domerian argillaceous formation is calculated in 1D, along the z-axis, at steady-state (Eq. 5) considering purely Darcy's flow and chemical osmosis. Hence, the excess-head build-up is calculated for a given concentration profile, considering the system is in pseudo-equilibrium at each time ($q \simeq 0$). Steady-state hypothesis avoid reconstructing the flow and transport history in the basin. This assumption is supported by the very low filtration and mass transport flux rates in the formation. The measured heads in the surrounding Carixian and Aalenian aquifers are introduced as boundary conditions and the present-day composition profile as chemical forcing (Fig. 7). The purely hydraulic flow with a constant permeability leading to a linear hydraulic head profile is taken as the reference state. Then two calculations were performed: i) purely hydraulic flow with variable hydraulic permeability; and ii) hydraulic and osmotic flows with chemo-osmotic efficiency and permeability vertical variations. The calculated head obtained considering purely hydraulic flow with permeability variations is shown in Fig.

8 and presents an important deviation compared with the reference linear head profile obtained using a constant permeability. Indeed, the calculated hydraulic head profile where permeability variations are considered can almost reproduce the measured excess-head. The deviation from the measured excess-head σ can be quantified as follows:

$$\sigma = \frac{|\Delta h_{data} - \Delta h_{model}|}{\Delta h_{data}} \times 100, \quad (7)$$

where Δh_{data} and Δh_{model} are, respectively, the measured and the calculated excess-heads compared with the linear head profile. Deviation σ is 24 % for the head obtained considering purely hydraulic flow and variable permeability.

The calculations of the hydraulic head profiles considering hydraulic flow and chemical osmosis together are made using the osmotic efficiency profile calculated from porewater composition but also using an osmotic efficiency profile calculated for a NaCl solution at the same salinity (Table 1). It allows evaluating the influence of porewater composition on the osmotic excess-head. The two calculated hydraulic head profiles are depicted in Fig. 8, together with the measured hydraulic heads.

Hydraulic head calculations considering chemical osmosis with ε computed using the natural composition allows improving the simulation of the observed excess-head profile. Indeed, a fairly good agreement is observed between the calculated and measured heads, with a deviation σ of 16 %. The influence of the porewater composition on the calculated head profile is illustrated in Fig. 8. Indeed, the osmotically induced hydraulic heads calculated for a NaCl solution are 10 to 15 m higher than the one calculated considering the natural porewater composition and present a deviation σ of 29 % compared with the measured heads. The measured excess-head is better reproduced when the natural composition of fluid is considered in the calculations though both calculated head profiles are

in the range of the measured one. A limited numerical uncertainty on the calculated head profile is found. Uncertainty on the hydraulic head was evaluated from the experimental uncertainty of the petrophysical parameters (Table 1) used to calculate the intrinsic permeability and the chemo-osmotic efficiency. A maximum numerical uncertainty of $\pm$ 1 m on the heads is calculated where the highest changes in mineralogy and petrology are observed in the formation, i.e in the lower Toarcian.

These calculations suggest that the measured excess-head profile in the Toarcian/Domerian argillaceous formation of Tournemire can be explained by chemical osmosis and vertical variations of the permeability. However, this analysis of the excess-head is partial because thermo-osmosis, a fluid flow driven by a temperature gradient, was also observed and quantified in the Tournemire argillite [*Tremosa et al.*, 2010] and is expected to have an influence on fluid flows and the hydraulic head profile in the formation.

Regarding the fluid flow and mass transport, modifications induced by chemical osmosis are relatively limited compared with the case considering only hydraulic flow with variable permeability. Fluid flow remains directed downward in both cases. The Peclet Number, which is the ratio of the characteristic time for diffusion to the characteristic time for convection, is 0.28 when only the hydraulic flow is considered and 0.30 when chemo-osmotic and hydraulic flows are considered together. Then, mass transport remains mainly governed by diffusion.

5. Conclusion

The effect of natural water compositions compared to simple NaCl solutions, commonly used in experiments and in calculations, on the osmotic efficiency and on the abnormal pressures in natural clay-rocks was evaluated. This evaluation was based on an electrical

triple-layer-model (TLM) developed to calculate the chemo-osmotic efficiency of compacted clay-rocks characterized by complex pore-fluid compositions. Compared to the osmotic overpressures predicted considering purely NaCl solutions, lower overpressures are predicted when Ca^{2+}/Na^{+} mixed solutions are considered. Considering porewater solutions with both monovalent and divalent cations tends to decrease the extent of the diffuse layer in the pore space. Consequently, the osmotic efficiency of the shale also decreases and tends to lower abnormal pressures. For a Na to Ca ratio of 18:1, the osmotic efficiency is predicted to be half compared as the one for a pure Na solution and the resulting overpressure is also divided by 2. However, the TLM was only calibrated on osmotic efficiencies obtained during experiments using NaCl as test solution. Indeed, no chemo-osmotic experiments have been performed on natural shales considering different test water compositions for a same salinity, so far. Thereby, the predicted osmotic efficiency of a shale for natural water compositions remains to be validated by experiments. Since natural waters are generally composed of species of various valences, lower osmotic efficiencies than those measured in most experiments using NaCl solutions can be expected in shale layers. Considering the natural water compositions is then a probable cause to explain the disparity between the osmotic overpressures predicted by *Neuzil and Provost* [2009] and the observed ones in basins.

Excess fluid pressures were calculated in sedimentary basins at steady-state conditions for salinity. These conditions are not usually considered as suitable conditions for the occurrence of such overpressures. Indeed, osmotic overpressures are exclusively studied as a transient-state situation depending on the concentration difference between the center of the argillaceous layer with a high salinity and the surrounding aquifers. In spite of

being moderated (less than 0.1 MPa), overpressures can be generated considering a linear concentration profile because of the chemo-osmotic efficiency coefficient dependence to the concentration, composition and pore size. However, such moderated osmotic overpressures can sorely be measured in shales.

The case study of the Toarcian/Domerian argillaceous formation of Tournemire showing moderate excess-hydraulic head of about 30 m was considered in support of the theoretical calculations and discussions previously carried out. The measured excess-head was correctly reproduced when hydraulic and chemo-osmotic flows are considered together with the vertical variations of the hydraulic permeability and the chemo-osmotic efficiency calculated with our model. Our results suggest that the variations of the permeability and chemical osmosis explain the excess-head profile measured at Tournemire. A noticeable difference of 10 to 15 m was observed between the calculated hydraulic heads for the natural porewater composition and for NaCl solution at the same salinity. A better agreement was thus obtained using the natural porewater composition to estimate the osmotic efficiency.

Although several explanations for the lower than predicted overpressures generated by osmosis are proposed in this paper, overpressures remains rarely detected or investigated [*Neuzil and Provost*, 2009]. Their detection is again more complicated since different causes can be invoked to explain abnormal pressures [*Rousseau-Gueutin et al.*, 2009].

Appendix A: Triple-layer-model TLM establishment for mixed Ca/Na solutions

The electrical triple-layer-model (TLM) developed herein to describe the interactions between the charged solid surface of a clay-rock and the pore solution is an improvement

of the *Avena and De Pauli* [1998] double-layer-model (DLM) and *Leroy and Revil* [2004] TLM. This model was modified by *Gonçalvès et al.* [2007] to account for diffuse layers overlapping. Multi-component solutions were introduced herein to this latter version following the approach by *Leroy et al.* [2007]. The advantage of the TLM compared to the DLM is the treatment of ions as particles of finite size, so high ionic concentrations near the surface can be considered [*Horseman et al.*, 1996]. Introducing the interaction of diffuse layers, by a truncation of these layers, is related to the small pore size in such rocks. As stated, osmosis phenomena results from this truncation. Multi-component solutions with monovalent and divalent cations are introduced in the model allowing exchange of various cations on surface sites.

Geometrically, the TLM considers two compacted layers constituted by ions sorbed at the mineral surface, i.e. the Stern layer. These layers are limited by the Inner Helmotz Plane (IHP) and Outer Helmotz Plane (OHP). This last plane forms the limit of the Stern layer and the diffuse layer, i.e. the third layer considered in the TLM, starts at the OHP. The diffuse layer extends towards the pore center and is limited by the interaction with the diffuse layer of another clay mineral particle. A schematic description is depicted in Figure 9. TLM considers the surface sites linked to the permanent negative charge due to isomorphic substitutions and the variable charge hydroxyl surface sites of protonation/deprotonation. Permanent exchange surface sites are represented here as X sites and each site carries one negative charge X^-. The exchange half-reactions for Na^+, Ca^{2+} and H^+ with their respective reaction constants correspond to:

$$XNa = X^- + Na^+, K_{Na}, \tag{A1}$$

$$X_2Ca = 2\,X^- + Ca^{2+}, K_{Ca}, \tag{A2}$$

$$XH = X^- + H^+, K_H. \tag{A3}$$

The surface site density Γ_i^0 (in sites m^{-2}) for each species i is expressed from the reaction constant expressions, in the *Gaines and Thomas* [1953] convention :

$$\Gamma_{XH}^0 = \frac{\Gamma_{X^-}^0 a_{H^+}}{K_H}, \tag{A4}$$

$$\Gamma_{XNa}^0 = \frac{\Gamma_{X^-}^0 a_{Na^+}}{K_{Na}}, \tag{A5}$$

$$\Gamma_{X_2Ca}^0 = \frac{(\Gamma_{X^-}^0)^2 a_{Ca^{2+}}}{K_{Ca}}, \tag{A6}$$

where a_i is the activity of species i. The $\Gamma_{X^-}^0$ expression is obtained using the total surface site density of the X sites, Γ_3^0, by the Newton method:

$$\Gamma_3^0 = \Gamma_{X^-}^0 + \Gamma_{XH}^0 + \Gamma_{XNa}^0 + \Gamma_{X_2Ca}^0. \tag{A7}$$

Γ_1^0 and Γ_2^0 correspond to the total surface site density of aluminol and silanol hydroxyl sites, obtained from the following complexation reactions:

$$AlOH_2^{1/2+} = AlOH^{1/2-} + H^+, K_1, \tag{A8}$$

$$SiOH_2^{1/2+} = SiOH^{1/2-} + H^+, K_2, \tag{A9}$$

The surface charge density of the clay minerals Q_0 (C m^{-2}) is obtained, using the surface site density, by the following equation:

$$Q_0 = -e[\frac{1}{2}(\Gamma^0_{AlOH_2^{1/2+}} - \Gamma^0_{AlOH^{1/2-}} + \Gamma^0_{SiOH_2^{1/2+}} - \Gamma^0_{SiOH^{1/2-}}) - \Gamma_3^0], \tag{A10}$$

where e is the elementary charge (1.6×10^{-19} C). The charge density in the Stern layer Q_β can be expressed as:

$$Q_\beta = e(\Gamma_{XNa}^0 + 2\Gamma_{X_2Ca}^0 + \Gamma_{XH}^0). \tag{A11}$$

Potentials in the IHP and the OHP drop linearly and are related to the charge densities by the relationships:

$$\varphi_0 - \varphi_\beta = Q_0/C_1, \tag{A12}$$

$$\varphi_\beta - \varphi_d = Q_S/C_2, \tag{A13}$$

where φ_0, φ_β and φ_d are, respectively, the electrical potentials (V) at the surface, at the β plane (IHP) and the d plane (OHP). C_1 and C_2 are the capacities (F m^{-2}) between the surface and the IHP and between the IHP and the OHP, respectively.

In the diffuse layer, the electrical potential and the ionic concentrations are obtained by the Poisson-Boltzmann equation. The charge density in the diffuse layer Q_S is written as follows, for a solution with N species i and a distance from the mineral surface x_d to b, i.e. from the OHP to the truncation plane:

$$Q_S = \int_{x_d}^{b} \sum_{i=1}^{N} \frac{C_i^f \gamma_i^f}{\gamma_i} \, e \, z_i \, exp\Big(- \frac{z_i e \varphi}{k_B T} \Big) dx, \tag{A14}$$

where k_B is the Boltzmann constant (1.38×10^{-23} J K^{-1}), T is the temperature (K), z_i is the valence of the ion i and C_i^f is the concentration of species i in the equilibrium solution (mol L^{-1}). This concentration C_i^f is the concentration in the porous media out of the electrostatic field influence denoted as the equilibrium solution and corresponds to the concentration obtained by a classical geochemical model. γ_i^f and γ_i are the activity coefficients, calculated with the *Davies* [1962] equation, in the equilibrium solution and in the diffuse layer, respectively. The *Davies* [1962] equation can be used for solutions with salinity lower than 0.7 M [*Langmuir*, 1997], i.e. up to seawater salinity.

The last equation of the TLM is its global electroneutrality constraint:

$$Q_0 + Q_\beta + Q_S = 0. \tag{A15}$$

587 The chemo-osmotic efficiency coefficient is obtained from the resolution of the Navier-
588 Stokes equation integrating the chemical force [*Bolt*, 1979], for a porous medium with a
589 plane parallel geometry:

$$\varepsilon = \frac{\int_0^b (1 - \frac{\overline{C-}(x)}{C_f})(2bx - x^2)dx}{\frac{2b^3}{3}}, \tag{A16}$$

590

591 where $\overline{C-}(x)$ is the anion concentration at a distance x from the clay surface, C_f is the
592 anion concentration in the equilibrium solution and $2b$ is the pore size. It is worth noting
593 that anion exclusion expression is applicable for both symmetric and non-symmetric so-
594 lutions [*Bolt*, 1979].

595

596 The predictions of the TLM for multi-ionic solutions with interacting diffuse layers
597 were calibrated against osmotic efficiency data of various natural clay-rocks in a NaCl-
598 clay system [*Neuzil*, 2000; *Cey et al.*, 2001; *Al-Bazali*, 2005; *Garavito et al.*, 2006, 2007;
599 *Horseman et al.*, 2007; *Rousseau-Gueutin et al.*, 2009, 2010]. Resulting parameters are
600 Γ_1^0=0 sites nm^{-2}, Γ_2^0=0.52 sites nm^{-2}, Γ_3^0=2.58 sites nm^{-2} (obtained with the CEC and
601 the specific surface area), K_1 undetermined, K_2=1.3×10^{-6}, K_H=1×10^{-2}, K_{Na}=1.3×10^{-1},
602 K_{Ca}=5×10^{-3} [*Avena and De Pauli*, 1998; *Leroy and Revil*, 2004; *Gaucher et al.*, 2006;
603 *Gonçalvès et al.*, 2007], C_1=1 F m^{-2} and C_2=0.2 F m^{-2}. As observed by *Gonçalvès et al.*
604 [2007], the more sensitive parameters are K_{Na} and C_2.

Acknowledgments. This work was performed during J. Tremosa PhD thesis, funded by IRSN and Amphos 21. J. Gonçalvès acknowledges the French National Center for Scientific Research (CNRS) through the GNR FORPRO II. PhD examiners, P. Cosenza and P. Gouze, are strongly acknowledged for their constructive comments on this work.

References

Al-Bazali, T. M. (2005), Experimental study of the membrane behavior of shale during interaction with water-based and oil-based muds, Ph.D. thesis, University of Texas, Austin.

Ambert, M., and P. Ambert (1995), Karstification des plateaux et encaissement des vallées au cours du Néogène et du Quaternaire dans les Grands Causses méridionaux (Larzac, Blandas), *Géologie de la France*, *4*, 37–50.

Avena, M. J., and C. P. De Pauli (1998), Proton adsorption and electrokinetics of an argentinean montmorillonite, *Journal of Colloid and Interface Science*, *202*, 195–204.

Bertrand, L., R. Laviguerie, J. Cabrera, J. M. Matray, and S. Savoye (2002), Instrument for measuring pore pressure and permeability in low permeability rock, in *Clays in natural & engineered barriers for radioactive waste confinement*, Andra.

Boisson, J.-Y. (2005), Clay club catalogue of characteristics of argillaceous rocks, *Nuclear Energy Agency Report 4436*, OECD.

Boisson, J. Y., L. Bertrand, J. F. Heitz, and Y. Moreau Le Golvan (2001), *In-situ* and laboratory investigations of fluid flow through an argillaceous formation at different scales of space and time, Tournemire tunnel, southern France, *Hydrogeology Journal*, *9*, 108–123.

Bolt, G. H. (1979), *Soil Chemistry, B. Physico-Chemical models*, Elsevier, Amsterdam.

Bresler, E. (1973), Anion exclusion and coupling effects in nonsteady transport unsatured soils : I. Theory, *Soil Science Society of America Proceedings*, *37*(5), 663–669.

Cey, B. D., S. L. Barbour, and M. J. Hendry (2001), Osmotic flow through a Cretaceous clay in southern Saskatchewan, Canada, *Canadian Geotechnical Journal*, *38*(5), 1025–

1033.

Chilingar, G. V., V. A. Serebryakov, and J. O. J. Robertson (2002), *Origin and prediction of abnormal formation pressures*, Developments in Petroleum Science, Volume 50.

Davies, C. W. (1962), *Ion Association*, Butterworths, Washington DC.

de Marsily, G. (1986), *Quantitative Hydrogeology, Groundwater Hydrology for Engineers*, 440 pp., Academic Press, New-York.

Fritz, S. J. (1986), Ideality of clay membranes in osmotic processes: A Review, *Clays and Clay Minerals*, *34*(2), 214–223.

Gaines, G. I., and H. C. Thomas (1953), Adsorption studies on clay minerals. II. A formulation of the thermodynamics of exchange adsorption, *Journal of Physical Chemistry*, *21*, 714–718.

Garavito, A. M., H. Kooi, and C. E. Neuzil (2006), Numerical modeling of a long-term in situ chemical osmosis experiment in the Pierre Shale, South Dakota, *Advances in Water Resources*, *29*, 481–492.

Garavito, A. M., I. De Cannière, and H. Kooi (2007), *In situ* chemical osmosis experiment in the Boom Clay at the Mol underground research laboratory, *Physics and Chemistry of the Earth*, *32*, 421–433.

Gaucher, E., P. Blanc, F. Bardot, G. Braibant, S. Buschaert, C. Crouzet, A. Gautier, J.-P. Girard, E. Jacquot, A. Lassin, G. Negrel, C. Tournassat, A. Vinsot, and S. Altmann (2006), Modelling the porewater chemistry of the CallovianOxfordian formation at a regional scale, *Comptes Rendus Geoscience*, *338*, 917–930.

Gonçalvès, J., S. Violette, and J. Wending (2004), Analytical and numerical solutions for alternative overpressuring processes : Application to the Callovo-Oxfordian sedimentary

sequence in the Paris basin, France, *Journal of Geophysical Research*, *109*, B02,110, doi :10.1029/2002JB002,278.

Gonçalvès, J., P. Rousseau-Gueutin, and A. Revil (2007), Introducing interacting diffuse layers in TLM calculations. A reappraisal of the influence of the pore size on the swelling pressure and the osmotic efficiency of compacted bentonites., *Journal of Colloid and Interface Science*, *316*, 92–99.

Gonçalvès, J., P. Rousseau-Gueutin, G. de Marsily, P. Cosenza, and S. Violette (2010), What is the significance of pore pressure in a saturated shale layer?, *Water Resources Research*, *46*, W04,514, doi:10.1029/2009WR008,090, doi:10.1029/2009WR008090.

Hendry, M. J., and L. Wassenaar (1999), Implications of the distribution of dD in porewaters of groudwater flow and the timing of geological events in a thick aquitard system, *Water Resources Research*, *35*(6), 1751–1760.

Horseman, S. T., J. J. W. Higgo, J. Alexander, and J. F. Harrington (1996), *Water, Gas and Solute Movement Trough Argillaceous Media*, Nuclear Energie Agency (NEA).

Horseman, S. T., J. F. Harrington, and D. J. Noy (2007), Swelling and osmotic flow in a potential host rock, *Physics and Chemistry of the Earth*, *32*, 408–420.

Kemper, W. D., and J. B. Rollins (1966), Osmotic Efficiency Coefficients Across Compacted Clays, *Soil Science Society of America Proceedings*, *30*(5), 529–534.

Langmuir, D. (1997), *Aqueous Environmental Geochemistry*, Prentice Hall.

Lee, Y., and D. Deming (2002), Overpressures in the anadarko basin, southwestern oklahoma: Static or dynamic?, *AAPG Bulletin*, *86*, 145–160.

Leroy, P., and A. Revil (2004), A triple-layer model of the surface electrochemical properties of clay minerals, *Journal of Colloid and Interfacial Science*, *270*, 371–380.

Leroy, P., A. Revil, S. Altmann, and C. Tournassat (2007), Modeling the composition of the pore water in a clay-rock geological formation (Callovo-Oxfordian, France), *Geochemica and Cosmochemica Acta*, *71*, 1087–1097, doi:10.1016/j.gca.2006.11.009.

Magara, K. (1980), Comparison of porosity-depth relationships of shale and sandstone, *Journal of Petroleum Geology*, *3*, 175–185.

Marine, I. W., and S. J. Fritz (1981), Osmotic model to explain anomalous hydraulic heads, *Water Resources Research*, *17*(1), 73–82.

Matray, J. M., S. Savoye, and J. Cabrera (2007), Desaturation and structure relationships around drifts excavated in the well-compacted Tournemire's argillite (Aveyron, France), *Engineering Geology*, *9*, 1–16.

Mazurek, M., P. Alt-Epping, A. Bath, T. Gimmi, H. N. Waber, S. Buschaert, P. De Cannière, M. De Craen, A. Gautschi, S. Savoye, A. Vinsot, I. Wemaere, and L. Wouters (2011), Natural tracer profiles across argillaceous formations, *Applied Geochemistry*, *26*, 1035–1064.

Mitchell, J. K., and K. Soga (2005), *Fundamentals of Soil Behavior*, 3rd ed., 558 pp., John Wiley & Sons, New-York.

Neuzil, C. E. (1994), How permeable are clays and shales?, *Water Resources Research*, *30(2)*, 145–150, doi:10.1029/93WR02,930.

Neuzil, C. E. (1995), Abnormal Pressures as Hydrodynamic Phenomena, *American journal of Science*, *295*, 742–786.

Neuzil, C. E. (2000), Osmotic generation of "anomalous" fluid pressures in geological environments, *Nature*, *403*, 182–184.

Neuzil, C. E. (2003), Hydromechanical coupling in geologic processes, *Hydrogeology Journal*, *11*, 41–83.

Neuzil, C. E., and A. M. Provost (2009), Recent experimental data may point to a greater role for osmotic pressures in the subsurface, *Water Resources Research*, *45*, W03,410, doi:10.1029/2007WR006,450.

Patriarche, D., E. Ledoux, J.-L. Michelot, R. Simon-Coinçon, and S. Savoye (2004), Diffusion as the main process for mass transport in very low water content argillites: 2. Fluid flow and mass transport modeling, *Water Resources Research*, *40*, W01,517, doi: 10.1029/2003WR002700.

Pearson, F. J., D. Arcos, A. Bath, J. Y. Boisson, A. M. Fernández, H. E. Gabler, E. Gaucher, A. Gaustchi, L. Griffault, P. Hernán, and H. N. Waber (2003), Geochemistry of water in the Opalinus Clay Formation at the Mont Terri rock laboratory, *Technical Report 2003-03*, Mont Terri Project.

Peyaud, J. B., J. Barbarand, A. Carter, and M. Pagel (2005), Mid-Cretaceous uplift and erosion on the northern margin of the Ligurian Tethys deduced from thermal history reconstruction, *International Journal of Earth Science*, *94*, 46247.

Revil, A., and P. Leroy (2004), Constitutive equations for ionic transport in porous shales, *Journal of Geophysical Research*, *109*, B03,208, doi : 10.1029/2003JB002,755.

Rousseau-Gueutin, P., V. de Greef, J. Gonçalvès, S. Violette, and S. Chanchole (2009), Experimental device for chemical osmosis measurement on natural clay-rock samples maintained at *in-situ* conditions. implications for pressure interpretation., *Journal of Colloid and Interface Science*, *337*, 106–116.

Rousseau-Gueutin, P., J. Gonçalvès, M. Cruchaudet, G. de Marsily, and S. Violette (2010), Hydraulic and chemical pulse-tests in a shut-in chamber imbedded in an argillaceous formation: numerical and experimental approaches, *Water Resources Research*, *46, W08516*, doi:10.1029/2008WR007,371.

Shackelford, C. D., and J. M. Lee (2003), The destruction role of diffusion on clay membrane behavior, *Clays and Clay Minerals*, *51*, 186–196.

Simon-Coinçon, R., and J. M. Schmitt (1999), Evolution géologique et histoire paléoenvironnementale du bassin des grands causses, *Rapport technique LHM/RD/99/52*, Centre d'Information Géologique, Ecole Nationale Supérieure des Mines de Paris.

Swarbrick, R., and M. Osborne (1998), *Mechanisms that Generate Abnormal Pressures : an Overview*, AAPG Memoir 70, 13-34. pp.

Tremosa, J. (2010), Influence of osmotic processes on the excess-hydraulic head measured in the Toarcian/Domerian argillaceous formation of Tournemire, Ph.D. thesis, Université Pierre et Marie Curie, Paris 6.

Tremosa, J., J. Gonçalvès, J. M. Matray, and S. Violette (2010), Estimating thermo-osmotic coefficients in clay-rocks: II. In situ experimental approach, *Journal of Colloid and Interface Science*, *342*, 175–184.

Tremosa, J., D. Arcos, J. M. Matray, F. Bensenouci, E. C. Gaucher, C. Tournassat, and J. Hadi (submitted), Geochemical characterization and modelling of the Toarcian/Domerian porewater at the Tournemire underground research laboratory, *Applied Geochemistry*.

Vinsot, A., S. Mettler, and S. Wechner (2008), In situ characterization of the callovo-oxfordian pore water composition, *Physics and Chemistry of the Earth*, *33*, S75–S86.

Walsh, J. B., and W. F. Brace (1984), The effect of pressure on porosity and the transport properties of rocks, *Journal of Geophysical Research*, *89*, 9425–9431.

Young, A., and P. Low (1965), Osmosis in argillaceous rocks, *AAPG Bulletin*, *49*, 1004–1008.

Figure 1. Model and data from several argillaceous formations of chemo-osmotic efficiency coefficient as a function of $b \times C_f$ for a NaCl-clay system. Data references: Oligocene Boom clay [*Garavito et al.*, 2007], Cretaceous Pierre shale [*Neuzil*, 2000; *Al-Bazali*, 2005; *Garavito et al.*, 2006], Cretaceous Bearpaw formation [*Cey et al.*, 2001; *Hendry and Wassenaar*, 1999], Jurassic Opalinus clay [*Boisson*, 2005; *Horseman et al.*, 2007], Paris basin Callovo-Oxfordian (COx) formation [*Rousseau-Gueutin et al.*, 2009, 2010] and shales from Al-Bazali [*Al-Bazali*, 2005; *Neuzil and Provost*, 2009].

Figure 2. Evolution of chemo-osmotic efficiency coefficient calculated with the TLM as a function of the Calcium Index $2\times Ca^{2+}/(Na^{+} + 2\times Ca^{2+})$ and $b \times C_f$.

Figure 3. Scheme of the abnormal pressure generation by osmosis due to a salinity gradient between the shale layer and the surrounding aquifers.

Figure 4. Overpressures (P_0 in MPa) generated by chemical osmosis as a function of the concentration difference, $C_{max} - C_{min}$, with C_{max}/C_{min}=10 and the pore size, b, for different Calcium Index a) 0, b) 0.1, c) 0.2, d) 0.5 and e) 1. Numbers on curves are P_0.

Figure 5. Pressure profile across a 100-m-thick argillaceous formation obtained at steady-state by chemical osmosis caused by variations of the osmotic efficiency with the concentration and for a constant porosity.

Figure 6. Pressure profile across a 100-m-thick argillaceous formation obtained at steady-state by osmosis caused by variations of the osmotic efficiency variations with the concentration and the porosity.

Figure 7. Profiles of intrinsic permeability, porosity, porewater composition and osmotic efficiency in the Toarcian/Domerian argillaceous formation of Tournemire. Triangles are the measured intrinsic permeabilities *Boisson et al.* [2001]; *Bertrand et al.* [2002].

Figure 8. Measured and calculated hydraulic head profiles in the Toarcian/Domerian argillaceous formation of Tournemire.

Figure 9. Schematic representation of solution - mineral surface interaction and associated electrochemical variables (electrical potentials φ_i and surface charges Q_i) in the TLM with interacting diffuse layers *Gonçalvès et al.* [2010].

Table 1. Parameters used in the calculations for the argillaceous formation of Tournemire. ω_{tot} is the total porosity, ρ_s is the grain density (g cm^{-3}), A_s is the specific surface area (m^2 g^{-1}), b is the half-pore size (nm), $\varepsilon_{natural}$ is the osmotic efficiency calculated for the natural porewater composition and ε_{NaCl} is the osmotic efficiency calculated for a NaCl solution. Elevation is in m NGF.

Formation unit	Elevation	ω_{tot}	ρ_s	A_s	b	$\varepsilon_{natural}$	ε_{NaCl}
upper Toarcian	551.3	0.111 ± 0.0006	2.732 ± 0.0005	28 ± 2	1.64 ± 0.12	0.513 [0.493 — 0.537]	0.846 [0.831 — 0.863]
upper Toarcian	534.4	0.111 ± 0.0006	2.721 ± 0.0005	25 ± 2	1.84 ± 0.15	0.425 [0.400 — 0.452]	0.794 [0.771 — 0.817]
upper Toarcian	512.2	0.111 ± 0.0005	2.723 ± 0.0004	24 ± 2	1.91 ± 0.16	0.323 [0.299 — 0.351]	0.733 [0.704 — 0.762]
upper Toarcian	463.1	0.096 ± 0.0006	2.709 ± 0.0005	23 ± 2	1.71 ± 0.14	0.204 [0.183 — 0.229]	0.646 [0.608 — 0.687]
upper Toarcian	411.5	0.084 ± 0.0006	2.735 ± 0.0004	22 ± 2	1.52 ± 0.13	0.104 [0.089 — 0.122]	0.572 [0.522 — 0.626]
int. Toarcian	387.5	0.100 ± 0.0006	2.734 ± 0.0007	25 ± 2	1.63 ± 0.17	0.129 [0.109 — 0.158]	0.560 [0.503 — 0.626]
lower Toarcian	372.9	0.047 ± 0.0006	2.424 ± 0.0028	5 ± 0	4.06 ± 0.07	0.025 [0.024 — 0.025]	0.169 [0.165 — 0.175]
lower Toarcian	359.1	0.027 ± 0.0007	2.385 ± 0.0010	5 ± 0	2.32 ± 0.06	0.085 [0.081 — 0.089]	0.435 [0.423 — 0.448]
Domerian	331.2	0.082 ± 0.0006	2.740 ± 0.0007	22 ± 2	1.48 ± 0.05	0.127 [0.120 — 0.134]	0.746 [0.729 — 0.761]
Domerian	316.7	0.077 ± 0.0006	2.733 ± 0.0006	23 ± 2	1.34 ± 0.13	0.206 [0.185 — 0.236]	0.827 [0.796 — 0.865]
Domerian	302.9	0.085 ± 0.0006	2.737 ± 0.0005	26 ± 2	1.30 ± 0.13	0.317 [0.290 — 0.348]	0.876 [0.851 — 0.903]

Figure 1

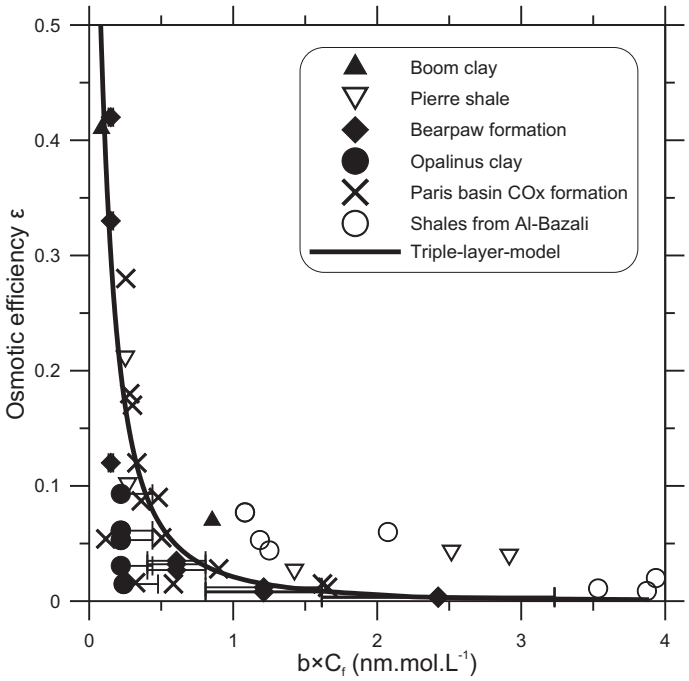

Figure 1. Model and data from several argillaceous formations of chemo-osmotic efficiency coefficient in function of $b \times C$ for a NaCl-clay system. Data references: Oligocene Boom clay [*Garavito et al.*, 2007], Cretaceous Pierre shale [*Al-Bazali*, 2005; *Garavito et al.*, 2006; *Neuzil*, 2000], Cretaceous Bearpaw formation [*Cey et al.*, 2001; *Hendry and Wassenaar*, 1999], Jurassic Opalinus clay [*Boisson*, 2005; *Horseman et al.*, 2007], Paris basin Callovo-Oxfordian (COx) formation [*Rousseau-Gueutin et al.*, 2009, 2010] and shales from Al-Bazali [*Al-Bazali*, 2005; *Neuzil and Provost*, 2009].

Figure 2

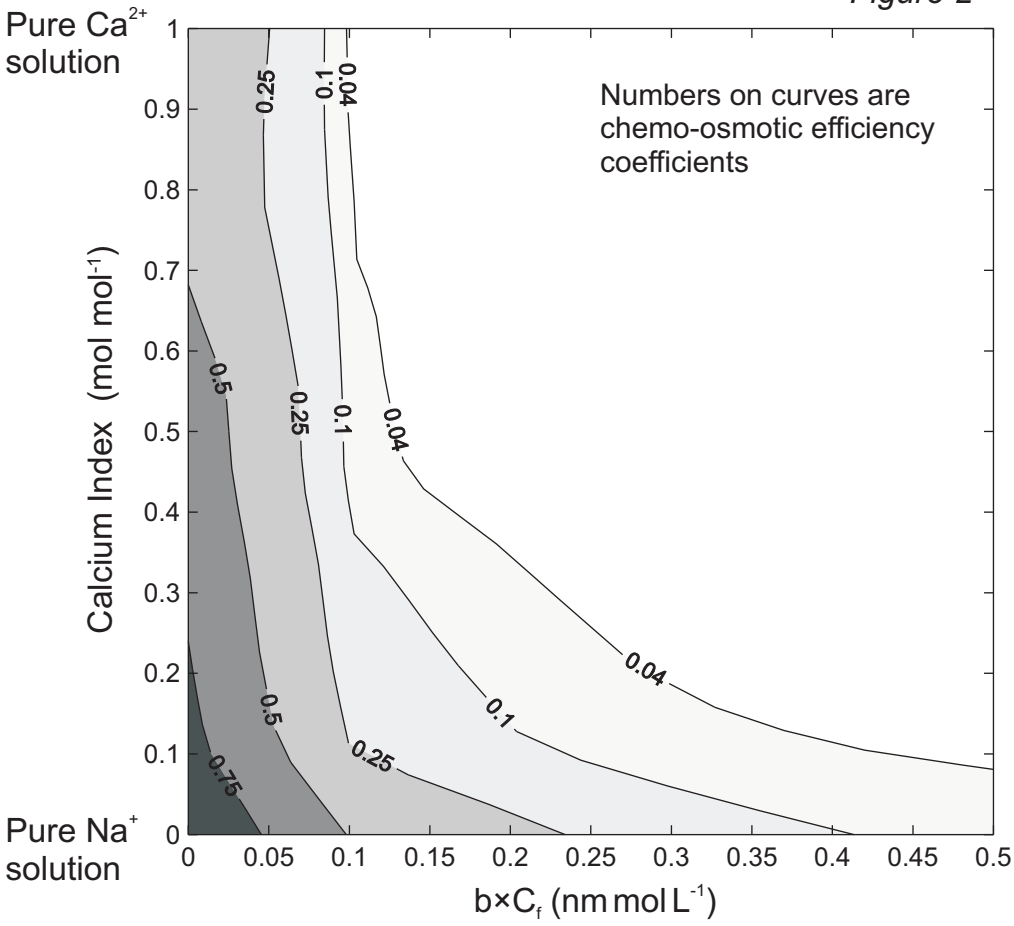

Figure 2. Evolution of chemo-osmotic efficiency coefficient calculated with the TLM as a function of the Calcium Index $2\times Ca^{2+}/(Na^{+} + 2\times Ca^{2+})$ and $b \times C_f$.

Figure 3

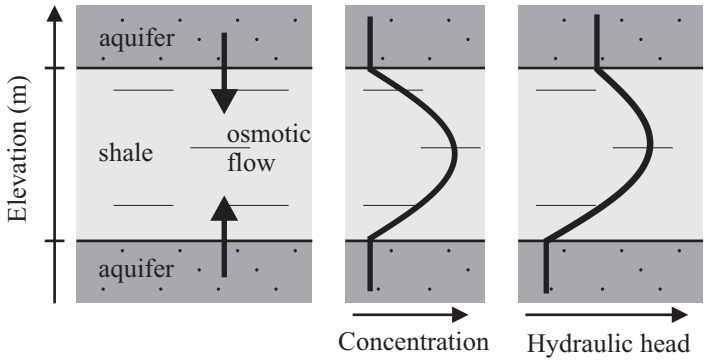

Figure 3. Scheme of the abnormal pressure generation by osmosis due to a salinity gradient between the shale layer and the surrounding aquifers.

Figure 4

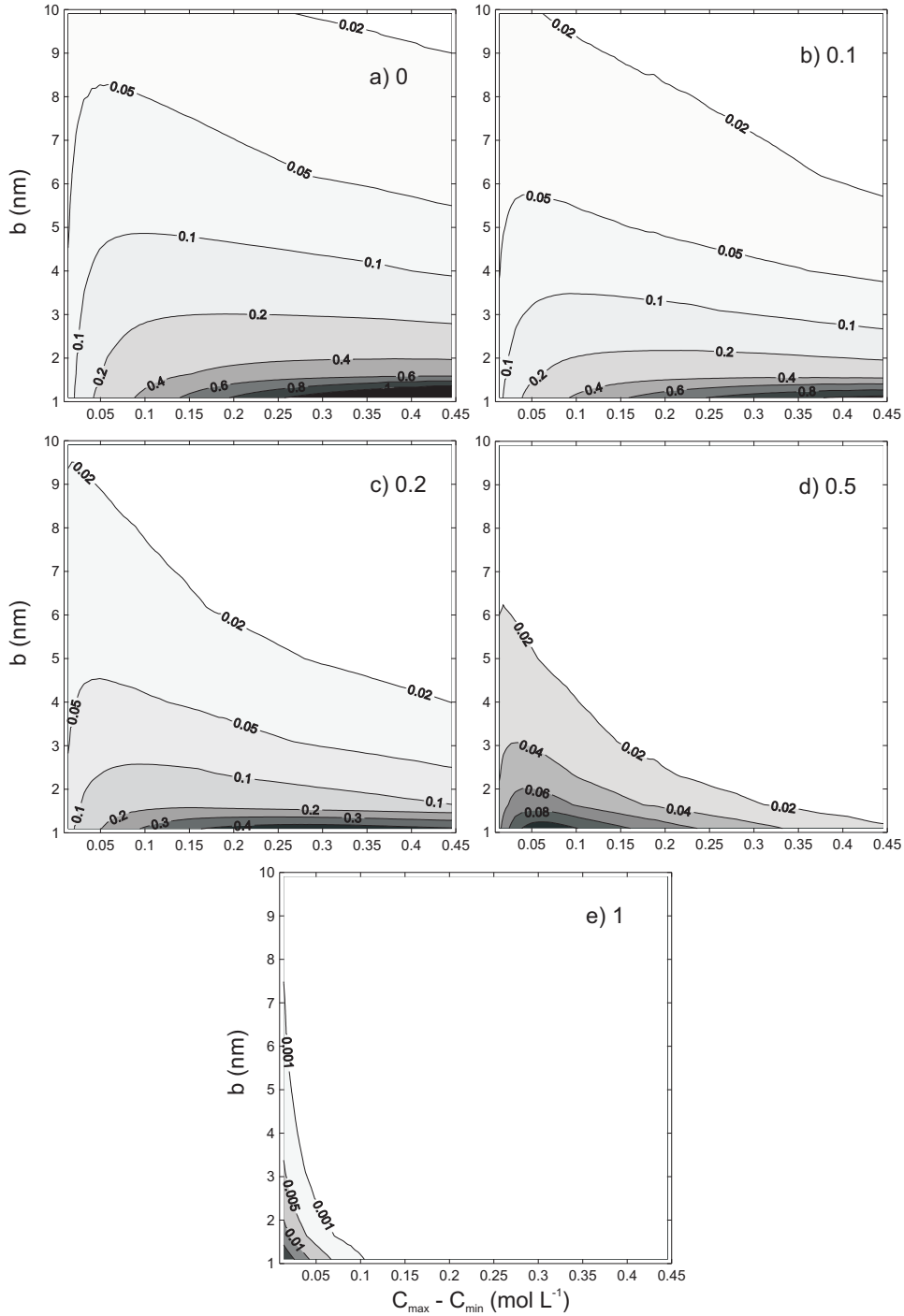

Figure 4. Overpressures (P_0 in MPa) generated by chemical osmosis as a function of the concentration difference, $C_{max} - C_{min}$, with C_{max}/C_{min}=10 and the pore size, b, for different Calcium Index a) 0, b) 0.1, c) 0.2, d) 0.5 and e) 1. Numbers on curves are P_0.

Figure 5

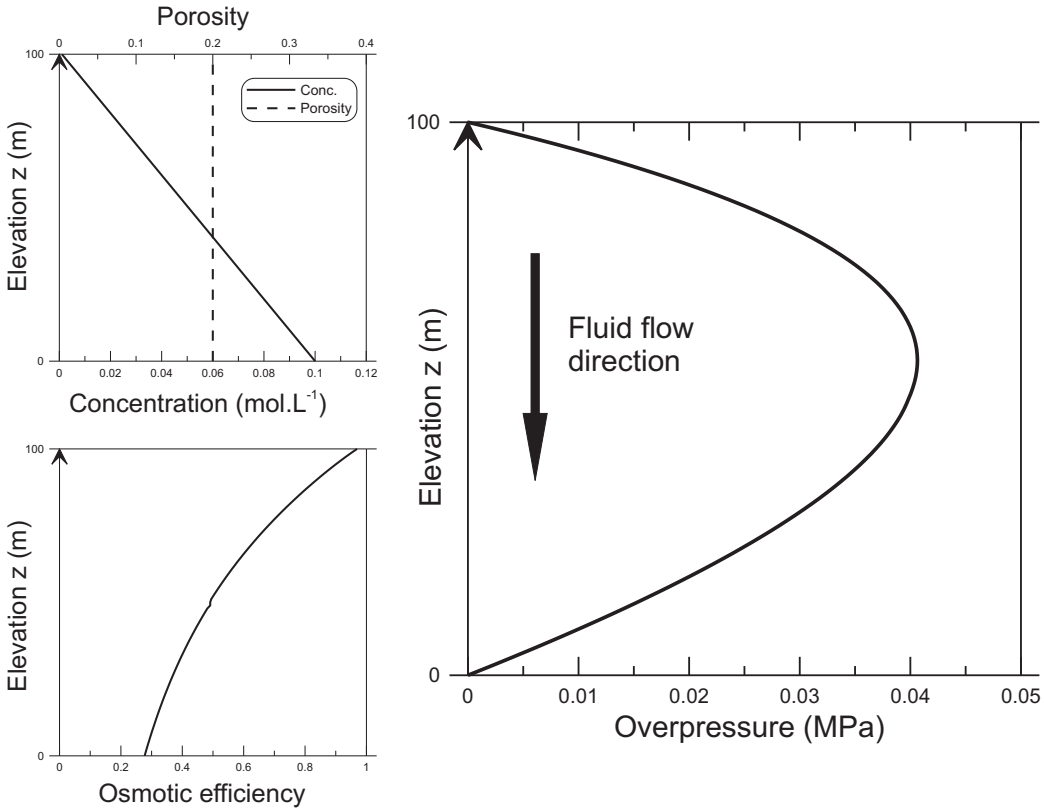

Figure 5. Pressure profile across a 100-m-thick argillaceous formation obtained at steady-state by chemical osmosis caused by variations of the osmotic efficiency with the concentration and for a constant porosity.

Figure 6

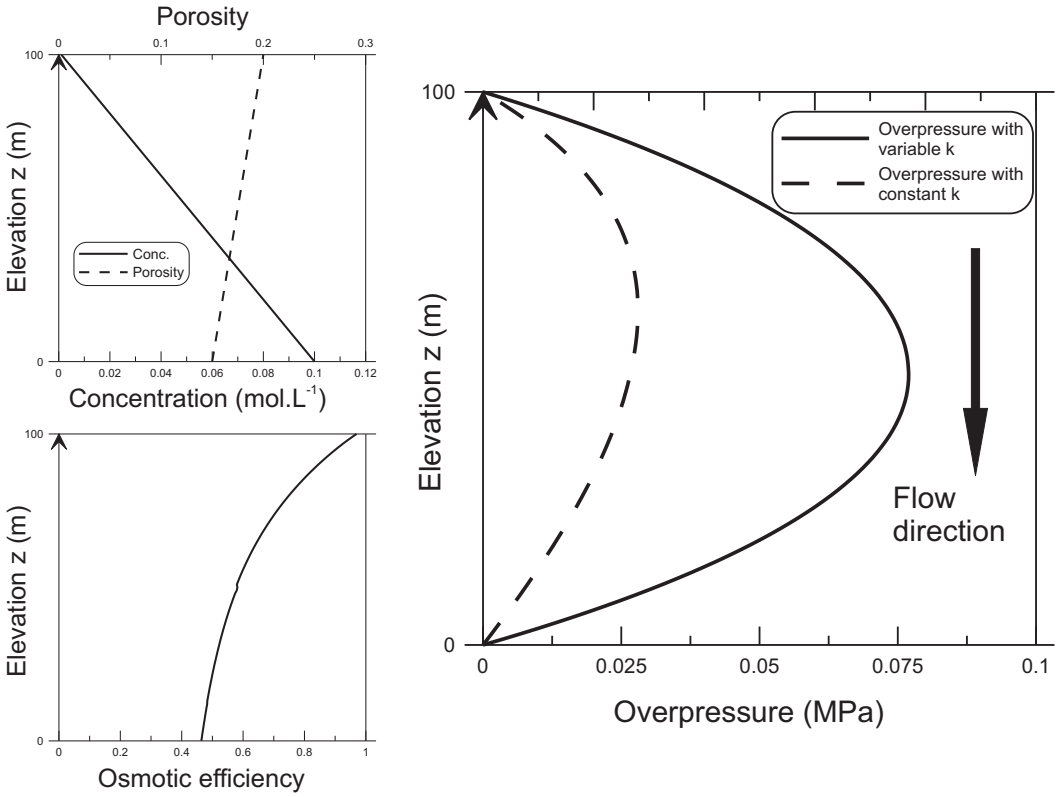

Figure 6. Pressure profile across a 100-m-thick argillaceous formation obtained at steady-state by osmosis caused by variations of the osmotic efficiency variations with the concentration and the porosity.

Figure 7

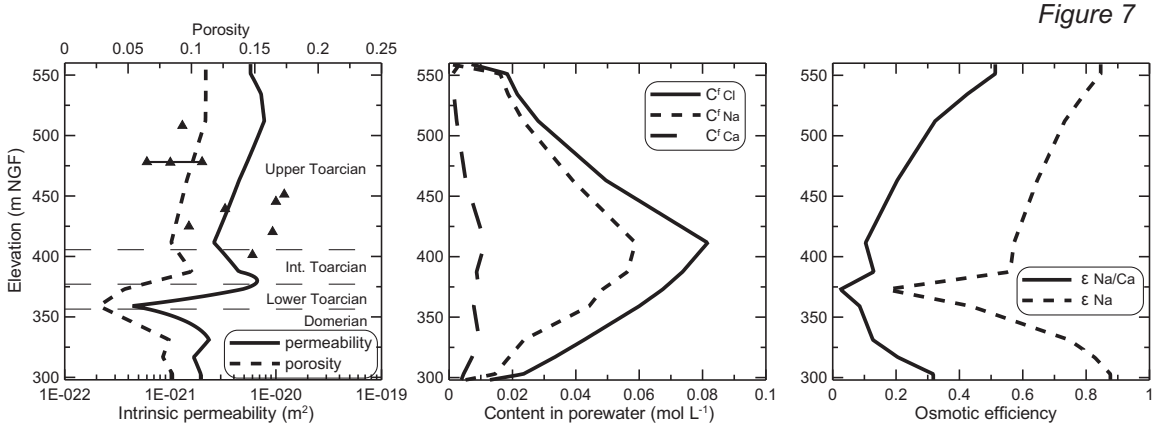

Figure 7. Profiles of intrinsic permeability, porosity, porewater composition and osmotic efficiency in the Toarcian/Domerian argillaceous formation of Tournemire. Triangles are the measured intrinsic permeabilities [*Boisson et al.*, 2001; *Bertrand et al.*, 2002].

Figure 8

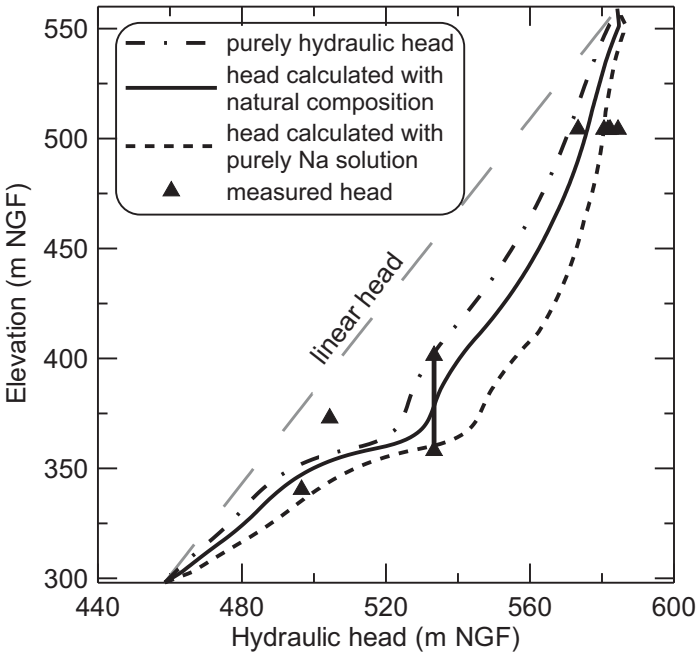

Figure 8. Measured and calculated hydraulic head profiles in the Toarcian/Domerian argillaceous formation of Tournemire.

Figure A1

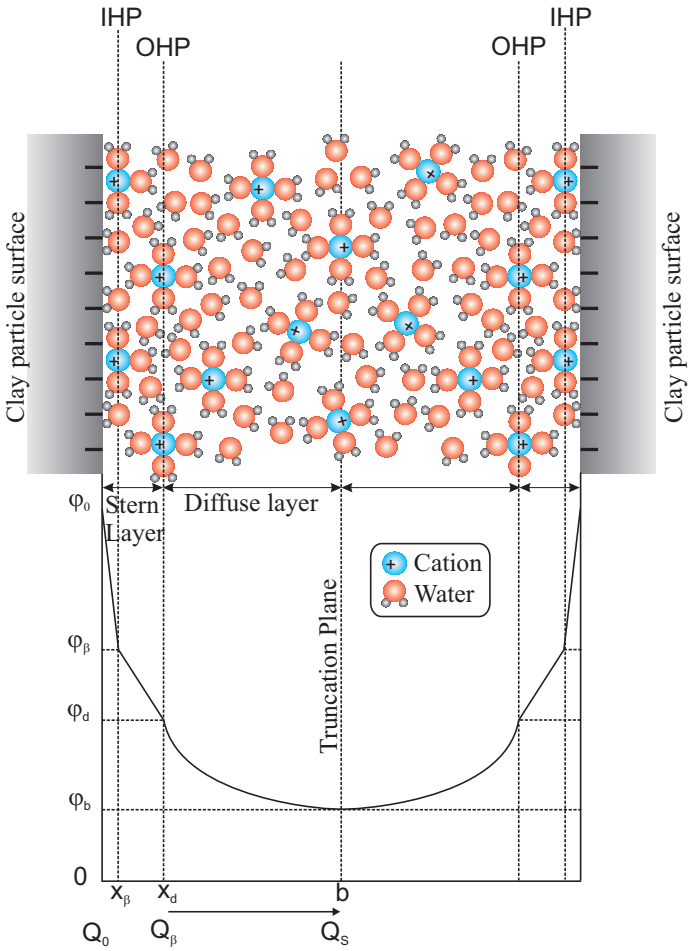

Figure 9. Schematic representation of solution - mineral surface interaction and associated electrochemical variables (electrical potentials φ_i and surface charges Q_i) in the TLM with interacting diffuse layers [*Gonçalvès et al.*, 2010].

Chapter 7

Interpretation of the pressures profile in the Tournemire argillaceous formation

7.1 Introduction

The interpretation of the hydraulic head profile in the Tournemire clay-rock is addressed in this last chapter.
The hydraulic head profile was established in the Chapter 2 by a collection of pressure measurements representative of the formation fluid pressure and a slight excess-head, compared with the hydrostatic head profile, was observed. The aim is now to identify the processes which contribute to the establishment of the actual pressure profile and, thus, to characterize the effective flow processes acting at the formation scale.
The previous chapters mainly dealt with the characterization of the osmotic processes (chemo- and thermo-osmosis) because of their suspected relevance for the fluid flow in the Tournemire clay-rock. Indeed, the occurrence of such processes was identified for this clay-rock by experiments. Osmotic processes were also studied because of their ability in generating abnormal pressures under conditions close to the ones found at Tournemire, i.e. a low permeability clay-rich formation in an old sedimentary basin affected by vertical salinity variations.
A special attention is thus paid to the osmotic processes in the interpretation of the hydraulic head profile. Other causes of abnormal pressures are also examined for the Tournemire argillaceous formation. It mainly includes hydromechanical processes, studying more particularly the visco-plastic behaviour of the clay-rock, and changes in the hydraulic boundary conditions.

7.2 Osmotic processes

7.2.1 Calculations hypothesis

Conceptual model and boundary conditions

The aim of these calculations is to establish the effect of the osmotic flows on the pressure field in the formation. The individual and conjugated effects of chemical osmosis and thermo-osmosis were, in particular, studied.
Calculations are made in 1D, along the z-axis, in the Domerian and Toarcian layers from the Carixian/Domerian to the Toarcian/Aalenian boundaries using the pressure, chemical and temperature conditions of the aquifers as boundary conditions. These calculations enable obtaining a pressure profile across the argillaceous formation and, after transformation as a hydraulic head, comparing it with the hydraulic head monitored in the formation (see section 2.2).
In the present calculations, a pressure build-up is calculated for a given profile of concentration and temperature, considering that at a given time, the modeled system is in pseudo-equilibrium, so that the variations of pressure with time can be assumed null. This simplification can be made because of the very low hydraulic diffusivity and diffusion coefficient of the Tournemire clay-rock. The election of steady-state conditions for the calculations presents the interest to avoid performing a reconstruction of the basin evolution including the flows and transfers in the argillaceous formation, required for transient-state calculations. Then, the pressure field in the formation is calculated by solving the pressure - diffusion equation including osmotic coupled flows at steady-state:

$$\frac{\partial}{\partial z}\left(\rho_f \frac{k}{\eta}(\nabla P + \rho_f g \nabla z) - \rho_f \varepsilon(b, C)\frac{k}{\eta}\nabla\Pi + \frac{k}{\eta}\frac{\Delta H}{T}\nabla T\right) = 0 \qquad (7.1)$$

with, from the left to the right in the right-hand-side term, the contributions of the Darcy's flow with the gravity term, the chemical osmosis flow and the thermo-osmosis flow.
A simple calculation at transient-state, considering diffusion from an initial porewater presenting sea water salinity [15, 123] but without calibrating the transfer time, was also made to assess that the fluid flows calculated at stead-state are realistic.

The Figure 7.1 presents the hydraulic head, concentration and temperature conditions used for the calculations. It corresponds to the hydraulic heads measured in the surrounding aquifers and to the concentration and

temperature profiles obtained across the Tournemire clay-rock (see section 3 and 2.3, respectively).

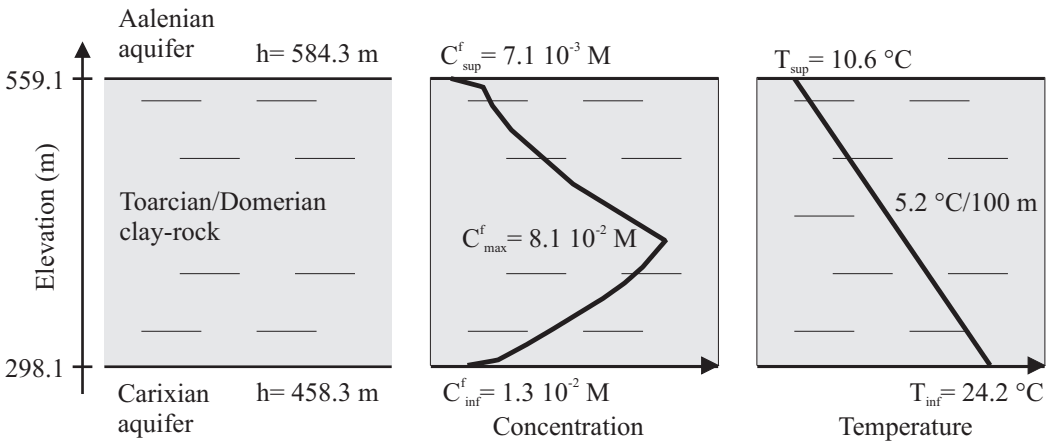

Figure 7.1: Hydraulic boundary conditions and temperature and salinity profiles for abnormal pressures calculations linked to osmotic processes.

It appears in Eq.(7.1) that additional parameters than the gradients are needed in the calculations: the osmotic coupling coefficients (ε and k_T), the intrinsic permeability (k), the dynamic viscosity of water (η) and the fluid density (ρ_f). Their variations across the formation are thus required.

Chemical osmosis efficiency

The chemical osmotic efficiency of the Tournemire clay-rock was determined by two ways: by calculations with a predictive model and by measurements on clay-rock samples. However, the measurements are only available at a single depth in the formation. The modelled osmotic efficiencies were thus used in the following calculations to obtain a complete profile accounting for its spatial variations.
The theoretical chemical osmosis efficiency was determined in section 4.2.5 using Bolt *et al.* [22]'s expression and through the resolution of an electrical model describing the interactions between the charged solid surface of a clay-rock and the porewater. This electrical model takes into account the interactions of adjacent diffuse layers and both monovalent and divalent counter-ions. A profile of chemical osmosis efficiency was then established (see Table 4.3) in agreement with rock properties and solution composition variations across the formation. This is depicted in Fig. 7.2.
The experimental chemical osmosis efficiency was determined on one sample

of the Tournemire clay-rock. It consisted in inducing a fluid flow through the sample upon a salinity gradient (see section 4.3). Efficiency values ranging between 0.014 and 0.31 as a function of the salinity were obtained during these experiments, in the range of the predicted osmotic efficiencies.

Thermo-osmotic coefficient

In a similar way as the chemical osmotic efficiency, the thermo-osmotic permeability of the Tournemire clay-rock was obtained by both predictive calculations and experimental measurements, but only the modelled k_T allows considering its variations across the formation.
The predictions of the thermo-osmotic permeability were obtained (section 5.2.2) by a model calculating the excess specific enthalpy in the pore space responsible of the occurrence of thermo-osmosis by molecular interaction considerations. Model input are a set of petrophysical parameters (porosity, specific surface area and cation exchange capacity) and the salinity of the bulk porewater. Taking into consideration the variations of these parameters across the Toarcian/Domerian argillaceous formation, a profile of k_T/k was monitored (see Table 5.1 and Fig. 7.2).
The thermo-osmotic permeability of the Tournemire clay-rock was also measured during in situ experiments (see section 5.3 and [148]), in equipped boreholes. A temperature gradient was induced between the measurement chamber of the borehole and the clay-rock. The inversion of the pressure evolution in the chamber allowed to identify a range of thermo-osmotic permeabilities. k_T ranges between 6×10^{-12} and 2×10^{-10} m^2 s^{-1} K^{-1} (Fig. 7.2).
Like for chemical osmosis calculations, pressure field calculations with thermo-osmosis were performed using the profile of theoretical coefficients. However, to interpret the effects of thermo-osmosis, it is worth noting that the comparison between the model and the data (see section 5 and Fig. 7.2) indicates that the model tends to underestimate the thermo-osmotic permeability.

Intrinsic permeability

The intrinsic permeability profiles available for the Tournemire formation [20, 21, 123] show k variations on 6 orders of magnitude, between 10^{-22} and 10^{-16} m^2. These variations are for a large extent related to differences in measurement methods and conditions (e.g., duration of the test, transient or equilibrated initial pressures, preservation conditions of the samples, under confinement or not) and in the absence or presence of fractures in the rock.

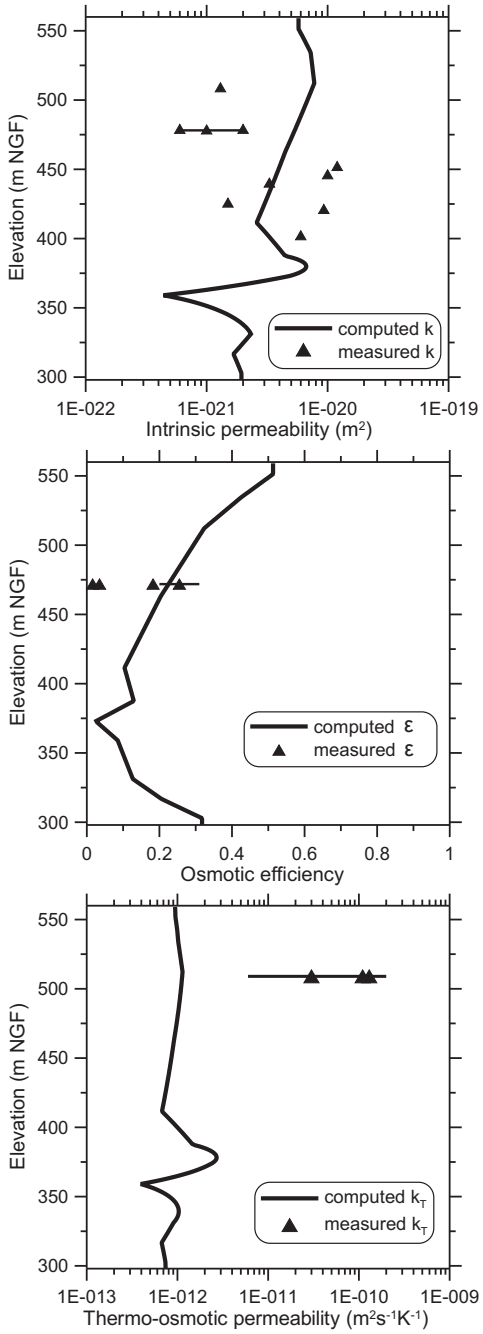

Figure 7.2: Profiles in the Tournemire argillaceous formation of the computed intrinsic permeability (k, in m^2), chemical osmosis efficieny (ε) and thermo-osmotic permeability (k_T, in m^2 s^{-1} K^{-1}). The measured ε, k_T and k are also reported at the elevation where they were determined.

Nevertheless, permeability measurements performed during pulse-tests, an adequate method for hydraulic parameters determination in very low permeability media, on confined samples were collected. These measurements suggest intrinsic permeability values between 10^{-21} and 10^{-20} m^2, though the possible variations of k with depth are overcome by measurements artefact. In situ measurements in unperturbed conditions with a suitable experimental borehole device in PH1 borehole [17] indicates a lower intrinsic permeability, between 6×10^{-22} and 2×10^{-21} m^2.
Because of these uncertainties, the intrinsic permeability is computed across the formation as a function of petrophysical parameters from the Kozeny-Carman equation. Based on plane-parallel geometry hypothesis, it writes:

$$k = \frac{b^2}{3F} \tag{7.2}$$

where, b is the half-pore size (m) and F is the formation factor. The formation factor is determined by the relationship $F = \omega^{-m}$, where ω is the porosity and m the cementation factor. In Chapter 1, m was fitted on natural clay-rocks permeabilities and diffusion coefficients giving a value of 2.3. The application of the Kozeny-Carman relation (7.2) to the argillaceous layers of Tournemire gives an intrinsic permeability ranging between 10^{-21} and 10^{-20} m^2 (see Fig. 7.2), as a function of the petrophysical parameters variations. The higher values (around 8×10^{-21} m^2) are obtained in the upper Toarcian and the lower values (around 2×10^{-21} m^2) in the Domerian. It corresponds to the range of permeabilities determined for this rock.
The following calculations are then made with the permeability determined using the Kozeny-Carman relation.

Fluid viscosity

The dynamic viscosity of water η (in Pa s) is determined using the relation by Mercer *et al.* [102], as a function of temperature:

$$\frac{1}{\eta} = (5.38 + 3.8A - 0.26A^3) \times 10^3 \tag{7.3}$$

where $A = (T - 150)/100$, with T the temperature expressed in ℃. The temperature variations across the formation induce η variations between 8.95 $\times 10^{-4}$ Pa s, for the higher temperature, and 1.27×10^{-3} Pa s.

Fluid density

The fluid density ρ_f (in kg m^{-3}) is determined by the UNESCO equation of state 1980 [150]. This equation of state for water density considers the

influence of salinity, temperature and pressure on the computed fluid density. Its application to the Tournemire formation induces slight variations of fluid density between 998.5 and 1002.3 kg m^{-3}, with the higher values corresponding to the most salted porewater. Owing to this little density variation, the fluid can be estimated as incompressible and the pressures across the formation can be transformed as hydraulic heads.

7.2.2 Influence of the variations of the hydraulic parameters on the hydraulic head profile

Before introducing the osmotic processes in the calculations of the pressure field across the Tournemire clay-rock, this calculation is made considering Darcy's flow alone (Fig. 7.3). The equation to be solved is then:

$$\frac{\partial}{\partial z}\left(\rho_f \frac{k}{\eta}(\nabla P + \rho_f g \nabla z)\right) = 0 \tag{7.4}$$

The aim is to establish the effect of the variations of the intrinsic permeability and the fluid viscosity and density on the calculated pressure profile. Different calculations were performed: with constant hydraulic parameters (k=10^{-21} m^2, η=10^{-3} Pa s and ρ_f=10^3 kg m^{-3}); with variable parameters, in agreement with the expressions previously established; with only fluid viscosity constant; and with only the fluid density constant.

First of all, a linear hydraulic head profile is logically obtained for constant hydraulic parameters (Fig. 7.3). Amongst the calculations performed with spatially varying parameters, the results of the case using variable intrinsic permeability, dynamic viscosity of water and fluid density are reported in Fig. 7.3. The obtained hydraulic head profile is in the range of the measured one and a deviation of 35 % is observed between the modelled excess head profile and the measured head profile, estimated from the head measurements (Fig. 2.5), where the excess-head Δh is defined as $\Delta h = h - h_{hydrostatic}$, with h and $h_{hydrostatic}$ are, respectively, the hydraulic head and the hydrostatic one. This deviation σ is calculated as follows:

$$\sigma = \frac{|\Delta h_{data} - \Delta h_{model}|}{\Delta h_{data}} \times 100 \tag{7.5}$$

where Δh_{data} and Δh_{model} are, respectively, the measured and the calculated excess-heads compared with the hydrostatic head.
The effect of spatial variations of the intrinsic permeability is the more noticeable on the head profile, although the variations of the fluid viscosity are

also non-negligible as the calculation with only the fluid viscosity constant presents a deviation of 24 % compared with the calculated head using all the parameters variable, which corresponds to a deviation of 24 % compared with the measured head (Eq. 7.5). A deviation of only 2 % is observed with only the fluid density as constant parameter, compared with the calculated head using all the parameters variable.
Using a purely hydraulic flow (Eq. 7.4), the water movement is directed downward and a specific discharge of -1.3 $\times$ 10^{-14} m s^{-1} is calculated, the negative specific discharge corresponding to a downward water movement.

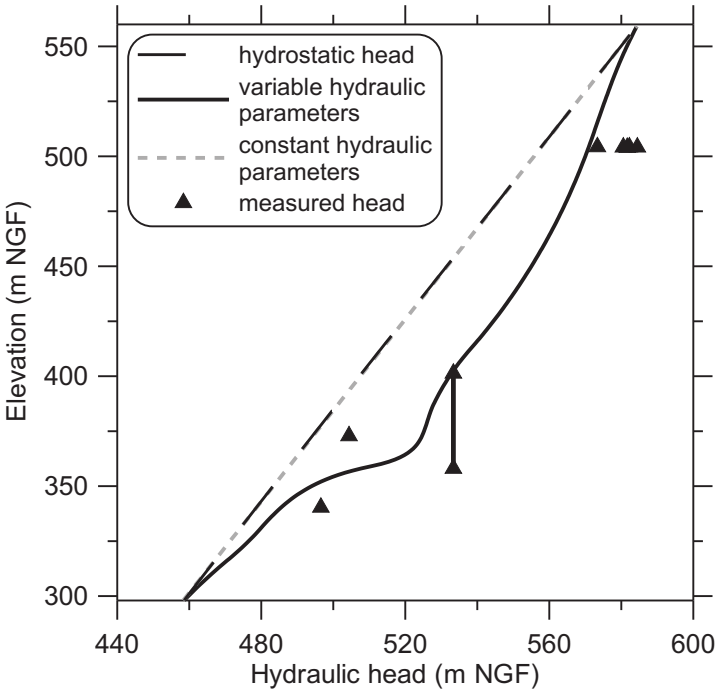

Figure 7.3: Hydraulic head profile calculated with a purely Darcy's flow in the Tournemire clay-rock.

7.2.3 Influence of chemical osmosis on the hydraulic head profile

In this section, the pressures profile across the formation induced by chemical osmosis is calculated. Consequently, Eq.(7.1) is restricted to Darcy's flow and chemical osmosis so that the solved equation becomes:

$$\frac{\partial}{\partial z}\left(\rho_f \frac{k}{\eta}(\nabla P + \rho_f g \nabla z) - \rho_f \varepsilon(b, C)\frac{k}{\eta}\nabla \Pi\right) = 0 \qquad (7.6)$$

The calculation conditions were presented in the previous section and the resulting pressure fields were calculated with the computed osmotic efficiency profile (Fig. 7.4) using space variable intrinsic permeability, water viscosity and fluid density.

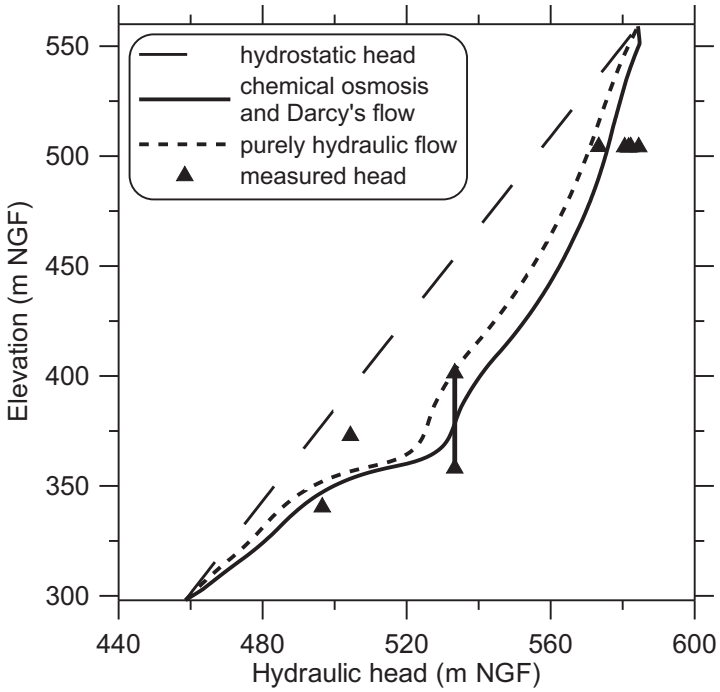

Figure 7.4: Hydraulic head profile induced by chemical osmosis in the Tournemire clay-rock. For comparison, the hydraulic head profile obtained with purely hydraulic flow (section 7.2.2) is also represented.

The addition of chemical osmosis to the Darcy's flow leads to 8 m higher excess-heads (Fig. 7.4) than those obtained only with Darcy's flow, at the formation center. The calculated hydraulic head profile is close to the measured one, so that a deviation of 16 % is found between the model and the data.

Chemical osmosis does not seem to induce consequent modifications on the water movement in the Tournemire clay-rock, which is still directed downward and the specific discharge is of the same order as when only Darcy's flow is considered i.e., -1.4 $\times$ 10^{-14} m s^{-1}.

7.2.4 Influence of thermo-osmosis on the hydraulic head profile

In a similar way than in the previous section, the individual contribution of the thermo-osmotic flow to the fluid pressure is evaluated. Considering only thermo-osmosis and Darcy's flow, Eq.(7.1) becomes:

$$\frac{\partial}{\partial z}\left(\rho_f \frac{k}{\eta}(\nabla P + \rho_f g \nabla z) + \frac{k}{\eta}\frac{\Delta H}{T}\nabla T\right) = 0 \tag{7.7}$$

The pressures profile is calculated using the computed $\Delta H/T$ dependent on the rock properties and the medium conditions (Fig. 7.5) using space variable hydraulic parameters.

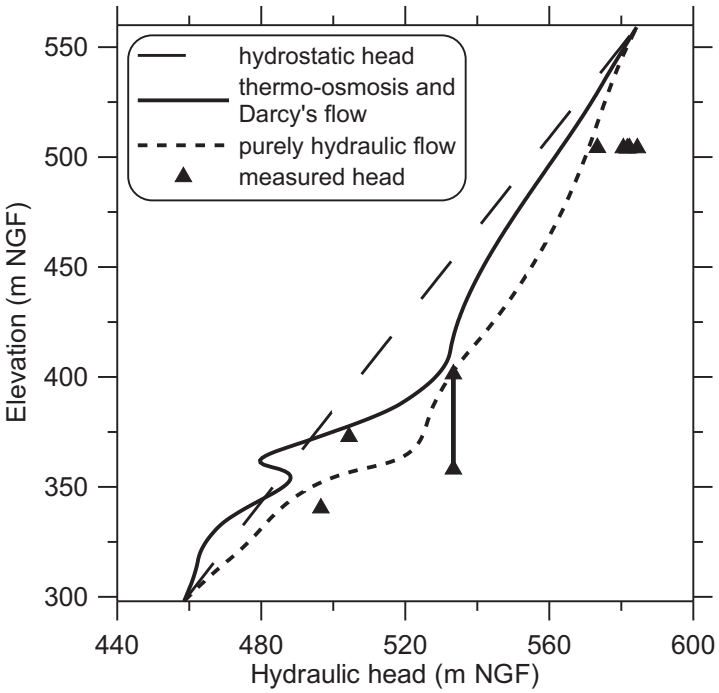

Figure 7.5: Hydraulic head profile induced by thermo-osmosis in the Tournemire clay-rock. For comparison, the hydraulic head profile obtained with purely hydraulic flow (section 7.2.2) is also represented.

The introduction of thermo-osmosis, together with the Darcy's flow, leads to a hydraulic head lower than the one calculated with a purely hydraulic flow (Fig. 7.5). The resulting head profile is between 10 and 15 m lower in the upper Toarcian and up to 35 m lower in the lower Toarcian. In the deeper

part of the formation, the head is even slightly lower than the hydrostatic head. It results in a higher deviation (84 %) of the modelled hydraulic head profile to the measured head than the ones calculated from the profiles obtained with the Darcy's flow alone or including chemical osmosis.
The water movement in the formation is modified by the thermo-osmotic flow and becomes directed upward, presenting a specific discharge of 3.3×10^{-14} m s^{-1}.

7.2.5 Influence of coupled osmotic flows on the hydraulic head profile

The individual contributions of chemical osmosis and thermo-osmosis on fluid pressures in the Tournemire argillaceous formation were evaluated in the sections 7.2.3 and 7.2.4, respectively. Their fully coupled effects are now calculated, using Eq.(7.1).
Calculations are made using the profiles of chemical osmotic efficiency and thermo-osmotic permeability and using the spatially variable hydraulic parameters, as described in section 7.2.1.

Considering in the calculations the combination of Darcy's flow, chemical osmosis and thermo-osmosis an excess-head, compared with the hydrostatic head, is observed (Fig. 7.6) in the upper and in the intermediate Toarcian but the excess-head vanishes in the deeper part of the formation where the calculated hydraulic head profile lies on the hydrostatic one. In the upper part of the argillaceous formation, the calculated excess-head is lower than the measured one, with a maximal excess of 25 m for the intermediate Toarcian. A deviation of 59 % to the measured hydraulic head profile is found. The influence of the thermo-osmosis on the trend of the calculated hydraulic head with coupled flows is particularly obvious.
When both chemo- and thermo-osmosis and Darcy's flow are considered, a specific discharge of 3.2×10^{-14} is computed, close to the one calculated for thermo-osmosis and Darcy's flow, indicating an upward water movement.

7.2.6 Conclusions on osmotic processes

The calculations performed in the previous sections highlight the contribution of osmotic processes on the pressure field and the water movement, though its uncertainties on parameters introduce some complexity in the interpretation.

First of all, it is worth noting that spatially variable parameters have to be used in these calculations. This approach is entirely justified by

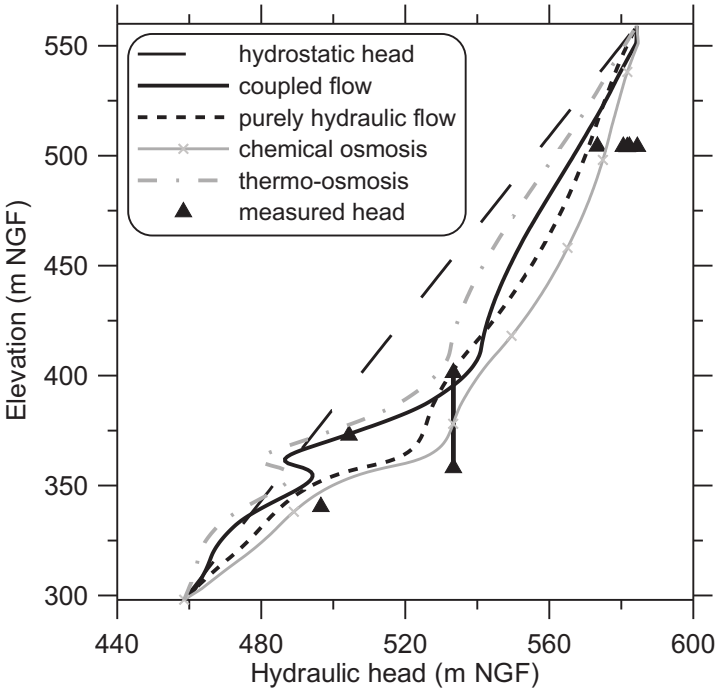

Figure 7.6: Profile of the hydraulic head induced by the coupling of the chemical osmotic, the thermo-osmotic and the Darcy's flows in the Tournemire clay-rock. For comparison, the hydraulic head profiles obtained with purely hydraulic flow (section 7.2.2), with chemical osmosis and the Darcy's flow (section 7.2.3) and with thermo-osmosis and the Darcy's flow (section 7.2.4) are also represented.

the variations across the Tournemire formation of the medium conditions such as salinity, porewater composition, temperature or petrophysical parameters. This holds also for the flow coefficients and the state parameters. Mathematical relations were established to consider this dependence and were calibrated versus experimental data. These relations were thus applied as a function of the medium properties, allowing the flow coefficients and the state parameters of water to account for the observed spatial changes.

Quasi-steady-state calculations conditions were postulated because of uncertainties on the conditions that constrain the calculations of evolution of the flows and transfers at geological time-scales. Nevertheless, because of the transient conditions of the concentration profile, two simple calculations at transient-state were performed. One of these calculations considers chemical osmosis and Darcy's flow and the second one gathers chemical osmosis, thermo-osmosis and Darcy's flow. The diffusion scenario for the Tournemire argillaceous formation [15, 123, 138] was reproduced in these calculations and a Fick's diffusion was involved from a sea water salinity to a salinity profile close of the actual profile using a diffusion coefficient in the range of those measured at Tournemire. At final transient-state, the obtained hydraulic head profiles and specific discharges were very close to the ones calculated assuming a quasi-steady-state. This observation allows asserting that the hypothesis of a pseudo-equilibrium of fluid flow for a given concentration profile is valid. The steady-state conditions can then be assumed with confidence and the calculations results are most likely realistic.

In the previous sections, the modification of the fluid movement caused by osmotic processes were shown. In particular, when thermo-osmosis is introduced in the calculations, the flow regime is modified and the flow direction, while it is downwards for Darcy's flow and chemo-osmosis alone, turns upward. However, the real interest of the fluid flow direction lies in its potential impact on advection mass transport. For this purpose, the Peclet number is calculated for estimating the convective contribution to the mass transport in comparison to the diffusion contribution. The Peclet number can be established as the ratio of the characteristic time for diffusion $\tau = L^2/D_p$ to the characteristics time for convection $\tau = L/u$, where L is the thickness (m) of the porous medium crossed by the solute, $D_p = D_e/\omega_{anions}$ with D_p and D_e the pore diffusion coefficient and the effective diffusion coefficient, respectively ($m^2\ s^{-1}$) and ω_{anions} is the anions accessible porosity. u is the pore fluid velocity ($m\ s^{-1}$) related to the specific discharge q by the relation

$u = q/\omega_c$, where ω_c is the cinematic porosity. The Peclet number thus writes:

$$P_e = \frac{\frac{L^2}{D_p}}{\frac{L}{u}} = \frac{L\,u}{D_p} = \frac{L\,q}{D_p\,\omega_c} \tag{7.8}$$

The Peclet numbers for the Tournemire argillaceous formation are determined for a Br^- or Cl^- ion located at the center of the 250 m thick formation (L = 125 m), using an effective diffusion coefficient for Br^- and Cl^- of 4 $\times$ 10^{-12} m^2 s^{-1} [15] and the specific discharges reported in the previous sections. The kinematic porosity value is between the total porosity and the accessible porosity, which present average porosities of 8.8 % for the total porosity and 6.6 % for the Cl^- and Br^- accessible porosity [15]. Calculation is here made using the total porosity. The resulting Peclet number is 0.28 for the purely hydraulic flow, 0.30 for chemical osmotic and Darcy's flows, 0.71 for the thermo-osmotic and Darcy's flows and 0.69 for the case where chemo- and thermo-osmosis and Darcy's flows are at work. These calculated Peclet numbers slightly lower than 1 suggests that diffusion is dominant but the convective flow is not negligible for mass transport at the formation scale. Convection also has to be taken into consideration for mass transport especially if thermo-osmosis is considered, because of the underestimation of the modelled thermo-osmotic permeability compared to the measured values. This is in contradiction with the assumption of a mass transport mainly controlled by diffusion, as proposed in the scenario describing the transport at the formation scale and in the interpretation of the natural tracers profile, where convection is neglected.

With regard to the excess hydraulic head, compared with the hydrostatic head, measured across the argillaceous formation of Tournemire, the calculations show that the pressure profile is largely explained by a purely hydraulic flow. Indeed, the intrinsic permeability variations with depth, and also the fluid viscosity changes with the temperature, are able to explain up to two-thirds of the measured excess-head.
However, the best representation of the measured hydraulic head profile is achieved by considering the chemical osmosis and the Darcy's flow. The pressure field resulting from the chemical osmotic process is related to the non-equilibrated salinity profile in the formation and the dependency of osmotic coefficient on the porewater composition and the pore size. In this case, around 85 % of the measured excess-head is reproduced and a maximum excess-head of 35 m compared with the hydrostatic head is obtained at the center of the formation. Thermo-osmosis tends to lower the calculated hydraulic head decreasing the quality of the model.

Indeed, only half of the observed excess-head is predicted when chemo- and thermo-osmosis and Darcy's flow are considered. It is worth noting that, though calculated excess-head profile represents half of the measured one, the difference is weak ($\sim$ 10 m). This is also associated with moderate measured excess-head compared with the hydrostatic head. However, both chemo- and thermo-osmosis processes were identified in the Tournemire clay-rock. The hydraulic head profile calculated with both osmotic processes and Darcy's flows gives a plausible view of the contribution of hydraulic and osmotic processes to the abnormal fluid pressures.

This profile depends on the accuracy of the predictions of the flow coefficients and variable profiles. Some uncertainties and misestimates of these parameters and variable could explain part of the discrepancy between calculated and measured excess-heads. The prediction of the flow coefficients was made with models, using petrophysical parameters and medium conditions as input parameters and both can present uncertainties. In particular, the effect of thermo-osmosis on the hydraulic head are only linked to the variations of the thermo-osmotic permeability across the formation, because of the linear temperature profile. Consequently, the prediction of the thermo-osmotic permeability and its variations with depth have an important influence on the calculated pressure field. As an example of the pressure calculations sensitivity to the predicted thermo-osmotic permeability, when the predicted k_T is divided by 2 (according to the model agreement versus experimental data, which states that data are reproduced within a factor 2; see section 5.2.1), the deviation between the measured head and the calculated one using both identified flows becomes 35 %, to compare with the deviation of 59 % obtained with the original calculated k_T. Furthermore, the main variation of k_T along the vertical profile occurs in the lower Toarcian horizon. This level is characterized by a high solid surface charge density, most likely because of the high content in organic matter, and by a small porosity, because of the high carbonates content. Such a high surface charge density and low porosity lead to a high k_T.
Other sources of uncertainty on the resulting hydraulic head profile can also be pointed out. Based on the fact that the permeability is scale independent in most of the argillaceous formation [114], an extrapolation at the formation scale of the flow coefficients determined at the local scale was performed in the pressures field calculations. This approach remains probably to validate as it only stands if there are no connected fractures in the formation. For the intrinsic permeability, this approach de facto excludes a possible contribution of the flow and transport by fractures. Indeed, its influence is still discussed at Tournemire and its constrain could undoubtedly improve

the understanding of the transport issue in the formation.
The last uncertainty to point out concerns the hydraulic head profile estimated from the different head measurements across the formation. Indeed, measured head can present a deviation of ± 10 m compared with the average excess-head profile (see Chapter 2).

To summarize the contribution of the osmotic processes on the hydraulic head profile, the combination of chemo- and thermo-osmosis and Darcy's flow explains about half of the excess hydraulic head measured across the formation, using computed flow coefficients. It was also noted that in fact, a large part of the calculated hydraulic head is explained by a purely hydraulic flow. Despite apparently explaining only a part of the measured excess-head in the Tournemire argillaceous formation, the combination of the uncertainties linked to the model and the data allows to conclude that a large part of the measured excess-head is likely caused by osmotic and Darcy's flows. Furthermore, the difference, expressed as meters of hydraulic head and not as a deviation (Eq. 7.5), is moderate and clearly indicates that the osmotic and hydraulic processes control a large part of the fluid pressures field in the formation.

7.3 Hydromechanical processes

7.3.1 Effect of the variation of total stress

Until now, the used pressure-diffusion equation implicitly assumed that the total stress σ (in Pa) is constant, so that $d\sigma = 0$.
If the total stress varies with time, the continuity equation writes [69, 139, 60]:

$$\frac{\partial}{\partial z}\left(\rho_f \frac{k}{\eta}(\nabla P + \rho_f g \nabla z)\right) = \frac{S_s}{g}\frac{\partial P}{\partial t} - \rho_f \alpha \frac{\partial \sigma}{\partial t}, \tag{7.9}$$

where, α is the compressibility coefficient of the porous medium (kg^{-1} s^2). Changes in the total stress is a source term of pressure through the hydromechanical coupling [24, 115]. Deformation or fracturing of the geological medium, like sediment compaction, erosional decompaction or tectonic deformation, can give rise to variations of the total stress and thus pore pressure [60, 72, 109, 115].

Among the causes of overpressures generation by variations of the total stress, the most frequently invoked process is linked to a compaction disequilibrium [69, 72]. Sediments compaction, by deposition of the upper

sediments, induces an increase of the vertical effective stress. When the pore fluid can not be expelled, the pore pressure increases and can lead to elevated overpressures, mainly controlled by the sedimentation rate. However, at the end of the geological forcings, when sedimentation ceases, such overpressures tend to dissipate rapidly according to the hydraulic diffusivity [60]. As an example, an excess pressure of 10 MPa relatively to the hydrostatic pressure in the Tournemire clay-rock is calculated to dissipate in 100 ka, using values of 10^{-21} m^2 and 10^{-6} m^{-1} for k and S_s, respectively. Since the sedimentation in the Grands Causses basin stopped at the early Cretaceous [127], the effect of disequilibrium compaction is not relevant for the actual pressure profile interpretation.

Opposite to disequilibrium compaction, erosional unloading can generate abnormally low pressures linked to a decompaction of the porous solid [72]. This phenomena is observed when the fluid flowing towards the rock porosity does not compensate the porosity increase. However, this process mainly affects soft-clays and is only able to generate moderate subpressures. Consequently, since the Tournemire detrital clay-rock is well compacted with a cemented matrix and that about 1300 m of sediments were eroded before the Pyrenean tectonic event [127], massif exhumation occurred at the Eocene and valley incision at the Miocene, this process can be discarded as a potential cause for the resulting pressure profile.

Lateral tectonic compression [16, 72, 100] can strongly increase the difference between the largest and lowest principal stresses. It results in a change in total stress and a compaction of the porous medium, leading to an increase of the fluid pressure. The last tectonic activity evidenced by faulting and by calcite twinning at Tournemire is the Eocene compression during the pyrenean orogeny [30, 35]. Since this event, a regional extension occured during the Oligo-Miocene but without evidences in the Grands Causses basin [30]. The recent paleo-seismicity is poorly constrained, although some evidences of local deformations were found in karstic fillings [30]. An evolution with time, including recent tectonic activity, of the total stress is not available and then, the effect of tectonic compression on the present pressure profile can not be evaluated. However, it is worth noting that such an effect is possible because of the geodynamic context of the Grand Causses basin, located between the two tectonically active zones of the Pyrénées and the Cévennes. Nevertheless, the relevance of this hypothesis is probably limited because of the Tournemire massif geomorphology, which is not favorable to a tectonic compression propagation. Indeed, massif exhumation and valley incision tend to individualize the massif which most likely partially impede

the compression propagation.
Further studies on the total stress evolution with time are needed to conclude on the relevance of tectonic compression as a cause of the present-day pressure profile in the Tournemire argillaceous formation.

7.3.2 Effect of the visco-plastic behaviour of clays

The visco-plastic behaviour of argillaceous rocks consists in a delayed deformation. Here, our interest to the visco-plastic behaviour of clays is limited to the time dependent volumetric deformation which prolongs the rock compaction and can lead to a persistence of overpressures during large geological time scales. The macroscopic volumetric creep of the rock, or compaction creep, can result from granular mechanisms like pressure dissolution, in carbonates and sandstones, or sliding and rotation of grains and platelets leading to an aggregate deformation, in clays [45].
The deformation rate $\dot{\varepsilon}$ for the viscous deformation writes [139]:

$$\dot{\varepsilon_{vol}} = \frac{1}{V}\frac{dV}{dt} = -\frac{\sigma}{\eta_s} \tag{7.10}$$

where $\dot{\varepsilon_{vol}}$ is the volumetric deformation rate (s^{-1}), V the porous medium volume, dV the variation of porous medium volume, σ the total stress (Pa) and η_s is a volumetric viscosity coefficient of the porous medium (Pa s). Accounting for the viscous effect in a simple hydromechanical coupling (e.g., [38]), the expression of the porosity variations with time writes:

$$\frac{d\omega}{dt} = (1-\omega)(\alpha-\alpha_s)\frac{\partial P}{\partial t} - (1-\omega)\frac{\sigma}{\eta_s} \tag{7.11}$$

where α and α_s are the compressibility coefficients (kg^{-1} s^2) of the porous medium and the solids, respectively.
The introduction of the viscous behaviour yields a pressure source term in the pressure-diffusion equation:

$$\frac{\partial}{\partial z}\left(\rho_f \frac{k}{\eta}(\nabla P + \rho_f g \nabla z)\right) = \frac{S_s}{g}\frac{\partial P}{\partial t} - \rho_f \alpha \frac{\partial \sigma}{\partial t} - \rho_f \frac{\sigma}{\eta_s} \tag{7.12}$$

Consequently, if the creep source term is characterized, one can calculate its effect on the fluid pressure and flow. The main difficulty in this characterization lies in estimating the viscosity coefficient η_s. Indeed, this coefficient depends on the temporal and spatial scale at which the process is considered [62]. As an example, for the Callovo-Oxfordian formation of the Paris basin η_s values between 10^{16} and 10^{17} Pa s are obtained during

laboratory creep tests on samples lasting from some hours to some weeks. At the basin scale in the Bure URL area, the deformation measured by GPS suggests a η_s value around 10^{22} Pa s [62]. Similarly, the viscosity coefficients used in models of compaction in sedimentary basin taking volumetric creep into consideration at the geological scale are higher than the measured at sample scale viscosity coefficients and range between 10^{19} and 10^{22} Pa s [104, 139].
These results show an increase of η_s when larger duration time or larger area are considered. Added to the fact that the granular mechanisms responsible of the visco-plastic behaviour of the rock lose their efficiency with time, these observations suggest that the viscosity coefficient η_s is most likely time dependent.

The rock viscosity of the Tournemire clay-rock can be estimated from a creep experiment performed on a sample submitted to an uniaxial compression [45]. The volumetric deformation and the mean stress evolution during the creep experiment are reported in Fig. 7.7, considering that $\sigma = \frac{\sigma_1+\sigma_2+\sigma_3}{3}$ with σ_2 and σ_3 equals to zero because of the uniaxial stress. Note that the convention used in this study [45] considers that, in compression conditions the volumetric deformation ε_{vol} is positive but dV is negative, so that:

$$\varepsilon_{vol} = -\frac{dV}{V}, \tag{7.13}$$

and

$$\dot{\varepsilon_{vol}} = \frac{1}{V}\frac{dV}{dt} = \frac{\sigma}{\eta_s}, \tag{7.14}$$

at the contrary to Eq.(7.10), used in the continuity equation (Eq. 7.12).
Assuming that the viscosity coefficient η_s is time dependent, the general trend of the ε_{vol} evolution curve as a function of time Fig. 7.7 and the ε_{vol} evolution during the first step of constant stress suggest that the function describing η_s is of the form $\eta_s(t) = at^b$, where a and b are constants. Thus, the integration of Eq.(7.14) gives:

$$\varepsilon_{vol}(t) = \int_0^t \frac{\sigma}{\eta_s(t)} dt, \tag{7.15}$$

and noting that:

$$\int \frac{1}{\eta_s} dt = \int \frac{dt}{at^b} = \frac{1}{a(1-b)} t^{1-b}, \tag{7.16}$$

for $t \in [t_i, t_{i+1}]$, where i corresponds to a step of constant stress applied during the creep experiment and $i+1$ to the following step of constant stress, we

have:

$$\varepsilon_{vol}^{i+1}(t) = \varepsilon_{vol}^{i+1}(t_i) + \int_{t_i}^{t} (\sigma_{i+1} - \sigma_i) \frac{1}{\eta_s(t - t_i)} dt, \tag{7.17}$$

where $\sigma_{i+1} - \sigma_i$ is constant. For the first step of stress applied to the sample, $i = 0$ and for $t \in [0, t_1]$ the volumetric deformation writes:

$$\varepsilon_{vol}^{1}(t) = \varepsilon_{vol}^{0}(0) + \int_{0}^{t} \frac{\sigma_1}{\eta_s(t)} dt. \tag{7.18}$$

Eq.(7.17) and Eq.(7.18) indicate that viscous deformation starts when the stress state is changed. Consequently, the beginning of creep at the formation scale corresponds to the last geological event leading to the actual stress conditions.
An inversion of the volumetric deformation measured by Fabre and Pellet [45] is performed (Fig. 7.7) and allows to identify the a and b constants (Eq. 7.16). A relation describing the viscosity coefficient evolution with time is thus obtained and writes:

$$\eta_s(t) = 3.510^{11} t^{0.9}. \tag{7.19}$$

This time dependent relationship gives a η_s value of 10^{16} Pa s for $t = 1$ day and a value of 6×10^{23} Pa s after 1 My of creep.

A calculation of the excess pressure caused by the visco-plastic behaviour of the Tournemire clay-rock can be made to evaluate the possible contribution of creep to the present measured pressure profile. This calculation is made for a 1D geometry, along the z axis, on the basis of Eq.(7.12) since the actual stress conditions is reached. The total stress is assumed constant since this last event, so that $\partial\sigma/\partial t = 0$. Including this simplification, the solved equation is:

$$K \frac{\partial P}{\partial z} = S_s \frac{\partial P}{\partial t} - \rho_f \frac{\sigma}{\eta_s(t)} \tag{7.20}$$

where K is the hydraulic conductivity (m s^{-1}).
The main uncertainty in the calculation input lies in fixing when the present total stress conditions are established. On the basis of the geological evidences [30] the calculation is made considering different starting times. The last noticeable tectonic activity dated from the end of the Eocene during which the basin was affected by the pyrenean orogenesis and a calculation is made with a constant total stress since 34 Ma. Major erosion and valley incision of the Grands Causses basin occurred during the Neogene and two starting times for creep are tested: 5 Ma ago, at the end of the Miocene and

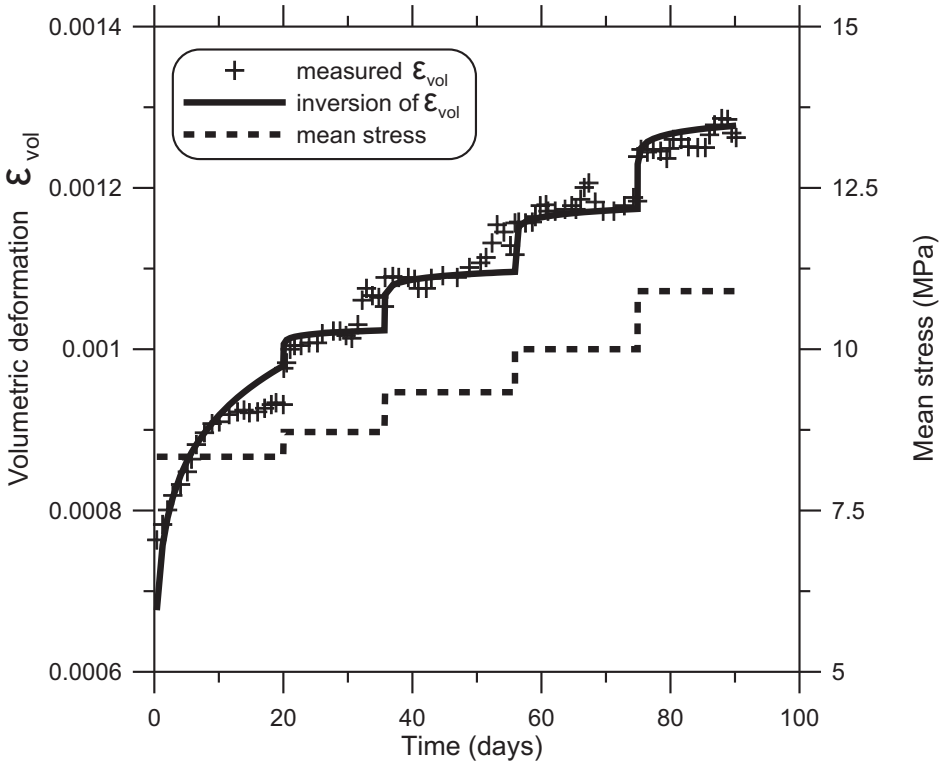

Figure 7.7: Creep experiment on a sample of Tournemire clay-rock [45]. The successive applied mean stress and the resulting volumetric deformation ε_{vol} are represented, as well as an inversion of the measured ε_{vol} suggesting that $\eta_s(t) = 3.5\,10^{11} t^{0.9}$.

the Messinian, and 2 Ma ago, corresponding to the end of the Pliocene and the Neogene.
The effect of creep is represented as hydraulic head together with the hydrostatic head and the heads measured across the Tournemire argillaceous formation (Fig. 7.8). These results show a very limited influence of this phenomena on the pressure profile. The excess head, related to the hydrostatic head, is of few meters and tends to decrease with time without completely vanishing. Indeed, after 2 Ma of viscous behaviour an excess head around 3.7 m is calculated while after 5 Ma the excess head is around 1.6 m and around 1.3 m after 34 Ma.

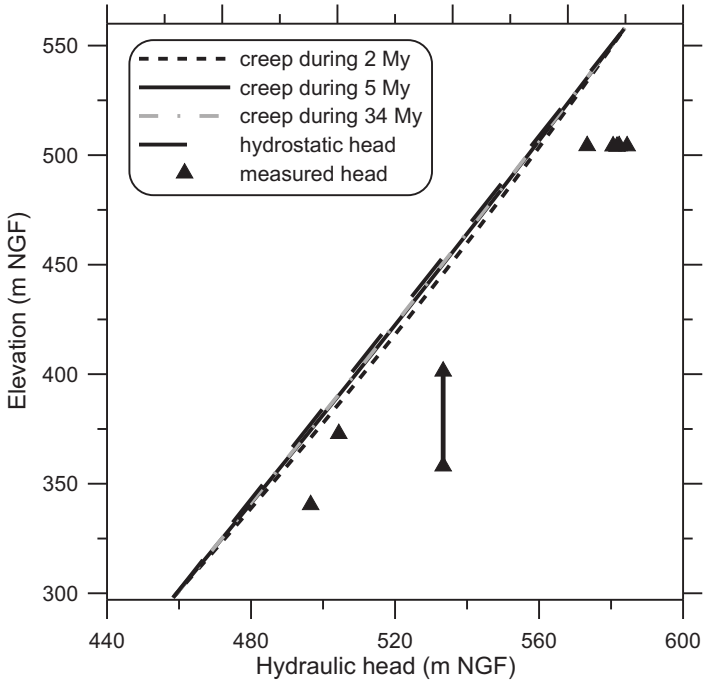

Figure 7.8: Calculated contribution of creep on the hydraulic head profile in the Tournemire clay-rock. Calculations made with $K = 10^{-14}$ m s^{-1}, $S_s = 10^{-6}$, $\sigma = 4$ MPa [30] and $\eta_s(t) = 3.5\,10^{11} t^{0.9}$.

As a conclusion on the visco-plastic behaviour of the Tournemire clay-rock, we conclude that this hydromechanical process presents a very small influence on the fluid pressures in the formation. The main difficulty in this evaluation was the determination of the viscosity coefficient η_s, dependent on the considered temporal and spatial scales. However, an attempt to constrain the behaviour of η_s on geological time scales was made from laboratory creep experiments [45]. The excess pressures calculated with this η_s seems

very limited and creep can be reasonably discarded as a relevant process for explaining the excess head profile at Tournemire. This conclusion is similar than that of Kazmierczak et al. [77] about the influence of clay viscoplasticity on the excess-head measured in the Paris basin Callovo-Oxfordian formation, which state that the measured overpressures in the formation can not been explained by such a process.

7.4 Overview of alternative processes

Two alternative processes can be added to the review of the processes potentially able to cause overpressures and explain the weak excess-head measured in the Tournemire formation, namely the diagenetic effects and the effects of changes in the hydraulic boundary conditions.

Some reactions occurring during the clay-rock late diagenesis, i.e. illitization and organic matter maturation, expel water molecules as a consequence of the mineral or organic matter molecules reorganization. It leads to a fluid pressure increase in the pore space and can result to formation overpressures. However, such effects on the actual pressure profile at Tournemire can be discarded as the exhumation of the massif occurred at the latest during the pyrenean orogenesis at the Eocene [30], stopping diagenesis because temperature is needed for these reactions [33] and dissipating the potential excess-head linked to diagenesis processes.

Changes in the hydraulic boundary conditions can generate apparent overpressures in a low permeability formation because of the delay in the recovering of the pore pressure equilibrium. Valley incision can lead to this situation in which a fluid excess pressure is found in an argillaceous formation during the transient-state until pressures recover the regional hydraulic equilibrium.
Gonçalvès *et al.* [60] show that this process could be relevant if the hydraulic boundary conditions would have recently changed since the pressures equilibrate in the low permeability formation (the Callovo-Oxfordian clay-rock of the Paris basin, in their study) in some tens of thousand years. In the Tournemire geological history, the main hydraulic boundary changes are the karstification and the valley incision. The present-day karstification started at the Eocene and its major episode occurred during the Neogene [2, 15, 30], whereas the valley incision likely occurred during the early or middle Miocene. Both events are too old for still being recorded in the present pressure profile in the Tournemire clay-rock.

A recent origin of changes in the hydraulic boundary conditions could come from the establishment of a permafrost during the last glaciation event, for a sufficient duration time so that pressures in the clay-rock equilibrated with this regional hydrodynamic modification, and its melting in the following greenhouse period [74]. However, such a paleo-permafrost was not observed in the Tournemire area.

7.5 Conclusion

An attempt to explain the hydraulic head profile measured in the Tournemire clay-rock was addressed in this chapter by a review of the processes able to cause abnormal fluid pressures in an argillaceous formation and by a calculation of the resulting hydraulic head profile for the relevant processes.

Based on the description of the occurrence of phenomena prone to cause abnormal pressures and on geological evidences at Tournemire and in the Grands Causses basin, some phenomena were discarded as potential causes of the present hydraulic head. It concerns compaction disequilibrium, erosional unloading, tectonic compression, diagenetic processes and changes in the hydraulic boundary conditions. Note that the effect of a variation of the tectonic compression was not addressed since the evolution of the total stress during the last million years is unknown. A definitive statement on this process remains for future work.

The visco-plastic behaviour of the Tournemire clay-rock was estimated to be a possible cause of abnormal pressures in the formation and its effect was studied. Its study required an estimate of the time-dependent viscosity coefficient at the geological scale. It was established from laboratory creep experiments [45]. This evaluation showed that the visco-plastic behaviour of clay could only generate very weak excess-head and has a negligible influence on the hydraulic head profile.

The only processes able to explain the measured hydraulic head profile is a combination of “normal” hydrodynamics and osmotic processes. Considering together chemical osmosis, thermo-osmosis and Darcy’s flow allows to reproduce about half of the measured excess-head in the Tournemire formation, using a-priori parameters.
The study on the influence of the osmotic effects also pointed out that variations in the intrinsic permeability are responsible for a large part of the calculated excess-head. It was also observed that some discrepancy could

be attributed to an insufficient accuracy of the theoretical expression of the thermo-osmotic permeability.
However, both hydraulic and osmotic permeability coefficients determination and measured hydraulic head profile are subjected to uncertainties. Furthermore, the difference between model and data is limited, when expressed as meters of hydraulic head.
It leads to the conclusion that, despite an unperfect agreement between measured and calculated hydraulic heads, the combination of both osmotic and hydraulic processes is a plausible explanation of the the observed excess-head. According to our evaluation of the alternative causes of overpressures, the osmotic and hydraulic processes are most likely the only reasonable causes of excess-head in the Tournemire argillaceous formation.

Part VI

Conclusions and perspectives

The aim of this thesis was the interpretation of the excess of hydraulic head measured in the Toarcian/Domerian argillaceous formation of Tournemire, with a particular focus on the osmotic processes. Understanding the origin of the excess-head raises the question of the relevant characterization of the flow processes and hydrodynamic phenomena in the formation, which can contribute to the mass transport, together with the Fick's diffusion.

A part of this work dealt with the improvement of the hydraulic head profile, by collecting the non perturbed pressure measurements across the formation. Indeed, in a low permeability and low water content rock such as the Tournemire argillaceous formation, the obtention in an equipped borehole of a pressure measurement equilibrated with the formation pressure can last from months to years. Moreover a depression is observed around the excavated tunnel and galleries and the required pressure profile aimed at representing the natural formation conditions and not the perturbed one. A hydraulic head profile was then established and a moderate excess-head of 30 ± 10 m compared with the relative hydrostatic head given by the heads in the surrounding aquifers is observed. Even moderate, a hydraulic head slightly different from the hydrostatic head can provide informations on the flow processes in the Toarcian and Domerian layers at Tournemire.

Another contribution of this thesis to the characterization of hydrogeochemical system of Tournemire was the establishment of the porewater composition profile. Owing to the very low permeability and water content in the rock, a direct sampling of porewater is impeded and an indirect method is required. This method is the geochemical modelling which, by considering the reactions occurring between the rock and the solution and a selection of rock and solution parameters characterizing the geochemical system, allows calculating the porewater composition. A model including various sites of cation exchange related to the mineral phases content was developed and, considered together with another model [53], an acceptable estimation of the porewater composition was achieved. Once validated corrected fracture waters assumed in equilibrium with the formation porewater, the developed model was then applied across the formation to obtain a profile of the porewater composition in the argillaceous layers at Tournemire.

The temperature profile was also established and leads to a linear profile presenting a relatively high geothermal gradient of 5.2 ℃100 m^{-1}.

The larger part of this thesis was dedicated to the characterization of the chemical osmosis and thermo-osmosis processes. A dual approach was

chosen for each osmotic process, developing and using theoretical models and carrying in situ and laboratory experiments.
The calculation of the chemical osmotic efficiency lies on the anionic exclusion processes occurring in the rock porosity related with the charged surface of clay minerals. It requires the resolution of an electrical model and here a triple-layer model accounting for overlap of diffuse layers [59, 89] was improved to account for solutions composed by both monovalent and divalent ions, like in natural waters. Considering divalent counterions or a mix of monovalent and divalent counterions instead of only monovalent ions leads to a substantial decrease of the osmotic efficiency. From this observation a discussion is addressed on the resulting effect on abnormal pressures in argillaceous layers in sedimentary basins. We show that overpressures lower than expected, using the osmotic efficiencies determined during experiments with only Na^+ as counterion, can be reached in argillaceous formations.
Chemical osmosis was also characterized by experiments on the Tournemire clay-rock. Several attempts of experiments in boreholes and on samples were carried out but only the chemical osmosis experiments performed on disk shape samples in a confining device were successful. During these experiments, a chemo-osmotic flow is induced by a concentration gradient applied across the sample. Pressure evolution in the reservoirs is measured and their inversion allow estimating a chemical osmotic efficiency ranging between 0.014 and 0.31 for this sample, at different salinities. A new set of experiments is planned using solutions with Ca^{2+} and no more Na^+ like in the previous experiments to study the osmotic behaviour of the natural clay-rock when submitted to divalent counterions. Indeed, the effect of divalent cations on the osmotic properties of natural shales is poorly documented and further experimental data are needed.

The thermo-osmotic process in clay-rock required a better characterization as well theoretically as experimentally. Indeed, neither predictive models nor experiments on natural shales were available, so far. Attempts to characterize thermo-osmosis by theoretical models and in situ experiments were performed during this thesis. A macroscopic expression, at the representative elementary volume, relating the thermo-osmotic permeability to the intrinsic permeability and the excess specific enthalpy was obtained and two models were developed for determining the excess specific enthalpy of the pore fluid. The first one proposed an expression of the excess specific enthalpy related to the excess Gibbs energy of the fluid but its determination required the structural component of the disjoining pressure, a poorly constrained parameter. Due to these uncertainties, a semi-quantitative model for the thermo-osmotic permeability was proposed. The second model went

down to the molecular scale and related the excess specific enthalpy to the concentrations of hydrogen bounds around the water molecules sorbed at the solid surface and in the first shells of ions compared with their concentration in bulk water. We were able to achieve a fully predictive model which only requires petrophysical parameters and concentration and temperature conditions as input parameters.
Thermo-osmotic process was observed and quantified in the Tournemire clay-rock during in situ experiments in an equipped borehole. The temperature gradient induced between the test interval of the borehole and the formation led to a pressure decrease related to a thermo-hydraulic behaviour and to a thermo-osmotic flow. A thermo-osmotic permeability for the Tournemire argillite ranging between 6×10^{-12} and 2×10^{-10} m^2 K^{-1} s^{-1} was deduced from these experiments.
A difference of at least half an order of magnitude was observed but not clearly identified between the measurements and the model. Further characterization of this process are undoubtedly required, in particular by experiments on natural clay-rocks.

The last part of the thesis was dedicated to the interpretation of the pressure profile measured in the Toarcian/Domerian argillaceous formation. The profiles of hydraulic head, chemical composition and temperature were required, as well as the profiles of hydraulic and osmotic flow permeabilities. The flow coefficients profiles were obtained using the predictive models previously developed which require the petrophysical parameters, chemical composition and temperature variations across the formation as input parameters.
For the interpretation of the measured excess-head, the hydraulic and osmotic processes were considered, as well as alternative processes due to a hydromechanical behaviour of the clay-rock or changes in the hydraulic boundary conditions. Nevertheless, only the hydraulic and osmotic processes are able to generate, in the present-day conditions, an excess-head in the Tournemire formation. A satisfactory reproduction of the measured excess-hydraulic head was achieved considering together chemical osmosis, thermo-osmosis and the purely Darcy's flow. It is worth noting that a large part of the excess-head can be explained only by variations of the intrinsic permeability across the formation, calculated with a Kozeny-Carman relationship and mainly due to the observed decrease of porosity with depth in the Tournemire argillaceous formation.
The important dependency of the calculated pressure profile to the intrinsic permeability, chemo-osmotic efficiency and thermo-osmotic efficiency emphasizes the interest of better constrains by experimental determination

of the flow coefficients variations across the formation. However, in such impervious rocks, it appears difficult to estimate the flow coefficients with an accuracy better than the order of magnitude. The interest of the predictive models based on petrophysical parameters is clear, however further data from the Tournemire clay-rock are required for a better constrain of the calculated coefficients accuracy.
During the hydraulic head profile calculations using the hydraulic and osmotic flows, it was observed that the introduction of thermo-osmosis leads to an increase of the specific discharge and an inversion of the water movements which became directed upward. This specific discharge was calculated to increase up to values so that advection is perhaps non-negligible in solute transport (Peclet number around 0.7).

At least, it seems important to state that the origin of the pressure profile across the Tournemire is now understood and the most plausible mechanisms, hydraulic and osmotic processes, are identified. However, owing to the accumulated uncertainties during the successive steps to calculate the resulting hydraulic head, some improvement can be expected.

The work performed during this thesis highlights some improvements required for a better constrain of the fluid flow and pressure fields in argillaceous formation and in particular in the Toarcian/Domerian formation of Tournemire. The understanding of the osmotic flows in shales can be clearly improved by performing osmotic experiments, essentially focused on two points.
For chemical osmosis, it appears interesting to perform a set of experiments on a clay-rock at a same salinity but using solutions presenting different compositions. The multi-ionic TLM developed during this thesis pointed out a decrease of the shale osmotic efficiency using solutions with divalent cations or mixed solutions and no monovalent cations as usually considered. These results also showed that this could have noticeable effects on the osmotically induced abnormal pressures in argillaceous formations. However, there is a lack of experimental data for assessing and calibrating these predictions. Indeed, almost all chemical osmosis experiments performed on natural shales were made using NaCl solutions.
Concerning thermo-osmosis, first experiments of such a kind of flow on natural clay-rock were carried out during this thesis. Further experiments on Tournemire clay-rock and on other argillaceous formations are required for a better constrain of this osmotic process. In particular, the discrepancy between thermo-osmotic permeability predictions and measurements is to clarify. Off-site laboratory thermo-osmotic experiments using a device simi-

lar to the device used for the chemo-osmotic experiments but modified to be able to induce a temperature gradient across the sample seem an interesting development for a better constrain of the experimental uncertainties.
Hydrogeological and hydraulic settings of the Tournemire argillaceous formation can also be improved by completing the profile of different parameters. The hydraulic head profile could be improved obtaining further long term and non-perturbed pressure measurements, particularly in the middle part of the Toarcian/Domerian formation. Pressure profile calculations highlighted the importance of the permeability variations across the formation on the resulting pressure profile. However, few reliable permeability measurements are available and performing a set of permeability measurements by pulse-test on confined samples, preserved in the same conditions (e.g., in triaxial cells) could be interesting for constraining the permeability profile. Completing chemical efficiency and thermo-osmotic permeability profiles appears also as an interesting development.

Some results presented in this manuscript can directly be used for the safety evaluation of the installation of nuclear wastes repository in deep argillaceous formations. This is particularly the case of the predictive model for estimating the thermo-osmotic permeability of clay-rocks. Thermo-osmotic process was apparently not considered in the fluid flow calculations around a repository, so far [4]. However, because of modifications of the temperature gradient in the vicinity of the repository by the heat emitted by decay of radioactive matters in waste canisters, such an osmotic process could have an impact on the fluid flow. This impact can be evaluated integrating the results of the thermo-osmotic predictive model in a safety model. In a general manner, it appears interesting to investigate the influence of the osmotic flows on water movement and on the evolution of the excess-hydraulic head with the evolution of the hydraulic, chemical and thermal transient states induced by a radioactive wastes repository installed in an argillaceous formation.

Bibliography

[1] Al-Bazali, T. *Experimental study of the membrane behavior of shale during interaction with water-based and oil-based muds.* PhD thesis, University of Texas, Austin, 2005.

[2] Ambert, M., and Ambert, P. Karstification des plateaux et encaissement des vallées au cours du Néogène et du Quaternaire dans les Grands Causses méridionaux (Larzac, Blandas). *Géologie de la France 4* (1995), 37–50.

[3] Anderson, R. V. V. Tertiary stratigraphy and orogeny of the northern punjab. *Geological Society of America Bulletin 38* (1927), 665–720.

[4] ANDRA. Dossier 2005. Référentiel du Site Meuse / Haute Marne - Tome 2: Caractérisation comportementale du milieu géologique sous perturbation. C.RP.ADS.04.0022/A, ANDRA, Châtenay-Malabry, France, 2005.

[5] ANTEA. Laboratoire souterrain de Tournemire (Aveyron) Réalisation de mesures hydrauliques Rapport n 2 de suivi des mesures et mesure périodique de perméabilité. Technical Report A 25665/A, ANTEA, 2001.

[6] ANTEA. Station expérimentale de Tournemire (Aveyron) Réalisation de mesures hydrauliques dans la couche argileuse (forages PH1 et PH3) et suivi de pression des aquifères (forages CA et DC) Rapport dintervention du 07 Avril 2003. Technical Report A 30372/A, ANTEA, 2003.

[7] Archie, G. E. The electrical resistivity log as an aid in determining reservoir characteristics. *Petroleum Transactions of AIME 146* (1942), 54–61.

[8] Athy, L. F. Density, porosity and compaction of sedimentary rocks. *American Association of Petroleum Geologists Bulletin 14* (1930), 1–24.

[9] AVENA, M. J., AND DE PAULI, C. P. Modeling the interfacial properties of an amorphous aluminosilicate dispersed in aqueous nacl solutions. *Colloids and Surfaces A: Physicochemical and Engineering Aspect 118* (1996), 75–87.

[10] AVENA, M. J., AND DE PAULI, C. P. Proton adsorption and electrokinetics of an argentinean montmorillonite. *Journal of Colloid and Interface Science 202* (1998), 195–204.

[11] AZAR, J. J., AND ROBELLO SAMUEL, G. *Drilling engineering*. PennWell books, 2007.

[12] BARBOUR, S., AND FREDLUND, D. Mechanisms of osmotic flow and volume change in clay soils. *Canadian Geotechnical Journal 26* (1989), 551–562.

[13] BEAUCAIRE, C., MICHELOT, J. L., SAVOYE, S., AND CABRERA, J. Groundwater characterisation and modelling of water-rock interaction in an argillaceous formation (Tournemire, France). *Applied Geochemistry 23* (2008), 2182–2197.

[14] BENHAMIDAA, A., DJERAN-MAIGRE, I., DUMONTETA, H., AND SMAOUI, S. Clay compaction modelling by homogenization theory. *International Journal of Rock Mechanics & Mining Sciences 42* (2005), 996–1005.

[15] BENSENOUCI, F. *Apport des traceurs naturels à la compréhension des transferts au travers d'une couche argileuse : Application aux argilites de Tournemire (Aveyron, France)*. PhD thesis, Université Paris-Sud 11, 2010.

[16] BERRY, F. A. F. High fluid potentials in California Costal Ranges and their tectonic significance. *American Association of Petroleum Geologists Bulletin 57* (1973), 1219–1249.

[17] BERTRAND, L., LAVIGUERIE, R., CABRERA, J., MATRAY, J. M., AND SAVOYE, S. Instrument for measuring pore pressure and permeability in low permeability rock. In *Clays in natural & engineered barriers for radioactive waste confinement* (2002), Andra.

[18] BOISSON, J., CABRERA, J., AND DE WINDT, L. Etude des écoulements dans un massif argileux. Laboratoire souterrain de Tournemire. Rapport DPRE/SERG n 98/06, IPSN, 1998.

[19] Boisson, J.-Y. Clay club catalogue of characteristics of argillaceous rocks. Nuclear Energy Agency Report 4436, OECD, 2005.

[20] Boisson, J. Y., Bertrand, L., Heitz, J. F., and Moreau Le Golvan, Y. *In-situ* and laboratory investigations of fluid flow through an argillaceous formation at different scales of space and time, Tournemire tunnel, southern France. *Hydrogeology Journal 9* (2001), 108–123.

[21] Boisson, J. Y., Cabrera, J., Bertrand, L., and Heitz, J. F. Mesures de très faibles perméabilités in-situ et en laboratoire sur les argilites de Tournemire (Aveyron). Méthodologies comparées et effets d'échelle. *Bulletin Sociétée Géologique de France 169* (1998), 595–604.

[22] Bolt, G. H. *Soil Chemistry, B. Physico-Chemical models*. Elsevier, Amsterdam, 1979.

[23] Borchardt, G. *Minerals in soil environments*. Soil Science Society America Book Series, No. 1. Soil Science Society of America, Madison, WI. 1989, p. 675.

[24] Bredehoeft, J. D., and Hanshaw, B. B. On the maintenance of anomalous fluid pressures: I. Thick sedimentary sequences. *Geological Society of America Bulletin 79* (1968), 1097–1106.

[25] Bredehoeft, J. D., Neuzil, C. E., and Milly, P. C. D. Regional flow in the dakota aquifer: A study of the role of confining layers. *U.S. Geological Survey Supply Paper 2237* (1983), 1–45.

[26] Bredehoeft, J. D., and Papadopoulos, S. A method for determining the hydraulic properties of tight formations. *Water Resources Research 16* (1980), 233–238.

[27] Bresler, E. Anion exclusion and coupling effects in nonsteady transport unsatured soils : I. Theory. *Soil Science Society of America Proceedings 37*, 5 (1973), 663–669.

[28] Brunauer, S., Emmett, P. H., and Teller, E. Adsorption of gases in multimolecular layers. *Journal of the American Chemical Society 60* (1938), 309–319.

[29] Bruxelle, L., Simon-Coinçon, R., Guendon, J. L., and Ambert, P. Formes et formations superficielles de la partie oust du Causse de Sauveterre. *Karstologia 49* (2007), 1–14.

[30] CABRERA, J., BEAUCAIRE, C., BRUNO, G., DE WINDT, L., GENTY, A., RAMAMBASOA, N., REJEB, A., SAVOYE, S., AND VOLANT, P. Projet Tournemire. Synthèse des programmes de recherche. Rapport DPRE/SERGD 01-19, IRSN, 2001.

[31] CARNAHAN, C. L. Thermal osmosis near a buried heat source. *International Communications in Heat and Mass Transfer 13* (1986), 659–664.

[32] CEY, B. D., BARBOUR, S. L., AND HENDRY, M. J. Osmotic flow through a Cretaceous clay in southern Saskatchewan, Canada. *Canadian Geotechnical Journal 38*, 5 (2001), 1025–1033.

[33] CHILINGAR, G. V., SEREBRYAKOV, V. A., AND ROBERTSON, J. O. J. *Origin and prediction of abnormal formation pressures*. Developments in Petroleum Science, Volume 50. 2002.

[34] COELHO, D., SHAPIRO, M., THOVERT, J., AND ADLER, P. Electroosmotic phenomena in porous media. *Journal of Colloid and Interface Science 181* (1996), 169–190.

[35] CONSTANTIN, J., LAURENT, P., VERGELY, P., AND CABRERA, J. Paleo-deviatoric stress magnitudes from calcite twins and related structural permeability evolution in minor faults: Example from the toarcian shale of the French Causses Basin, Aveyron, France. *Tectonophysics 429* (2005), 49–77.

[36] COSENZA, P., GHOREYCHI, M., MARSILY, G. D., VASSEUR, G., AND VIOLETTE, S. Theoretical prediction of poroelastic properties of argillaceous rocks from in situ specific storage coefficient. *Water Resources Research 38* (2002), 1207.

[37] DAVIES, C. W. *Ion Association*. Butterworths, Washington DC, 1962.

[38] DE MARSILY, G. *Quantitative Hydrogeology, Groundwater Hydrology for Engineers*. Academic Press, New-York, 1986.

[39] DERJAGUIN, B. V., CHURAEV, N. V., AND MULLER, V. M. *Surface Forces, 1st Ed.* ed. Kitchener, J. A., New York : Consultants Bureau, 1987.

[40] DESCOSTES, M., BLIN, V., BAZER-BACHI, F., MEIER, P., GRENUT, B., RADWAN, J., SCHLEGEL, M., BUSCHAERT, S., COELHO, D., AND TEVISSEN, E. Diffusion of anionic species in

Callovo-Oxfordian argillites and Oxfordian limestones (Meuse/Haute-Marne, France). *Applied Geochemistry 23* (2008), 655–677.

[41] Dick, P. Rapport de fin de creusement des nouvelles galeries 2008 dans la Station Expérimentale de Tournemire. Note Technique DEI/SARG/2010-027, Institut de Radioprotection et de Sûreté Nucléaire, 2010.

[42] Dickinson, G. Geological aspects of abnormal reservoir pressure in Gulf Coast, Louisiana. *American Association Petroleum Geological Bulletin 37* (1953), 410–432.

[43] Dirksen, C. Thermo-osmosis through compacted saturated clay membranes. *Soil science society of America proceedings 33* (1969), 821–826.

[44] Elimenech, M., Gregory, J., Jia, X., and Williams, R. *Particle Deposition & Aggregation - Measurement, Modelling and Simulation*. ButterworthHeineman, Oxford, 1995.

[45] Fabre, G., and Pellet, F. Creep and time-dependent damage in argillaceous rocks. *International Journal of Rock Mechanics and Mining Science 43* (2006), 950–960.

[46] Fritz, S. J. Ideality of clay membranes in osmotic processes: A Review. *Clays and Clay Minerals 34*, 2 (1986), 214–223.

[47] Fritz, S. J., and Marine, I. W. Experimental support for a predictive osmotic model of clay membranes. *Geochimica and Cosmochimica Acta 47* (1983), 1515–1522.

[48] Gable, R. *Terrestrial heat flow in Europe*. Springer Verlag, 1979, ch. Draft of geothermal flux map of France, pp. 179–185.

[49] Gaines, G. I., and Thomas, H. C. Adsorption studies on clay minerals. II. A formulation of the thermodynamics of exchange adsorption. *Journal of Physical Chemistry 21* (1953), 714–718.

[50] Garavito, A., Kooi, H., and Neuzil, C. Numerical modeling of a long-term in situ chemical osmosis experiment in the pierre shale, south dakota. *Advances in Water Resources 29* (2006), 481–492.

[51] Garavito, A. M., De Cannière, I., and Kooi, H. *In situ* chemical osmosis experiment in the Boom Clay at the Mol underground

research laboratory. *Physics and Chemistry of the Earth 32* (2007), 421–433.

[52] GAUCHER, E. C., BLANC, P., BARDOT, F., BRAIBANT, G., BUSCHAERT, S., CROUZET, C., GAUTIER, A., GIRARD, J. P., JACQUOT, E., LASSIN, A., NEGREL, G., TOURNASSAT, C., VINSOT, A., AND ALTMANN, S. Modelling the porewater chemistry of the CallovianOxfordian formation at a regional scale. *Comptes Rendus Geoscience 338* (2006), 917–930.

[53] GAUCHER, E. C., TOURNASSAT, C., PEARSON, F., BLANC, P., CROUZET, C., LEROUGE, C., AND ALTMANN, S. A robust model for pore-water chemistry of clayrock. *Geochimica et Cosmochimica Acta 73* (2009), 6470–6487.

[54] GIRAUD, A., AND ROUSSET, G. Time-dependent behaviour of deep clays. *Engineering Geology 41* (1996), 181–195.

[55] GONÇALVÈS, J. Hydrogéologie des couches argileuses. Mémoire d'habilitation à diriger des recherches, Université Pierre et Marie Curie, Paris 6, 2008.

[56] GONÇALVÈS, J. A slug test to assess the osmotic and hydraulic properties of argillaceous formations. *Water Resources Research 44* (2008), W07501, doi:10.1029/2007WR006547.

[57] GONÇALVÈS, J., AND ROUSSEAU-GUEUTIN, P. Molecular-scale model for the mass density of electrolyte solutions bound by clay surfaces: Application to bentonites. *Journal of Colloid and Interface Science 320* (2008), 590–598.

[58] GONÇALVÈS, J., ROUSSEAU-GUEUTIN, P., DE MARSILY, G., COSENZA, P., AND VIOLETTE, S. What is the significance of pore pressure in a saturated shale layer? *Water Resources Research 46* (2010), W04514, doi:10.1029/2009WR008090.

[59] GONÇALVÈS, J., ROUSSEAU-GUEUTIN, P., AND REVIL, A. Introducing interacting diffuse layers in TLM calculations. A reappraisal of the influence of the pore size on the swelling pressure and the osmotic efficiency of compacted bentonites. *Journal of Colloid and Interface Science 316* (2007), 92–99.

[60] Gonçalvès, J., Violette, S., and Wending, J. Analytical and numerical solutions for alternative overpressuring processes : Application to the Callovo-Oxfordian sedimentary sequence in the Paris basin, France. *Journal of Geophysical Research 109* (2004), B02110, doi :10.1029/2002JB002278.

[61] Gray, D. H., and Mitchell, J. K. Fundamental aspects of electro-osmosis in soils. *Journal of the Soil Mechanics and Foundations Division ASCE 93* (1967), 209–236.

[62] Gunzburger, Y., and Cornet, F. H. Rheological characterization of a sedimentary formation from a stress profile inversion. *Geophys. J. Int. 168* (2007), 402–418.

[63] Gupta, A., Coelho, D., and Adler, P. M. Electroosmosis in porous solids for high zeta potentials. *Journal of Colloid and Interface Science 303* (2006), 593–603.

[64] Gupta, A., Coelho, D., and Adler, P. M. Universal electro-osmosis formulae for porous media. *Journal of Colloid and Interface Science 319* (2008), 549–554.

[65] Habib, P., and Soeiro, F. In *Proceedings 4th International Congress of Soil Mechanics* (1957), p. 40.

[66] Hendry, M. J., and Wassenaar, L. Implications of the distribution of dD in porewaters of groudwater flow and the timing of geological events in a thick aquitard system. *Water Resources Research 35*, 6 (1999), 1751–1760.

[67] Hiemstra, T., and Van Riemsdijk, W. H. On the relationship between charge distribution, surface hydration, and the structure of the interface of metal hydroxides. *Journal of Colloid and Interface Science 301* (2006), 1.

[68] Horseman, S. T., Harrington, J. F., and J., N. D. Swelling and osmotic flow in a potential host rock. *Physics and Chemistry of the Earth 32* (2007), 408–420.

[69] Horseman, S. T., Higgo, J. J. W., Alexander, J., and Harrington, J. F. *Water, Gas and Solute Movement Trough Argillaceous Media*. Nuclear Energy Agency (NEA), 1996.

[70] HUNT, J. M. Generation and migration of petroleum from abnormally pressure compartements. *American Association of Petroleum Geologists Bulletin 74* (1990), 1–12.

[71] HYDROINVEST. Installation d'une complétion multiobturateurs et tests hydrauliques sur le forage PH4 du site de Tournemire. Rapport d'installation HI 200811222NF, HydroInvest, 2008.

[72] INGEBRITSEN, S., SANFORD, W., AND NEUZIL, C. *Groundwater in Geological Processes*. Cambridge University Press, 2006.

[73] IRSN. Avis de l'Institut de Radioprotection et de Sûreté Nucléaire sur le Dossier 2005 Argile. Rapport DSU N 106, IRSN, 2005.

[74] JOST, A., VIOLETTE, S., GONCALVES, J., LEDOUX, E., GUYOMARD, Y., GUILLOCHEAU, F., KAGEYAMA, M., RAMSTEIN, G., AND SUC, J.-P. Long-term hydrodynamic response induced by past climatic and geomorphologic forcing: The case of the Paris basin, France. *Physics and Chemistry of the Earth 32* (2007), 368–378.

[75] JURY, A., AND HORTON, R. *Soil physics*. John Wiley & Sons, 2004, 6th Ed.

[76] KATCHALSKY, A., AND CURRAN, P. F. *Nonequilibrium Thermodynamics in Biophysics*. Harvard University Press, Cambridge, Massachusetts, 1967.

[77] KAZMIERCZAK, J. B., LAOUAFA, F., GHOREYCHI, M., LEBON, P., AND BARNICHON, J. D. Influence of creep on water pressure measured from borehole tests in the Meuse/Haute-Marne Callovo-Oxfordian argillites. *Physics and Chemistry of the Earth 32* (2007), 917–921.

[78] KEEP, C. E., AND WARD, H. L. Drilling against high rock pressures with particular reference to operation conducted in the Khaur field, Punjab. *Journal of Institutional Petroleum Technology 20* (1934), 990–1013.

[79] KEIJZER, T. J. S., AND LOCH, J. P. G. Chemical Osmosis in Compacted Dredging Sludge. *Soil Science Society of America Journal 65* (2001), 1045–1055.

[80] KEMPER, W. Water and Ion Movement in Thin Films as Influenced by the Electrostatic charge and Diffuse Layer of Cations Associated With

Clay Mineral Surfaces. *Soil Science Society of America Proceedings* (1960), 10–16.

[81] Kemper, W. D., and Evans, N. A. Movement of Water as Effected by Free Energy and Pressure Gradients III. Restriction of Solutes by Membranes. *Soil Science Society of America Proceedings 27*, 5 (1963), 485–490.

[82] Kemper, W. D., and Quirk, J. P. Ion Mobilities and Electric Charge of external Clay Surfaces Inferred from Potential Differences and Osmotic Flow. *Soil Science Society of America Proceedings 36* (1972), 426–433.

[83] Kemper, W. D., and Rollins, J. B. Osmotic Efficiency Coefficients Across Compacted Clays. *Soil Science Society of America Proceedings 30*, 5 (1966), 529–534.

[84] Kohler, E., Pozo, C., Raynal, J., Jullien, M., Beaucaire, C., Pitsch, H., and Cabrera, J. Characterization of argilites heated by a basaltic Intrusion at Laumiere (Aveyron, France), evolution of mineral combination with depth and intrusion proximity. *Geophysical Research Abstracts Vol. 5* (2003).

[85] Kostek, S., Schwartz, L., and Johnson, D. Fluid permeability in porous media: Comparison of electrical estimates with hydrodynamical calculations. *Physical Review B 45(1)* (1992), 186–194.

[86] Krief, M., Garta, J., Stellingwerff, J., and Ventre, J. A petrophysical interpretation using the velocities of p and s waves (full-waveform sonic). *The Log Analyst 31* (1990), 355–369.

[87] Langmuir, D. *Aqueous Environmental Geochemistry*. Prentice Hall, 1997.

[88] Law, B., Ulmishek, G., and Slavin, V. Abnormal pressures in hydrocarbon environments. Memoir 70, AAPG, 1998.

[89] Leroy, P., and Revil, A. A triple-layer model of the surface electrochemical properties of clay minerals. *Journal of Colloid and Interfacial Science 270* (2004), 371–380.

[90] Leroy, P., Revil, A., Altmann, S., and Tournassat, C. Modeling the composition of the pore water in a clay-rock geological formation (Callovo-Oxfordian, France). *Geochemica and Cosmochemica Acta 71* (2007), 1087–1097.

[91] LETEY, J., AND KEMPER, W. D. Movement of Water and Salt through a Clay-Water System : Experimental Verification of Onsager Reciprocal Relation. *Soil Science Society of America Proceedings*, 33 (1969), 25–29.

[92] LUO, X. *Modélisation des surpressions dans les bassins méditerranéen et des phénomènes associés*. PhD thesis, Université de Montpellier 2, 1994.

[93] LUO, X., AND VASSEUR, G. Contributions of compaction and aquathermal pressuring to geopressure and the influence of environmental conditions. *The American Association of Petroleum Geologists Bulletin 76, 10* (1992), 1550–1559.

[94] MAGARA, K. Importance of aquathermal pressuring effect in Gulf Coast. *American Association Petroleum Geological Bulletin 59* (1975), 2037–2045.

[95] MAGARA, K. *Compaction and fluid migration, practical petroleum geology*. Developments in petroleum science 9. Elsevier, 1978.

[96] MALUSIS, M. A., AND SHACKELFORD, C. D. Coupling Effects during Steady-State Solute Diffusion through a Semipermeable Clay Membrane. *Environmental Science & Technology 36* (2002), 1312–1319.

[97] MARINE, I. W., AND FRITZ, S. J. Osmotic model to explain anomalous hydraulic heads. *Water Resources Research 17*, 1 (1981), 73–82.

[98] MATRAY, J.-M., SAVOYE, S., AND CABRERA, J. Desaturation and structure relationships around drifts excavated in the well-compacted Tournemire's argillite (Aveyron, France). *Engineering Geology 9* (2007), 1–16.

[99] MAZUREK, M., ALT-EPPING, P., BATH, A., GIMMI, T., AND WABER, H. N. CLAYTRAC project: Natural tracer profiles across argillaceous formations - review and synthesis. Nuclear Energy Agency (OECD/NEA) report, 2009.

[100] MCPHERSON, B. J. O. L., AND GARVEN, J. D. Hydrodynamics and overpressure mechanisms in the Sacramento Basin, California. *American Journal of Science 299* (1999), 429–466.

[101] MEIER, C., AND PIEDEVACHE, M. Laboratoire souterrain de Tournemire. Complétion multi-obturateur PH5. Rapport d'installation 1426-17, SolExperts, 2008.

[102] Mercer, J. W., Pinder, G. F., and Donalson, I. G. A Galerkin-finite element analysis of the hydrothermal system at Wairakei, New-Zealand. *Journal of Geophysical Research 80* (1975), 2608–2621.

[103] Mitchell, J. K., and Soga, K. *Fundamentals of Soil Behavior*, 3rd ed. John Wiley & Sons, New-York, 2005.

[104] Morency, C., Huismans, R. S., Beaumont, C., and Fullsack, P. A numerical model for coupled fluid flow and matrix deformation with applications to disequilibrium compaction and delta stability. *Journal of Geophysical Research 12* (2007), B10407.

[105] Motellier, S., Devol-Brown, I., Savoye, S., Thoby, D., and Alberto, J.-C. Evaluation of tritiated water diffusion through the Toarcian clayey formation of the Tournemire experimental site (France). *Journal of Contaminant Hydrology 94* (2007), 99–108.

[106] Mouchet, J., and Mitchell, A. Abnormal pressures while drilling. Manuels techniques 2, Elf Aquitaine, 1989.

[107] Moyne, C., and Murad, M. Electro-chemo-mechanical couplings in swelling clays derived from a micro/macro-homogenization procedure. *International Journal of Solids and Structures 39* (2002), 6159–6190.

[108] Munro, R. G. Analytical representations of elastic moduli data with simultaneous dependence on temperature and porosity. *Journal of Research of the National Institute of Standards and Technology 109* (2004), 497–503.

[109] Neuzil, C. Hydromechanical coupling in geologic processes. *Hydrogeology Journal 11* (2003), 41–83.

[110] Neuzil, C., and Provost, A. Recent experimental data may point to a greater role for osmotic pressures in the subsurface. *Water Resources Research 45* (2009), W03410, doi:10.1029/2007WR006450.

[111] Neuzil, C. E. On conducting the modified 'slug' test in tight formations. *Water Resources Research 18* (1982), 439–441.

[112] Neuzil, C. E. Groundwater Flow in Low Permeability Environements. *Water Resources Research 22*, 8 (1986), 1163–1195.

[113] Neuzil, C. E. Low fluid pressure within the pierre shale: a transient response to erosion. *Water Resources Research 29* (1993), 2007–2020.

[114] NEUZIL, C. E. How permeable are clays and shales? *Water Resources Research 34* (1994), 145–150.

[115] NEUZIL, C. E. Abnormal Pressures as Hydrodynamic Phenomena. *American journal of Science 295* (1995), 742–786.

[116] NEUZIL, C. E. Osmotic generation of "anomalous" fluid pressures in geological environments. *Nature 403* (2000), 182–184.

[117] NEUZIL, C. E., COOLEY, C., SILLIMAN, S. E., BREDEHOEFT, J. D., AND HSIEH, P. A. A transient laboratory method for determining the hydraulic properties of 'tight' rocks II. Application. *International Journal of Rock Mechanics and Mining Science 18* (1981), 253–258.

[118] NOY, D., HORSEMAN, S., HARRINGTON, J., BOSSART, P., AND FISH, H. *An Experimental and Modelling Study of Chemico-osmosis Effect in the Opalinus Clay of Switzerland.* Rapports de l'OFEG, Série Géologie, 2004, pp. 95–126.

[119] OLSEN, H. W. Liquid Movement trough Kaolinite under Hydraulic, Electric and Osmotic Gradients. *The American Associationof Petroleum Geologists Bulletin 56* (1972), 2022–2028.

[120] ONSAGER, L. Reciprocal relations in irreversible processes. i. *Physical Review 37* (1931), 405–426.

[121] ONSAGER, L. Reciprocal relations in irreversible processes. ii. *Physical Review 38* (1931), 2265–2279.

[122] PAPE, H., CLAUSER, C., AND IFFLAND, J. Permeability prediction based on fractal pore-space geometry. *Geophysics 1447-1460* (1999), 64.

[123] PATRIARCHE, D., LEDOUX, E., MICHELOT, J.-L., SIMON-COINÇON, R., AND SAVOYE, S. Diffusion as the main process for mass transport in very low water content argillites: 2. Fluid flow and mass transport modeling. *Water Resources Research 40* (2004), W01517.

[124] PATRIARCHE, D., LEDOUX, E., MICHELOT, J.-L., SIMON-COINON, R., AND SAVOYE, S. Diffusion as the main process for mass transport in very low water content argillites: 1. Chloride as a natural tracer for mass transport - Diffusion coefficient and concentration measurements in interstitial water. *Water Resources Research 40* (2004), W01516.

[125] Pearson, F. *Muds and muds: physical and fluid flow properties.* 1999, special publication of the geological society of london 158 What is the porosity of a mudrock?, pp. 9–21.

[126] Pearson, F., Arcos, D., Bath, A., Boisson, J., Fernández, A., Gbler, H., Gaucher, E., Gaustchi, A., Griffault, L., Hernán, P., and Waber, H. Geochemistry of water in the Opalinus Clay Formation at the Mont Terri rock laboratory. Technical Report 2003-03, Mont Terri Project, 2003.

[127] Peyaud, J. B., Barbarand, J., Carter, A., and Pagel, M. Mid-Cretaceous uplift and erosion on the northern margin of the Ligurian Tethys deduced from thermal history reconstruction. *International Journal of Earth Science 94* (2005), 46247.

[128] Powers, M. C. Fluid release mechanisms in compacting marine mudrocks and their importance in oil exploration. *American Association Petroleum Geological Bulletin 51* (1967), 1240–1254.

[129] Revil, A., and Glover, P. W. J. Nature of surface electrical conductivity in natural sands, sandstones, and clays. *Geophysical Research Letters 25*, 5 (1998), 691–694.

[130] Revil, A., and Leroy, P. Constitutive equations for ionic transport in porous shales. *Journal of Geophysical Research 109* (2004), B03208, doi : 10.1029/2003JB002755.

[131] Revil, A., Leroy, P., and Titov, K. Characterization of transport properties of argillaceous sediments : Application to the Callovo-Oxfordian argilite. *Journal of Geophysical Research 110* (2005), B06202, doi : 10.1029/2004JB003442.

[132] Revil, A., and Pessel, M. Electroosmootic flow and the validity of the classical Darcy equation in silty shales. *Geophysical Research Letters 29*, 9 (2002), 10.1029/2001GL013480.

[133] Rosanne, M., Paszkuta, M., and Adler, P. Thermodiffusional transport of electrolytes in compact clays. *Journal of Colloid and Interface Science 299* (2006), 797–805.

[134] Rouire, J., and Rousset, C. *Causses, Cévennes, Aubrac — Guide Géologiques Régionaux.* Masson, 1980.

[135] ROUSSEAU-GUEUTIN, P. *Les processus couplés dans les argilites du Callovo-Oxfordien sur le site de Bure : implications pour les mouvements de fluide et de solutés.* PhD thesis, Université Pierre et Marie Curie, Paris VI, 2008.

[136] ROUSSEAU-GUEUTIN, P., DE GREEF, V., GONÇALVÈS, J., VIOLETTE, S., AND CHANCHOLE, S. Experimental device for chemical osmosis measurement on natural clay-rock samples maintained at *in-situ* conditions. implications for pressure interpretation. *Journal of Colloid and Interface Science 337* (2009), 106–116.

[137] ROUSSEAU-GUEUTIN, P., GONÇALVÈS, J., CRUCHAUDET, M., DE MARSILY, G., AND VIOLETTE, S. Hydraulic and chemical pulse-tests in a shut-in chamber imbedded in an argillaceous formation: numerical and experimental approaches. *Water Resources Research* (2010), doi:10.1029/2008WR007371, in press.

[138] SAVOYE, S., MICHELOT, J. L., BENSENOUCI, F., MATRAY, J. M., AND CABRERA, J. Insight given by stable isotope profiles in pore-water for understanding transfers through Toarcian/Domerian argillaceous rocks over large space and time scales. *Physics and Chemistry of the Earth 33* (2008), S67–S74.

[139] SCHNEIDER, F., POTDEVIN, J. L., WOLF, S., AND FAILLE, I. Mechanical and chemical compaction model for sedimentary basin simulators. *Tectonophysics 263* (1996), 307–317.

[140] SIMON-COINÇON, R., AND SCHMITT, J. M. Evolution géologique et histoire paléoenvironnementale du bassin des grands causses. Rapport technique LHM/RD/99/52, Centre d'Information Géologique, Ecole Nationale Supérieure des Mines de Paris, 1999.

[141] SOLER, J. M. The effect of coupled transport phenomena in the Opalinus Clay and implications for radionuclide transport. *Journal of Contaminant Hydrology 53* (2001), 63–84.

[142] SPENCER, C. W. *Studies in abnormal pressure.* Elsevier, 1994, ch. Abnormal formation pressure caused by hydrocarbon generation, pp. 343–375.

[143] SPOSITO, G. *The surface chemistry of soils.* Oxford University Press, 1984.

[144] Srivastava, R., and Avasthi, P. Non-equilibrium thermodynamics of thermo-osmosis of water though kaolinite. *Journal of Hydrology 24* (1975), 111–120.

[145] Srivastava, R., and Jain, A. Thermo-osmosis of water through bentonite. *Indian Journal of Chemistry 12* (1974), 1276–1279.

[146] Swarbrick, R., and Osborne, M. *Mechanisms that Generate Abnormal Pressures : an Overview.* AAPG Memoir 70. 1998.

[147] Tournassat, C., Ferrage, E., Poinsignon, C., and Charlet, L. The titration of clay minerals. part ii. structural-based model and implications for clay reactivity. *Journal of Colloid and Interface Sciences 273* (2004), 234–246.

[148] Trémosa, J., Gonçalvès, J., Matray, J. M., and Violette, S. Estimating thermo-osmotic coefficients in clay-rocks: II. In situ experimental approach. *Journal of Colloid and Interface Science 342* (2010), 175–184.

[149] Ullman, W. J., and Aller, R. C. Diffusion coefficients of nearshore marine sediments. *Limnology and Oceanography 27 (3)* (1982), 5526–5555.

[150] UNESCO. Tenth report on the joint panel on oceanographic tables and standard. Sidney, BC, Canada. 1-5 september 1980. Unesco technical paper in marine science 36, 1981.

[151] Van Olphen, H. *An introduction to clay colloid chemistry for clay technologists, geologists and soil scientists.* 1974.

[152] Vasseur, G. *Advances in European Geothermal Research.* 1980, ch. Some aspects of heat flow in France, pp. 170–175.

[153] Wittebroodt, C., Savoye, S., and Gouze, P. Influence of initial iodide concentration on the iodide uptake by the argillite of Tournemire. *Physics and Chemistry of the Earth 33* (2008), 943–948.

[154] Yang, Y., and Aplin, A. C. Permeability and petrophysical properties of 30 natural mudstones. *Journal of Geophysical Research 112* (2007), doi:10.1029/2005JB004243.

[155] Young, A., and Low, P. Osmosis in argillaceous rocks. *AAPG Bulletin 49* (1965), 1004–1008.

[156] ZHENG, L., AND SAMPER, J. A coupled THMC model of FEBEX *mock-up* test. *Physics and Chemistry of the Earth 33* (2008), S486–498.

Abstract

In the framework of the studies dealing on ability to store radioactive wastesin argillaceous formations, signification of interstitial pressures is an importantpoint to understand water and solutes transport. In very low permeabilityargillaceous formations, like those studied in the Callovo-Oxfordian ofthe Paris basin by ANDRA, pore pressure is frequently higher than the theoreticalhydrostatic pressure or than the pressure in the surrounding aquifers.
Such an overpressure is also measured in the Toarcian/Domerian argillaceousformation ($k = 10^{-21}m^2$), studied by the IRSN in the undergroundresearch laboratory of Tournemire (Aveyron, France). The hydraulic headprofile has been specified in this manuscript and found to present a 30 ±10m excess-head. This excess-head can be due to compaction disequilibriumof the argillaceous formation, diagenetic evolution of the rock, tectonic compression,changes in hydrodynamic boundary conditions or osmotic processes.
Amongst these potential causes, chemical osmosis and thermo-osmosis, a fluid flow under a chemical concentration and a temperature gradient, respectively,are expected to develop owing to the small pore size and theelectrostatic interactions related to the charged surface of clay minerals.
The goal of the work presented here was to study and quantify the contributionof each cause to the measured excess-head. Chemo-osmotic andthermo-osmotic permeabilities were obtained by experiments and using theoreticalmodels. Theoretical models are based on the reproduction of theinteractions occurring between the charged surface of clay minerals and poresolution and their upscaling at the representative elementary volume macroscopicscale. Chemical osmosis phenomenon is related to anionic exclusionand the determination of the chemo-osmotic efficiency requires the resolutionof an electrical interactions model. A triple-layer-model which considersdiffuse layers overlapping was improved during this thesis to be able to takeinto account the effect of multi-ionic solutions, i.e. nearest than the naturalwaters composition, and, thus, to constrain better the chemo-osmoticefficiency ". Thermo-osmosis process is poorly characterized so that no satisfactorymacroscopic expression to calculate the thermo-osmotic permeabililty$k_T$was available nor thermo-osmotic experiments performed on naturalshales, so far. This process is interpreted as being related to changes propertiesof water sorbed at clay minerals surface compared with bulk water.A thermo-osmotic permeability predictive model is proposed here, based on the modifications of the hydrogen bounds associated with water moleculeslocated at the vicinity of the solid surface. Input parameters of this modelonly consist in petrophysical parameters and medium conditions (porewaterconcentration and temperature). Chemical osmosis and thermo-osmosisexperiments were performed on Tournemire argillite samples and in a testinterval equipped borehole at the Tournemire URL. These experiments haveconsisted in inducing a concentration or temperature gradient across a samplefor the laboratory experiments and between the borehole test intervaland the formation for the in situ experiments. Osmotic flows were identifiedby the interpretation of the pressure evolution in the test interval using ahydro-thermo-chemo-mechanical model based on the mass balance equationsand the coupled-flow equations. Inversion of the measured pressure signalsallowed identifying a chemo-osmotic efficiency " ranging between 0.014 and0.31 and a thermo-osmotic permeability $k_T$ranging between $6 \times 10^{-12}$and $2 \times 10^{-10} m^2K^{-1}s^{-1}$for the Tournemire clay-rock.In parallel to the characterization of the osmotic processes in the argillaceousformation of Tournemire, porewater composition and temperature profiles were established. Temperature profile was obtained by direct measurementin different boreholes. Porewater composition profile was calculatedby a geochemical model developed to reproduce the thermodynamic equilibriumreactions with mineral phases and cation exchange between the clayrockand the pore solution. Added to the requirement of the temperature and concentration profiles across the Tournemire argillaceous formation asforce gradients to reproduce the osmotic flows through the formation, theporewater composition is also needed as it is an essential input parameter topredict the chemo-osmotic efficiency coefficient.
At last, the characterization of the osmotic processes and the different force gradient profiles allowed estimating the contribution of the osmoticand hydraulic processes to the measured excess-hydraulic head profile measuredin the argillaceous formation of Tournemire. Considerations on thehydro-mechanical behaviour of the argillaceous formation allowed rule outthe other possible causes of excess-head and lead to the conclusion that onlythe hydraulic processes, related to the intrinsic permeability variation acrossthe formation, and osmotic processes can explain the pressure field in theToarcian/Domerian formation. The results particularly highlight the importanceof the spatial variations of the hydraulic and osmotic permeability coefficients in the generation of an excess-hydraulic head.